A STUDY OF LOW TEMPERATURE MAGNETIC ANOMALIES IN DILUTE ALLOYS BY SPECIFIC HEAT MEASUREMENTS

Thesis Submitted

for the

Degree of Doctor of Philosophy

of the University of London

by

JOHN WILLIAM LORAM

Physics Department,
Imperial College of Science and Technology,
London.

August, 1965.

ABSTRACT

The specific heat of several dilute magnetic alloys has been measured in the temperature range 1.3° to 20°K, using an adiabatic calorimeter. The design and construction of the calorimeter are described in detail.

Measurements are presented of the specific heat of copper, gold, and a series of copper-gold alloys, all containing a fixed quantity (0.6 at %) of iron. Details of the specific heat anomalies in these systems are discussed in relation to the appearance of a low temperaturemaximum in the electrical resistance with increasing gold concentration. The differing shapes of the specific heat anomalies in the Cu 0.6% Fe and Au 0.6% alloys are correlated with the marked differences in the Mossbauer spectra of the two systems. A Cu 0.6% Fe 0.1% Mn alloy has been investigated to observe the effect of the Mn ions on the magnetic ordering of the Fe. The specific heat of Rh 0.5% Fe and Pd 0.19% Fe alloys have been measured to throw light on the origins of their unusual resistive and magnetic properties.

The extensive body of experimental data on the anomalous properties of dilute magnetic alloys is surveyed, and current theories are discussed which purport to explain these properties.

ACKNOWLEDGEMENTS

I should like to express my sincere thanks to Dr. B. R. Coles for his stimulating interest and unfailing enthusiasm shown throughout the course of this work, which was carried out under his supervision. I am also grateful to other members of the Metal Physics group for their help and forbearance. I am indebted to Dr. H. Montgomery for his help in the design of the calorimeter, and to Mr. C. Trubridge for its construction. Finally, I should like to thank my wife for her considerable assistance in the computation of the results and in the preparation of this thesis.

C O N T E N T S

GENERAL INTRODUCTION

The study of the changes in electronic structure which occur when a foreign atom is introduced into a pure metal has attracted much theoretical and experimental attention. The behaviour of the system is largely determined by the requirement that the excess or defect charge of the impurity is screened out by the conduction electrons approximately within its atomic volume. The problem is especially interesting when the impurity comes from the first transition series, as the screening can be accomplished either by equal numbers of conduction electrons of both spin directions, giving an unmagnetised impurity state, or by conduction electrons of mainly onespin direction, giving a magnetised state. Magnetic susceptibility measurements show that both situations are to be found amongst the various alloys of non-transition metals containing small amounts of transition metals, and that the impurity state, when magnetised, behaves in a manner similar to paramagnetic ions in non conductors.

It has also been observed that whenever the impurity exists in a magnetised state, the thermal and transport properties of the alloy show striking anomalies at low temperatures. Thus even with very dilute alloys, there is a large excess specific heat at low temperatures, suggesting magnetic ordering. The ordering temperature is too high to be accounted for by magnetic dipole coupling, and occurs for concentrations that are too low for direct exchange coupling to be important. A mechanism involving the conduction electrons, which is intimately connected with the screening mechanism, is probably responsible for this long range interaction, though other models have been proposed.

In Chapters 1 and 2 the properties of dilute magnetic alloys are reviewed. (The recent review article by Van den Berg[1] was found to be a valuable source of references). Current theories deriving the conditions necessary for the formation of magnetised states, and the interaction between such states, are discussed in Chapter 3, and in Chapter 4 several theoretical models are considered which endeavour to account for particular properties. After the description of the adiabatic calorimeter and measuring technique in Chapter 5, experimental values of the specific heat of several dilute magnetic alloys are presented in Chapter 6, and these are discussed in Chapter 7 in the light of present theoretical and experimental knowledge.

CHAPTER 1

PROPERTIES OF DILUTE MAGNETIC ALLOYS

1.1 Introduction

Many experiments have demonstrated that the addition of a small amount of non-transition metal solute to a pure metal leads to an approximately temperature independent increase in its electrical resistance (Matthiesson's rule)[1]. As the temperature is reduced, electron-phonon scattering becomes negligable compared with impurity scattering, and the resistance falls to a constant value proportional to the solute concentration. This will be called normal behaviour. In 1933, de Haas[2], de Boer and Van den Berg noticed that the resistance of 'pure' gold (containing less than 10^{-4} % impurity) did not tend to a constant value at low temperatures, as expected, but went through a minimum, and started to increase on cooling below 4°K. Careful investigation showed that this effect was due to the presence of transition metal impurities. Similar results were found for silver wires, and in 1951 Gerritsen[3] and Linde showed that the resistance minimum of a Ag 0.1% Mn alloy* was followed by a maximum at still lower temperatures. The temperature of the maximum was proportional to the concentration, and for concentrations of less than 0.05% Mn, it fell below 1°K. These authors also showed that the Ag Mn alloy had a large negative magnetoresistance, which was consistant with a magnetic

* A dilute alloy of solute B in solvent A will be written A B, and the concentration, if quoted, will be in atomic percent.

origins for the resistance anomalies.

In 1956, Owen et al[4] published the results of a series of significant experiments on the magnetic properties of Cu Mn (which had also been shown to exhibit a resistance maximum and minimum). They observed a rapid increase in the magnetic susceptibility with decreasing temperature, which could be well described by a Curie-Weiss law, with a positive Curie temperature suggesting a ferromagnetic interaction between the paramagnetic impurities. However, instead of becoming ferromagnetic at low temperatures, the susceptibility showed a broad maximum at a temperature T_N, rather greater than θ, indicating a gradual antiferromagnetic ordering.

Their experiments on the Electron Spin Resonance of the Mn ions, and their demonstration of the absence of a Knight shift in the Nuclear Magnetic Resonance of the Cu nuclei, showed that there was no uniform polarisation of the conduction electrons, and that the interaction of the Mn ions and Cu nuclei was only appreciable up to a few inter-atomic distances.

In 1930, Borelius had observed large negative thermoelectric powers in the liquid helium temperature range, for Cu and Au containing small amounts of transition metals, several orders of magnitude larger than those observed for normal metals and alloys. Later work showed that this large anomalous thermopower persisted to extreme dilution (a few parts per million) of the transition metal impurity.

The thermal resistance is also found to be affected by the scattering processes that lead to the anomalies in the electrical resistance. Spohr and Webber[5] found a rapid increase in the thermal resistivity of Mg .043% Mn below 15°K which correlated well with the increase in electrical resistance below the resistance minimum. Chari and Nobel[6] observed a large negative thermal magnetoresistance, and Berman et al[7] have found similar effects in a Au.03% Fe alloy. In 1956 de Nobel measured the specific heat of a Ag 0.09% Mn alloy, and found a very large excess specific heat at very low temperatures over that of pure Ag. Such specific heat anomalies have since been found to exist in all alloys for which there is a resistance anomaly.

The low temperature anomalies that have just been described, occur in systemsof extreme dilution. For the face centred cubic lattice, an impurity has a 50% chance of having another impurity as one of its nearest neighbour atoms if the concentration is 8%, and this probability decreases as c^2 at lower concentrations. Thus, the influence of direct interactions between impurity atoms which are nearest neighbours is likely to be small if the concentration is less than one or two per-cent, and the alloy may be considered to be dilute in this concentration range. The crystal structure of a dilute alloy will be the same as that of the pure metal.

The solubility of transition metals in other metals is, in some cases, extremely small. This is particularly marked when the

solvents are Cu or Ag, though Mn dissolves easily in both metals. The solubility of the transition metals in Au is very much higher than in Ag or Cu. Concentrations greater than the room temperature equilibrium limit have often been obtained by quenching the alloy from high temperatures. Table 1, using results taken from Hansen[8], shows the solubility limit at room temperature and 700°C for several alloy systems.

Table 1 Solubilities of Transition Metals in the Noble Metals[8]

	Au Cr	Au Mn	Au Fe	Au Co	Au Ni
0°C	23	25	11	0.1	7
700°C	23	30	40	4	37
	Ag Cr	**Ag Mn**	**Ag Fe**	**Ag Co**	**Ag Ni**
0°C	-	14	-	-	-
700°C	-	30	-	-	-
	Cu Cr	**Cu Mn**	**Cu Fe**	**Cu Co**	**Cu Ni**
0°C	-	25	-	-	100
700°C	0.13	70	0.35	1	100

*

1.2 Electrical Resistance

The alloys of first row transition metals in non-transition metals can be classified in their resistive behaviour as follows.

a) Those exhibiting a resistance minimum only. These include Cu Cr, Cu Fe, Mg Fe, Zn Cr, Zn Mn, Cd Mn.

b) Those for which both a resistance minimum and maximum have been observed. These are Au Cr, Au Mn, Au Fe, Ag Mn, Cu Mn and Mg Mn.

c) Ill defined anomalies. Au Co, Cu Co.

d) No anomaly observed. Au Ni, Cu Ni, Au V, Zn Fe, Al Mn, Al Fe.

* Solubilities are expressed in atomic percentages
-, Solubility less than 10^{-3} %

It is often assumed that the resistance minimum is a result of the addition to the resistance of the pure metal, of an anomalous resistivity which decreases monatonically with temperature, and which approaches a constant value at high temperatures. The measurements of Gerritsen[9] and Linde between 1.5 and 300°K of the resistivity of Au Mn, Au Cr, and Cu Mn, and those of Domenicali[10] and Christenson (between 4° and 1200°K) of Cu containing Cr, Mn, Fe, Co, Ni and Au containing Mn, Fe, and Co show, however, that in all cases except Cu Ni and Au Co, the excess resistivity itself (the resistance of the alloy minus that of the pure metal) goes through a low temperature minimum, followed by a broad maximum at temperatures between 60°K and 200°K, the temperature of the maximum increasing only very slowly with concentration. At higher temperatures the resistance continues to decrease slowly up to 1200°K. Similar high temperature maxima have been observed in dilute alloys with non-magnetic impurities, so that it is doubtful if this high temperature hump in the excess resistance has a magnetic origine.

The behaviour of the excess resistance of Cu Fe, which shows a low temperature resistance minimum only, and of Au Fe, which shows a low temperature minimum and maximum, is shown schematically in Fig.1.

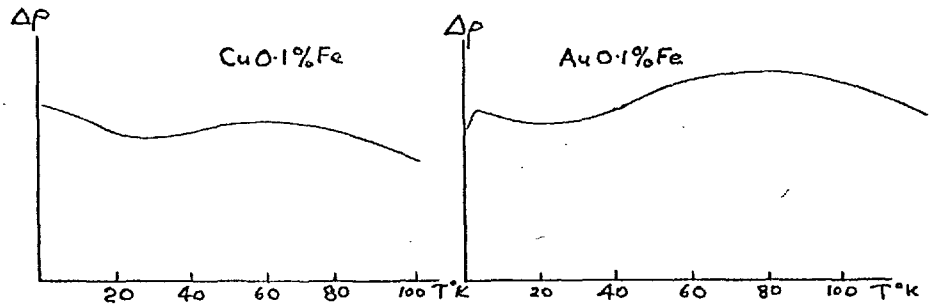

Fig. 1. Schematic behaviour of excess resistance $\Delta\rho$ of Cu Fe and Au Fe

Resistance Minimum

The temperature dependence of the resistance of very dilute gold alloys, which exhibit only a resistance minimum in the temperature range of measurement (the maximum falling at very much lower temperatures), has been measured by several workers. (Croft et al[11] on impure gold wires down to 0.006°K, Dugdale and Macdonald[12] on similar alloys down to 0.1°K, and Macdonald[13] et al on dilute Au Fe alloys containing less than 0.0% Fe down to 0.02°K) and for temperatures well below 4°K, their results are consistant with a relation of the form

$$R(T) = R_{pure}(T) + R_1 - R_2 \log T \quad \ldots\ldots\ldots 1.1$$

where R_1 and R_2 are constants for the alloy.

This relation, which describes the monatonic decrease in the

excess resistance with increasing temperature, breaks down at higher temperatures when the excess resistance starts to increase. Such a relation does not apply to the resistance of Cu Fe, as the R - T curve for this system has a pronounced negative curvature below the temperature of the resistance minimum. White[14], and Dugdale and Macdonald[12] have examined a Cu 0.056% Fe alloy down to 0.05°K and find that the resistance is approximately constant below 1°K.

Knook[15] has found that the depth of the minimum in Cu containing 0.0005 to 0.1% Fe is proportional to the resistance at the minimum, and is about 11% of this resistance. Measurements of Kjekshus and Pearson[16] on Cu Fe containing between 0.0025 and 1% Fe suggest that this relation breaks down at high concentrations, with the depth increasing less rapidly than linearly.

Kjekshus and Pearson have found that Cu Cr has the deepest minimum of any of the systems that have been investigated; it is about 40% of R_{min} - the resistance at the minimum. This may be compared with the value of 11% for Cu Fe and 16% for very dilute Au Fe. ($c < 0.03\%$). R_{min} is however, only 4μΩ c.m. / % for Cu Cr, whilst it is about 8μΩ c.m. / at % for Au Fe and Cu Fe.

The most concentrated Cu Cr alloy investigated by Kjekshus et al contained only about 0.06% Cr (the solubility of this system is extremely small), and no maximum was observed down to 1.5°K. Because of the very low solubility, measurements to lower temperatures are

required to decide whether this system will exhibit a resistance maximum.

Muto[17] has measured the resistance of dilute Zn Mn alloys, and finds that the resistance passes through a minimum at around 20°K, and then becomes constant on cooling below 5°K, without exhibiting a maximum above 1.5°K.

Resistance Maxima

The temperature T_{max} of the resistance maximum observed in the systems Au Cr[9, 13], Au Mn[9, 13], Au Fe[13, 18], Ag Mn[3], Cu Mn[9, 16] and Mg Mn[19] increases approximately linearly with concentration at very low concentrations, being given by T_{max} °K = 31 c for Au Cr, 26 c for Au Mn, 24 c for Au Fe, 27 c for Ag Mn and 30 c for Cu Mn and 10 c for Mg Mn, where c is the concentration. This linear dependence has not been tested for concentrations less than 0.04% for which T_{max} should fall below 1°K, though it would be of considerable interest in determining the range of the interaction between impurities to find whether there is a critical concentration necessary for the existance of the resistance maximum.

The low temperature resistance maximum is very broad, with no sharp change of slope. The measurements of Macdonald on a Au 0.1% Fe alloy, and a Au 0.04% Mn alloy, having maxima at 2.4°K and 1.3°K respectively, show that the resistance is still decreasing rapidly at 0.01°K. From these results, the magnitude of the quantity

$\frac{R_{max} - R(0)}{R_{max}}$, where R(0) is the resistance extrapolated to 0°K, is 2% for the Au Fe alloy, and 6% for the Au Mn alloy.

At higher concentrations T_{max} increases less rapidly with concentration, and the maximum and minimum finally disappear altogether, having presumably merged with the high temperature increase in the excess resistance. This occurs at about 0.25% for the Au Fe system and at about 0.4% for the other systems.

c) and d) Ill Defined and Absent Anomalies

Measurements of the low temperature resistivity of Au Ni[20], Au Co[21], Cu Ni[20] and Cu Co[22, 16] show very shallow minima ($<1\% R_{min}$) whose depth vary in a random manner with the solute concentration. It therefore seems likely that these minima are due to iron or manganese impurities in the alloy and not to the solute. (Their magnitude could be explained by the presence of less than 0.005% Fe). For Cu Co alloys containing 1% and 2% Co, Jacobs and Schmitt[22] have found rather deeper minima, (up to $3\% R_{min}$) which may be due to the Co itself. Domenicali has found that the excess resistivity in Cu Co alloys goes through a broad maximum at around 100°K, similar to that found for the systems exhibiting low temperature maxima and minima. These authors find that the excess resistance of Au 2.1% Co and Au 4.3% Co decreases continuously

as the temperature increases from 4°K to 1000°K, and does not pass through the high temperature maximum found for the other systems. They also find that the excess resistance of Cu Ni increases monatonically over the entire temperature range 4° - 1000°K.

1.3 Magnetic Susceptibility

Because of their comparitively extensive solubility the systems Au Cr, Au Mn, Au Fe, Ag Mn and Cu Mn have been investigated over a wide concentration range.

The susceptibilities of more concentrated alloys of all of these systems have the following features in common.

1) At high temperatures the susceptibility χ can be represented by a Curie-Weiss Law of the form

$$\chi = \chi_o + \frac{C}{T-\theta}$$

where χ_o is the susceptibility of the pure metal.

2) As T is reduced, there is a broad maximum in χ at a Néel Temperature T_n, which increases with the concentration.

3) At temperatures below about $2T_n$, where deviations from the Curie Weiss law become apparent, field dependence of the susceptibility, suggestive of partial magnetic saturation, is observed for fields less than 10 Koe, the effect increasing as the temperature is reduced.

4) At temperatures below T_n, hysteresis and a small remenant magnetisation are observed, the latter increasing as T is reduced , to a few per cent of the saturation moment of the alloy.

If the linear dependence of $\frac{1}{\chi-\chi_o}$ on T at high temperatures is assumed to be due to independent magnetic moments localised on impurity atoms, then the effective magneton number μ of each impurity can be calculated from the Curie constant C. The spin S of the impurity is then given by

$$\mu = g\mu_b \sqrt{S\ (S+1)}$$

if the orbital angular momentum is assumed to be suppressed. μ_b is the Bohr magneton, and g = 2. The Curie temperature θ may be regarded as a measure of an effective high temperature interaction between the magnetic moments, being positive if the interaction is ferromagnetic and negative if it is antiferromagnetic. In the temperature region where the magnetisation is no longer a linear function of the applied field, the susceptibility is a somewhat ambiguous quantity. Some authors quote the zero field susceptibility, and others the susceptibility at high fields, which choice can lead to considerable variation of the temperature of the susceptibility maximum.

In addition to the general features described above, details of the results for particular systems will now be given.

Cu Mn

Author	Temperature Range °K	Concentration%	μ/μ_b	θ °K	T_n °K
Owen et al[23]	4-300	0.029	4.95	0±0.5	-
		1.4	5.05	+7	10-13
		5.6	5.19	+37	30-50
		11.1	4.7	+100	80-120
Van Itterbeek et al[24]	1.2-290	1.40	4.54	-3.4	-
		1.61	4.55	-0.3	-
		2.57	4.45	+8.3	10.6
		4.82	4.35	+20	11.5

(- , a susceptibility maximum was not observed within the temperature range of measurement).

The divergence in the values of μ found by these two authors is probably due in part to errors in the estimations of the Mn concentration. The results indicate that the spin value of Mn in Cu is approximately 2 (corresponding to $\mu = 4.9$) and is independent of the concentration. The considerable differences in sign and magnitude of θ and T_n as found by the two authors suggest that these quantities are particularly susceptible to the distributions of the Mn atoms in the alloy. The general trend of T_n and θ is, however, to increase with concentration.

Schmitt and Jacobs[25] have published magnetisation curves for Cu Mn alloys containing 0.05, 0.2, 0.4, 1.0 and 1.8 % Mn in the temperature range 1.8 to 20°K. Because of the strong field dependence of the magnetisation and the onset of hysteresis at low temperatures, susceptibility values are not quoted.

Ag Mn

Author	Temperature Range°K	Concentration%	μ/μ_b	θ°K	T_n °K
Owen et al[23]	4-300	4.2	5.58	+13	10-20
Van Itterbeek[24] et al	1.2-290	1.24	6.03	-13.7	-
		1.67	5.89	-4.5	-
		3.50	5.74	+11.3	6
		5.10	5.66	+17.6	-
		5.30	5.65	+19	11.4

The spin value of Mn in Ag is therefore close to 5/2 (μ = 5.9). As for the Cu Mn alloys, Van Itterbeek finds a susceptibility maximum above 1.2°K only for those alloys with a positive θ.

Au Mn

Author	Temperature Range°K	Concentration%	μ/μ_b	θ°K	T_n °K
Lutes and[26] Schmit	0.5 - 35	1	5.8	+1.5	4.2
		2	6.6	+2.9	7.0
Gustafsson[27]	300 - 700	.72	5.5		
		2.08	5.8		

The spin value of Mn in Au is therefore close to 5/2.

Lutes and Schmit quote results of measurements by Cohen et al of Au Mn alloys containing 1.8 to 18 % Mn in the temperature range 4-400°K. They find ferromagnetic transitions in alloys containing more than 6% Mn, at temperatures close to the paramagnetic Curie temperature, and given by $T_c = \theta_c$.

Au Cr

Author	Temperature Range°K	Concentration%	μ/μ_b	θ°K	T_n °K
Lutes and[26] Schmit	0.5 - 35	0.5	4.0	-2	6.3
		1.0	3.7	-3	11.5

The susceptibility of these two alloys is found to be almost independent of concentration below 5°K. The spin value of Cr in Au is approximately 3/2.

Well defined antiferromagnetism, with a sharp Neel point, has been found to occur in the concentration range 21-29% Cr.

Au Fe

Author	Temperature Range°K	Concentration%	μ/μ_b	θ°K	T_n °K
Lutes and Schmit[26]	0.5 - 30	0.5	3.6	-3	4
		1.0	3.3	+1	7.4
Kaufmann et al[28]	14 - 300	0.63	3.4	-23	-
		1.3	3.6	-18	-
		2.8	3.7	-6	-
		4.3	4.4	+8	-
		6.6	4.9	+25	-
Henry[29]	4 - 295	5		+23	

Kaufmann did not observe a susceptibility maximum above 14°K for any of the alloys, but found a small remnant magnetisation in the most concentrated alloy at 14°K. The rapidly increasing value of the effective moment with concentration suggests that the true Curie Weiss region may not have been reached at 300°K.

At concentrations above 11%, long range ferromagnetic order exists below a temperature close to the high temperature paramagnetic Curie temperature. This well defined critical temperature increases rapidly with concentration.

Cu Fe

Author	Temperature Range°K	Concentration%	μ/μ_b	θ°K	T_n °K
Bitter et al[30]	14-295	.008	2.0	-16	-
		.065	2.4	-6	-
		.13	3.1	-10	-
		.32	4.1	-4	-
		.56	4.7	-2	-
		.71	6.9	0	-

Measurements made between 100°K and 1300°K indicate a value of $\mu = 4.7$ for all concentrations, whilst θ increases from large negative to large positive values with increasing concentration . Bitter does not find a susceptibility maximum or remenance in any of the alloys above 14°K, though the susceptibility is found to be field dependent at 14°K for all concentrations greater than 0.1% by an amount which is too large to be accounted for by simple paramagnetic saturation, and which suggests that ordering would occur at lower temperatures.

Cu Co

The measurements of Hildebrand[31] on alloys containing between 0.1 and 0.5 % Co between 90° and 300°K, and those of Jacobs and Schmitt[22] on alloys containing 0.5, 1.0, 2.0 % Co between 2°K and 77°K, show that the susceptibility does not obey a Curie-Weiss law at any temperature below 300°K. χ tends to a constant value (approximately $+0.25 \times 10^{-6}$ emu/gm for c = 0.5%) at high temperatures, and increases rapidly on cooling below 100°K. At low temperatures the susceptibility is very field dependent, though the magnetisation curves show no signs of remenance or hysteresis, and is also strongly concentration dependent, increasing more rapidly than c^2.

Au Co

Hildebrand[31], measuring specimens containing between 0.3 and 2% Co in the temperature range 90 - 300°K, and Lutes and Schmit[26] measuring a Au 1% Co alloy between 0.5 and 10°K, have shown that a Curie Weiss law is not applicable to this system, but that the susceptibility tends to a constant value at high temperatures (+ 0.8 x 10^{-6} emu/gm for 1% Co) and increases rapidly on cooling to low temperatures. No remenance was observed by Lutes et al, and the field dependence of the suseptibility was not measured. The behaviour is therefore very similar to that of Cu Co.

Cu Ni

Pugh[32] et al have measured the susceptibility of Cu containing between 0.59 and 2.48% Ni in the temperature range 2.5 to 300°K, and find that the increase in susceptibility over pure copper is independent of temperature and equal to 0.023 x 10^{-6} emu/gm per atomic%, apart from a small paramagnetic increase at low temperatures that could be accounted for by the presence of less than one part per million of iron impurity. The temperature independent increase in χ is therefore very much smaller than that found at high temperatures in Cu Co or Au Co.

Mg Mn and Zn Mn

Author	Temperature Range°K	Concentration%	μ/μ_b	θ°K	T_N °K
Owen et al[23]	4 - 300	Mg 0.67 Mn	3.5	0	-
Collings et al[33]	1.3- 300	Mg 1.34 Mn	4.1	0	-
Collings et al[34]	15- 300	Zn 0.43 Mn	4.8	+12	-

The Mn spin is therefore approximately 3/2 in Mg and 2 in Zn.

Discussion

Curie Weiss behaviour is to be found in all systems exhibiting well defined low temperature resistance anomalies. Susceptibility maxima occur in those systems exhibiting resistance maxima, provided the concentration is sufficiently high.

The situation regarding systems exhibiting a resistance minimum only is still not clear. The only systems of this group to be investigated are Cu Fe and Zn Mn. The measurements on Cu Fe were taken down to 14°K, and no maximum in the susceptibility was observed; this is not surprising as the highest concentration of Fe was only 0.7%, (because of the very low solubility of the system). Similarly, the Zn 0.43 Mn specimen measured by Collings et al is probably too dilute to give a maximum above 1.5°K if the behaviour is similar to that of Cu, Ag or Au containing Mn.

Thus it is not know whether susceptibility maxima occur in systems exhibiting resistance minima only. Nor has it been definitely established that susceptibility maxima occur at very low concentrations in systems exhibiting resistance maxima and minima.

There is little correlation between the temperature T_n of the susceptibility maximum, and the temperature T_{max} of the resistance maximum. This is partly because the concentration of those systems exhibiting susceptibility maxima tend to be so high that the resistance maximum has disappeared ($c > 0.4\%$). However, assuming that T_n and T_{max} vary linearly

with concentration. T_n takes the approximate values of 2c for Ag Mn, 4c for Au Mn, 8c for Au Fe and 12c for Au Cr, whilst T_{max} takes values between (25 and 30) c, for all of these systems.

The rapid variations of μ andθ with temperature, found for some systems suggest that

1) The interaction constant θ may be temperature dependent, or

2) The assumptions involved in the derivation of Curie's law may not be valid, namely that the impurities may be treated as a system of independent magnetic moments in thermal equilibrium and unaffected by the Pauli Exchusion Principle.

In such systems, the value of the effective moment μ calculated from the slope of $1/\chi$ vs.T may be of little significance. This is probably the case for Au Fe and Cu Fe, and is certainly true of Cu Co, Au Co and Cu Ni.

The onset of well defined ferromagnetism at c >11% in the Au Fe system, and at c > 6% in the Au Mn system, and of well defined anti-ferromagnetism in the Au Cr system at high concentrations, is almost certainly due to short range interactions between nearest neighbour impurity atoms. This interaction is presumably ferromagnetic in Au Fe and Au Mn, and anti-ferromagnetic in Au Cr.

1.4 Magnetic Remenance

Magnetic hysteresis, and remenance on removal of the applied field, is observed in all systems which exhibit a susceptibility maximum, and

the results of Lutes and Schmit[26] on Au Cr, Au Mn and Au Fe alloys suggest that it occurs only at temperatures lower than the susceptibility maximum. The remenance has several interesting properties.

1) The application and removal of a magnetic field at a constant temperature produces an isothermal remenance M which increases with the applied field up to some maximum M_s, which is never more than a few per cent of the saturation moment of the alloy. Jacobs and Schmitt[22] have shown that no further increase in the saturation remenance is possible even with the application of fields of up to 140 kg, ten times greater than that just needed to produce M_s.

2) The field H_s needed to produce M_s increases as the temperature is reduced and the concentration is increased, and for Cu Mn, H_s can be approximately calculated from H_s kg = 35 c/T where the concentration c is in %.

3) M_s increases as T is reduced, varying approximately as 1/T at low temperatures, and falling to zero as T approaches the temperature of the susceptibility maximum.

4) At a given temperature M_s can be reversed by the application of a reverse field of about 2 kg, far smaller than the field necessary to create M_s, and can be restored to its original value by the application of a forward field of about 2 kg.

5) M_s can be produced by cooling from higher temperatures in a field which is considerably smaller than H_s. A field which is sufficiently high

to saturate the remenance is applied at a high temperature (this will be smaller than the field required at lower temperatures). On cooling, the remenance remains saturated, and thus increases in magnitude to the value obtained by isothermal saturation at the given low temperature.

6) The remenance decays with time at a rate which increases with the temperature, and is of the order of a few hours at low temperatures.

1.5 Electron Spin Resonance

Measurements of Owen Browne Knight and Kittel[4] on the electron spin resonance of Mn spins in Cu Mn alloys containing 0.5, 1.4, 5.6, and 11.1% Mn, at a few fixed temperatures between 2° and 300°K, show the following behaviour. At high temperatures (77 - 300°K) the line width increases approximately linearly with temperature due to spin lattice interactions, with a relaxation time decreasing from 4×10^{-10} sec at 77°K to 1×10^{-10} sec at 300°K. This is considerably shorter than the spin-lattice relaxation time observed for Mn ions in non-metallic crystals. The electronic Knight shift is very small in this temperature range, and the g-factor is close to 2.00 at all temperatures above the Neel point T_n.

As T is reduced below T_n the resonance line width becomes constant, and the resonance field shifts to lower values, from the free spin value Ho found at high temperatures to a lower field H. The line shift $H_o - H$ increases rapidly as T is reduced, and may become so large that the resonance disappears altogether. The line shift increases with the wavelength, and is approximately three times larger for $\lambda = 3.3$ cm ($H_o = 3250$ gauss) than for $\lambda = 1.3$ cm ($H_o = 8250$ gauss)

The shifts for the two frequencies can be described rather closely by the relation[23]

$$H = (H_o^2 - H_c^2)^{\frac{1}{2}}$$

where the critical field H_c decreases as the temperature increases, and approaches zero as T approaches T_n. H_c does not depend on the frequency.

This behaviour is similar to that found in non-metallic anti-ferromagnets, in which the large shift is caused by small anisotropy fields at right angles to the applied field. The effect for the Cu Mn alloys was found to be isotropic, and is therefore not due to crystal anisotropies. Owen[23] et al show that these large field shifts could be caused by a rather small interaction between the conduction electrons and the Mn spins assuming the existance of long range anti-ferromagnetic ordering of the Mn spins below T_n.

Owen[23] et al also observed an electron spin resonance in Ag containing 2.0 and 4.2% Mn, and a Mg 0.67% Mn alloy, and found a rather small line shift which increased on cooling from 4° to 2°K.

Collings and Hedgecock[33] have measured the spin resonance of a Mg 0.6% Mn alloy which exhibits a resistance maximum at 6.5°K. They find that at high temperatures the g-value is 2.00, but that below the temperature of the resistance maximum the resonance field falls, the field shift increasing rapidly as the temperature decreases.

Collings [23] et al did not detect a resonance in Al 1% Mn, which is consistant with the absence of anomalies in the other properties of Al Mn alloys. They[35] were also unable to detect a resonance in Au 7% Fe at 77°K or 4°, in Cu 4.5% Fe and Cu 0.55% Fe at the same temperatures, and Cu 0.57% Co Cu at 77°K. This is rather surprising as the susceptibility suggests the existance of localised magnetic moments on the transition metal atoms. It is possible that spin-orbit coupling, stronger than for the Mn atoms, (Mn atoms are probably in a state of zero orbital angular momentum, as in the free atom) broadens the resonance so much that it cannot be detected.

1.6 Magnetoresistance

The resistance of a normal metal or alloy generally increases when measured in a magnetic field due to the deflection of the conduction electrons by the magnetic field away from the direction of the electric field, by an amount which depends on the ratio of the mean free path to the radius of curvature of the electrons in the magnetic field. The effect is therefore large when the mean free path is long, and decreases when the resistance increases, due either to thermal or impurity scattering. The increase $\Delta\rho$ due to a field H can be represented by the formula due to Kohler, $\frac{\Delta\rho}{\rho} = f\left(\frac{H}{\rho}\right)$, where ρ is the total resistivity in zero field. The function $f(x)$ is generally a power of x, close to 2 for low fields and decreasing at higher fields.

Marked deviations from Kohler's Law are observed for several of the dilute magnetic alloys, there being a negative contribution to the magneto-resistance which increases as the temperature is reduced. At low enough

temperatures, and sufficiently high concentrations, this may exceed the normal positive contribution, and the total magnetoresistance becomes negative.

It is also found that the negative contribution is isotropic with respect to the relative directions of the magnetic field and the current, in contrast to the normal contribution, which is strongly anisotropic.

Schmitt and Jacobs[25] have made a careful study of the relation between the magnetoresistance and the magnetisation of Cu Mn alloys containing between 0.05 and 1.8% Mn. They find that whilst both the magnetisation and magnetoresistance show hysteresis at high concentrations and low temperatures (below the susceptibility maximum), and the magnetisation shows considerable saturation effects, the magnetoresistance is proportional to the square of the magnetisation. Writing the magnetisation I as a fraction of the saturation moment (assumed to be $4\mu_b$ / Mn atom in Cu), and the magnetoresistance as $\frac{\Delta\rho}{\rho}$, where ρ is the zero field resistance, they find

$$\frac{\Delta\rho}{\rho} = - S\,(T)\, I^2$$

The coefficient S(T), which is close to 1 as T -> o, decreases as the temperature increases. The rate of decrease is greatest for the lowest concentration.

Jacobs and Schmitt[22] have made measurements of the electrical resistance, magnetisation, and magnetoresistance of Cu Co alloys containing 0.5, 1.0 and 2.0% Co, at temperatures down to 1.6°K. They find

that despite strong saturation effects in the magnetisation and megneto-resistance curves as a function of magnetic field, that the negative magneto-resistance can be represented by $\Delta\rho = A M^2$. If M is the magnetisation in emu/gm (it is not possible to determine a relative magnetisation I for this system), and $\Delta\rho$ is expressed in $\mu\Omega$ cm, the constant "A", which is independent of temperature for this system, takes the values, A = 2.1 for c = 0.5, A = 0.87 for c = 1.0 and A = 0.23 for c = 2.0. Thus "A" falls rapidly as the concentration increases, but unlike the Cu Mn system, is independent of temperature.

It is unfortunate that this dependence of the magnetoresistance on I^2 has not been tested for other systems, and to magnetisationsapproaching saturation. This would be of interest at low temperatures as a value of unity for the coefficient S(T) suggests that the resistance should fall to zero if the alloy is completely saturated. Deviations from an I^2 dependence are therefore presumably to be expected before this occurs.

The behaviour of the earlier measurements of Gerritsen et al on the magnetoresistance of Cu Mn^{36}, Ag Mn^{3}, and of Mn^{36}, Cr^{36}, and Fe^{18} in Au, can be understood qualitatively in terms of the relative magnitudes of the normal positive and anomalous negative contributions, assuming that this latter quantity increases with the magnetisation. At very low concentrations the mean free path of the conduction electrons is long, and the positive term dominates. As the concentration increases, the mean free path decreases, the anomalous scattering of the magnetic impurities increases, and the

total magnetoresistance becomes negative. At higher concentrations the magnet resistance passes through a maximum value for a given applied field, and decreases rapidly as the concentration is further increased. This can be understood from the results of Schmitt and Jacobs[25] (that $\frac{\Delta\rho}{\rho}$ is proportional to I^2) if the relative magnetisation increases less rapidly than the concentration. This is consistent with the results of Lutes and Schmit[26] on the susceptibility at low fields of more concentrated alloys of Au Cr, Au Mn and Au Fe. The magnitude of the maximum negative value of the magnetoresistance increases as the temperature is reduced, and at 1.3°K, in a field of 20kg, it takes the value of 11% at c = 0.02 % for Cu Mn, 32% at 0.1% for Au Mn, and 27% at 0.1% for Ag Mn.

The very small negative component found for Au Cr is also understandable in these terms. Gerritsen[36] finds a small negative value of $\frac{\Delta\rho}{\rho}$ (about 2%) only for the most dilute alloy measured, containing 0.03% Cr, and at the lowest temperature measured, 1.7°K. This negative component has almost completely disappeared at 4°K for this alloy, and is also negligable when the concentration has increased to 0.3%. Lutes and Schmit[26] find small negative Curie temperatures, and high Néel temperatures for Au 0.5% Cr and Au 1% Cr, and therefore the susceptibility remains very low compared to that of say Au Mn, which has a positive Curie temperature and a low Néel temperature If this behaviour continues to very low Cr concentrations, the negative contribution to the magnetoresistance in Au Cr may be expected to be very small.

Gerritsen[18] has measured the magnetoresistance of Au Fe alloys containing between 0.02 and 0.24% Fe at 1.3, 4.2, 14.3 and 20.3°K. The behaviour is found to be similar to that of the alloys containing Mn, but the magnitude for a fixed field and temperature is rather smaller. At 1.3°K in a field of 23kg, $\frac{\Delta\rho}{\rho}$ reaches a maximum negative value of 12% for a concentration of 0.08%, and decreases rapidly for larger and smaller concentrations.

In order to investigate the magnetoresistance of systems exhibiting a resistance minimum only, Muto and Hedgecock[37] examined Cu Fe alloys containing between 0.01 and 0.1% Fe, and a Cu 0.007% Mn alloy, at 1.3°K and 4.2°K in fields up to 100kg. They find that all of the Cu Fe alloys have a negative component of magnetoresistance which increases on cooling, and that for those alloys containing more than 0.04% Fe, the total magnetoresistance in negative. The magnitude of the effect is $\frac{\Delta\rho}{\rho}$ = 12% for H = 100kg at 1.3°K, for the Cu 0.1% Fe alloy, and is therefore considerably smaller than the effect for a Au 0.1% Fe alloy. $\frac{\Delta\rho}{\rho}$ is proportional to H^2 for fields below 10kg, but no measurements were made of the magnetisation. At high fields there are signs of saturation, though this is not complete at 100kg. For a fixed field, $\frac{\Delta\rho}{\rho}$ is approximately independent of concentration, but there is only a 20 - 30% increase on cooling from 4.2°K to 1.3°K for any concentration, suggesting that the magnetisation does not increase much in this temperature range.

The Cu 0.007% Mn alloy exhibited only a resistance minimum in the temperature range down to 1.3°K (the maximum might be expected at about 0.2°K). There is a negative contribution to the magnetoresistance which is approximately isotropic, and which saturates completely at high fields.

At 4.2°K, it saturates at about 9% of the residual resistivity, at a field only slightly greater than the saturation field at 1.3°K. The lower saturation value at 4.2°K is consistant with the temperature variation of S(T) found by Schmitt and Jacobs[25], but it is rather surprising that the saturation field is much the same at the two temperatures.

Gerritsen[21] has measured the magnetoresistance of Au Co alloys containing between 0.01 and 0.44% Co, and finds very small negative values in alloys containing more than 0.1% Co at temperatures below 5°K, though only the 0.44% Co alloy has a total magnetoresistance which is negative. The behaviour is therefore probably similar to that of Cu Co, though this is not definitely established. The consistant correlation with the magnetisation in the Cu Co system shows that the negative magnetoresistance in this system is definitely due to the Co atoms, and not to iron impurity.

Los and Gerritsen[20] have measured the magnetoresistance of Cu Ni and Au Ni alloys. The very small negative deviations from Kohler's law that they find in the more concentrated alloys, could certainly be accounted for by iron impurity.

1.7 Mossbauer Effect

The Mossbauer effect provides a valuable method of determining the magnetic field existing at the nucleus of an atom which may decay from an excited state to a ground state with the recoilless emission of a γ-ray. The measurements yield values for the splitting of the nuclear energy levels in the hyperfine field, and from a knowledge of the nuclear magnetic moment,

this field can be calculated.

Unfortunately the technique has only limited application, as Fe^{57} is the only suitable member of the first transition series. It has a large nuclear moment, and emits a 14 kev γ-ray with a half life $\sim 10^{-7}$ secs., and has, therefore, a very small natural line width. Transitions between the four level excited state and the two level ground state give rise to a six line hyperfine spectrum. The lines are spaced at equal intervals by an amount proportional to the hyperfine field. If the hyperfine field varies from one iron nucleus to another, the final γ-ray spectrum will be a superposition of six line spectra of different widths, whose amplitudes are proportional to the number of iron nuclei in the given field. Thus an analysis of the γ spectrum enables the spectrum of hyperfine fields to be determined.

The hyperfine field arises from the interaction of the nucleus with both the conduction electrons, and the bound electrons of the Fe atom, and is proportional to the magnetisation of the atom and of the conduction electrons. As the atomic magnetic moment is continually flipping in the magnetic field in which it finds itself, the hyperfine field is also flipping, and the field which determines the energy of the γ ray is the thermal average of the hyperfine field over a time of the order of 10^{-7} secs., the lifetime of the excited state. Thus the hyperfine field is related to the field seen by the atomic moment, and in principle, it is possible to work back from the γ-spectrum to the spectrum of magnetic fields at the iron atoms.

The technique has been applied to Cu Fe containing between 0.2 and

2.6% Fe by Marshall et al[38, 39] at 290°, 77°, 4.2° and 1.3°K. At high temperatures (77°, 300°K) only a single paramagnetic resonance line is observed. With the 0.2% Fe alloy the line remains unresolved at 1.2°K, but is slightly broader than the line at 4.2°K and 290°K. The 0.5% alloy shows a single line at 4.2°K, approximately twice as broad as that at 290°K. At 1.95°K, the centre of the rather broad peak has split into two, and by 1.2°K four small peaks have appeared, superimposed on an approximately triangular shaped background whose maximum width is around 290kg. The 1.2% Fe alloy shows a broad spectrum at 4.2°K, of width around 250 kg, which at 4.2°K has become resolved into four well defined lines, and two ill defined lines, superimposed on a broad background.

The temperature at which lines first appear can be represented approximately by $T = 6c$, where c is the concentration, though the lines appear gradually, and there is no well defined transition temperature.

These results suggest that for the Cu Fe system, there is an approximately constant probability of finding any value of the internal field between zero and some maximum value.

Several authors have investigated the Au Fe system, and all find that the high temperature paramagnetic line splits into six well resolved lines below some well defined transition temperature Tc. Due to the long periods required to obtain a single spectrum, a study of the spectrum over a continuous range of temperatures has not been possible, but the results on specimens of different concentrations at a few fixed temperatures

suggest that for the Au Fe system the width of the spectrum increases rapidly at temperatures just below Tc, and tends to a constant value on further cooling, suggesting a cooperative increase in the internal field which varies with temperature in a manner similar to a Brillouin Function. The sharpness of the lines at temperatures well below Tc (only about five times the natural line width), and the absence of a paramagnetic line (Less that 1% of the six finger spectrum) suggest that most of the iron atoms are in large fields, and very few in low or zero fields.

Borg, Booth, and Violet[40] have studied the Mossbauer spectra of Au Fe alloys containing 0.84, 1.85, 7.38 and 11.5% Fe at 290°, 80°, 27.3°, 20.4°, 17°, 14°, 4.2° and 2.2°K. For all alloys except the Au 7.3 % Fe they find a splitting $g(T)$ which is either zero (at high temperatures) or large and close to the value for pure iron (at low temperature). For the Au 7.38% Fe alloy they find that at 27.3°K the spectrum is broad but unresolved, with the full spectrum appearing at 20°K and below. They therefore assume that 27°K is just below a cooperative transition temperature for this alloy. They then find the best Brillouin curve to fit the splitting found at different temperatures for each of the alloys, and from this calculate a splitting $g(0)$ at 0°K, and a transition temperature Tc at which the splitting would be zero. As it has not been established that a Brillouin curve is suitable to describe the temperature dependence of the splitting, due to the lack of points near to the transition, the value of Tc should be taken as approximate only. The splittings at 0°K are probably quite reliable, however.

Their results for Tc and g(0) (represented as a fraction of the 0°K splitting in pure Fe) are given below.

C%	0.84	1.85	7.38	10.2	11.5
Tc°K	7±2	12±2	28±1	31±1	35±1
g(0)	0.70	0.73	0.77	0.91	0.81

If it is assumed that the splitting at 0°K is proportional to the magnetic moment of the iron atom, (although because of the unknown contribution to the hyperfine field of the conduction electrons this may not be justified), and that the same constant of proportionality applies to the Fe^{57} nucleus in pure Fe, it can be seen that the magnetic moment of the Fe atom in Au varies between $1.5\mu_b$ for c = 0.84% and $2.0\mu_b$ for c = 10.2%. The trend of this moment with concentration is similar to that found by Kaufmann[28] from the high temperature susceptibility of Au Fe alloys, but the magnitude of the moment calculated from the Mossbauer results is rather lower than those of Kaufmann.

Craig and Steyert[41] have investigated the effect of an external magnetic field on the Mossbauer spectrum of a Au 5% Fe alloy. Measurements in zero field show that the transition temperature is 23±1°K, (the same value as the high temperature Curie temperature found by Henry[29] from the susceptibility of a Au 5% Fe alloy), though it is not made clear from the text whether this value is deduced by extrapolation from low temperature points, or by measurements close to Tc. At 4.2°K they find a hyperfine field equal to 250kg.

Nuclear selection rules forbid the emission of those γ-rays which give the 2nd and 5th lines of the spectrum, in the direction of the magnetic field. Thus in the Mossbauer spectra of ferromagnets, observed along the direction of an applied field which is large compared with the demagnetising field, these lines are found to be suppressed. The above authors have found that the spectrum of Au 5% Fe, observed in a direction parallel to an applied magnetic field of 30kg, is essentially the same as that measured in zero field. There is no obvious change in the relative magnitudes of the six lines of the spectrum though the lines are broadened slightly. They suggest that these results exclude the possibility of ferro- or ferri-magnetic ordering for the system, and deduce that there must be anti-ferromagnetic ordering with the Fe moments pointing in random directions that are only slightly effected by a magnetic field. The broadening is then due to some of the Fe nuclei feeling a slightly larger field, and some a slightly smaller field, as a result of their random orientations with respect to the applied field.

1.8 Thermoelectric Power

The thermopower of a pure metal can be separated into diffusion thermopower, and phonon drag thermopower. Diffusion thermopower, which is due to the reversible changes in thermal energy of the conduction electrons as they move to regions of different temperature in the electrical circuit, is linear in temperature, and may be of either sign depending on the

detailed shape of the Fermi surface. It has a magnitude which is less than $10^{-2}T$ μv / °K, and dominates the thermopower at high temperatures (above 100°K). For Cu, Ag and Au this term is positive, and of the order of $5 \times 10^{-3}T$ μv / °K.

Between 30° and 60°K there is a broad positive peak, whose maximum magnitude is around 1 μv / °K, which is attributed to electron-phonon scattering by Umklapp processes, which tend to scatter the conduction electrons predominantly in a direction opposite to the phonon heat current. This is called the phonon drag effect. This contribution falls off roughly as T^3 below the maximum, and is negligable below 20°K. Below 20°K, the pure metal may be expected to have a thermopower of less than 0.1 μv / °K.

Gold et al[42] showed that only in wires of extreme purity were such low values obtained. Slightly less pure specimens of Cu showed very large negative thermopowers, (between 1 and 10 μv / °K) in the temperature range 2 to 20°K, falling off to zero below 2°K, and, more gradually, above 20°K, the variation in magnitude bearing little relation to the residual resistivity of the wires. He showed that Fe (when in solution) was the impurity responsible for the large thermopower, and that other non-magnetic impurities reduced the effect of the iron by an amount which was in proportion to their relative contributions to the electron scattering, and thus to the residual resistivity. This dependence of the thermopower on the relative magnitudes of the different scattering mechanisms, rather than their actual magnitude, is expressed in the Nordheim-Gorter law.

$$S = \frac{\sum_i \rho_i S_i}{\sum \rho_i} = \frac{\sum_i \rho_i' S_i'}{\rho} \qquad \ldots\ldots\ldots\ldots\ldots\ldots 1.2$$

where S_i and ρ_i are the thermopower and resistivity that would obtain if only the i th scattering mechanism were present. (The conditions necessary for the validity of this relation are discussed by Gold[42]). ρ is the total resistivity, S the total thermopower.

If there are only two scattering machanisms present, S_1, ρ_1 and S_2, ρ_2, this may be written

$$S = \frac{\rho_1 S_1 + \rho_2 S_2}{\rho_1 + \rho_2} = S_1 + \frac{\rho_2}{\rho}(S_2 - S_1) \qquad \ldots\ldots\ldots\ldots 1.3$$

If it is assumed that the intrinsic thermo power of Fe in Cu increases rapidly from zero at T = 0 to a constant value of - 16 $\mu v / {}^{o}K$ above $20^{o}K$, and apply equation 2, the complex behaviour observed for alloys of different iron concentrations can be understood. (The assumption of a constant thermopower above $20^{o}K$ may not be correct, but it is not inconsistant with the limited experimental results).

At low temperatures, below $30^{o}K$, the charactoristic thermopower due to thermal scattering is close to zero, and therefore as the thermal scattering increases, the total thermopower decreases. Thus although the intrinsic thermopower of Fe in Cu saturates at a constant value, the total thermopower will pass through a maximum negative value, and then decrease to zero at

higher temperatures. The temperature of the maximum increases only slowly with Fe concentration because of the very rapid increase in thermal scattering above 20°K and its very small magnitude below that temperature. Variation in the magnitude of the maximum can be explained simply by the presence of other non-magnetic impurities with intrinsic thermopowers close to zero.

The intrinsic thermopower S_T at temperature T of any particular solute, can be found by measuring S for different solute concentrations, and plotting S against $1/\rho$ at constant temperature T. Equation 2 shows that this should be linear (if S_2 and ρ_2, due to all other scattering mechanisms are constant) and gives $S_1 = S_T$ on extrapolating to $1/\rho = 0$. Thus when the solute scattering predominates, the thermopower approaches the intrinsic thermopower of the solute. Gold applied this analysis to Cu containing Ag, Au, Ga, Ge, In, Si, and Sn as solutes, and found that the charactoristic thermopower at 15°K, S_{15}, was close to zero in each case. The large thermopower observed on the addition of small amounts of these substances was therefore probably due to the reduction of iron oxide impurity in the solvent, bringing Fe into solid solution. For Cu Ni they found $S_{15} = -1.2$ μv /°K; for Cu Cr, $S_{15} = 0$; and for Cu Fe containing less than .05% Fe, $S_{15} = -16.2$ μv / °K.

In attempting to make correlations between resistive and thermoelectric behaviour, (as between any other properties) it is essential that the measurements should be made on the same specimens, due to the sensitivity of the properties to heat treatment, cold work, aging etc., and to the difficulty in ascertaining the amount of solute in solution. Kjekshus and Pearson[16] have measured the thermopower of alloys of Cu containing Cr, Mn,

Fe and Co between 0.3° K and 20°K, and the resistivity of the same specimen between 2°K and 30°K.

Their results for Cu Fe containing less than 0.1%Fe are very similar to those of Gold. The S-T curves for concentrations between .0025 and 0.1% are independent of the concentration below 20° K, showing that scattering due to other impurities is negligable. The initial rate of increase of S at very low T is approximately -4.5 μ v/ ° K^2. A plot of S against $1/\rho$ is linear, and extrapolation to $1/\rho = 0$ gives $S_3 = -9\ \mu$ v/° K, and $S_{15} = -16.2\ \mu$v/°K. For concentrations greater than o.1%, the S- T curves are similar in shape to the lower concentration curves, but the initial slope is less rapid, and decreases as the concentration increases. S may reach the same saturation value as for the lower concentrations, but at a higher temperature. A plot of S against $1/\rho$ for c > 0.1% extrapolates to $1/\rho = 0$ to give a value of S close to zero at low temperatures, but which increases slowly as T increases. This suggests that the addition of iron in concentrations greater than 0.1% introduces a scattering of intrinsic thermopower which increases rather slowly with temperature.

The thermopower of Cu Mn alloys containing 0.01% and 0.03% Mn are small and positive below 0.4° K, then decrease at a rate of about 4 μ v/° K^2 to a maximum negative value of around -5 μ v/° K, and are then approximately constant up to 16°K. Higher concentrations, up to 1%, continue to exhibit the positive deviation at very low temperatures. The maximum positive value is approximately +1 μv/°K, and the temperature of the positive maximum increases with the concentration. For concentrations of 0.1%and greater

the negative component increases less rapidly than for lower concentrations, as was found for the Cu Fe system.

The S-T curves for Cu Cr alloys containing between 0.005 and .06% Cr are rather ambiguous. Two alloys, containing .005 and .012% Cr, show large negative thermopowers, approaching -6 μv/ °K. Alloys containing .016% and .03% Cr show a much smaller thermopower of about -1 μv/ °K, and an alloy containing 0.06% Cr has a thermopower which is close to zero. As the large negative thermopower can be explained by the presence of less than 0.003% Fe impurity, it seems very likely that the intrinsic thermopower of Cr in Cu is close to zero.

The S-T curves for Cu Co containing between 0.01 and 0.5% Co suggest that the intrinsic thermopower of Cu Co increases approximately linearly with temperature up to 16°K, with $S = -0.3T$ μv/ °K, independent of the Co concentration. There is no tendency for a reduction in the thermopower for higher concentrations, as was found for Cu Fe or Cu Mn, though the rate of increase in Cu Co is less than for the other systems.

Macdonald, Pearson and Templeton have measured the thermopower and resistivity of alloys of Au containing Cr, Mn, Fe, Co and Ni, though unfortunately the two properties were not measured on the same specimens.

The behaviour of the Au Fe alloys is similar to that of Cu Fe, though the initial increase is much more rapid, and saturation takes place at a lower temperature for Au Fe. For concentrations less than 0.05%, S is approximately independent of the concentration, and increases initially at

around -20 μv/ °K², reaching -10 μv/ °K at 1 °K and saturates at a value of around -15 μv/ °K above 6°K. There is then a broad, flat, maximum, followed by a decrease at higher temperatures which can be accounted for by the increasing thermal scattering. For concentrations greater than 0.05%, the initial rate of increase falls rapidly with increasing concentration, though the final saturation value may be the same as for the lower concentrations.

The S- T curves for Au Mn are similar to those for Cu Mn except that the initial increase is much more rapid when Au is the solute (about -12 μv/°K²). The small positive peak observed for Cu Mn is found in this system also, though the temperature of the peak occurs at lower temperatures in Au Mn. The Nordheim-Gorter plot suggests a value of S_s of about -4 μv/ °K for c < 0.04%, and about zero for c>> 0.04%.

Au Cr exhibits a negative thermopower which decreases rapidly with Cr concentration, and it is not possible to decide whether this is due to Fe impurity, or to the Cr. If it is not due to Fe, Cr in Au would appear to have an intrinsic thermopower at 8°K of -2μv/ °K for c < 0.2%, and zero or slightly positive for c > 1%. The Au 1% Cr alloy exhibits a very small positive thermopower (less than 0.1 μv/ °K) and the Au 3.7% Cr alloy has a rather larger positive peak which falls to zero at about 4°K. The S-T curves of Au Co containing between 0.002% and 2.1% Co are independent of concentration and linear in temperature at low temperatures, with an intrinsic thermopower given by S = -0.9T μv/ °K. When thermal scattering becomes important, the thermopower falls away from the linear curve.

Macdonald et al[13] have measured the thermopower of Au 0.2% Ni; up to 16°K, and Borelius[43] has measured Au Ni alloys containing 0.04, 0.18, and 1.16% Ni above 16°K. As the thermopower increases slightly with increasing Ni concentration, it seems likely that the intrinsic thermopower of Ni in Au at 16°K is -4 μv/°K.

Summary

It is apparent that the behaviour of the thermopower due to a particular transition metal solute is basically the same in either Cu or Au, although the rate of increase of the thermopower with temperature at low temperatures is generally three to four times larger with gold than copper. Thus Fe has a saturation thermopower of -16μv /°K in either solvent, Mn has a small positive peak (rather less than +1 μv/ °K) at very low temperatures followed by a maximum negative thermopower at higher temperatures of about -4 μv/ °K. In all these systems, the presence of more than about 0.1% of the solute reduces the thermopower considerably.

Co shows essentially the same behaviour in Au and Cu, giving a thermopower linear in T, and increasing much more slowly than for the Mn or Fe alloys, but showing no signs of saturation. It is also not reduced by the presence of large concentrations of solute. Ni also seems to have a negative intrinsic thermopower, which does not fall at high concentrations, being about -1 μv/ °K in Cu and -4 μv/°K in Au.

The situation for Cr is not quite clear, but it would appear that the

intrinsic thermopower is close to zero in Cu Cr, and slightly positive for Au Cr at moderate concentrations.

The small positive thermopowers found for Cu Mn and Au Mn at very low temperatures are particularly interesting, and may indicate a scattering mechanism which gives an intrinsic thermopower which changes from positive, at very low temperatures, to negative at rather higher temperatures. An alternative analysis is possible however. Two scattering machanisms may be present at all temperatures. One has a negative intrinsic thermopower which rises to a maximum value of $-5\ \mu v/^{\circ}K$ at above $4^{\circ}K$, and one has a positive thermopower which increases more rapidly, but saturates at a lower temperature than the negative one, saturating at a constant value of around $+\ 1\mu v/^{\circ}K$, above $2^{\circ}K$. The resultant of these two mechanisms would give the S-T curves observed.

There are no simple correlations to be found between the thermopower and the resistance anomalies. Thus large thermopowers are found for Cu Fe and Au Fe, the former having a resistance minimum only, the latter a minimum and a maximum. They are also found in Cu Co and Au Co which exhibit neither a minimum nor maximum. They are not found in Cu Cr, which has the largest resistance minimum of any alloy, and are small in Au Cr which has a maximum and minimum. They are also found in Cu Ni and Au Ni, for which there are neither resistance nor magnetic anomalies. The tempting association of the small positive thermopower observed for Cu Mn, Au Mn and possibly Au Cr, with the resistance maximum found in those systems, is refuted by its

absence in Au Fe which also exhibits a resistance maximum.

It is however, possible to correlate the concentration of Fe or Mn above which the intrinsic thermopower decreases, with the ratio of the depth of the resistance minimum to the resistivity at the minimum. It was noted in the section on resistance anomalies that this ratio was independent of the concentration at low concentrations, but falls rapidly at higher concentrations. The concentration at which this deviation takes place is also the concentration above which the thermopower falls. This may suggest either that the machanism which produces the resistance minimum also produces the thermopower anomaly, (in which case it is hard to account for the large thermopowers in Cu and Au containing Co or Ni,) or that the mechanism which is responsible for the breakdown in the linear relationship between the depth of the minimum and the resistivity at the minimum is also responsible for the reduction in the thermopower.

It should finally be mentioned that although it was suggested initially that the intrinsic thermopower of Cu or Au containing Fe (or Mn) saturates to a constant value, and that the high temperature decrease is entirely due to thermal scattering, this has not been definitely established, although it is clearly of the greatest importance in testing the predictions of any theory of the thermopower that the high temperature behaviour of the intrinsic thermopower should be established.

1.9 Dilute Transition Metal - Transition Metal Alloys

Susceptibility

Matthias et al[44] and Clogston et al[45] have measured the susceptibility of second row transition metals containing 1% Fe between 1.4°K and 300°K in a field of 14kg. They obtained a continuous variation in the electron per atom ratio of the solvent by choosing suitable binary alloys of consecutive second row transition elements. (Because of the difficulty of working with Tc, the Third Row Transition Element Re was used to produce alloys in the electron per atom ($\frac{e}{a}$) range 6 to 8). Their results are summarised in Fig. 2 (a).

Zr, and Nb rich NbMo alloys (all containing 1% Fe) exhibit a temperature independent susceptibility, showing that there is no localised moment associated with the Fe atoms.

With Nb Mo solvents containing more than 50% Mo, Curie Weiss behaviour is observed, and the effective moment per Fe atom is shown in Fig 2(a). The moment reaches a maximum value of $2.1\mu_b$ at $Mo_{0.6}$ $Re_{0.4}$ (equivalent to a spin of 0.7) and is zero at Re. It reappears at $Ru_{.75}$ $Rh_{.25}$, and increases to the very large value of $10.8\mu_b$ at $Rh_{.05}$ $Pd_{.95}$.

Several interesting features of these results should be noticed.

1) There is no localised moment on the Fe atom for solvents close to Ru, that is, when the perturbation of the lattice by the Fe impurity is smallest. (Fe lies directly above Ru in the periodic table).

2) The increase in magnitude of the moment as $\frac{e}{a}$ increases from

fig 2

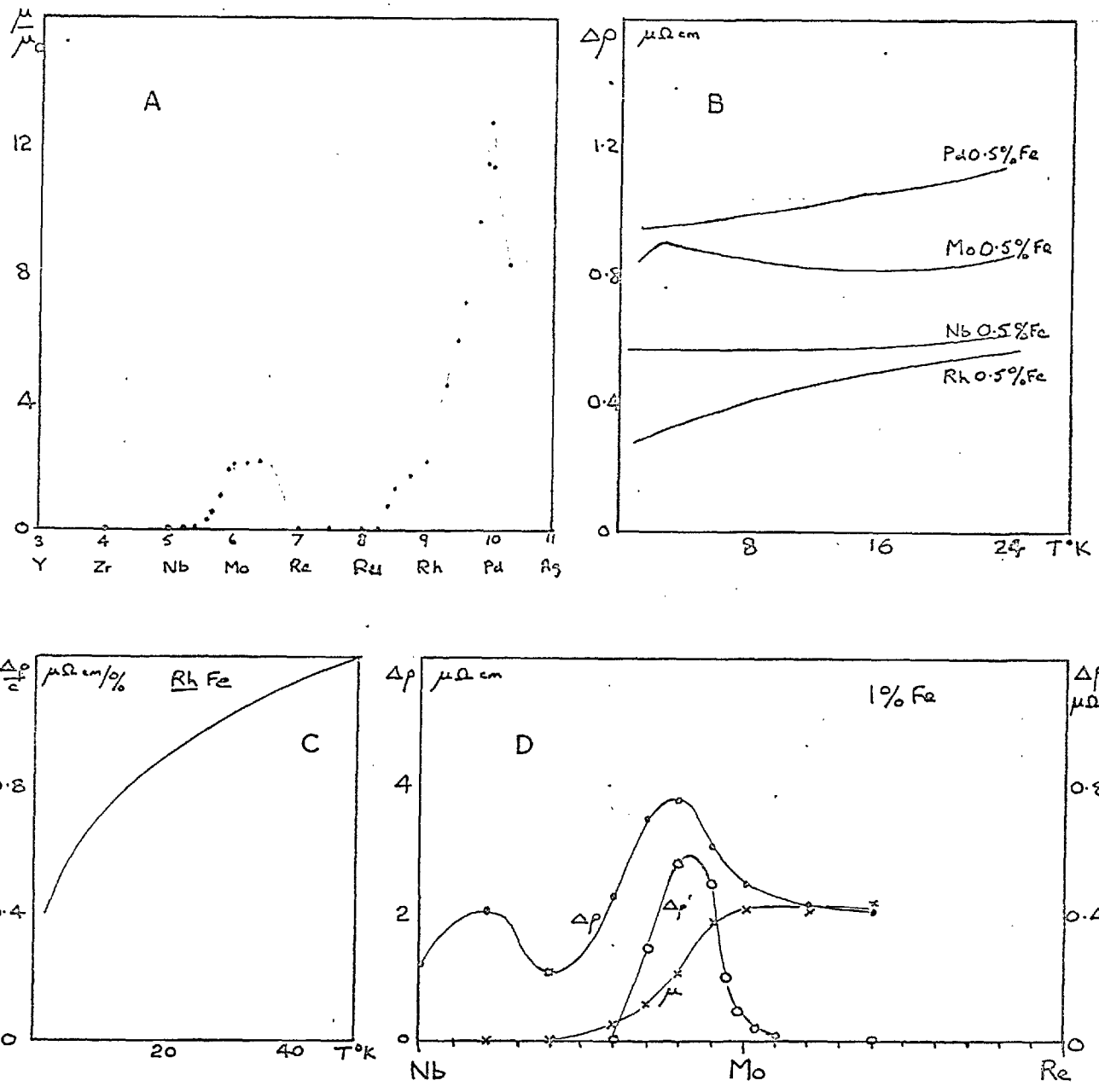
A
12
8
4
0
3 4 5 6 7 8 9 10 11
Y Zr Nb Mo Re Ru Rh Pd Ag
B
μΩ cm
1·2
0·8
0·4
0
Pd 0·5% Fe
Mo 0·5% Fe
Nb 0·5% Fe
Rh 0·5% Fe
8 16 24 T°K
C
μΩ cm/%
Rh Fe
0·8
0·4
0
20 40 T°K
D
μΩ cm
1% Fe
4
2
0
0·8
0·4
0
Δρ
Δρ'
μ
Nb Mo Re

5.5 to 6 (Nb Mo series), and between 8.3 and 9 (Ru Rh series) is extremely rapid, as is its disappearance as $\frac{e}{a}$ increases from 6.5 to 7.

3) The magnitude of the moment per Fe atom, when dissolved in V Ru alloys having $\frac{e}{a}$ values between 6 and 6.5, is similar to the magnitude found in Mo Re solvents of the same $\frac{e}{a}$ values, even though the Fe moment is zero in both pure V and Ru.

4) No susceptibility maxima were observed.

5) The $Rh_{0.2}$ $Pd_{0.8}$ alloy containing 1% Fe was found to become ferromagnetic at 11°K. The transition temperature increases as the Pd concentration increases and reaches a maximum value of 39°K in the Pd 1% Fe alloy. This value is consistant with earlier measurements of Gerstenberg[46], and Crangle[47], and it appears that arbitrarily small amounts of Fe (or Co) are capable of inducing ferromagnetism in Pd, with a transition temperature of approximately 40°K / %Fe. The very large moment per Fe atom associated with the RhPd Fe alloys is due to the polarisation of the Pd atoms in the neighbourhood of the Fe impurity atom. The magnetic moment per Fe atom is then the sum of the moment on the Fe atom itself, and the induced moment on the Pd atoms. Neutron diffraction studies of Low[48] on Pd Fe alloys show that the polarisation is significant on Pd atoms which are as far as 10 Å from the Fe impurity, and thus more than one hundred nearest Pd atoms are effected.

Waszink[49] has measured the susceptibility of a Rh 0.85% Fe alloy between 1.7°K and 295°K. χ was found to be field independent at all temperatures

but the results could not be fitted to a simple Curie Weiss law over the entire temperature range. The high temperature results ($T > 100^{\circ}K$) suggest a value of $\mu = 3.4$ and $\theta = -41^{\circ}K$. (Clogston et al found $\mu = 2.2$ and $\theta = -14^{\circ}K$). At low temperatures χ increases more rapidly than a simple extrapolation, based on these high temperature values, would suggest.

Resistivity

Coles has measured the electrical resistivity of Nb^{50}, Mo^{50}, Rh^{51} and Pd^{52} containing small amounts of Fe, above $1.8^{\circ}K$. The behaviour of the resistance at low temperatures is different in each of these systems, and is shown in Fig 2b for a fixed concentration of iron (0.5%).

No low temperature anomalies are observed in Nb Fe alloys, consistant with the absence of a localised moment on the iron atom.

In Mo Fe, resistance minima and maxima are observed which are similar to those found in noble metal - transition metal alloys. The temperature of the maximum increases with concentration, and is given approximately by $6c^{\circ}K$. This may be compared with the value of 24c for Au Fe and 10c for Mg Mn.

In Rh Fe, the behaviour of the resistance is quite different from that found in any other system. The variation with temperature of the excess resistance per atomic % Fe, $\frac{\Delta\rho}{c}$, is shown in Fig 2c, and it is seen to increase by a factor three between $1^{\circ}K$ and $50^{\circ}K$. The resistance is still decreasing rapidly at $0.4^{\circ}K$. The curve $\frac{\Delta\rho}{c}$ is seen to be independent of concentration, for concentrations between 0.1 and 0.85%. The magnitude of

the decrease between 1°K and 50°K is approximately 0.9 μΩ cm/%, which is comparable with the increase in resistance below the minimum in Cu Fe and very dilute Au Fe of 0.9 μΩ cm/% and 0.5 μΩ cm /% respectively. The fraction $\frac{\Delta\rho}{\rho(0°K)}$ is very much larger, however, for the Rh Fe alloy.

Measurements on a series of Pd Fe specimens containing between 0.1 and 0.5% Fe show that the excess resistance decreases rapidly below some well defined transition temperature Tc, and is constant above Tc.

Thus in this system there is no resistance minimum, and there is a sharp kink in the resistance at Tc, rather than the broad maximum found in Cu Mn and Mo Fe. Tc increases rather more rapidly than the concentration, and is 3°K for Pd 0.2% Fe, and 15°K for Pd 0.5% Fe. It is therefore slightly lower than the transition temperature for ferromagnetic ordering found by magnetic measurements.

Sarachik[53] et al have measured the resistivity of a series of Nb Mo and Mo Re alloys containing 1% Fe. They find that a shallow minimum first appears at $Nb_{0.5}\ Mo_{0.5}$ (where a localised moment first appears on the Fe atoms), and increases in depth with increasing Mo concentration. It reaches a maximum depth (10% of R_{min}) for $Nb_{.15}\ Mo_{.85}$, then decreases, and is zero at $Mo_{.6}\ Re_{.4}$. A resistance maximum first appears at $Nb_{.05}\ Mo_{.95}$, and is observed for all alloys up to $Mo_{.6}Re_{.4}$; The variation of the residual resistivity $\Delta\rho$ (measured at room temperature[54]), and the depth of the minimum $\Delta\rho$, are plotted against e/a in fig 2d. The variation of μ is also plotted for comparison.

Sarachik[55] has also measured the resistivity of a series of $Nb_{0.2}$ $Mo_{0.8}$ alloys containing between 0.2 and 2.27% Fe. (This solvent composition exhibited the deepest minimum in the Nb-Mo-Re system). The quantity $\frac{\Delta\rho'}{\Delta\rho}$ has the value of 10%, independent of concentration, up to 0.78% Fe. At higher concentrations the relative depth of the minimum decreases. No maximum is observed, however, even for the highest concentration, 2.27%. It is found that the resistance has the logarithmic temperature dependence expressed in eq.. 1.1 over quite a wide temperature range, though it breaks down at a low temperature which increases with concentration.

Magnetoresistance

Sarachik[55] also presents values for the magnetoresistance, and magnetisation of the $Nb_{0.2}$ $Mo_{0.8}$ alloys containing varying quantities of Fe, and finds that the magnetoresistance is negative, isotropic, and proportional to the square of the magnetisation for all alloys. The magnetisation is proportional to H^x, where x approaches 2 only for infinite dilution.

Coles[50, 56] has measured the magnetoresistance of Mo 0.65% Fe and Mo 1% Fe, and found it to be negative, and proportional to H^2 at low fields. He has also measured the magnetoresistance of Rh 0.5% Fe, down to 1.4°K, and finds it to be positive. The change in magnitude between 4.2°K and 2°K can be well described by Kohler's Law.

Thermopower

Coles[51] has measured the thermopower of a Rh 0.5% Fe alloy, and finds that it is anomalously large, and increases continuously with decreasing

temperature, reaching a value of 4.6 $\mu v/^{\circ}K$ at $1.5^{\circ}K$.

Specific Heat

Specific heat measurements on a Rh 0.5% Fe alloy and a Pd 0.19% Fe alloy are presented in Chapter 6 of this thesis and are discussed in detail in Chapter 7. A large excess specific heat at low temperatures is observed in both of these systems, though the specific heat falls off more rapidly in the Pd Fe alloy at high temperatures than is found in the Rh Fe alloy or in noble metal - transition metal alloys. Rayne[56] has measured the specific heat of a series of Pd Fe alloys containing between 0.1 and 0.7% Fe, and from the excess entropy determines a spin value of approximately 1.1.

Hake[57] et al have shown that Mn has a localised moment of $3.5\mu_b$ when dissolved in the first row transition element Ti. Definite Curie Weiss behaviour is not observed for Fe, Cr or Co in Ti. They find resistance minima in Ti Mn alloys, and also in Ti Fe and Ti Cr alloys, which is not consistant with the absence of a localised moment on the impurity atom in these latter systems. Resistance maxima were not observed in Ti Mn alloys above $2^{\circ}K$, even for concentrations as high as 2% Mn.

Their specific heat measurements on a series of Ti Mn alloys containin 0.17, 0.36, 0.85% Mn reveal low temperature anomalies very similar to those observed in Cu, Ag or Au containing Mn, (see Chapter 2) the maximum in $\frac{\Delta C}{T}$ occuring at $1.3^{\circ}K$ for the Ti 0.85% Mn specimen.

CHAPTER 2

THE SPECIFIC HEAT OF DILUTE ALLOYS- A BASIC THEORY

2.1 Introduction

The specific heat of a body is defined as the limit as $\Delta T \to 0$ of $\frac{\Delta Q}{\Delta T}$ where ΔT is the temperature increase when an amount of heat ΔQ is supplied to the body. If no external work is done in the process, ΔQ is the increase in internal energy. The specific heat is usually defined with certain parameters held constant, e.g. pressure p, volume v, or magnetic field H. The specific heat measurements to be described in the following pages have been performed under vacuum, and are therefore at constant pressure - C_p, whereas in calculations of the specific heat the volume is generally assumed constant, giving C_v. C_p will in general be larger than C_v because of the dependence of the internal energy on the volume, and because of the work done in expanding against the external pressure (this latter contribution is negligible for a solid body). The difference can be estimated using the thermodynamical identity,

$$C_p - C_v = T V \beta^2 k \qquad \ldots\ldots\ldots\ldots\ldots\ldots\ldots\ldots 2.1$$

where β is the expansion coefficient and k is the compressibility.

It is found experimentally that β is approximately proportional to C_v, and can be written as $\beta = \frac{S C_v}{V}$ where S is a constant and k is nearly

independent of temperature. Therefore,

$$\frac{C_p - C_v}{C_v} = \frac{TV\beta^2}{k\,C_v} = \frac{T\beta\,S}{k} \qquad \ldots\ldots\ldots 2.2$$

For Cu this fraction has the value 2.8% at 300°K, 0.1% at 50°K, and falls rapidly at lower temperatures, and is therefore negligible in the temperature range of interest. The measured values of C_p will therefore be compared with the calculated C_v without correction.

2.2 The Specific Heat of a Pure Metal

Contributions to the specific heat of a pure metal are to be expected from the nuclei, the core electrons and the conduction electrons. Because of the large energy separation of the core levels, electrons in these states contribute a negligible amount to the specific heat. The allowed vibrational energy levels of the atom cores, and the energy states of the conduction electrons lie so close together, however, that significant changes in the energy distribution of these particles take place when the temperature is altered, leading to the observed specific heat.

It is generally assumed that the electrons and lattice contributions may be calculated independently though this is at first sight surprising for the following reasons.

1) The restoring forces acting on the atom cores are in part dependent

on the nature of the electronic wave functions between the nuclei. These restoring forces determine the vibrational modes of the cores, and thus the lattice specific heat. This might therefore be expected to be affected by changes in the conduction electron distribution with change in temperature. Because of the high degeneracy temperature of the conduction electrons, however, their energy distribution is very little affected by changes in temperature in the range 0-20°K in which we are interested, so that the elastic constants are scarcely affected.

2) The conduction electrons move in the oscillating field of the vibrating cores, and the temperature dependent amplitude of these vibrations may be expected to affect the distribution of energy states occupied by the electrons, and thus their specific heat. However, because of the large zero point motion of the cores, their amplitude of vibration is very little affectedby changes of temperature, for temperatures small compared with the Debye temperature (to be discussed below), and thus the electronic specific heat will not be affected.

It is therefore permissable to treat the lattice and conduction electrons as two independent systems in thermal equilibrium, and their separate contributions will be discussed in the following sections.

2.3 Lattice Specific Heat

Atom cores, placed at regularly spaced sites in the crystal lattice, vibrate under the influence of approximately harmonic forces. Classically

they can be considered to be a set of simple harmonic oscillators, and their energy E at any temperature T can be calculated by applying Maxwell Boltzman Statistics, this being justified by the localisation of atoms on definite lattice sites, leading to the theoretical possibility of distinguishing between them.

It can be shown that the specific heat of N_o simple harmonic oscillators where N_o is Avogadro's number is,

$$C = 3 N_o k = 3R = 24.9 \text{ joules/mole}^\circ k,$$

and this is therefore the specific heat of 1 mole of a crystal of atom cores on a classical model. Experimentally it is found that the constant value of 3R is approximately true only at high temperatures. As the temperature is reduced the specific heat falls rapidly and tends to zero as T approaches zero. This failure of the classical theory at low temperatures can be traced to the assumption of a continuous spectrum of available energy states extending to zero energy. When a spectrum of discrete energy levels is assumed, and the temperature is such that kT is small compared with the energy difference ε between the ground state and the first excited state, the specific heat falls to zero as $1/T^2 e^{-\varepsilon/kT}$. The temperature dependence of the specific heat of any particular system can then be calculated by a suitable choice of the distribution of discrete energy levels.

As a first approximation Einstein suggested that the crystal lattice might be considered to be equivalent to a set of simple harmonic oscillators each of constant frequency ν, whose energies are quantised with the values

$$E = n h \nu + \tfrac{1}{2} h \nu$$

where $\frac{1}{2}h\nu$ is the ground state or zero point energy of each oscillator. Applying Maxwell Boltzman Statistics to determine the distribution of the particles among the various energy levels, the total energy of N_o oscillators is

$$\frac{3 N_o h\nu}{e^{h\nu/kT} - 1} + 3/2 N_o h\nu$$

and the specific heat is

$$3R \left(\frac{h\nu}{kT}\right)^2 \frac{e^{h\nu/kT}}{(e^{h\nu/kT} - 1)^2} \quad \ldots\ldots\ldots\ldots\ldots 2.3$$

This function tends to 3R, the classical value, at high temperatures, and at intermediate temperatures reasonable agreement with experiment can be obtained by an appropriate choice of the frequency ν. In the low temperature limit the formula predicts that

$$C = 3R \left(\frac{h\nu}{kT}\right)^2 e^{-h\nu/kT}$$

which is in disagreement with the experimentally observed T^3 dependence for the lattice specific heat as T tends to zero.

A better approximation to the vibrational spectrum of the crystal lattice was obtained by Debye, who treated the crystal lattice as a homogeneous elastic solid, and considered the energy to be distributed among the normal modes of vibration of the system up to some maximum frequency ν_D. ν_D is determined by the condition that the maximum number of independent vibrational modes is 3N, where N is the number of atoms in the crystal. The finite energy spacing of the vibrational modes of a finite elastic medium, which is a result of the requirement that each mode should contain an integral number of half wave-lengths to satisfy the boundary conditions, ensures that the specific heat will fall below the classical value of 3R at low temperatures and tend to zero at T=0. The approximation that the body is homogeneous will be reasonable at very low temperatures, where the atoms move coherently with wave-lengths which are long compared with the interatomic distance. Such modes have a low frequency and correspondingly low energy, and are the only ones to be excited significantly at low temperatures. The existance of these discrete long wave-length modes, with energies which extend nearly to zero, ensures that the specific heat need notfall to zero exponentially as in the Einstein theory.

If there are $g(\nu)\, d\nu$ modes in the frequency range $\nu \rightarrow \nu + d\nu$, they will give a contribution to the specific heat of

$$k \left(\frac{h\nu}{kT}\right)^2 \frac{e^{h\nu/kT}}{(e^{h\nu/kT}-1)^2} g(\nu)d\nu$$

The total specific heat is therefore

$$\int_0^{\nu_m} k \left(\frac{h\nu}{kT}\right)^2 \frac{e^{h\nu/kt}}{(e^{h\nu/kT}-1)^2} g(\nu)\, d\nu \quad \ldots\ldots\ldots 2.4$$

where ν_m is given on the Debye model by the condition that the number of independent modes is 3N, thus

$$3N = \int_0^{\nu_m} g(\nu)\, d\nu \quad \ldots\ldots\ldots 2.5$$

Assuming periodic boundary conditions, and remembering that for each frequency there are three independent waves, one longitudinal and two perpendicular transverse waves, it is easily shown that the number of modes between ν and $\nu + d\nu$ for a homogeneous solid is

$$g(\nu)\, d\nu = V \left(\frac{1}{C_\ell^3} + \frac{2}{C_t^3}\right) 4\pi\nu^2\, d\nu \quad \ldots\ldots\ldots 2.6$$

where V is the volume and C_ℓ and C_t are independent of ν (this is true for low ν, but does not hold as $\nu \to \nu_m$) e.g. Eq 2.5 may be written

$$\int_0^{\nu_m} g(\nu)\, d\nu = 3N = \int_0^{\nu_m} V \left(\frac{1}{C_\ell^3} + \frac{2}{C_t^3}\right) 4\pi\nu^2\, d\nu \quad \ldots\ldots 2.7$$

$$\therefore \quad \nu_m^3 = \frac{9N}{4\pi V} \quad \frac{1}{(1/C_\ell^3 + 2/C_t^3)} \qquad \ldots\ldots\ldots\ldots 2.8$$

and from 2.6 and 2.7

$$g(\nu) = 9N \frac{\nu^2}{\nu_m^3} \qquad \nu < \nu_m$$

$$= 0 \qquad \nu > \nu_m \qquad \ldots\ldots\ldots\ldots 2.9$$

This simple form for the density of states of the vibration spectrum is the central result of the Debye theory, and is a result of the assumption of a homogeneous and non-dispersive medium. The specific heat per mole then follows immediately

$$Cv = 9R \left(\frac{T}{\theta_D}\right)^3 \int_0^{x_m} \frac{e^x \; x^4}{(e^x - 1)^2} \, dx \qquad \ldots\ldots 2.10$$

where $x = \frac{h\nu}{kT}$ $\qquad$ $x_m = \frac{h\nu_m}{kT}$

$$\theta_D = \frac{h\nu_m}{k} = \frac{h}{k} \frac{1}{(1/C_\ell^3 + \frac{2}{C_t^3})^{\frac{1}{3}}} \left(\frac{9N}{4V}\right)^{\frac{1}{3}}$$

If $kT \ll h\nu_m$, $x_m \to \infty$ and the integral takes the value $\frac{4\pi^4}{15}$ so that

$$C_v = \frac{12\pi^4}{5} R \left(\frac{T}{\theta}\right)^3 = 1944 \left(\frac{T}{\theta}\right)^3 \text{ joules/mole as } T \to 0 \quad . \quad . \quad 2.11$$

thus giving the temperature dependence observed experimentally. It should be noted that the T^3 dependence at low temperatures is a result of the parabolic density of states function at low frequencies, and this is expected for any three dimensional crystal at sufficiently low frequencies and is not peculiar to the model discussed above.

On the Debye model, deviations from a simple T^3 law exceed 1% at above $\theta/15$, with the specific heat increasing less rapidly than T^3 as T increases. Deviations are usually found at temperatures much lower than this, however, as the parabolic density of states curve is true only in the low frequency limit. The ability of the Debye function to generate the experimental results may be represented numerically in the following way. The electronic contribution to the specific heat is subtracted from the total specific heat, to give the lattice specific heat at each temperature, and from this a value of θ appropriate to that temperature may be computed. If θ is independent of temperature, the simple Debye model describes the results exactly. It is commonly found that θ is constant at very low temperatures, below, say $\theta/30$, then falls as T increases, passes through a minimum at around $\theta/10$ and tends to a constant value at higher temperatures. The fall in θ and subsequent minimum are associated with a

peak in the density of states curve at frequencies well below the value ν_m calculated on the Debye model. More refined calculations of the density of states curves based on more realistic assumptions than those of Debye, namely a discrete lattice with its associated anisotropies in the force constants, and frequency dependent wave velocities, predict the existence of several peaks in the density of states curve.

In a review article, Blackman[58] discusses the background and developments in this study, and recent calculations include those of Leighton[59] on the f.c.c. lattice including Cu, Ag and Au, Neighbours and Alers[60] on Au and De Launay[61] on Cu, Ag and Au.

2.4 Electronic Specific Heat

Each electron moves in the coulomb field of the other conduction electrons and the atom cores. Because of the long range of the coulomb field, strong correlations between the motions of the electrons are to be expected. Bohm and Pines have shown that as a result each electron is surrounded by a local deficet of electrons or 'correlation hole', and the motion of the resulting quasi-particle is almost independent of that of other similar quasi-particles, interacting with them only by a short range potential of the form

$$V(r) = e^2/r \; e^{-r/\lambda}$$

where λ is a constant of the order of 1Å.

One may therefore consider the allowed energy states of these almost independent quasi-particles in the field of the atom cores.

The very rapid variations in potential in the neighbourhood of the ion cores might be expected to influence the allowed energy states of the electron very profoundly. The requirement that the conduction electron states be orthogonal to the occupied core states leads to a rapid increase in the kinetic energy of the conduction electrons in the region of the core. This may be considered to be equivalent to a reduction in the effective potential energy of the core and leads to the concept of the 'pseudo-potential' introduced by Phillips and Kleinman and by Heine, which is very much smaller in magnitude than the actual core potential. It thus becomes a reasonable approximation to think of the electrons as independent particles moving in a uniform potential, with the remaining influence of the cores included by giving the electrons an effective mass m^+. A density of states function $g(E)\,dE$, giving the number of allowed one electron states between energy E and E + dE, may be calculated.

The property that electrons are indistinguishable and obey the Pauli Exclusion principle dictates the use of Fermi Dirac statistics in deciding the distribution of electrons among the allowed energy states at any given temperature. This leads to the result that at T=0, electrons have energies up to the Fermi energy E_F, which for metals is generally several electron volts. For temperatures low compared to the degeneracy temperature $\frac{E_F}{k}$,

which is of the order of 10^5 °K for Cu, only a small number of electrons with the highest kinetic energies can be excited into unoccupied states, and thus the energy absorbed by the degenerate electron gas in raising its temperature is very small.

The fraction of electrons which are in excited states at temperature T is of the order of $\frac{kT}{E_F}$, and each will have gained an amount of energy of the order of kT. The total increase in energy of N electrons is therefore approximately $\frac{NkT}{E_F} \times kT$ and the specific heat is $C \sim \frac{Nk^2T}{E_F}$, and is therefore linear in T.

A more accurate value can be obtained by differentiating with respect to T the total energy

$$U = \int_0^\infty \frac{Eg(E)\,dE}{e^{\frac{E - E_F}{kT}} + 1}$$

which yields $C = \frac{\pi^2 k^2}{3} g(E_F) T = \gamma T$ for $kT \ll E_F$, provided $g(E_F)$ varies only slowly with energy. Thus under these conditions, C is proportional T and to the density of states at the Fermi surface.

If γ is expressed in milli joules/mole °K^2, and g(E) in electron states / electron volt atom, g(E) can be calculated from the observed electronic specific heat from the relation.

$g(E)/_{e.v.\ atom} = 0.425\ \gamma$ mj/mole °K^2 and may be compared with

the theoretical value found from the surface integral over the Fermi surface

$$g(E) = \frac{1}{8\pi^3} \int_S \frac{ds}{\text{grad}_k E(k)}$$

Total Specific Heat of Pure Metal

From the two preceeding sections, it follows that the specific heat of a pure metal may be written $C = \gamma T + \beta T^3$ at very low temperatures. A plot of C/T against T^2 is therefore a straight line with a slope β and γ its intercept at $T = 0$. Such a plot therefore yields the two contributions to the specific heat separately.

2.5 Magnetic Specific Heat

Because of its possible relevance to an understanding of the anomalous contribution to the low temperature specific heat of dilute magnetic alloys, the specific heat of isolated magnetic moments in a magnetic field will now be considered.

A magnetic carrier of spin S and magnetic moment $\mu = g \mu_b \sqrt{S (S + 1)}$ (complete quenching of the orbital angular momentum is assumed), placed in a magnetic field H, will have $2 S + 1$ allowed energy levels

$$E = - g \mu_b H S, - g \mu_b H (S-1) \ldots\ldots + g \mu_b H S$$

The distribution of carriers among these energy levels at a temperature

T can be found by applying Maxwell Boltzmann statistics, (required by the distinguishability of the carriers) and the total energy and specific heat may be calculated. The result is a specific heat curve, known as a Schottky anomaly, which increases from zero at T=0, passes through a maximum, and falls to zero as $T \to \infty$. The form of the curve is such that when kT is much smaller than the energy separation E between the ground state and the first excited state, the specific heat per carrier falls to zero as

$$k \left(\frac{E}{kT}\right)^2 e^{-\frac{E}{kT}}$$

As $E = g \mu_b H$, the specific heat in this region depends only on H, and not on S. When kT is large compared with μH, the specific heat per carrier falls as $\frac{\mu^2 H^2}{3k^2 T^2}$

In Appendix 1 the analysis is extended to show the influence on the specific heat curve of a distribution of magnetic fields. It is convenient to define a quantity P (H), such that P (H) dH is the probability that a magnetic carrier is in a field lying between H and H + dH. The high temperature specific heat is little changed, falling as $1/T^2$ for any temperature independent distribution of fields, provided kT is large compared with $\mu H_{max.}$ H^2 is replaced by $\overline{H^2}$, a suitable average of H^2 over the distribution of fields.

At low temperatures the behaviour of the specific heat will be affected dramatically if P (H) remains finite down to H=0. In this case C does not

fall to zero exponentially as T -> 0, but in the limit as T -> 0, the temperature dependence of C/T closely resembles the field dependence of the P (H) curve as H -> 0. In particular, if P(H) tends to a constant P (0) at H=0, C/T also tends to a constant.

The physical origine of this linear temperature dependence of C as T -> 0 can be seen from Fig. 3.

Fig. 3

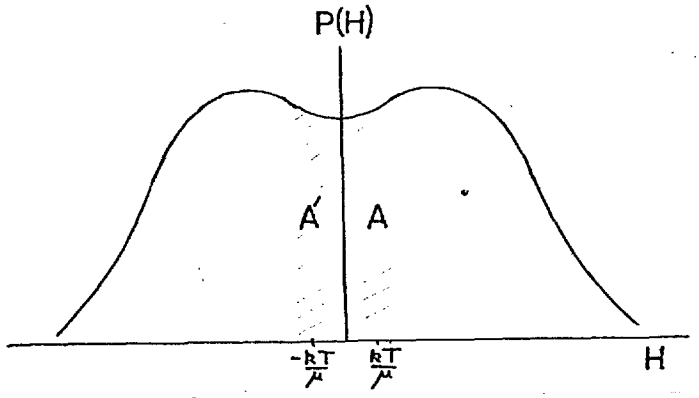

Suppose that P(H) has the general form shown in the figure, and that P (0) is finite. At very low temperatures those spins that lie in fields large compared with $\frac{kT}{\mu}$ will be almost completely aligned parallel to their local field, and will not contribute to the specific heat. They will, however, provide an approximately temperature independent distribution of magnetic fields. Those spins in fields very small compared with $\frac{kT}{\mu}$ will be completely disordered, and will also not contribute to the specific heat. Those spins lying in fields of the order of $\frac{kT}{\mu}$, and indicated by the shaded areas A, A', will be partially aligned, and will contribute an approximately classical value k to the specific heat. The number of such

spins will be of the order of $cN \frac{kT}{\mu} P(0)$, and thus will give a specific heat of $cNk \frac{k}{\mu} P(0)$. Thus in the limit as T -> 0, C is proportional to T if P (0) is finite. Graphs of C/T against T for a few simple P (H) curves are shown in Fig. 4.

B. EXISTING EXPERIMENTAL RESULTS

2.6 Dilute Non-Magnetic Alloys

If an impurity atom is introduced into a pure metal, and has a higher valency than the solvent, the extra valence electron joins the conduction band of the solvent. The average positive potential of the lattice is increased, and the energy of each electron state falls slightly, by an amount ΔE. If the band shape is unaltered by the perturbation, (Rigid Band Approximation), Friedel[62] shows that to a first approximation the extra electrons added with the impurity raise the Ferni level to the same value that it had in the pure metal. The density of states at the Fermi energy of the alloy, will, on this approximation, be the same as the density of states at an energy ΔE above the Fermi Energy of the pure metal. Thus, assuming the rigid band approximation, the addition or subtraction of conduction electrons by the addition of impurities having a valency higher or lower than that of the solvent, allows the density of states function of the pure metal to be determined from a measurement of the electronic specific heat of the alloy.

Measurements by Montgomery[63] of the Specific heat of dilute Ag Cd and

fig 4

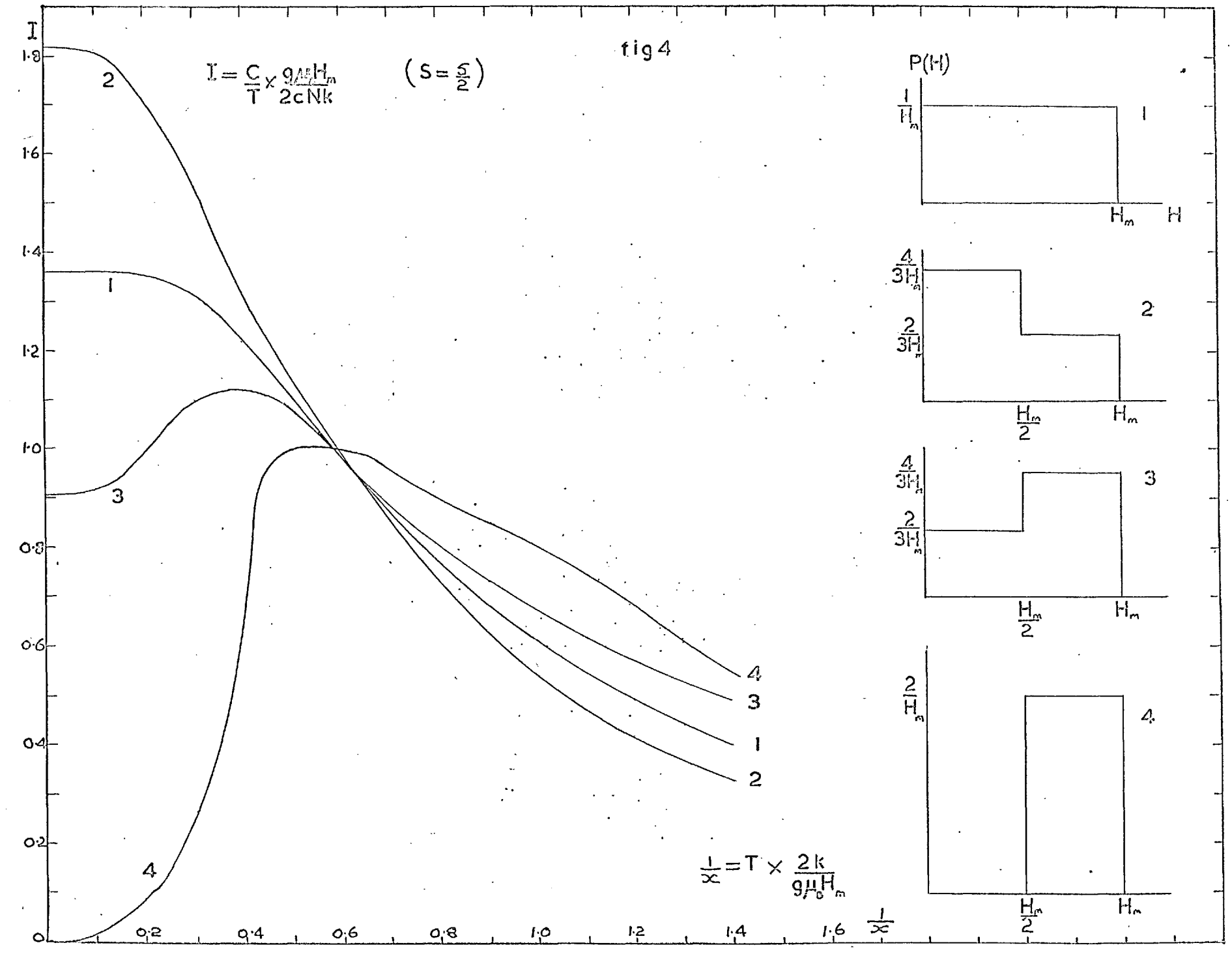
I
$I = \frac{C}{T} \times \frac{9\mu_B H_m}{2cNk}$ $(S = \frac{5}{2})$
2
1
3
4
1·8
1·6
1·4
1·2
1·0
0·8
0·6
0·4
0·2
0
0·2
0·4
0·6
0·8
1·0
1·2
1·4
1·6
$\frac{1}{\chi}$
$\frac{1}{\chi} = T \times \frac{2k}{9\mu_B H_m}$
P(H)
$\frac{1}{H_m}$
H_m
H
$\frac{4}{3H_m}$
$\frac{2}{3H_m}$
$\frac{H_m}{2}$
$\frac{2}{H_m}$

Ag Pd alloys, in which the number of conduction electrons is expected to be increased or decreased by one for each atom of Cd or Pd added, show that γ increases linearly with concentration in each system. Measurements on the ternary alloys Ag 4% Cd 4% Pd, which is isoelectronic with Ag, show an increase in γ which equals the sum of the increases in Ag 4% Cd and Ag 4% Pd. Similar results arefound for a Ag 2% Cd 2% Pd alloy.

Similar results seen to obtain for the Cu Zn, Cu Ni system. Guthrie[64] has measured a series of concentrated Cu Ni alloys, and finds a rapid increase in γ with Ni concentration, though the most dilute alloy measured was Cu 10% Ni. Rayne[63] has investigated the Cu Zn system and finds that γ increases at a rate of 2% per % Zn at low concentrations. Doubt has been cast on these results by the recent work of Isaacs and Massalski[66] on the same system. They find an initial decrease in γ followed by a minimum at about 3% Zn. Rayne also measured γ for the Cu Ge system, in which two extra electrons are introduced into the conduction band per Ge atom, and found an initial rate of increase twice as large as the rate found for Cu Zn.

De Haes van Alphen measurements on Cu, Ag and Au show that in each of these systems the Fermi surface touches the (111) faces of the Brillouin Zone, and therefore the density ofstates of these metals is expected to decrease with increasing energy at the Fermi energy. On the basis of the rigid band model, this is quite inconsistant with the increase in γ with electron / atom ratio found by Montgomery for Ag Cd and Rayne for Cu Zn, but is in agreement with the results of Isaacs and Masalski. It is evidently

not possible to explain the results of the ternary Ag Cd Pd alloys on this theory.

The magnitude of the change in γ is very much larger than would be expected from a rigid band calculation. A free electron model would give, for a divalent impurity in a monovalent solvent, an increase of 0.3% / at % impurity, and Ziman[67] finds that the rigid band model applied to a noble metal whose Fermi surface contacts the Brillouin zone, gives a decrease of 0.7%/at % impurity.

It therefore seems likely that the rigid band model is not applicable to the systems discussed above. The theory has greater success when applied to the alloys of members of the first row transition series (Cheng, Wei and Beck[68]). γ appears to be a function of the electron per atom ratio only, independent of the component metals, provided their difference in valency is not too great.

Several improvements on the rigid band metal have been proposed. Cohen and Heine[69] proposed a soft band model, in which the band gaps decrease on alloying, leading to a sphericalisation of the Fermi surface. Jones[70] has suggested that the greatly reduced mean free path of conduction electrons in a dilute alloy broadens their states in k-space, and allows the excitation of electrons from states well below the Fermi energy, even at very low temperatures. The existance of a peak in the density of states curve of the pure metal just below the Fermi surface, as is expected for the noble metals, will therefore increase the electronic specific heat. In the

explanation due to Friedel, the conduction electrons which screen the excess or defect charge of the impurity lie in a rather narrow range of energy states, and may give a large contribution to the density of states at the Fermi surface. Friedel's ideas will be discussed in more detail in Chapter 3. It is not at present clear whether any of the above suggestions can explain the experimental results.

2.7 Dilute Magnetic Alloys

The specific heat of those dilute transition metal in normal metal alloys which show anomalous resistive and magnetic behaviour, is profoundly different at temperatures below 20°K from the non-magnetic alloys that have just been discussed.

The excess specific heat increases linearly from zero at T=0, and at very low temperatures may be an order of magnitude larger than the specific heat of the pure metal. It reaches a rather broad maximum, then slowly decreases at higher temperatures, and is generally negligable compared with the rapidly increasing lattice specific heat above 20°K. At low temperatures the excess specific heat is approximately independent of concentration, but at higher temperatures the magnitudes increase rapidly with concentration.

Table 2 shows the systems that have been investigated, and the alloy concentrations and temperature ranges for which measurements have been made.

Table 2

Alloy	Author	Concentration %	Temperature °K	Anomaly in C	Anomaly in ρ or χ
Cu Cr	du Chatenier[72]	0.073, 0.56. .. 0.3	0.05–20 1.2 –20	Yes	Yes
Cu Mn	du Chatenier[72,76]	0.15, 1.15 0.35, 0.45	0.06–30 1.2 –30	Yes	Yes
	Zimmerman & Hoare[73]	0.135, 0.48, 1.0 2, 4, 10	1.8 –16 1.8 –4.2		
Cu Fe	Franck Manchester Martin[74]	0.05, 0.12, 0.24	0.4 –30	Yes	Yes
	du Chatenier[72]	0.086	0.4 –30		
Cu Co	Crane & Zimmerman[75]	0.25, 0.55, 1.1, 1.3, 1.5, 1.78, 2.21, 2.25	1.5 –4.5	Yes	Yes
Cu Ni	Guthrie[64]	10, 20, 30, 40	1.5 –4.5	No	No
Ag Cr	du Chatenier[72]	0.099, 0.28	1.3 –20	Yes	
Ag Mn	du Chatenier[72,76]	0.093, 1.01	0.03–0.5, 1.2 –30	Yes	Yes
		0.29, 0.41	1.2 –30		
Au V	du Chatenier[72]	0.1. 0.27, 0.7, 1.4	1.2 –4	No	No
Au Cr	du Chatenier[72]	0.11, 0.18	1.2 –4	Yes	Yes
Au Mn	du Chatenier[72]	0.083, 0.16	0.05–30	Yes	Yes
Au Fe	du Chatenier[72]	0.092	0.15–30	Yes	Yes
	Dreyfus[77]	0.2, 0.5, 1, 2, 3, 8	1.3 –4.2		
Au Co	Crane[75]	0.35, 0.57, 0.98, 1.8, 2.0, 2.6,	1.2 – 5	Yes	Yes
Mg Fe	Logan[78]			No	No
Mg Mn	Martin[79]	0.025, 0.15	0.4 –1.5	Yes	Yes
Zn Cr	du Chatenier[72]	0.21	1.5 –5	Yes	Yes
Zn Mn	du Chatenier[72]	0.071, 1.5	1.5 –5	Yes	Yes
Zn Fe	du Chatenier[72]	0.1	1.5 –20	No	No
Al Cr	du Chatenier[72]	-	1.5 –5	No	No
Al Mn	Martin[80]			No	No

As can be seen from the last two columns in table 2, the existance

of a specific heat anomaly correlates well with the existance of anomalies in the resistance and susceptibility. The distribution amongst the alloys of anomalies in these properties, can be seen more clearly in the Friedel diagram (section 3.5) the significance of which will be discussed in detail in Chapter 3.

Uncertainties in the shape of the C against T curves increase rapidly with temperature above the liquid helium range, because of the very rapidly increasing lattice specific heat, and the difficulties of accurate temperature calibration in this region. Although this is obviously more severe, at any given temperature, for low concentration alloys, the fact that the anomaly generally occurs at lower temperatures in these alloys, and may therefore fall in a more managable region, allows a greater proportion of the shape of the anomaly to be know accurately, particularly if measurements have been performed below 1°K. The difficulties are also greater when Au is the solvent, which, because of its low Debye temperature, gives a lattice specific heat approximately eight times larger than that of Cu.

Figures 5, 7, 8, 9, 11, 12 show the quantity $\frac{\Delta C}{T}$ against T found by other authors for several systems exhibiting anomalies in the specific heat. ΔC is the difference between the specific heat of the alloy and pure metal at a given temperature T. These have usually been taken by direct measurement from the authors published curves, and may not, therefore, be a very accurate representation of their actual results. They do, however,

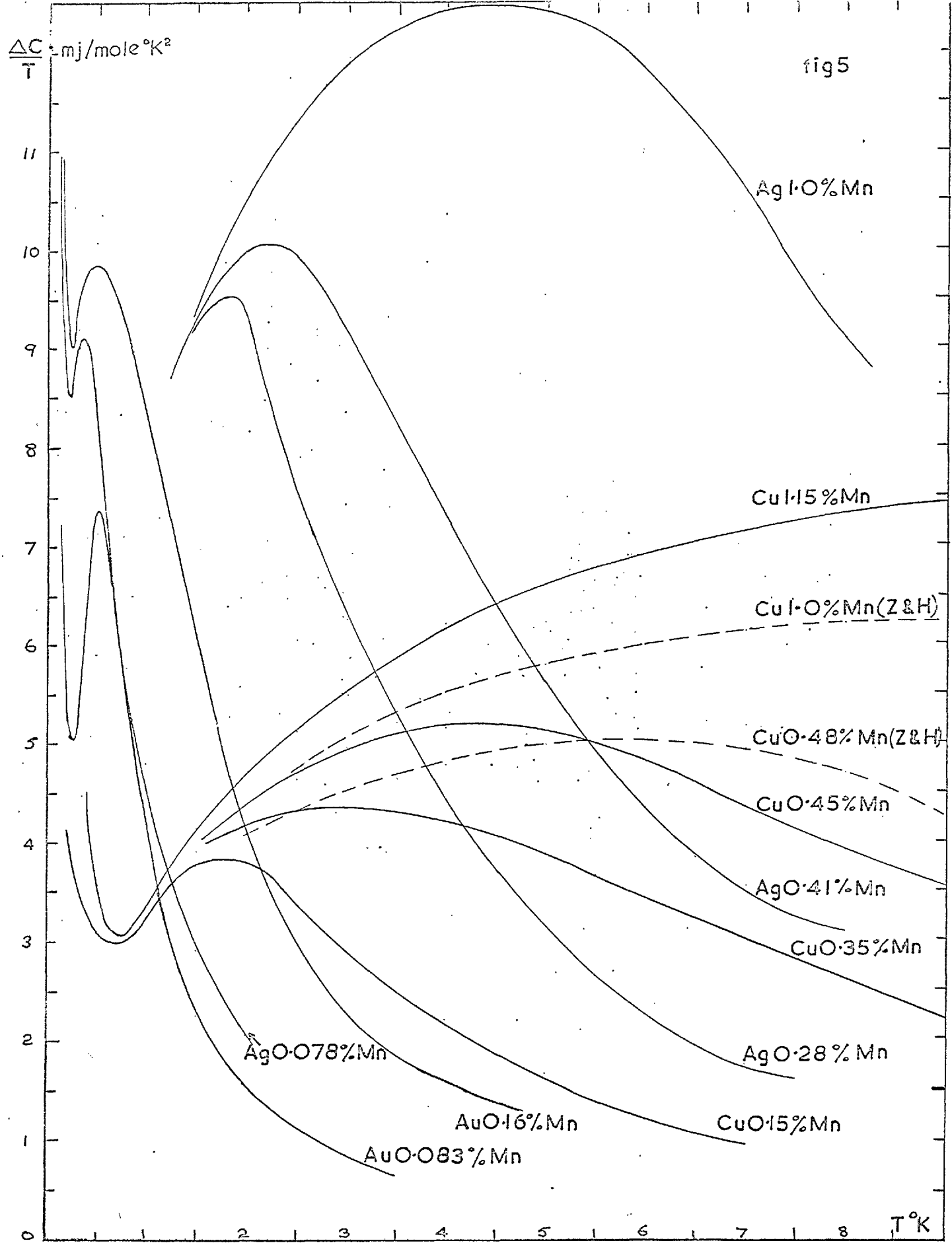
ΔC/T - mj/mole °K²
fig 5
Ag 1·0% Mn
Cu 1·15% Mn
Cu 1·0% Mn (Z&H)
CuO·48% Mn (Z&H)
CuO·45% Mn
AgO·41% Mn
CuO·35% Mn
AgO·28% Mn
CuO·15% Mn
AgO·078% Mn
AuO·16% Mn
AuO·083% Mn
0
1
2
3
4
5
6
7
8
9
10
11
T °K

show the main features of the anomalies in the different systems.

For systems in thermal equilibrium, $\frac{\Delta C}{T}$ is equal to $\frac{dS}{dT}$, where S is the entropy of the alloy minus that of the pure metal, and thus the magnitude of $\frac{\Delta C}{T}$ indicates the rate per degree at which disorder is increasing in the system of magnetic impurities. ΔC is the rate per degree at which the energy of the impurities is increasing.

Fig. 5 shows $\Delta C/T$ against T for Cu, Ag and Au containing Mn. These are mainly from measurements of du Chatenier, but those of Zimmerman and Hoare on Cu Mn have also been included. The curves exhibit the following features. At very low temperatures, generally below $0.5^{\circ}K$, $\Delta C/T$ is dominated by the specific heat of the nuclear magnetic moments ordering in the hyperfine field, giving a specific heat which varies as A/T^2. The constant A is proportional to the concentration, and for 1% of Mn, takes the values 0.12, 0.06, 0.07 mj/mole for Cu Mn, Ag Mn and Au Mn respectively. If this nuclear term is subtracted $\Delta C/T$ is found to become independent of Mn concentration as $T \rightarrow 0$.

The curves pass through maxima at temperatures which are proportional to the Mn concentration, and are given approximately by 4, 5.5, and 10 $^{\circ}K$ / at % Mn for Au Mn, Ag Mn and Cu Mn. $\frac{\Delta C}{T}$ decreases rapidly below the maximum and du Chatenier quotes the following values for $\frac{\Delta C}{T}$ at T = 0 after subtraction of the nuclear term; 7.8, 4.6, and 2.3 mj/mole $^{\circ}K^2$ for Au Mn, Ag Mn and Cu Mn. These figures must be regarded as approximate only, because of the large extrapolation of a non-linear function that is involved in their estimation,

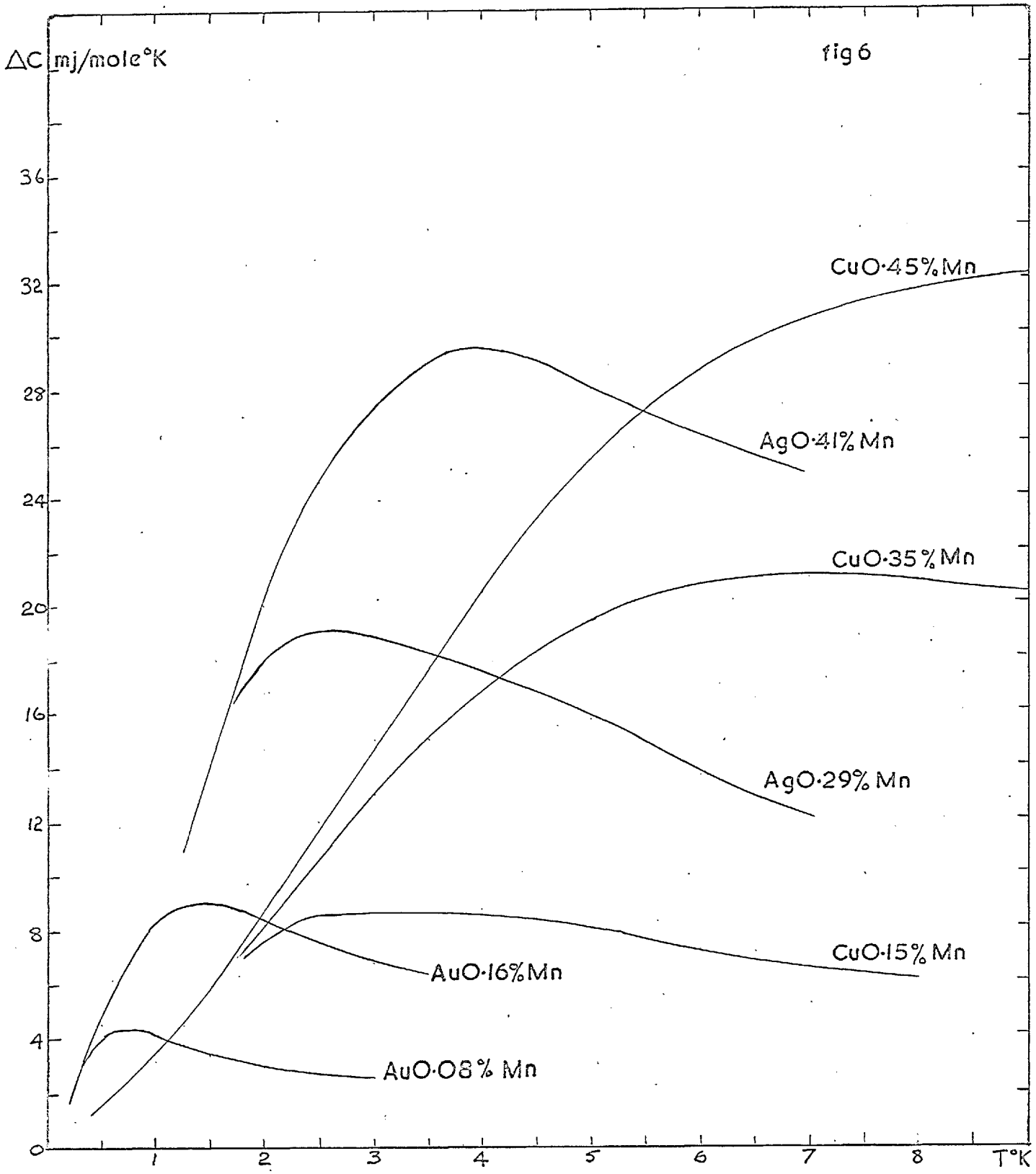
ΔC mj/mole°K
fig 6
36
32
28
24
20
16
12
8
4
0
1
2
3
4
5
6
7
8
T°K
CuO·45% Mn
AgO·41% Mn
CuO·35% Mn
AgO·29% Mn
CuO·15% Mn
AuO·16% Mn
AuO·08% Mn

and almost any value between zero and these values would seem possible from the published curves. The estimated entropy for each of these systems is found to approach $\sigma R \log_e 6$ at high temperatures, and is therefore consistant with a spin of 5/2 on the Mn atom.

Fig 7 - shows $\frac{\Delta C}{T}$ against T for Cu, Ag and Au containing Cr, as measured by du Chatenier. For Au Cr and Cu Cr, $\frac{\Delta C}{T}$ becomes concentration independent at low temperatures, and for Cu Cr, for which measurements were made on two alloys down to 0.05°K, $\Delta C/T$ is constant below about 0.8°K at 1.8 mj/mole $^{\circ}K^2$. At higher temperatures, the curves for different concentrations diverge, and those of higher concentration exhibit a maximum. The maximum for Au 0.18%Cr occurs at about 2.3°K, or 13°K/%Cr. The concentrations of the Cu 0.56% Cr and Cu 0.3% Cr are purely nominal, as they are so far in excess of the room temperature solubility limit of Cr in Cu. This probably accounts for the rather low spin values found for these alloys. (See Table 3).

The available data for the Au Fe system is shown Fig. 8. Measurements to very low temperatures on a series of Au Fe alloys of varying concentration do not exist, so that it is not possible to decide whether the behaviour of Au Fe is similar to that of the Mn alloys, with $\Delta C/T$ becoming concentration independent as T approaches zero. Du Chatenier has measured a Au 0.092% Fe alloy down to 0.15°K, and claims that $\Delta C/T$ is effectively constant at 2.26 mj/mole $^{\circ}K^2$ below 0.5°K. The measurements of Dreyfus et al on Au containing 0.2, 0.5, 1.0% Fe, and those of the author

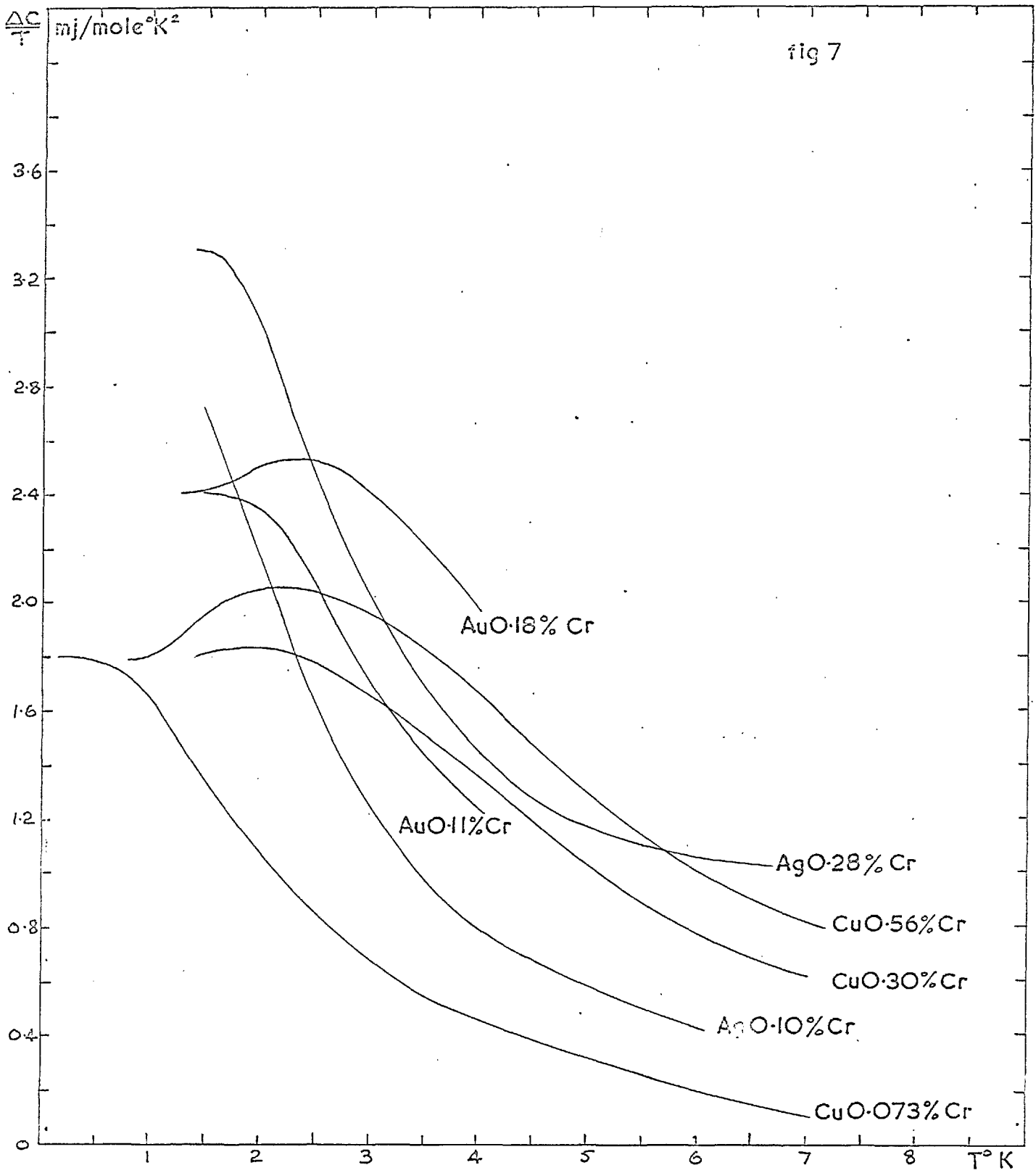
ΔC/T mj/mole°K²
fig 7
3·6
3·2
2·8
2·4
2·0
1·6
1·2
0·8
0·4
0
1
2
3
4
5
6
7
8
T° K
AuO·18% Cr
AuO·11% Cr
AgO·28% Cr
CuO·56% Cr
CuO·30% Cr
AgO·10% Cr
CuO·073% Cr

on a Au 0.6% Fe alloy, have reached a value which is almost independent of concentration, about 3.2 mj/mole $^{\circ}K^{2}$, at 1.3°K, and it is not impossible that these curves will approach that of the Au 0.092% Fe at lower temperatures. Du Chatenier finds a spin value of Fe of 0.65 from his measurements on the Au 0.092%Fe alloy, whilst a value of 0.5 is found for the Au 0.6% Fe alloy in the present investigation.

Fig. 9 shows the measurements of Franck Manchester and Martin on Cu Fe alloys containing 0.05, 0.12, 0.24 % Fe in the temperature range 0.4 to 30°K, measurements by du Chatenier on a Cu 0.086% Fe down to 0.4°K, and those on a Cu 0.6% Fe alloy between 1.3°K and 20°K described in the present work. None of the alloys reaches a concentration independent region in the temperature range of measurement, though one may speculate from the trends of all of the curves at low temperatures that they may approach a concentration independent value of around 2.4 mj/mole $^{\circ}K^{2}$ at a temperature below 0.4°K. The entropy associated with the alloys of Cu containing 0.05, 0.12, 0.24 and 0.6% Fe is consistant with a spin on the iron atom of 0.5.

Figures 11 and 12 show the measurements of Crane and Zimmerman on Cu Co alloys, and of Crane on Au Co alloys. These two systems have specific heat anomalies that are very similar to one another, with the anomaly rather larger in Au Co than Cu Co.

In the limited temperature range covered (1.5 - 5°K) they show little resemblance to the systems that have been described so far. For

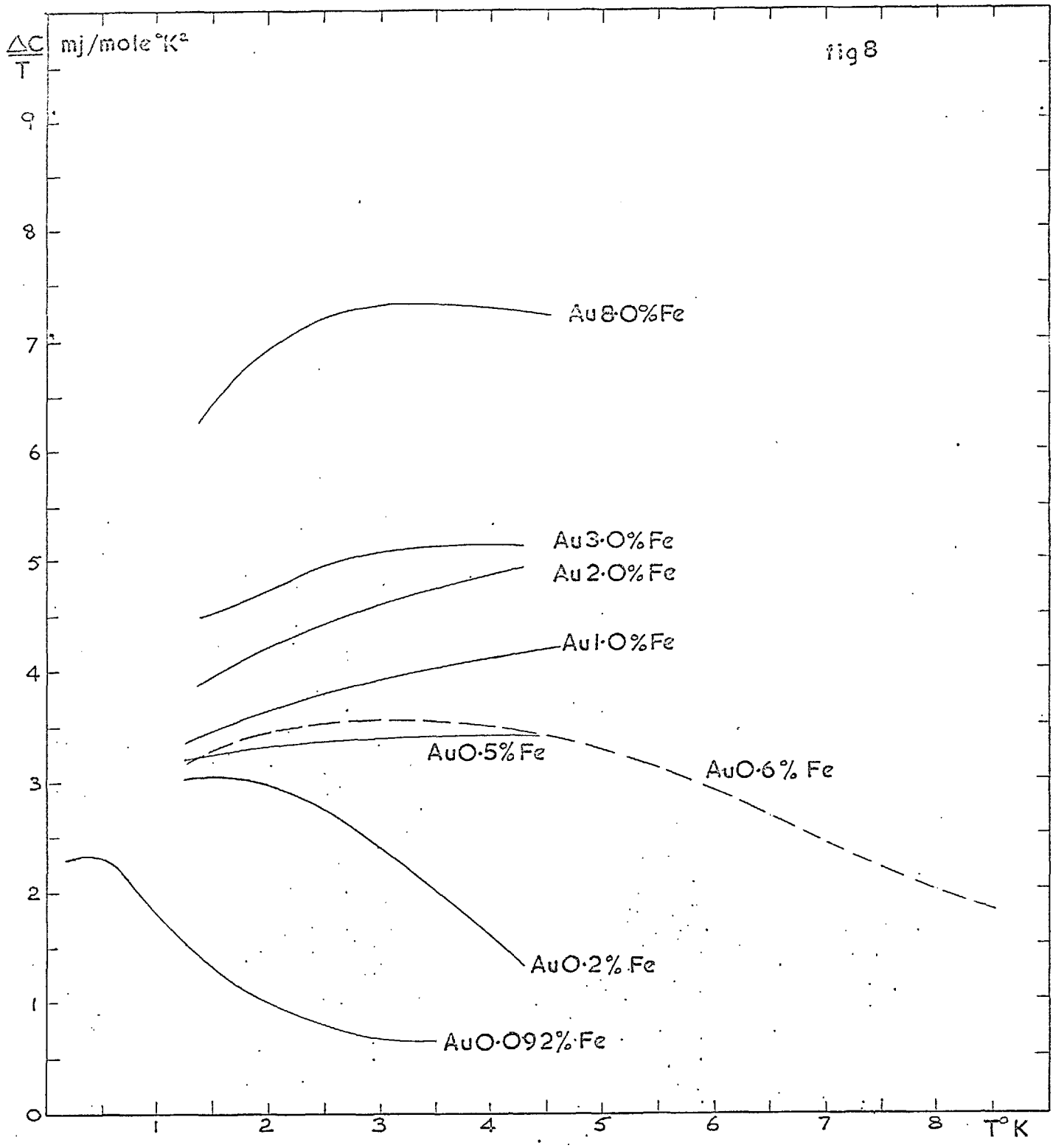
ΔC/T mj/mole °K²
fig 8
9
8
7
6
5
4
3
2
1
0
1
2
3
4
5
6
7
8
T°K
Au 8·0% Fe
Au 3·0% Fe
Au 2·0% Fe
Au 1·0% Fe
AuO·5% Fe
AuO·6% Fe
AuO·2% Fe
AuO·092% Fe

Co concentrations below 1%, there appears to be a small and almost temperature independent increase in $\Delta C/T$ which decreases rapidly with Co concentration. For higher concentrations $\Delta C/T$ increases as the temperature is reduced, suggesting that a large amount of ordering takes place below 1.5°K. Although for large concentrations $\Delta C/T$ reaches values higher than those observed for any of the other systems so far discussed, the entropy increase in the temperarange 1.5 to 5°K is only around 5% of the entropy associated with the disordering of isolated spins with $S = \frac{1}{2}$.

Other systems that have been shown to exhibit specific heat anomalies are Mg Mn (Martin), Zn Mn (du Chatenier) and Zn Cr (du Chatenier). Measurements below 1.5°K are needed to show whether the specific heat anomaly in Zn Mn is similar to those of Cu, Ag, and Au containing Mn, but results above 1.5°K suggest that this may be the case. Du Chatenier finds a spin value of 1.5 for Mn in Zn and 0.3 for Cr in Zn.

Other systems that have been investigated, Au V, Zn Fe, Cu Ni, Al Cr, Al Fe, Mg Fe and Al Mn show no signs of a specific heat anomaly, consistant with the absence of anomalies in their other properties.

Plots of ΔC against T for Cu, Ag and Au containg Mn are shown in Fig. 6, and for Cu Fe alloys in Fig 10. Because the large uncertainties in the values at higher temperatures (above 4°K), have a greater influence on the temperature of the maximum and the rate of decrease above the maximum, in ΔC than in $\Delta C/T$, it is unwise to draw definite conclusions from the high temperature. behaviour of these curves. It would appear, however, that

fig 9

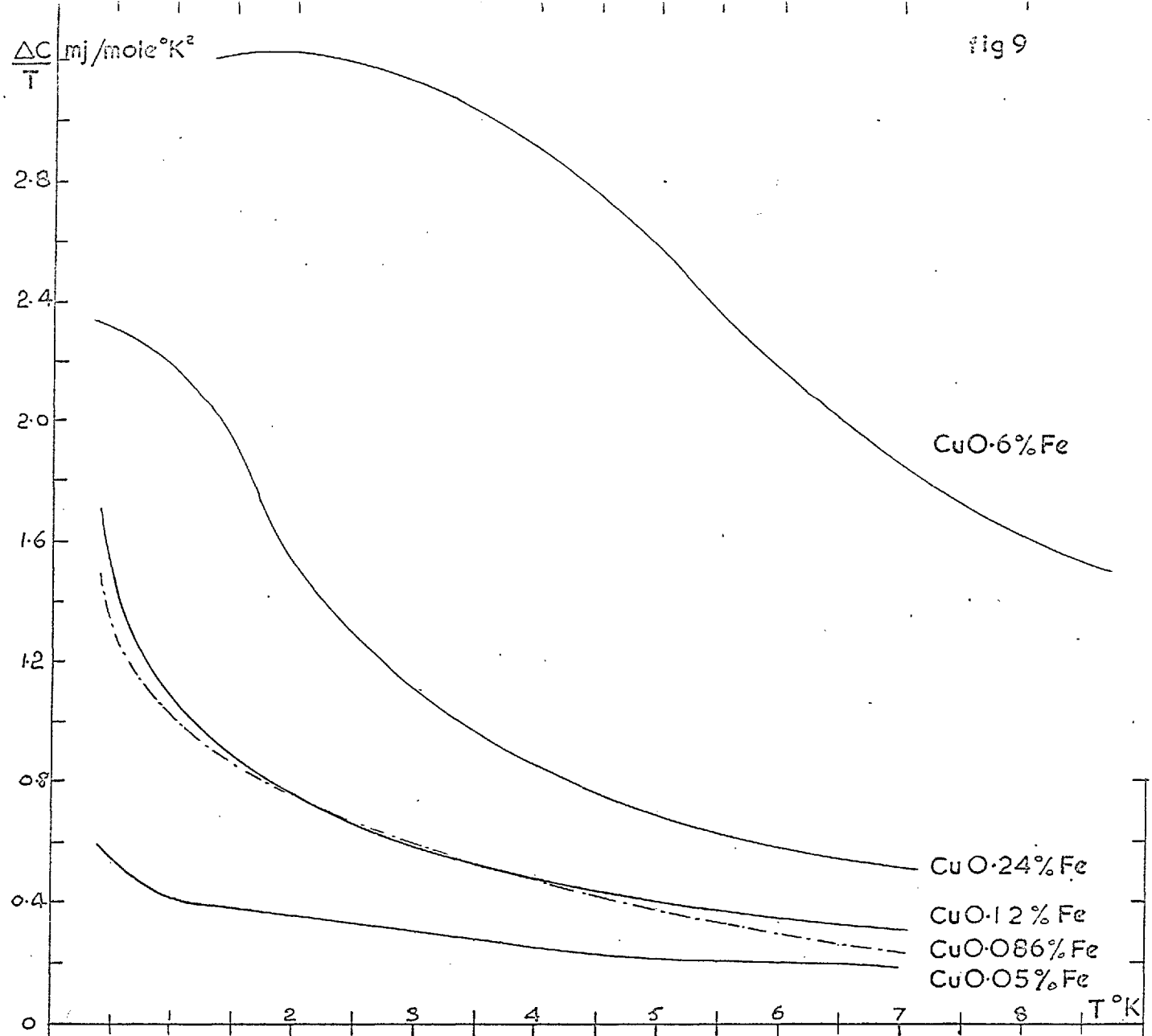
ΔC/T mj/mole°K²
2·8
2·4
2·0
1·6
1·2
0·8
0·4
0
2
3
4
5
6
7
8
T °K
CuO·6% Fe
CuO·24% Fe
CuO·12% Fe
CuO·086% Fe
CuO·05% Fe

fig 10

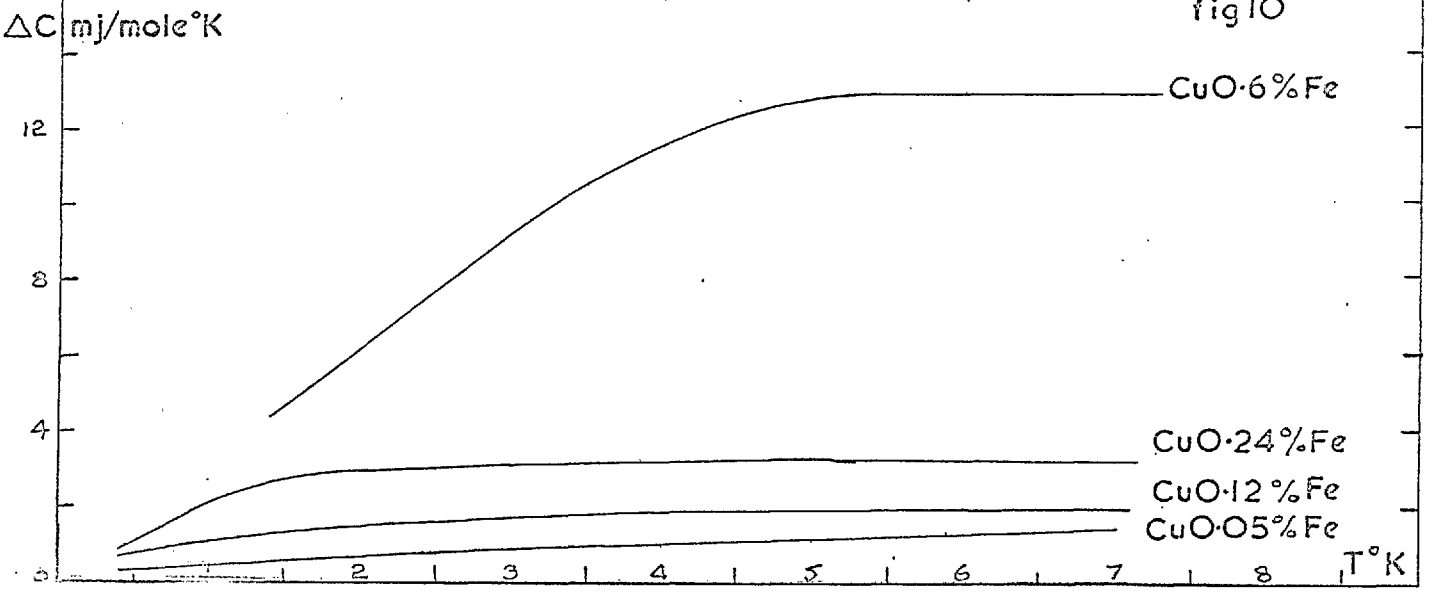
ΔC mj/mole°K
12
8
4
0
2
3
4
5
6
7
8
T °K
CuO·6% Fe
CuO·24% Fe
CuO·12% Fe
CuO·05% Fe

the rate of decrease in ΔC above the maximum is greater in the Mn alloys than the Fe alloys, and decreases only a little less rapidly than $1/T^2$ for the Mn alloys at high temperatures.

Table 3 shows the spin values on the solute atom, found from specific heat measurements, and compares them with the values found from high temperature susceptibility measurements. The value of $\Delta C/T$ at $T = 0$ is also included. When this quantity has been guessed from measurements above $1.5^\circ K$, in systems for which a concentration independent region has not definitely been reached, the value is followed by a question mark.

Table 3

Alloy	Author	Concentration	Spin from Specific Heat	Spin from Susceptibility	$\frac{\Delta C}{T}$ at T=0 mj/mole $^\circ K^2$
Cu Mn	du Chatenier	0.15, 0.35, 0.45	2.5	2.0	2.32
Ag Mn	du Chatenier	0.093, 0.285, 0.41, 1.01	2.5	2.5	4.6
Au Mn	du Chatenier	0.083, 0.16	2.4	2.5	7.8
Cu Cr	du Chatenier	0.073 0.30 0.56	0.8 0.3 0.2	-	1.8
Ag Cr	du Chatenier	0.099 0.28	1.4 0.7	-	3.27
Au Cr	du Chatenier	0.11, 0.18	1.3	1.5	2.4?
Cu Fe	Franck Manchester and Martin	0.05, 0.12, 0.24	0.5		2.4?
	This work	0.6	0.5		
Au Fe	Du Chatenier	0.092	0.67	1.3	2.26
	This work	0.6	0.5		<3.1
Zn Mn	du Chatenier	0.071	1.5	2 (34)	
Zn Cr	du Chatenier	0.21	0.3	-	

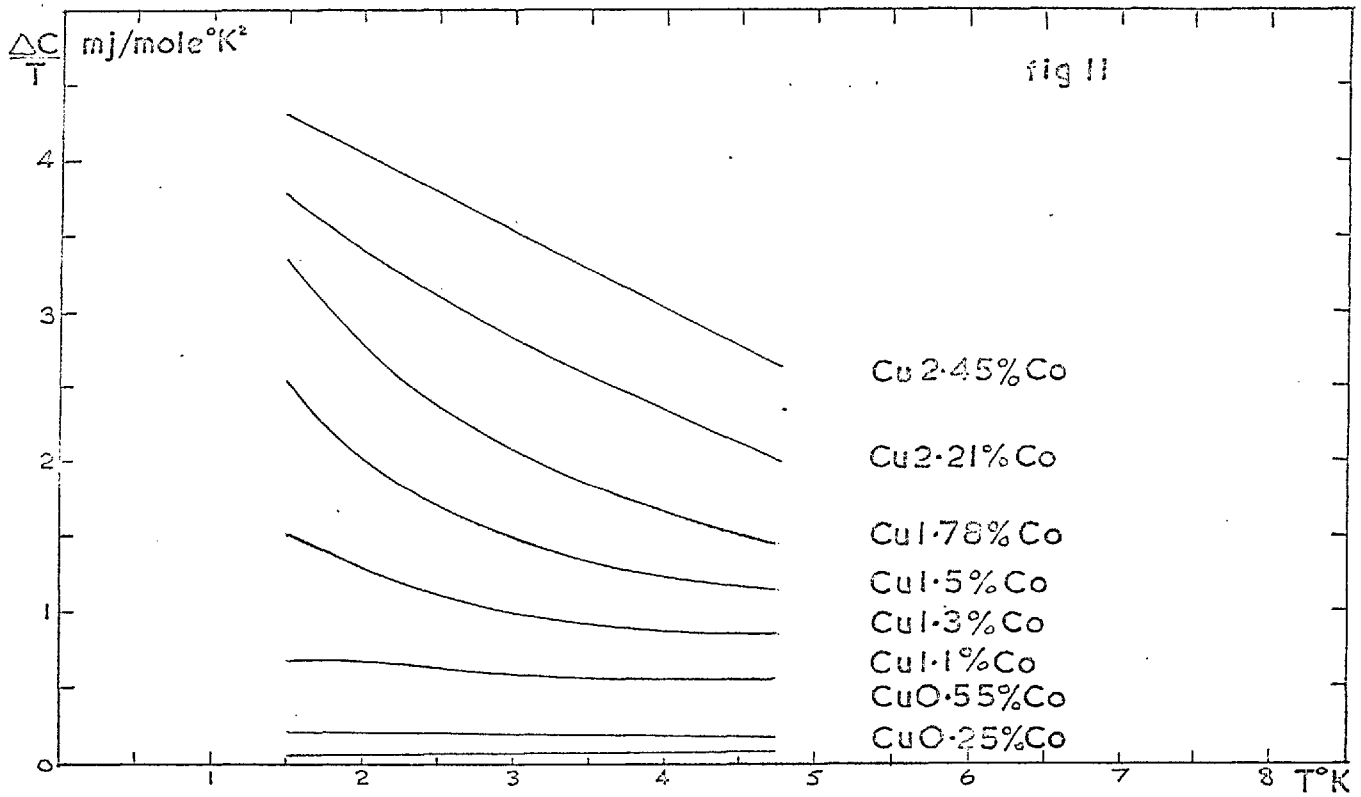
ΔC/T mj/mole°K²
fig 11
Cu 2·45%Co
Cu 2·21%Co
Cu 1·78%Co
Cu 1·5%Co
Cu 1·3%Co
Cu 1·1%Co
CuO·55%Co
CuO·25%Co
T°K

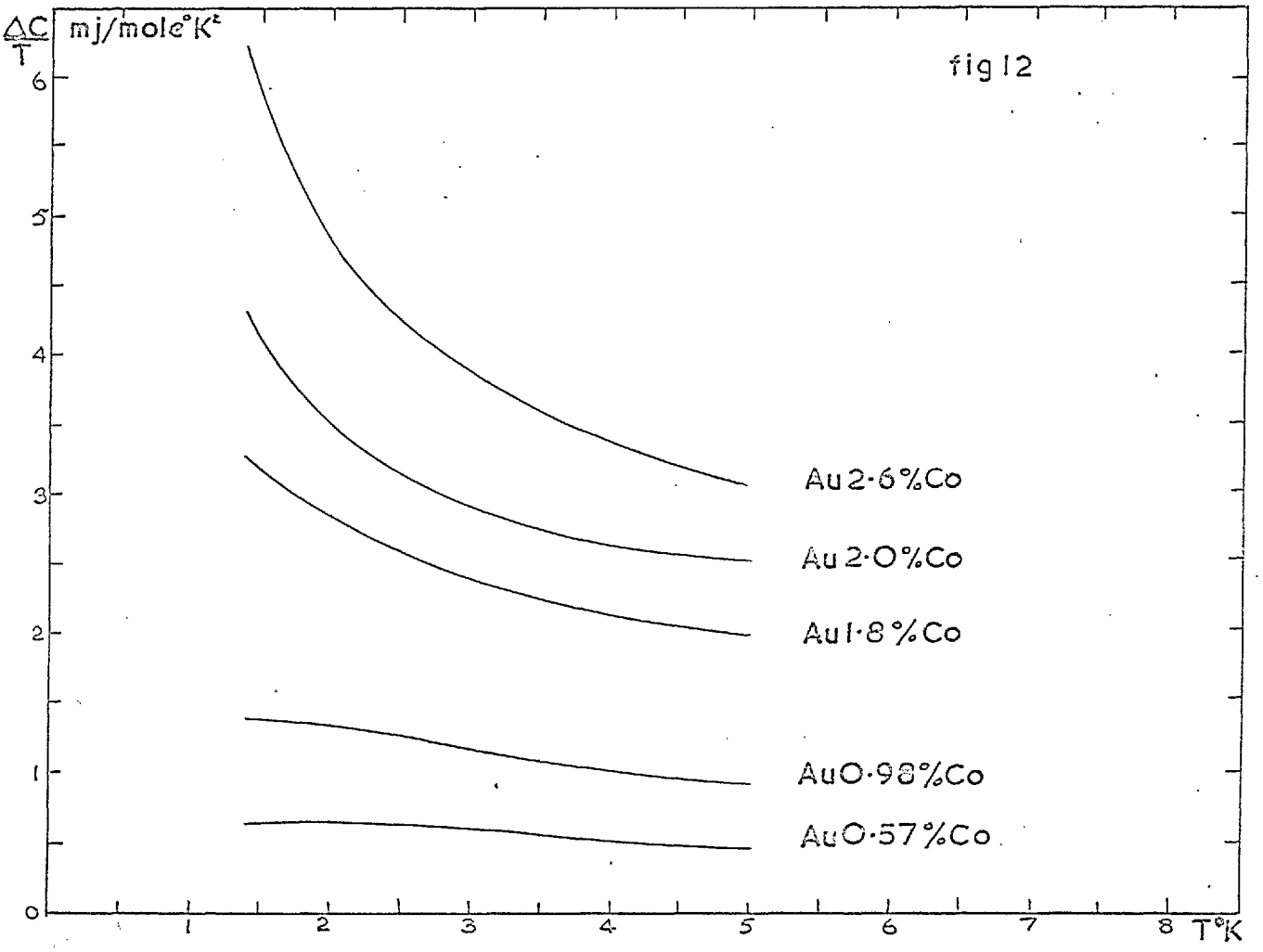
ΔC/T mj/mole°K²
fig 12
Au 2·6%Co
Au 2·0%Co
Au 1·8%Co
Au 0·98%Co
Au 0·57%Co
T°K

CHAPTER 3

THEORY OF DILUTE ALLOYS. A - IMPURITY STATES IN METALS

3.1 Introduction

When an impurity atom is introduced into a metal, the properties of the system depend largely on the interaction of the impurity with neighbouring solvent atoms, and with other impurity atoms. This in turn depends on the rearrangement of the electron wave functions around the impurity atom. The valence electrons of the impurity atom will be in states of positive kinetic energy throughout the volume of the metal, and will therefore enter the solvent conduction band. This leaves the impurity core with an excess positive charge + Ze, if its valency exceeds that of the solvent by Z. Classically, no long range electric fields can exist in a conductor, and it may therefore be expected that the conduction electrons will rearrange themselves around the impurity in such a way that the excess charge will be screened within a distance which is of the order of atomic dimensions.

3.2 Thomas-Fermi Screening

A semi classical model, due to Thomas and Fermi (see Friedel[81]) gives the density $\rho(r)$ of the screening electrons as a function of distance r from the impurity centre, assuming that the potential varies slowly in a distance of the order of the wavelength of the electrons. The result of this calculation is

$$\rho(r) = \frac{Z q^2}{4\pi r} e^{-qr} \quad \ldots\ldots\ldots\ldots\ldots\ldots\ldots\ldots 3.1$$

where $q^2 = 4\pi n(E_f)$ and $n(E_f)$ is the density of states at the Fermi surface. The influence of the impurity will only be felt up to a distance of a few times $1/q$, which is of the order of the interatomic distance for most metals. As this distance varies inversely as the density of states at the Fermi energy, it will be very small for alloys of transition metals in transition metals, for which $n(E_F)$ is large, and a typical value for $1/q$ is 0.3 Å. The excess charge will then be screened out within the atomic volume of the impurity, and there will be negligable interaction even with nearest neighbour solvent atoms. This explains the large solubility, low heat of solution, and absence of short range order in these alloys. Friedel also explains, on this basis, the linear variation of magnetic moment as a function of concentration in the alloys of the first row transition elements, and his conclusion that the magnetic moment on a nearest neighbour solvent atom is unaffected by the impurity is confirmed by the neutron diffraction experiments (Low)[82].

For normal-metal alloys, the density of states is lower, and the screening range is larger than for transition metals, and there is a small overlap of the screening charge at the nearest neighbour solvent atoms. The extensive solubility observed in many normal metal alloys, is due largely to this rapid screening out of the excess charge, though other factors must also be favourable, e.g. the sizes of the solute and solvent atoms must be comparable to prevent undue distortion of the lattice; the symmetry

of the impurity wave functions at the surface of the atomic cell must match suitably with those of the solvent atoms. This latter consideration probably accounts for the very low solubility of transition metals in noble metals, and possibly for the almost complete insolubility of Ag and Cu where the levels of the d-band differ greatly.

3.3 Friedel Screening

A more exact calculation of the screening of an impurity, in which the restriction of a slowly varying potential is removed, reveals several new and significant features. The increase in electron density $\rho(r) - \rho_o(r)$ at a distance r from the centre of a square potential well of depth Vo and radius 'a', is given by

$$\Delta\rho = \rho(r) - \rho_o(r) = \frac{-4\,U\,k_f^4}{\pi^3} \quad \frac{2k_f r \cos 2k_f r - \sin 2k_f r}{(2k_f r)^4} \quad \ldots 3.2$$

in atomic writs $e = \hbar = m = 1$

where $U = \frac{4\pi}{3} a^3 V_o$, and k_f is the Fermi wave number.

In this calculation it is assumed that $\sqrt{2\,V_o}\,a$ and $k_f a$ are $\ll \pi$, and that the potential is screened by free electrons from zero energy up to a Fermi energy $E_F = \frac{k_F^2}{2}$. This formula may also be written

$$\Delta\rho = \frac{-72\pi n^2\,U}{E_F} \quad F(2k_f r) \quad \ldots\ldots\ldots\ldots\ldots\ldots\ldots 3.3$$

where 2n is the mean electron density in the metal, and

$$F(x) = \frac{x\,\mathrm{Cos}x - \mathrm{Sin}x}{x^4} \quad \ldots\ldots\ldots\ldots\ldots\ldots\ldots\ldots 3.4$$

The function $F(x)$ is shown in fig. 13

Fig 13

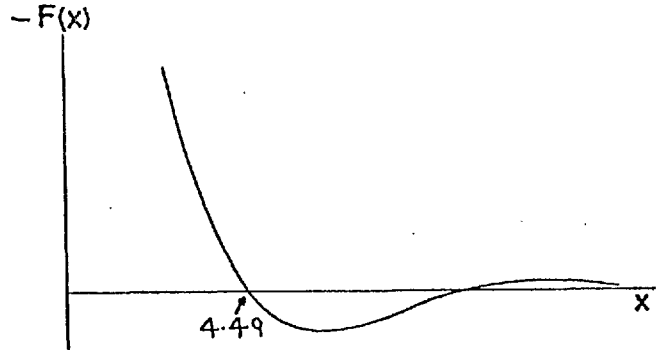

For $x < 4.49$, the electron density decreases rapidly with increasing distance, and the excess charge is effectively screened out within this range. For Cu, $k_f = 0.72$ atomic units, and the first zero in $\Delta\rho$ occurs at a distance $r = \frac{4.49}{2 \times 0.72} \times 0.53$ Å $= 1.7$ Å, which may be compared with the nearest neighbour distance in Cu of 2.55 Å.

At distances greater than the first zero, the electron density oscillates in sign, with an amplitude which falls off at large distances as $\frac{\mathrm{Cos}\ 2k_f r}{r^3}$. Despite their very rapid decrease in amplitude, these oscillations in the conduction electron gas may be considered to be of long range, compared with the exponentially decreasing amplitude of the atomic wave-

functions at large distances, and they may lead to interactions at much greater range than is possible by direct exchange of electrons in bound orbitals.

Evidence for the existance of such long range oscillations in the charge density comes from the strong attenuation and absence of Knight Shift of the nuclear magnetic resonance line of Cu or Al atoms in Cu or Al base alloys containing impurities (Kohn and Vosko[83]). The electric field gradients, of random sign and direction, associated with the oscillating charge density, interact with the electric quadrupole moment of the nuclei, and broaden the resonance. The magnitude of the effect in very low concentration alloys shows that the resonance of the first 80-100 neighbours of an impurity atom is effected. The importance of these long range oscillations in understanding the interactions between magnetic impurities, will be discussed in the second part of this chapter.

Friedel[84] has derived an expression for the screening charge density due to a strong potential by a partial wave analysis, in which the scattering potential appears implicitely in the phase shifts η_l of the scattered waves of angular momentum l. He finds that the total number of screening charges N(k) within a large sphere of radius R, per unit k, is

$$N(k) = \int_0^R \frac{d}{dk} \left[4\pi r^2 \Delta\rho(r)\right] dr = \frac{2}{\pi} \sum_l (2l+1) \left[\frac{d\eta_l}{dk} - \frac{1}{k} \sin\eta_l \cos(2kR + \eta_l - l\pi)\right] \quad \ldots\ldots\ldots 3.5$$

in which the degeneracy $2(2l + 1)$ of each state has been included.

For large r this gives

$$\Delta\rho = \frac{1}{2\pi^2 r^3} \sum_l (2l + 1) \int_0^{k_f} \text{Sim}\eta_l \, \text{Sin}\,(2kr + \eta_l - l\pi)\, 2r\,dk \quad . . \quad 3.6$$

η_l is in general a function of k. If the integration is performed, $\Delta\rho$ is found to exhibit long range oscillations of the same general form as those in equation 3.2.

From 3.5 the total number of screening charges N is

$$N = \frac{2}{\pi} \sum_l (2l + 1) \int_0^{k_f} \left[\frac{d\eta_l}{dk} - \frac{1}{k} \text{Sim}\eta_l \, \text{Cos}\,(2kR + \eta_l - l\pi) \right] dk$$

$$= \frac{2}{\pi} \sum_l (2l + 1)\, \eta_l\,(k_f) + \text{oscillating term} \quad . . . . . \quad 3.7$$

The second, oscillating term inthe integration contributes a negligable amount to N. $\eta_l\,(k_f)$ is the phase shift of electrons at the Fermi level. For the screening to be complete within the radius R, the number of screening charges N must equal the excess charge Z of the impurity, and therefore

$$Z = \frac{2}{\pi} \sum_l (2l + 1)\, \eta_l\,(k_f) \quad . . . . . \quad 3.8$$

This expression is known as the Friedel Sum Rule, and it imposes conditions that must be satisfied by any self consistant impurity potential.

The residual resistance $\Delta\rho$ of a dilute non-magnetic alloy can be calculated in terms of the phase shifts $\eta_\ell\ (k_f)$ from the scattering cross section σ.

$$\sigma = \frac{4\pi}{k_f^2} \sum_\ell (\ell + 1)\ \mathrm{Sin}^2\ (\eta_\ell - \eta_{\ell+1}) \qquad \ldots\ldots\ldots\ldots\ 3.9$$

and

$$\Delta\rho = \frac{c\ k_f \sigma}{p} = \frac{4\pi c}{p k_f} \sum_\ell (\ell + 1)\ \mathrm{Sin}^2\ (\eta_\ell - \eta_{\ell+1}) \qquad \ldots\ldots\ 3.10$$

where c is the impurity concentration, p is the number of electrons per atom of the matrix, and the phase shifts are taken at the Fermi level. $\Delta\rho$ is expressed in atomic units, where 1 a.u. = 21.8 $\mu\Omega$ c.m.

Calculations by Casteljau [85] et al, and others, for Cu containing polyvalent non-magnetic impurities, in which the potential is chosen to satisfy the sum rule, have given results in good agreement with experimental values.

3.4 Energy distribution of the screening electrons (Friedel)

In the last sections, the spacial distribution of the screening

charge was discussed, and was found to be localised in a small region around the impurity. The energy distribution of the screening electrons will now be considered.

If the impurity has a valency which is positive with respect to the solvent metal, and the potential is sufficiently strong, a bound state may exist below the bottom of the conduction band. This will then be filled by an electron from the conduction band, and the excess charge of the impurity will be decreased by one unit. This situation has been dealt with in detail by Slater and Koster[86], who find that the wavefunction of such a bound electron is of the form $\frac{e^{-ar}}{r}$.

If the strength of the potential is progressively reduced, the energy level rises, and crosses the bottom of the conduction band. It will then be in a state which has a positive kinetic energy throughout the whole lattice, and is therefore no longer a truely bound state. The state, which had a discrete energy value when it lay below the conduction band, now resonates with the conduction electron states, and broadens out into a region of finite energy width, centred on the energy that it would have had in the absence of the band states. The behaviour can be seen more clearly from an analysis due to Mott and Massey[87] of the similar problem of the resonant scattering of free electrons by free atoms in a gas.

Writing the electron wave function as

$$\psi (r, \theta, \phi) = R(r)\, u (\theta, \phi)$$

the radial part of the wave equation associated with an angular momentum $\ell\hbar$ in a potential V(r) may be written,

$$-\frac{\hbar^2}{2m}\frac{d^2\chi}{dr^2} + \left(V(r) + \ell\,\frac{(\ell+1)}{2mr^2} \right)\chi = E\chi$$

where $\chi = \frac{R(r)}{r}$

The quantity $\ell\,\frac{(\ell+1)}{2mr^2}$ may be thought of as an extra positive potential, and the quantity $V(r) + \ell\frac{(\ell+1)}{2mr^2}$ may be of the form shown in Fig. 14, for $\ell > o$

Fig. 14

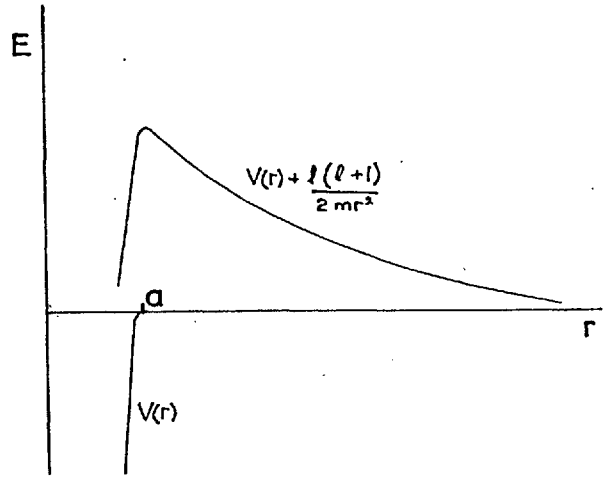

For E -ve, only bound states separated by large energies are allowed, to satisfy the boundary conditions that $\chi = 0$ at $r = a$. For E + ve, a

continuum of states exist which extend through the whole lattice. The amplitude of the wavefunctions in the region $r < a$ is determined by the normal conditions of continuity of the wave function and its derivative at the barrier, and a large amplitude for χ will generally only be possible if there are <u>almost</u> an integral number of half wavelengths in the region $r < a$, that is for energies centred around a value at which a bound state would have existed if the barrier had been very wide. When this condition is not satisfied the amplitude of χ for $r < a$ will be very small. The narrow region of states which have a large amplitude in the neighbourhood of the impurity is called a Virtual Bound State (Friedel[84]). The symmetry of the virtual state resembles that of the bound state from which it was derived, and the total amplitude summed over all the extended states equals that of the bound state. The energy width of the virtual state decreases rapidly as ℓ increases, and is only significantly narrower than the band for $\ell \geq 2$. In future therefore, only virtual states with $\ell = 2$ will be considered.

Because of their large amplitude at the impurity, electrons within the energy range of the virtual state will suffer strong resonant scattering. The phase shift of an electron whose energy is just greater than the energy of a bound state is π (Schiff[88]) and it decreases slowly as the energy increases. The phase shift of an electron whose energy lies at the bottom of the conduction band is 0, and as the energy increases through the virtual state, the phase shift increases rapidly, reaching a value of almost π at

high energies. This behaviour has been analysed in detail by Blandin and Friedel[89], and their plot of phase shift against energy for different strengths of the impurity potential is shown in Fig. 15. They assume a square potential well of depth V and radius 1.4 Å, and consider only the phase shifts for $\ell = 2$.

The potential V = 19.6 e.v. is just sufficient to capture a bound state.

fig 15

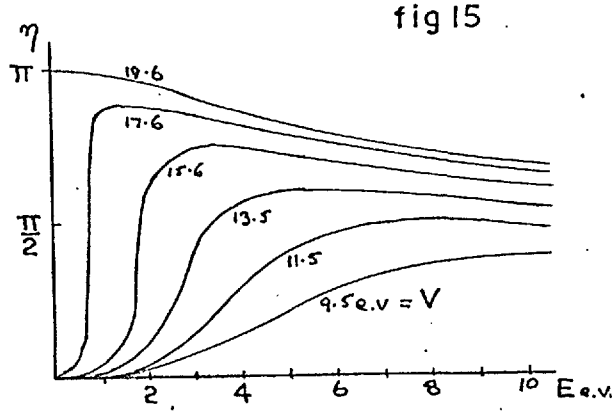

From Eq. 3.8 the density of states between E and E + dE may be written

$$n(E) = \frac{dZ}{dE} = \frac{2}{\pi} \sum_{\ell} (2\ell + 1) \frac{d\eta}{dE} \quad \ldots\ldots\ldots\ldots\ldots\ldots\ldots\ldots 3.11$$

Thus the density of states is proportional to the slope of the η - E curve, and this will therefore have a maximum value at the energy for which the curve has a point of inflection. It is convenient to take this energy Eo as the

centre of the virtual state. The width of the state may be defined as the difference between the energies for which the phase shift is $\eta = 3/2\ \eta$ (Eo) and $\eta = \frac{1}{2}\ \eta$(Eo). The above authors find that the width is approximately $\frac{1}{3}$ of the mean energy E_o of the virtual state, for $\ell = 2$, and also that Eo decreases with increasing impurity potential.

3.5 Magnetic and Non-magnetic Virtual States

Screening by means of the virtual state is of particular importance in dilute solutions of transition metals in normal metals. A self consistant impurity potential will be of such a strength that the position of the virtual state with respect to the Fermi level will ensure that approximately that part of the excess charge which in the free atom is screened by electrons of d-symmetry is screened by the $\ell = 2$ virtual state.

Friedel[90] explains the observed behaviour of the residual resistance of alloys of transition metals in Aℓ (Aℓ T alloys), shown in Fig. 16A.

fig16

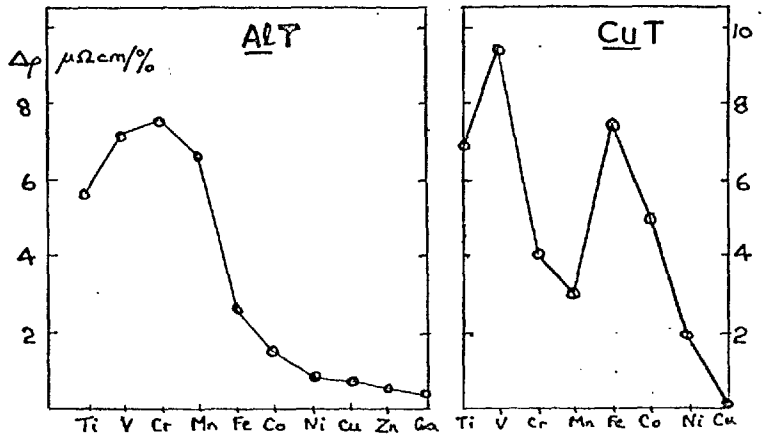

He assumes that as the atomic number increases, from Sc to Ni, the

virtual state is pulled down through the Fermi level, giving a strong maximum in the resonant scattering when the phase shift at the Fermi energy passes through $\pi/2$. If only one phase shift is assumed to be large, Eq. 3.10 can be written

$$\Delta\rho = \frac{4\pi c}{p k_F} \sum_{\ell} (2\ell + 1) \sin^2 \eta_\ell (k_F)$$

and the maximum value of $\Delta\rho$, assuming $p = 3$, $\ell = 2$ and $k_f = 1$ a.u., is 4.6 $\mu\Omega$ cm / %.

The room temperature thermopower is related to the quantity $\frac{1}{\Delta\rho} \frac{d}{dE} (\Delta\rho)$, and therefore to $\cot \eta \frac{d\eta}{dE}$. A variation consistant with this relation is observed experimentally, with the thermopower changing sign at Al Cr, and passing through a maximum at Al Fe.

Direct comparison with theory of the extra density of states at the Fermi energy by measurements of the electronic specific heat of these systems has not so far been possible because of the very low solubility of transition metals in Al. The large increase in γ (0.7 / e.v. %) for Cu Ni alloys found by Guthrie is, however, consistant with a screening of the d-electrons of Ni by a virtual state of width around 2.5 e.v.[89].

The residual resistance of dilute Cu T alloys is shown in Fig. 16B. Two peaks are visible, with a strong minimum at Mn. Friedel explains these

results by assuming that the virtual d state of Cu is split by exchange interactions into two broad, partially overlapping virtual states, one containing spin up electrons, and the other, spin down electrons. These two displaced states are now drawn down through the Fermi level, as the atomic number increases, giving the two maxima observed. The polarisation of the virtual bound state gives rise to a magnetised impurity, and the resistive behaviour is therefore consistent with the observation of magnetised impurity states in Cu T alloys, but not in Al T alloys. Using the observed magnetic moments in Cu T alloys to estimate the degree of polarisation, and the position of the virtual state with respect to the Fermi level, and assuming the Friedel sum rule, Daniel[91] has calculated values of the resistivity from Eq. 3.9. which are in good agreement with the experimental values shown in Fig. 16B.

Assuming that the decoupling of the spins is due entirely to exchange, and that crystal field splitting and coulomb correlation effects are negligable, Blandin and Friedel[89] give the conditions necessary for total, partial or zero splitting of the virtual state. Their detailed calculations give results that are similar to an earlier condition due to Friedel[90], that for total splitting,

$$p\Delta E > W \quad \ldots\ldots\ldots\ldots\ldots\ldots\ldots\ldots\ldots\ldots\ldots\ldots \quad 3.12$$

where p is the number of electrons or holes in the d virtual state, ΔE is the exchange coupling between two spins of equal

sign, and W is the width of the virtual state, and is approximately $\frac{1}{3} E_F$. This relation simply expresses the requirement that the exchange energy gained by splitting should be greater than the width of each virtual state. If this condition is not satisfied, the state will be unmagnetised, or be magnetised with a very small moment. Using this relation, assuming that $\Delta E = 0.8$ ev, and that each impurity gives one electron to the s or p conduction band, they have constructed a table showing the distribution of magnetised states among the normal metal - transition metal alloys. This is shown in Fig. 17. A magnetised state is only to be expected within the area bounded by the thick line. The symbols show whether or not an anomaly is in fact observed.

Fig 17

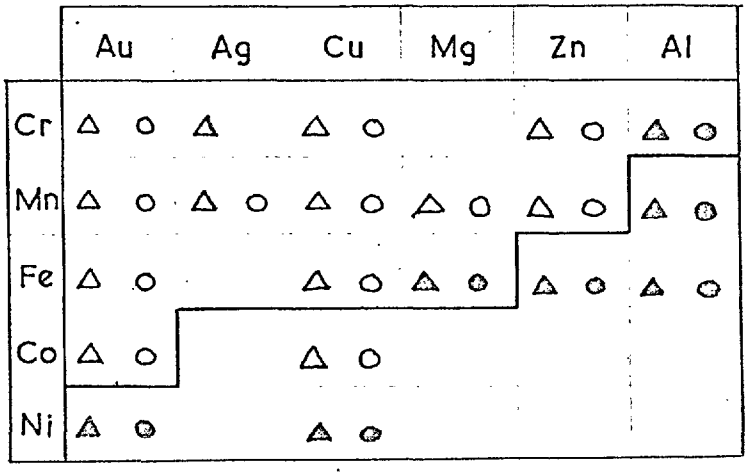

△ An anomaly has been observed in the specific heat

▲ No " " " " " " " " "

○ An " " " " " " resistance or susceptibility

● No " " " " " " " " "

The agreement between the predicted and actual distribution of magnetised states can be seen to be surprisingly good, considering the approximations that are involved in its derivation. Magnetised states are most likely when Cu, Ag or Au are solvents, because of their low Fermi energies, and correspondingly small values of W, (the density of states at the Fermi surface is presumably the significant quantity in determining the width, but Friedel assumes a free electron model throughout). They are not found in Al because of its large Fermi energy. Magnetised states occur most readily when Mn is the solute, as p takes its maximum value of 5.

3.6 Wolff[92] and Clogston[93]

Wolff[92] has discussed the formation of a virtual state, and the conditions necessary for its magnetisation, using an approach which is essentially a refinement of that of Friedel. The impurity potential V is assumed to scatter electrons from and to states of a single band, and it is shown that under certain circumstances the amplitude of the scattered waves may be large in a narrow energy range within the band, and thus form a virtual state.

Expanding the wave function in terms of Wannier functions derived from a single band, and assuming that the potential V is of such short range that it does not appreciably overlap Wannier functions centred on neighbouring atoms, and also does not mix states from different bands, Wolff

finds that the amplitude of the Wannier function centred on the impurity is given by

$$U(Ro) = \frac{e^{ik.Ro}}{1 - V_1 F(E) + i\pi V_1 n(E)} \quad \ldots\ldots\ldots\ldots\ldots 3.13$$

where V_1 is the matrix element of V between states within the band, and n(E) is the density of states of the band. The function F(E) depends on n(E), and is shown in Fig 18A for a typical density of states curve.

Fig 18

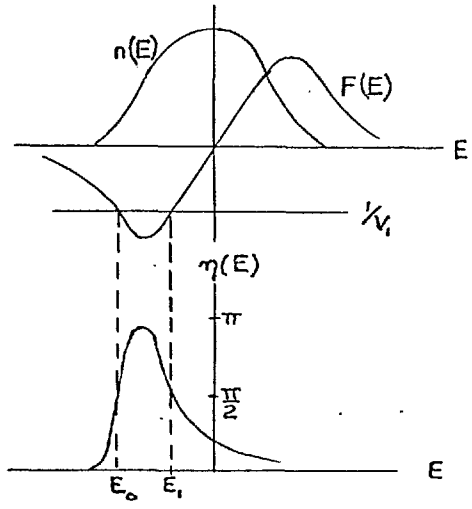

The amplitude U(Ro) will be a maximum when $1-V_1 F(E)$ is zero, that is, when the line $1/V_1$ intersects F(E) at the points A and B. Wolff

shows that the energy Eo of the point A may be considered to be the centre of the virtual state formed by the states of large amplitude of energies close to Eo. As V increases, the point A moves to lower energies. When it lies below the bottom of the band, n(E) is zero, U(Ro) is infinite, and the state is bound.

Using a similar approach, Clogston derived an expression for the phase shift as a function of energy,

$$\eta(E) = \tan^{-1} \frac{\pi\, n(E)}{F(E) - \frac{1}{V_1}} \qquad \ldots\ldots\ldots\ldots\ldots\ldots 3.4$$

This is shown for different values of V_1, in fig 18 B, and it can be seen that $\eta(E)$ passes through the value $\pi/2$ when $F(E) = 1/V_1$ that is, when U(Ro) is a maximum. Clogston concludes that the virtual state has been created in the region of Eo, and to conserve the numbers of states, has been removed from the vicinity of E_1.

The restriction of a single band limits the application of the model to cases for which the impurity and band states have the same symmetry, and is therefore not well suited to the problem of transition metal impurities in normal metals, though is possibly suited to the problem of th magnetic state of Fe dissolved in the s econd row transition metals, for which it was devised. Clogston also shows that for such a short range potential, only the $\ell=0$ phase shift is significant, and not more than one state can

be displaced below the Fermi level. The model is therefore better suited to the treatment of normal metal impurities than transition metal impurites.

Both authors then consider the conditions for the magnetisation of the virtual state, by methods which are basically equivalent. In Wolff's treatment, a small spin dependent potential $\Delta V +$ or $\Delta V -$ is added to V, to describe the scattering of electrons of spin up (+) and spin down (-). Equation 3.13 shows that the amplitude of the spin up and spin down states will now be different. These new wave functions are used to calculated the new Hartree-Fock field of the impurity. Here it is shown that theexchange interaction is just cancelled by the coulomb integral for states of parallel spin, and the energy of the spin state is entirely due to the coulomb repulsion of states of opposite spin. Thus the resulting change in the energy of the spin up electrons depends on the amplitude of the spin down electrons, which in turn depends on the original change in energy of the spin down electron ΔV_-. The equations are made self consistant by putting the resulting change of energy of the spin up electrons equal to $\Delta V+$.

An expression for $\Delta V+$ is therefore obtained in terms of ΔV_-, and a similar expression for ΔV_- in terms of $\Delta V+$. These equations are solved graphically, assuming that $\Delta V/V$ is small, and two sets of solutions may be found. i) a stable one with $\Delta V+ = \Delta V_-$ corresponds to an unmagnetised state, ii) two stable solutions $\Delta V+ \neq \Delta V_-$, and an unstable solution $\Delta V+ = \Delta V_-$. This situation corresponds to a magnetised state. Taking as the criterion for magnetisation that $\frac{d(\Delta V+)}{d(\Delta V_-)} > 1$ it is shown that

this is equivalent to

$$\left| \frac{J}{\pi^2 V^4 \, n(E) \, F^1} \right| > \frac{\Delta^2 + (E_F - E_o)^2}{\Delta^2} \quad \ldots\ldots\ldots 3.15$$

where J is the coulomb integral between opposite spins, F^1 is $\frac{d\,F(E)}{dE}$, Δ is the width of the virtual state, defined by $\Delta = \frac{\pi n(E)}{F^1}$, and Eo is the energy of the centre of the virtual state. The conditions that are most favourable for the formation of a magnetised state are 1) that Eo should be close to E_F, 2) n(E) should be low, and hence the state will be narrow.

3.7 Anderson[94]

Anderson[94] considers the situation in which the symmetry of the impurity state is different from that of the band states, and assumes, therefore, that the impurity state retains its atomic charactor (assumed to be of d-symmetry). This state is then broadened by interaction with band states, and may be split by exchange self energy. The conditions necessary for magnetisation are established.

The theory starts with an electron of spin $\uparrow$ in a singly degenerate atomic d-state, with energy E, assumed to be below the Fermi level of the conduction band. For reasons which were outlined in the previous section, only the coulomb repulsion U between electrons of opposite spin is effective, and this quantity may be particularly large (up to 10 e.v.) in the present case of a localised atomic state as screening by the conduction electrons

will be small. Thus the energy of a d-electron with spin $\downarrow$ will be E + U. If this energy lies above the Fermi level, it will not be occupied, and the impurity will be magnetised. This situation is shown in Fig. 19.

Fig 19

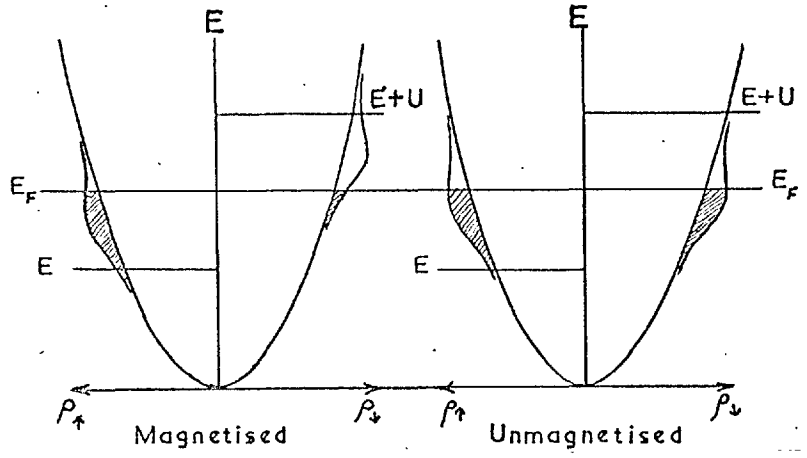

The effect of s-d interaction between band states and the localised state is to broaden the impurity state. This will reduce the number of electrons in the spin $\uparrow$ state, and increase the number in the spin $\downarrow$ state, thus reducing the magnetic moment. Because of the interaction between electrons in opposite spin states, this will effect the energies of the spin states, raising the spin $\uparrow$ state from E to E+ U δn, and lowering the spin $\downarrow$ state from E + U to E + U - Uδn. δn is the number of electrons transferred from the $\uparrow$ to the $\downarrow$ state, and it increases with the density of states of the free electrons, and with the s-d interaction. It also increases as the energy difference between $\uparrow$ and $\downarrow$ states decreases, and therefore if either of the other parameters leads to an

increase in δn, the energy difference decreases cooperatively, and the state ceases to be magnetised.

As in the previous theory, a self consistant calculation of the Hartree Fock field leads to two equations, which contain the dependence of the number of up spins $n_\uparrow$ on the number of down spins $n_\downarrow$, and vice versa. These must be solved simultaneously by graphical methods.

$$n_\uparrow = \frac{1}{\pi} \operatorname{Cot}^{-1} \frac{E-E_F + Un_\downarrow}{\Delta} \quad \ldots\ldots\ldots\ldots\ldots 3.16$$

$$n_\downarrow = \frac{1}{\pi} \operatorname{Cot}^{-1} \frac{E-E_F + Un_\uparrow}{\Delta} \quad \ldots\ldots\ldots\ldots\ldots 3.17$$

Where Δ, the width of the level, is given by

$$\Delta = \pi \langle V^2 \rangle n(E) \quad \ldots\ldots\ldots\ldots\ldots\ldots\ldots\ldots 3.18$$

and $\langle V^2 \rangle$ is the matrix element associated with the s-d interaction between the localised and band states. The width therefore increases with the density of states of the conduction electrons, and the strength of the s-d interaction. The density of states in the broadened d-state of spin $\uparrow$ is given by

$$\rho_{\uparrow}(E) = \frac{1}{\pi} \frac{\Delta}{(E-Eo)^2 + \Delta^2} \quad \ldots\ldots\ldots\ldots\ldots\ldots 3.19$$

where Eo is the centre of the extended spin $\uparrow$ state, given by

$$Eo = E + n_{\downarrow} U$$

The conditions for the magnetisation of the impurity state are found by solving equations 3.16 and 3.17. Writing $x = \frac{E_F - E}{U}$ and $y = \frac{\Delta\pi}{U}$, a magnetised state is found to be possible within the shaded area of Fig 20.

Fig 20

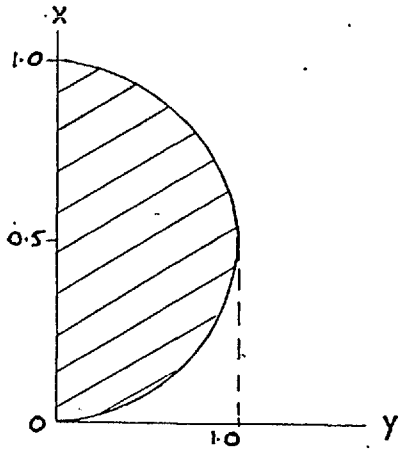

Conditions are most favourable when $x = 0.5$, that is, when E and E + U are symmetrically placed about the Fermi level. They are most

unfavourable when $x = 0$ or 1, that is when either E or E+U lies at the Fermilevel (the virtual state will then be completely above or completely below the Fermi level.) A magnetised state cannot occur if $\Delta > U/\pi$. (This condition is similar to that of Friedel, page 105).

U may be of the order of 10 e.v., and n(E) around 0.3/e.v. atom. If V is taken to be 1 e.v. Δ is then approximately 1 e.v. Thus $y = \frac{\pi\Delta}{U} \sim 0.3$, and magnetisation is possible.

The conditions will be most favourable for Mn, as the virtual state will lie symmetrically placed about the Fermi level in order to provide a screening charge of five electrons. Thus almost complete polarisation of the virtual state may be expected for Mn. For atoms like Co, or Ni, the state will lie almost entirely below the Fermi level to provide sufficient screening, and the conditions for polarisation are very poor. A non-magnetised state is therefore to be expected, though a ciritical intermediate state may exist for Co.

B. INTERACTIONS BETWEEN MAGNETIC STATES

3.8 Introduction

The experimental properties discussed in Chapters 1 and 2 suggest that interactions exist between the magnetised impurities in many of the systems. The magnitude of the interaction is too large to be accounted

for by magnetic dipole - dipole coupling, and is observed in systems which are too dilute for direct or super-exchange between impurites to be significant as entropy measurements suggest that all of the impurities are ordered at very low temperatures. It is also found that the temperature of the region of magnetic ordering increases approximately linearly with concentration to very low concentrations. Any interaction with a finite range, would lead to a finite cut off concentration below which ordering of all of the impurities is impossible. A long range interaction is required to explain this complete ordering. As these large interactions are not observed in non-conducting crystals containing magnetic impurities, the conduction electrons of the metal are certainly involved in the interaction mechanism.

3.9 Yosida[95]

Zener[96] proposed that the ferromagnetic coupling between atomic moments in pure ferromagnetic metals may be due to a uniform polarisation of the conduction electron spins, induced by exchange interactions with the impurity. The uniform polarisation resulted from a first order perturbation calculation of the energy of the system assuming an exchange interaction between the conduction electrons and a localised atomic d-orbital.

Yosida[95] showed that if the first order perturbation of the conduction electron wavefunction is also included, the conduction electron

polarisation is no longer uniform, but that the charge density for each spin direction oscillates with rapidly decreasing amplitude at large distances from the impurity. As the sign of the exchange interaction depends on the relative directions of conduction electron spin and impurity spin, the oscillating spin densities for the two spin directions are out of phase, and a total spin density is produced which oscillates in sign and magnitude with increasing distance from the impurity. The sign and magnitude of the interaction with a second impurity is then calculated from the magnitude of the spin density at the second impurity, and the s-d exchange energy.

Yosida finds an expression for the spin density of up and down spins at a distance r from an impurity with spin up.

$$\rho\pm\ (r) \;=\; \frac{n}{V}\left[1 \mp 18\pi \left(\frac{n}{N}\right) \frac{JS_1}{E_F} F(2k_F r)\right] \quad \ldots\ldots\ldots 3.20$$

Where 2n is the total number of conduction electrons, V is the total volume, N is the total number of lattice points. Thus $\frac{n}{V}$ and $\frac{n}{N}$ are the number of conduction electrons of one spin direction per unit volume, and per atom, respectively. $F(x) = \frac{x\,\mathrm{Cos}x - \mathrm{Sin}x}{x^4}$. and is shown in Fig 13. J is an s-d exchange integral, and S_1 is the z component of the impurity spin. The form of this equation is identical to eq 3.3 due to Friedel, apart from a numerical factor of 4 which arises from the different definitions of J and U.

The function $F(x)$ goes to infinity as $x \to 0$, and therefore gives an infinite spin density at the origine. This is in disagreement with Knight shift measurements on Mn nuclei in Cu. (Owen et al). This behaviour at low x arises because the exchange integral $J(q)$ has been put equal to the constant J for all q. (q is the change in wavenumber of the scattered electron). $J(q)$ is expected to decrease as q increases, and if $J(q)$ is arbitrarily cut off at $q = 2k_F$ by assuming that the quantity

$$J(q)\, f(q) = 2J \quad \text{for} \quad q < 2k_F$$

$$= 0 \quad \text{for} \quad q > 2k_F$$

where $$f(q) = 1 + \frac{4k_F^2 - q^2}{4k_F q} \log \left| \frac{2k_F + q}{2k_F - q} \right|$$

equation 3.20 becomes

$$\rho \pm (r) = \frac{n}{V} \left[1 \mp 36 \left(\frac{n}{N}\right) \frac{J g_1}{E_F} \left\{ 2k_F r\, F(2k_F r) \right\} \right] \quad \ldots\ldots 3.21$$

This is now finite at r=0, but decreases as $1/r^2$ at large distances, in contrast to the $1/r^3$ dependence in eq. 3.20. Thus it appears that the range of the spin polarisation depends critically on the q dependence

of J(q). Abrikosov and Gorkov[97] have criticised Yosidas analysis, asserting that if the conditions for a uniform polarisation are required, only the values of q close to zero need be considered. This is effectively Zener's approximation, and leads directly to a uniform polarisation.

The interaction with a second spin S_2 at a distance R from the first can now be found, assuming a spin polarisation of the form 3.20. This gives

$$E = 18\pi \left(\frac{n}{N}\right)^2 \frac{J^2}{E_F} \; S_1 . S_2 \; F(2k_F \; R) \quad \ldots\ldots\ldots\ldots\ldots\ldots \quad 3.22$$

This result is identical to an earlier relation due to Rudermann and Kittel[98], who calculate the spin polarisation due to the hyperfine interaction between conduction electrons and nuclear spins, and the consequent interaction between nuclear spins. The result will therefore be referred to as the Rudermann-Kittel-Yosida (RKY) interaction.

If R is taken to be the nearest neighbour distance, 2.55Å, in Cu, k_F = 0.72 a.u. $\simeq$ 1.4 x10^8 cm^{-1}, $F(2k_F R) = 2.2 \times 10^{-3}$. Taking $n/N = \frac{1}{2}$, E_F = 7e.v. and $S_1 = S_2 = 2$, and assuming J = 0.1e.v., Eq. 3.22 gives

$$E = 0.2 \times 10^{-3} \text{ e.v. } \left(\sim \frac{2^\circ K}{k}\right)$$

for the interaction between two nearest neighbour Mn atoms.

3.10 Blandin and Friedel[89]

Instead of considering the polarisation in the conduction electrons induced by exchange with a bound impurity state, as was considered by Yosida, Blandin and Friedel[89] assume that the strength of the self consistant impurity potential is such that the impurity is screened by the conduction electrons themselves, concentrated into a virtual bound state. They show that the spin density associated with this state oscillates in sign at large distances, and provides the long range coupling mechanism.

Eq. 3.6 shows the charge density of the conduction electrons at a large distance r from the centre of an impurity in terms of the phase shifts, η_ℓ. The selfconsistant potential, and therefore the phase shifts, depend on the sign of the electron spin. If the state is completely decoupled, with electrons of spin $\downarrow$ lying completely above the Fermi level, as for Mn, it may be assumed for all $k < k_F$, the phase shifts $\eta_\downarrow$ of the spin $\downarrow$ electrons are zero. It is also assumed that only the $\ell = 2$ phase shifts for the spin $\uparrow$ electrons are greater than zero.

They can then write $\Delta\rho_\downarrow = 0$, and from eq. 3.6

$$\Delta\rho_\uparrow = \frac{5}{4\pi^2 r^3} \int_0^{k_F} \sin\eta_2 \sin(2kr + \eta_2)\, 2r\,dk$$

η_2 is a function which increases rapidly from 0 to π on passing through the virtual state. Assuming a variation of η_2 with k of the form shown in fig 21

Fig 21

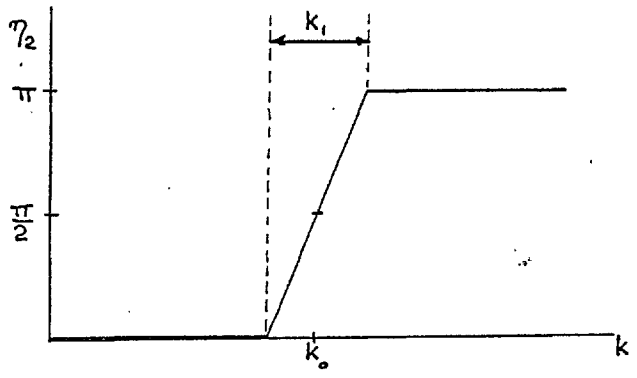

and taking k_o as the centre of the state, and k_1 as the width, then if k_F lies above the top of the state of spin ↑ and below the bottom of the state of spin ↓ ,

$$\Delta\rho_{\uparrow} = \frac{5}{4\pi r^3} \frac{\text{Sin } k_1 r \text{ Cos } 2 k_o r}{k_1 r + \pi} \quad \ldots\ldots\ldots\ldots\ldots\ldots 3.23$$

$\Delta\rho_{\uparrow}$ calculated from this expression is very much larger up to several times the interatomic distance, than the spin density calculated by Yosida. The reason for this is that the very short range potential considered by Yosida will give a rather small $\ell = 0$ phase shift ($\eta_o \sim 0.1$), and all other phase shifts will be zero. It is therefore quite incapable of holding the five charges needed to screen the Mn atom. The much extended, self consistant, potential associated with the virtual state, which does satisfy the sum rule, will produce a correspondingly larger polarisation of the conduction electrons. $\Delta\rho_{\uparrow}$ calculated from 3.23 does, however, decrease as $\frac{1}{r^4}$ at large distances, and therefore falls to zero more rapidly than the R.K.Y. polarisation.

The coupling between two spins at a distance R on the Blandin-Friedel

model is given by

$$E = \Delta\rho\ (R)\ \ v_A\ \ F \qquad \ldots\ldots\ldots\ldots\ldots\ldots\ldots\ldots\ 3.24$$

where v_A is the atomic volume of the second spin S, F is the s-d exchange energy, and may be obtained from the quantity J, as $F \sim J(S+\frac{1}{2})$.

Taking $v_A = 1.2 \times 10^{-23}$ cm^3, the atomic volume of the Cu atom, $k_o = 0.72$ a.u. and $k_1 = 0.15$ a.u. (equivalent to a width of 2 e.v.), and the same values for the constantsJ, S, R, that were used in the previous section, 3.24 gives for the energy of two nearest neighbour Mn spins a value of $E = 8 \times 10^{-3}$ e.v. $\frac{(\sim 100^\circ K)}{k}$.

3.11 Overhauser[99]

Overhauser[99] has proposed a mechanism that can lead to antiferromagnetic ordering, which is quite different from the mechanisms described above. He suggests that a single static spin density wave exists as an excitation of the conduction electron gas. Exchange interactions tend to orient each impurity spin parallel to the local direction of the spin density wave, and the inter action energy gained compensates for the energy required to create the wave. Because the spin density wave is a property of the electron gas and not the lattice, the wave length of the wave is incommensurate with the lattice parameters, and impurities therefore have a probability of experiencing effective fields of either sign, and of any magnitude between zero and some maximum value, depending on the amplitude of the spin density wave at the impurity. Overhauser shows that the amplitude of the spin density wave at the point R is given by

$$S(R) = bN\Sigma \quad \text{Cos } q.R \qquad \ldots\ldots\ldots\ldots\ldots\ldots\ 3.25$$

where N is the number of atoms per unit volume, bN is the maximum amplitude of the wave, and q is the wave number of the wave. This is shown to be made up of two waves of opposite spin, having equal amplitude but opposite phase, thus leaving the charge density uniform.

Overhauser then examines the conditions necessary for the stability of such a wave, and finds that this is possible for a well defined value of q if the electron-electron exchange is sufficiently strong. He also shows that in the Hartree Fock approximation, the kinetic energy of the wave is just balanced by the exchange energy gained, and the energy of the state is therefore zero. If correlation energy is included, the energy of the state is positive, so that it is no longer the ground state of the electron gas of a pure metal. He shows that the energy density of the wave is

$$W(b) = \frac{8n\,C'b^2}{9\,\xi\,\eta^2} \qquad \ldots\ldots\ldots\ldots\ldots\ldots\ldots\ldots\ldots\ldots\ldots\ldots\ldots\ldots\ldots\ldots 3.26$$

where C' is the correlation energy per electron, n is the number of electrons per unit volume, ξ is a constant of the order of 1 and η is the number of conduction electrons per atom.

Writing the Hamiltonion for the exchange interaction between the spin density wave of amplitude s_i at r_i and the impurity spin S_j at R_j as

$$H^1 = -\frac{G}{N}\sum_{i\,j} s_i \cdot S_j\, \delta(r_i - R_j)$$

where G is the s-d interaction, the effective field may be written

$$H_j = G\,b\,\varepsilon\,\mathrm{Cos}\,q \cdot R_j \qquad \ldots\ldots\ldots\ldots\ldots\ldots\ldots\ldots\ldots\ldots\ldots\ldots\ldots\ldots 3.27$$

Fields will therefore be distributed over lattice points with a probability given by

$$P(H) = \frac{1}{\pi} \frac{1}{(G^2b^2 - H^2)^{\frac{1}{2}}} \quad \ldots\ldots\ldots\ldots\ldots\ldots\ldots 3.28$$

for all H between + Gb and - Gb, and P (H) = 0 for $|H| > Gb$. P (H) against H is shown in Fig 22. The specific heat of the impurities, calculated on this model, will be discussed in section 4.17.

fig 22

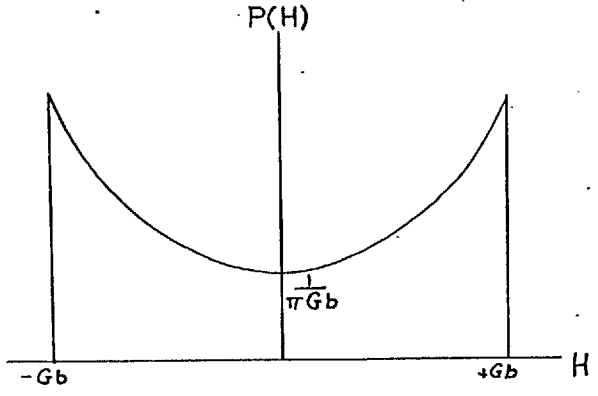

CHAPTER 4

THEORETICAL MODELS FOR VARIOUS PHYSICAL PROPERTIES

4.1 General Introduction

The experimental survey in chapters 1 and 2 showed that in those dilute alloys in which the solute atom is magnetised, the low temperature transport properties have an anomalous temperature dependence, there is a negative component in the magnetoresistance, and a large excess specific heat. In systems in which the solute atoms are not magnetised, these effects are not observed. It is not surprising, therefore, that all the theoretical models that follow account for the anomalous behaviour in terms of the interaction between the solute spin and the conduction electrons. It has been shown in the previous section how this interaction leads first to the existance of magnetised impurity states, and then to the interaction between them. The calculation of the properties of the system presents many formidable problems, of which the way to include the random distribution of the solute atoms and therefore the random strength of interaction between them is certainly the most severe, and is the major distinguishing feature between the models.

A - MAGNETIC SUSCEPTIBILITY

4.2 Introduction

The experimental results to be accounted for are as follows.

1) The Curie Weiss behaviour at high temperatures.

2) An effective moment which in some cases varies with the concentration in the intermediate temperature range, but which becomes concentration independent at very high temperatures.

3) A paramagnetic Curie temperature T_c which may be of either sign, but which generally increases with concentration.

4) A broad low temperature maximum in the susceptibility of more concentrated alloys at a temperature T_n, which increases with concentration.

Any model which treats the magnetic states as distinguishable and therefore uses Maxwell Boltzman statistics, predicts that $1/\chi$ is linear in T at temperatures large compared with the interaction energy between impurities, and has a slope which is proportional to $1/\mu^2$, where μ is the magnetic moment of the impurity. The high temperature Curie constant and the low temperature susceptibility depends critically, however, on the assumptions made in the model concerning the sign and range of the interactions, and distribution of the particles.

4.3 Owen, Browne, Arp and Kip[23]

The simplest way of including the interaction between the impurities is to assume the existence of a molecular field acting on each impurity, proportional to the magnetisation of the system, (for low concentrations this is equivalent to assuming an interaction of very long range). Owen, Browne, Arp and Kip suggest that the observed susceptibility behaviour of Cu Mn can be accounted for by assuming the existance of two types of magnetic sites, labelled A and B, such that A-A interactions are short range ferromagnetic, and A-B interactions are short range antiferromagnetic. They also included a small uniform polarisation of the conduction electrons, giving a small ferromagnetic interaction.

They had originally expected this latter contribution to be the

dominant one, but the absence of a Knight shift in the Mn resonance line indicated that such a uniform polarisation was at most very small. They were not aware of the possibility of a long range oscillating interaction of the R.K.Y. type . From a simple molecular field calculation they were able to show that a positive high temperature Curie temperature was consistant with a low temperature antiferromagnetic transition, if the ferromagnetic coupling was very large compared with the antiferromagnetic coupling. In this case the restriction of the sublattices isno longer essential, and the system may be replaced by the more physically acceptable one of domains relatively rich in Mn atoms, in which the Mn atoms are coupled by short range ferromagnetic interactions, with a weak antiferromagnetic coupling between the domains. At high temperatures the system is completely disordered, and the most important interactions are the short range ferromagnetic ones, giving the positive T_c. At a temperature close to T_c, spontaneous alignment of spins within a domain occurs, and antiferromagnetic ordering of the domain results at a temperature T_n close to T_c.

Such a cooperative alignment of sublattices would naturally lead to a sharp Neel temperature. The much broader transition which occurs is attributed to the random nature of the alloy and consequent distribution of molecular fields. Although it is not suggested by Owen et al, the strong short range ferromagnetic interaction and weak antiferromagnetic interaction could be of the R.K.Y. type, the sign of which varies rapidly with distance .

4.4 Dekker[100]

Dekker has attempted to calculate the susceptibility of a system in

which the sign and magnitude of the interaction depends on the distance between impurities. He assumes that nearest neighbour (n.n.) solute atoms are coupled antiferromagnetically with strength θ_A and that more distant neighbours are coupled ferromagnetically with a strength θ_F which decreases rapidly with distance. He then calculates the number of nearest neighbour pairs, next nearest neighbour (n.n.n.) pairs and isolated solute atoms (those with no n.n. or n.n.n. impurites) as a function of concentration, assuming a f.c.c. lattice.

At high temperatures the system is completely disordered and only n.n. antiferromagnetic coupling and n.n.n. ferromagnetic coupling need be considered. A positive Curie temperature T_c is then only possible if $\theta_F > 2\theta_A$. T_c is proportional to concentration at very low concentrations, but significant departures are expected at concentrations greater than $\sim$ 1%, T_c increasing less rapidly than c.

As the temperature is reduced, the n.n. and n.n.n. pairs are aligned, and isolated atoms become aligned by the ferromagnetic interaction with distant neighbours. These then form ferromagnetic domains, coupled antiferromagnetically by n.n. pairs. A very simplified model (linear chain) shows that such a system will exhibit a broad maximum in the susceptibility. Dekker shows that in order that the susceptibility maximum should not be lost in the increasing paramagnetic contribution of the isolated spins as T is reduced, the strength of the interaction must be a few per cent of θ_A or θ_F up to at least the seventh nearest neighbours, that is, at approximately three times the n.n. distance. The origin of the broad susceptibility maximum on this model is that the antiferromagnetic interactions between domains are independent of

one another, and do not increase cooperatively as on the molecular field model.

4.5 Blandin and Friedel[89]

Blandin and Friedel have assumed a long range oscillating interaction between impurities of the type described in section 3.10 (due to long range oscillations in the spin density of a magnetised virtual state). The field at any point in the lattice may therefore be in any direction, and of any magnitude between zero and some maximum value. At low temperatures, the spins will be frozen into a kind of random antiferromagnetic structure, with each spin oriented along its local magnetic field.

At high temperatures, using the statistical method of the Opechovski[101], they find a series expansion for $1/\chi$ in terms of T. (χ is the susceptibility per atom).

$$1/\chi = \frac{3k}{4g^2\mu_B^2 S(S+1)} \left[T - \frac{yJ}{2k} + \frac{y(y+1)I^2}{4k^2T} + O\left(\frac{1}{T^2}\right) \right] \quad \ldots 4.1$$

Where $y = 4/3\ S(S+1)$

$$J = \sum_B J_{OB}$$

$$I^2 = \sum_B J_{OB}^2$$ and J_{OB} is the exchange integral between the central impurity at O and another impurity at B, such that the exchange energy is $-J_{OB}\ S_o \cdot S_B$. The second term in the brackets is the Curie temperature T_c, and as J is shown to be positive (it is dominated by the interaction between Mn atoms which are nearest neighbours, which is positive), Tc is positive and proportional to the concentration, and of a magnitude which is inr easonable agreement with experiment.

The third term in the brackets arises from the fluctuations in the internal field, and is always positive, and therefore reduces the susceptibility by an amount which increases as T decreases.

Because of the strong positive interaction between impurities which are nearest neighbours, all nearest neighbour pairs of spins S can be considered to be rigidly aligned with total spin 2S at low temperatures. The low temperature magnetisation is calculated by a molecular field theory assuming the existance of Nc (1-cZ) impurities of spin S, and $Nc^2 \frac{Z}{2}$ nearest neighbour pairs of spin 2S, where Z is the number of nearest neighbours (twelve in the f.c.c. lattice). This yields a sharp Neel temperature T_n given by

$$kT_n = \frac{4}{3} Nc\, n\mu_b^2\, S(S+1)\, (1+ \frac{S}{S+1}\ cZ)$$

where n is a molecular field coefficient.

The second term in the brackets is due to the pairs of spins, and is of the order of 0.20 for c = 0.05. The Neel temperature is therefore proportional to c at low concentrations.

An effective number of neighbours required to give a value n appropriate to the experimental values of T_n can be calculated assuming an interaction of the form given by equations 3.23 and 3.24. This shows that approximately the seven nearest impurity atoms are responsible for the molecular field on an impurity for c < 10%. As in all molecular field theories, the Neel temperature is sharp, and the observed broad peak is attributed to a spread in internal fields.

4.6 Sato Arrott and Kikuchi[102]

Sato et al discuss the various statistical methods that have been

applied to the determination of the magnetic properties of random magnetic alloys, and consider their relevance to dilute magnetic alloys with only short range forces. They conclude that a molecular field approach based on short range interactions between sublattices, is not applicable to very dilute systems, as this gives equal weight to the interactions between allpairs on neighbouring sublattices, independent of their separation. Thus long range cooperative ordering is impossible in very dilute systems assuming interactions between nearest neighbours only.

In Bethe's method, only nearest neighbour interactions are considered, and the possible fluctuations in the field at a central spin is calculated, as a result of all possible orientations of the nearest neighbour spins. Extending this method to the present problem, Sato et al assume that the co-ordination number of each impurity is cZ, where c is the concentration, and Z is the lattice coordination number. Thus they do not consider random fluctuations in the density of impurities. Applying Bethe's results they find that the temperature at which $1/\chi = 0$ is only greater than zero if $cZ > 2$, that is long range ordering can only occur if each impurity has at least two nearest neighbour impurities. If $cZ < 2$, $1/\chi = 0$ only at $T = 0$. The Curie temperature in the limit of very high temperatures is, however, the same as on the Curie Weiss model. In low concentration alloys pronounced curvature of the $1/\chi$ against T curve is necessary at low temperatures to satisfy both of these conditions, even though there is no long range ordering. In this way, Sato et al account for the apparent variation of moment with concentration found in the Cu Fe and Au Fe systems.

The dramatic change in the magnetic behaviour of Au Fe at concentrations above 11% Fe is consistentwith the above model. In this high concentration

region, long range order exists because of short range ferromagnetic interactions between iron atoms. The condition cZ > 2 gives c>17% for the f.c.c. lattice, which is in reasonable agreement with the critical concentration found. Similar long range ferromagnetism at high concentrations is also observed in the Au Mn system.

At concentrations below 11%, the magnetic behaviour suggests long range antiferromagnetic ordering, with ordering apparently occuring for arbitrarily small concentrations. Evidently a long range interaction is required to explain this. The small remenant magnetisation observed in the low concentration region, is possibly due to cooperative ferromagnetic ordering of small clusters of ∴ Fe atoms under the action of these short range forces.

B - RESISTANCE AND MAGNETORESISTANCE

4.7 Introduction

The early theories of the low temperature resistance anomalies (Korringa and Gerritsen[103], and Schmitt[104]) soughtto account for the resistance minimum and maximum as one phenomenon, whereas in later theories, these have been considered separately. The theories of Schmitt and Jacobs[25], and Yosida[105], yield a resistance which decreases as T decreases, whilst those of Overhauser and Brailsford[106], Dekker[107], and Kondo[108] lead to an increasing resistance with decreasing temperature. Combinations of the later theories, and the addition of normal phononscattering, are therefore needed to provide the resistance minimum and maximum.

4.8 Korringa and Gerritsen[103]

Korringa and Gerritsen showed that a very energy dependent relaxation

time τ for conduction electrons with energies very close to the Fermi energy, could lead to resistive anomalies at low temperatures. (The residual resistance of normal alloys is temperature independent because the scattering cross section of the impurities is approximately independent of energy). In particular, if it is assumed that τ is zero in a small energy range containing the Fermi level, and finite at all other energies, a resistance minimum results. If τ is assumed to be zero only within a small energy range Δ centred around energies $\pm E_0$, a resistance minimum and maximum results. By a suitable choice of Δ and E_0, the experimental results can be reproduced very satisfactorily. The required values of Δ and E are very small, of the order of a few times 10^{-4} e.v. The required energy dependence of τ could be explained by the presence of localised impurity states with energies very close to the Fermi energy. These cannot be one electron states, as they would be broadened by resonance with the conduction states to widths of the order of 1 e.v. Korringa and Gerritsen therefore proposed that a cooperative interaction between the conduction electrons, stabilised by the impurity spins, could lead to a very narrow peak in the density of states close to the Fermi energy. No further theoretical justification for this model has been advanced.

4.9 Schmitt[104]

Schmitt suggested that if the degeneracy of the impurity levels is split by a ferromagnetic interaction between the impurities, and the elastic scattering cross section of the impurity ground state is greater than that of the excited states, then a resistance maximum and minimum would result.

Because of the increasing number of impurities in the ground state, elastic scattering will increase as the temperature falls, giving an increasing contribution to the resistance that will roughly follow the increasing magnetisation. As a cooperative increase in the molecular field is assumed below some transition temperature Tc, the shape of this contribution to the resistance will be a Brillouin function.

Inelastic scattering may occur, with reversal of the spin direction of the conduction electron and impurity spins. To conserve total spin, this can only take place when the two spins are anti-parallel. A contribution to the resistance which decreases rapidly with decreasing temperature, and which falls to zero at T=0, results from this inelastic scattering. This is because at $0^{o}K$ a scattering in which the electron loses energy in exciting the impurity is forbidden by the absence of empty electron states of lower energy. A scattering in which the electron gains energy from an impurity in an excited state is forbidden at $0^{o}K$ as all the impurities are in their ground states. As the temperature increases, inelastic scattering increases, and is effectively constant when the temperature is large compared with the energy splitting of the impurity levels. The decrease (known as freezing out) of inelastic scattering at low temperatures, which falls exponentially as T approaches zero, is the cause of the low temperature decrease in the resistance in all of the theories to be described. The combined effect of the competing processes assumed by Schmitt is a resistance that is constant above $T_{c'}$, increases rapidly as T falls below T_{c}, passes through a maximum, and decreases rapidly to zero as $T \rightarrow 0$.

4.10 Schmitt and Jacobs[25]

Schmitt and Jacobs assume the model considered by Owen et al[23], of ferromagnetic domains coupled antiferomagnetically, and include both inelastic scattering and spin dependent elastic scattering in calculating the temperature dependence of the resistance. They make the significant observation that as the experimental results indicate that the negative magnetoresistance $\Delta\rho(H)$ is proportional to I^2, where I is the total magnetisation of the sample, then in zero field, the average magnetisation in a region of the order of the electron mean free path must be zero. If the mean free path were shorter than the domain size, $\Delta\rho(H)$ would be proportional to M^2, where M is the domain magnetisation, and this would bear only an indirect relation to the total magnetisation of the sample. Such a condition may easily be satisfied for, say a Cu 1% Mn alloy, as the mean free path is around 200 Å, and the mean distance between impurities is 10Å.

With this assumption, Schmitt and Jacobs show that the temperature variation of the resistance in zero field depends only on the inelastic scattering, and the resistance therefore decreases monotonically with decreasing temperature.

Because of the changes in the populations of the spin up and spin down impurity states on the application of an external magnetic field, the elastic scattering of spin up and spin down conduction electrons will be effected, if the cross section D_1 for parallel spins is different from the cross section D_2 for anti-parallel spins. This leads to a reduction in the resistance by an amount $\Delta\rho$ proportional to I^2, where I is the relative magnetisation of the sample.

$$\frac{\Delta\rho}{\rho_T} = -\left(\frac{\rho_o}{\rho_T}\right)^2 \gamma^2 I^2 \qquad \ldots\ldots\ldots\ldots\ldots\ldots 4.2$$

Where ρ_o and ρ_T are the resistances in zero field at 0^oK and T^oK, and

$$\gamma = \frac{D_2 - D_1}{D_2 + D_1}$$

Thus the dependence of the magnetoresistance on I^2 is accounted for on this model, though the authors suggest that this dependence would be found on any similar model which included spin dependent elastic scattering. The temperature dependence of the coefficient of I^2 found for Cu Mn is not well accounted for however, as $\left(\frac{\rho_o}{\rho_T}\right)^2$ does not vary strongly with temperature, and γ^2 was assumed to be temperature independent.

4.11 Yosida[105]

Yosida has given a more detailed discussion of the low temperature resistance on the lines of Schmitt and Jacobs, taking into account both the spin independent and spin dependent elastic scattering and the inelastic spin flip scattering. The spin independent potential V arises from the screening charge on the impurity atom, whilst the spin dependent potential 2JS.s is due to the exchange between the impurity spin S and conduction electron spin s. This latter potential is of opposite sign for the two conduction electron spin directions, so that the effective potential seen by the up and down spins is different, and may be written

$$V - 2JS.s \qquad \ldots\ldots\ldots\ldots\ldots\ldots\ldots\ldots\ldots\ldots 4.3$$

The transition probability for elastic scattering from state $k \rightarrow k^1$ in

which the spin of conduction electron and impurity are unchanged is,

$$W(k\pm, m \rightarrow k'\pm, m) \propto | V_{kk'} \mp m J_{kk'} |^2$$

where m is the magnetic quantum number of the impurity spin and $V_{kk'}$ and $J_{kk'}$ are matrix elements of V and J between states k, k'. Thus the scattering probability depends on the direction of the conduction electron spin relative to the impurity spin. When this expression for the transition probability is summed over all impurity spin directions, it can be written in the form,

$$W = Wo \mp wI$$

where the negative sign is to be taken when the spins are parallel, and the positive sign when they are antiparallel. Wo depends on V^2 and J^2, and w depends on the cross term JV. I is the relative magnetisation. The resistance is then given by

$$R \propto \left[\frac{1}{Wo - wI} + \frac{1}{Wo + wI} \right]^{-1} \propto Wo - \frac{w^2}{Wo} I^2 \quad \ldots 4.4$$

Thus there is a negative magnetoresistance proportional to I^2 which has its origine in the spin dependence of the elastic scattering potential.

The transition probability for spin flip inelastic scattering can also be obtained from equation 4.3, and is found to decrease monatonically with decreasing T, and provides the temperature dependence of the resistance in zero field.

The detailed nature of the calcul tion makes it possible to check experimental results with the estimation of very few unknown parameters. It is found that a value of the exchange energy J, which is approximately twice as large as the value found in the free Mn atom, is required to explain the

magnitude of the resistance decrease in zero field at low temperatures. The theory predicts a saturation value of the magnetoresistance

$$\frac{\Delta\rho}{\rho} = -0.68 \text{ in infinite field}$$

The sharp decrease of the resistance below the Neel point, suggested by the theory, is a result of the use of molecular field model. Yosida emphasises that even though I, the total magnetisation, has gone to zero at temperatures above the Neel point, local fluctuationsin the magnetic field will continue to provide a resistance which increases with temperature up to temperatures considerably in excess of the Neel temperature. The temperature dependence of the resistance is therefore much more susceptible to short range order than is the magnetic susceptibility.

4.2 Overhauser and Brailsford[106]

Overhauser and Brailsford have shown that the degeneracy of the energy levels of a pair of nearest neighbour impurity atoms is split by the interaction between them and that if this interaction is ferromagnetic in sign, the scattering cross section of the ground state is larger than that of the excited states. This was the situation assumed arbitrarily by Schmitt[104], who showed that the resistance will increase as the temperature falls because of the increasing population of impurity pairs in the ground state.

In the presence of an interaction, $-WS_1 \cdot S_2$ between the pair of spins S_1 and S_2, the energy states of the pair are given by

$$W_I = \frac{W}{2}\left[2S(S+1) - I(I+1)\right]$$

where I takes all integral values between 0 and 2S. Each level has $(2I+1)$ -

fold degenerate. The scattering cross section of the pair increases as the degeneracy of the state, and therefore I, increases. If the interaction W is ferromagnetic, the ground state will have the largest value of I, and as the population of this state increases with decreasing temperature, the resistance increases, giving a resistance minimum.

Competing with this increasing contribution, is the decreasing inelastic scattering. Inclusion of the effects of interference between the scattering amplitudes from the two impurities, shows that under certain conditions the elastically scattered waves may interfere constructively, and the inelastically scattered waves interfere destructively. The resistance will then increase with decreasing temperature.

One obvious result of the description of the resistance minimum in terms of pairs of impurities is that its magnitude must depend on c^2. This is in disagreement with experimental results which show a linear or less than linear dependence on c. Overhauser and Brailsford suggest that the concentration dependence of their model may be improved by the inclusion of inelastic scattering effects from pairs, and single impurities coupled by a molecular field. It is, however, rather difficult to account for the depth of the minimum by considering pairs only.

Dekker[107] has also considered the scattering from neighbouring pairs of impurities and obtained results in general agreement with those of Overhauser and Brailsford.

4.13 Kondo[108]

Kondo agues that as the scattering processes leading to the resistance

minimum are still temperature dependent at temperatures far in excess of the resistance and susceptibility maxima in very dilute alloys, and that as the depth of the minimum is proportional to concentration, then the resistance minimum phenomenon must result from temperature dependent scattering from single, isolated ions, without the requirement of an internal field.

Assuming a spin dependent scattering potential J between the conduction electrons and the impurity, and complete degeneracy of the energy states of the impurity spin system, the scattering cross section is calculated to second Born approximation. First Born approximation gives a scattering probability that is independent of energy, and is a suitable approximation for nonmagnetic impurities, giving a temperature independent resistance. Second Born approximation considers the possibility of intermediate states in the scattering process, and for magnetic impurities these can lead to a scattering cross section which varies rapidly with energy.

Consider (for example) a scattering process in which the initial and final states of the conduction electron have spin up and are labelled by k+ and k^1+, and the initial and final spin of the impurity is M. The electron may first be scattered by the impurity into the empty spin down state q^1-, with the impurity spin being increased from M -> M + 1. The electron is then again scattered to a spin up state k^1 +, and the impurity spin is reduced from M + 1 -> M.

An alternative path between the initial and final states is also possible. An electron of spin down from the Fermi sea, denoted by q-, may be scattered by the impurity into a state k^1+, and the impurity spin is decreased from M -> M -1. The conduction electron in the state k+ is then scattered into

the empty state q-, and the impurity spin increases from M - 1 -> M.

The matrix elements for these two paths are found to be different, and because of the dependence of the paths on the occupation of the states q- and q^1-, they also contain a factor f(q), where f(q) is the Fermi function. Matrix elements are found for all possible intermediate paths and are summed over all values of M, and all values of q. This yields a transition probability between the states k and k^1.

$$W(k+ \rightarrow k^1+) = \left[\frac{2\pi J^2}{3\hbar N} \; S(S+1)\, c \right] \left[1 + 4J\, g(E_k) \right] \times \delta (E_k - E_k^1) \quad . . \; 4.5$$

the function $g(E_k)$ is given by

$$g(E_k) = \frac{1}{N} \sum_q \frac{f(q)}{E_q - E_k} \quad . . . . . \; 4.6$$

A similar analysis for the case when the spin of the conduction electron is reversed gives a scattering probability W(k + -> k^1 -) which is twice the magnitude given by eq. 4.5

At T = 0, f(q) = 1 if $q < k_F$, and 0 if $q > k_F$, where k_F is the fermi wave number, and $g(E_k)$ is readily shown to be

$$g(E_k) = \frac{3Z}{2E_F} \left(1 + \frac{k}{2k_F} \log \left| \frac{k_F - k}{k_F + k} \right| \right) \quad \text{at } T = 0 \quad . . . . . \; 4.7$$

where Z is the number of conduction electrons / atom. The singularity in the scattering probability at $k = k_F$ is a result of the sharpness of the Fermi surface at T = 0.

At higher temperatures, the resistance is calculated by summing W(k) over all k, which involves mainly those electrons which lie within a range

of the order of kT of the Fermi energy. The logarithmic temperature dependence of the resistance is evident from equation 4.7 as the average value of $(k - k_F)$ for thermally excited electrons, is proportional to T. It is also evident from equations 4.5 and 4.7 that the resistance will increase with decreasing temperature only if J is negative.

A careful analysis shows that the resistivity can be written

$$\rho_{total} = \rho_L + c\rho_A + c\rho_m \left[1 + \frac{3Z\,J}{E_F} \log T \right] \quad \ldots\ldots\ldots\ldots 4.8$$

where ρ_L is the resistivity of the pure metal ρ_A is the resistance due to spin indepent coulomb scattering, Z is the number of conduction electrons per atom, c is the concentration and quantity $c\rho_m \left(1 + \frac{3ZJ}{E_F} \log T\right)$ is the contribution from spin dependent scattering described above. The logarithmic temperature dependence and the linear concentration dependence are in good agreement with the results for very dilute Au Fe in the limited temperature range below the resistance minimum and well above the resistance maximum. It does not describe satisfactorily the temperature dependence of the Cu Fe resistance below the minimum. From Knook's[15] results on the resistance of Cu Fe, Kondo deduces a value for J of -0.15 e.v., and from Macdonald's[13] results on Au Fe he finds a value of J = -0.25 e.v.

Possible objections to Kondo's approach are his use of perturbation theory to a system on which the interaction is strong and of short range and also the requirement of a negative value for J. J is generally assumed to be positive, but Kondo has shown that it can take negative values when strong mixing of conduction electrons and orbital d- electrons occurs.

Another difficulty is that the magnetic and specific heat results suggest that the degeneracy of the spin system is certainly removed up to temperatures at least as high as the resistance minimum even in rather dilute alloys, and Kondo suggests that when this degeneracy is removed, the resistance becomes constant. (This prevents the resistancebecoming infinite at $T = 0$).

C - THERMOELECTRIC POWER

4.14 Introduction

It may be shown (Mott and Jones 1936) that the thermopower due to elastic scattering can be written

$$S = \frac{\pi^2 k^2 T}{3e} \frac{\partial}{\partial E} \ln \sigma (E) \quad \ldots\ldots\ldots\ldots\ldots\ldots\ldots 4.9$$

if $\sigma(E)$ varies only slowly with energy. $\sigma(E)$ is the electrical conductivity that the metal would have, at absolute zero, if the Fermi level came at the energy E.

These conditions are met in electron phonon scattering in pure metals at high temperatures. In this case $S \sim \frac{kT}{E_F} \times \frac{k}{e}$. As $k/e \sim 86\ \mu v/^{\circ}K$. S will be of the order of 10^{-3} T $\mu v/^{\circ}K$. This is the order of magnitude observed for normal metals. In the case of inelastic scattering, or of a relaxation time that varies very rapidly with energy, eq 4.9 no longer holds. The rate of change of relaxation time at the Fermi energy is still the important quantity in determining the thermopower as can be seen from very general physical arguments. Several authors have sought to explain the anomalous thermopowers on the basis of the rapidly varying relaxation time of conduction electrons at the Fermi energy which is inherent in all of the theories of

the low temperature resistance anomalies.

4.15 De Vrooman and Potters[109]

De Vrooman and Potters have analysed in detail the thermo power anomaly to be expected from the model considered by Yosida[105] in his discussion of the low temperature decrease in resistance. They assume that the degeneracy of the magnetic impurity state is removed by an internal field, and that the conduction electrons interact with the impurities via a spin independent elastic scattering, and also inelastic spin flip scattering.

Elastic scattering can be shown to vary only slowly with the energy of the conduction electron, but because of the dependence of inelastic scattering on the occupation of the conduction electron and ion states, the relaxation time for inelastic scattering depends strongly on the energy of the conduction electron, (this led to the rapid fall in resistance with decreasing temperature in Yosida's theory). For a conduction electron with spin parallel to the excited state spin direction of the impurity, this relaxation time increases rapidly as its energy passes through the Fermi level. This is because to conserve spin, it can only scatter inelastically from an ion in the ground state, and thus lose energy, and this requires a vacant energy level at lower energies. The opposite is the case for a conduction electron whose spin is in the opposite direction. Thus the final relaxation time, although varying rapidly with energy, is symmetrical about the Fermi energy, and gives a zero thermopower. In the case of a molecular field with a unique direction, the elastic scattering for conduction electron spins of one direction will be different from that of spins of the other direction, because of the cross terms between the spin dependent and spin independent scattering potential

discussed in Yosida's theory of the magnetoresistance. The inclusion of these terms will tend to make the total relaxation time asymmetrical about the Fermi energy and a thermopower approaching the maximum possible value $k/e = 86\ \mu v / {}^{o}K$ is possible under favourable circumstances. However, if an antiferromagnetic molecular field couples the spins and thus the impurity spin directions are random, the elastic scattering, averaged over many scatterings, becomes the same for both spin directions and the thermopower is zero. Intermediate cases are possible if the number of up impurity spins differs from the number of down spins.

The thermopower is found on such a model to decrease to zero exponentially as $T \rightarrow 0$, because of the freezing out of the inelastic scattering, and falls as $1/T^2$ at very high temperatures. The temperature dependence is therefore similar to that of the specific heat of the ions themselves, on the molecular field model.

The general features necessary for a large thermopower, which emerge from this treatment, and which appear to be common to all the current theories, are an inelastic scattering of electrons of mainly one spin direction, this asymmetry of the electron spin scattering being due (possibly) to spin dependent elastic scattering. Thus it is possible to generate large thermopowers using models of the Yosida type, though it is not easy to see how they can be reconciled with Schmitt and Jacob's[25] criterion of a magnetisation which is zero over a distance of the order of an electron mean free path.

Other models, such as that of Overhauser and Brailsford[106], give a relaxation time which varies only slowly with energy, and will not therefore yield large thermopowers. Kondo has suggested that his mechanism could produce

large thermopowers, but this is still in doubt.

D - SPECIFIC HEAT

4.16 Introduction

The significant features of the specific heat anomalies which current theories seek to explain are the concentration and temperature independence of C/T as T -> 0, and the concentration and temperature dependence at high temperatures.

The broad peak in the density of states near the Fermi level associated with the virtual bound state can only give an extra contribution to γ of the order of

$$\frac{\delta\gamma}{\gamma} \sim \frac{cZ}{W/\frac{p}{E_F}} \sim \frac{3cZ}{p}$$

where c is the concentration, Z is the valency difference of solute and solvent, p is the number of electrons per solvent atom, and W is the width of the virtual state, which is of the order of $\frac{1}{3} E_F$ (Friedel Section 3.4). Thus for Cu Ni, Z = 1, p = 1, $\therefore \frac{\delta\gamma}{\gamma} \sim 3\% / \%Ni$. This probably accounts for the rapid increase in γ with Ni concentration in Cu Ni alloy, where the magnetic susceptibility suggests that the solute atoms are not magnetised, but cannot account for the very large anomalies observed in the dilute magnetic alloys. These are generally attributed entirely to the ordering of the impurity spins in the local field in which they find themselves. The origine and distribution of the fields distinguishes the various theories.

4.17 Overhauser[99]

The static spin density wave theory of Overhauser has been discussed in section 3.11. It was shown that an effective field H acts on each impurity with a probability given by eq. 3.28, and shown in fig. 22,

$$P(H) = \frac{1}{\pi} \quad \frac{1}{(G^2 b^2 - H^2)^{\frac{1}{2}}}$$

The total energy of the system includes both the positive energy W(b) required to produce the wave of amplitude b, and the negative interaction energy of the solute spins with the spin density wave. Minimising the total energy with respect to b shows that b decreases with temperature as

$$b(T) = b(o)\left[1 - \left(\frac{T}{Tc}\right)^2\right]^{\frac{1}{2}} \qquad \text{for } T < Tc$$

$$= 0 \qquad T > Tc \qquad \ldots\ldots\ldots\ldots 4.10$$

where $$b(o) = \frac{9\,\xi\,\eta\,S\,G\,c}{8\pi C'} \qquad \ldots\ldots\ldots\ldots\ldots\ldots\ldots\ldots 4.11$$

and $$kTc = \frac{3\,\xi\,\eta\,S(S+1)\,G^2}{32\,C'}\,c \qquad \ldots\ldots\ldots\ldots\ldots\ldots\ldots\ldots 4.12$$

There is a finite value of P(o), and therefore $\mathcal{G}$ is proportional to T as T -> 0, and is given by

$$\frac{C}{T} = \frac{32\pi^2\,NC'k^2}{27\,\xi\,\eta\,(2S+1)\,G^2} = \gamma_o \quad \text{as } T \to 0 \qquad \ldots\ldots\ldots 4.13$$

$\frac{C}{T}$ is therefore finite, and independent of concentration at T = 0. Taking C' = 1 e.v., $\eta = \xi = 1$, S = 5/2 and C/T = 2.3 mj/mole $^{\circ}K^2$ as found by Du Chatenier

for Cu Mn, Eq. 3.32 gives G = 0.8 e.v., which may be compared with the spectroscopic value of 0.4 e.v. found for the free Mn atom.

At higher temperatures, detailed calculations show that C/T increases slightly above its value at T = 0, to a maximum value of $\frac{30}{\pi^2}\left(\frac{2S+1}{2S^2+2S+1}\right)\gamma_0$ just below Tc, and drops discontinuously to zero at T = Tc.

From 4.12 and 4.13,

$$\gamma_0 T_c = \frac{\pi^2}{9}\,\frac{S(S+1)}{2S+1}\,cNk \sim 13c$$

If γ is in mj/mole $^\circ K^2$, and S = 5/2, this gives Tc = 55°K / at % for Cu Mn.

Evidently the high temperature behaviour of the specific heat is not well described on this model, a broad maximum in C/T occuring at much lower temperatures than this (~ 10°K / at % for Cu Mn) followed by a gradual decrease at higher temperatures. Overhauser attributes the residual tail of the specific heat curve at temperatures above the cooperative decrease in the amplitude of the spin density wave to short range forces of the R.K.Y. type between nearest neighbour impurities. He considers this interaction to be of too short a range to produce the long range order at lower temperatures.

Marshall[110] has objected to the theory on the grounds that the perturbation theory has only been taken to first order, yielding a spin polarisation, and thus a coupling, of infinite range. Higher order perturbation theory would then reduce the range of the polarisation in the same way that the second order theory of Yosida modified the infinite range of the Zener interaction.

4.8 Marshall[110]

Marshall assumes that as a result of the R.K.Y. interaction between impurities, the impurity spins freeze into an antiferromagnetically ordered state at very low temperatures. Because of the alternating sign of the interaction with distance, there is an effective field H acting on an impurity, which may be of any sign, and of any magnitude up to some maximum value. He assumes, however, that this field has a unique axis, and as an impurity spin of $\frac{1}{2}$ is assumed, the spin can only be parallel or antiparallel to this axis. Arguments are presented which suggest that the shape of the P(H) curve is similar to that shown in Fig. 3., the curve being symmetrical about H = 0, and P(0) is finite. $\Delta C/T$ therefore tends to a constant value for the reasons outlined in section 2.5.

Assuming a Hamiltonion of the form

$$\mathcal{H} = \sum_{n<m} f(R_{nm}) S_n \cdot S_m \qquad \ldots\ldots 4.14$$

where S_n, S_m are the spins of the n^{th} and m^{th} impurities, R_{nm} is their separation, and f(R) is the R.K.Y. interaction discussed in section 3.9. Putting $n/N = \frac{1}{2}$ in eq. 3.22,

$$f(R) = \frac{9\pi J^2}{2E_F} F(2k_F R)$$

and $$F(x) = \frac{x \cos x - \sin x}{x^4}$$

The energy of the spin S_n may be written

$$E = - g\mu_b S_n \cdot H$$

and the effective field defined by this equation is

$$H = \sum_m \frac{9\pi}{4} \frac{J^2}{g\mu_b E_F} F(R_{nm})\, S \quad \ldots\ldots\ldots\ldots\ldots\ldots\ldots 4.15$$

The mean field h(T) is then given by

$$h(T) = \int_{-\infty}^{\infty} dH \; |H| \; P(H,T) \quad \ldots\ldots\ldots\ldots\ldots\ldots\ldots 4.16$$

as the P(H) curve will in general be a function of T.

As the amplitude of the interaction decreases rapidly with distance, H will be dominated by the few spins closest to S_n, and h can therefore be written

$$h = \lambda\, H(Ro) = \frac{\lambda}{2} \frac{f(R_o)\, S^2}{g\mu_b S} = \frac{\lambda}{8\mu} f(Ro) \quad \ldots\ldots\ldots\ldots\ldots 4.17$$

if $S = \frac{1}{2}$. λ is a number of the order of unity, representing the effective spin coordination number, and Ro is the mean distance between impurity atoms.

If the P(H) curve is similar to that shown in Fig. 3. P(0) may be written $P(o) = \frac{1}{4\lambda^1} h$ $\quad \ldots\ldots\ldots\ldots\ldots\ldots\ldots\ldots 4.18$

where λ^1 is a number of the order of unity.

If P(H) varies only slowly with T for T small, the specific heat as $T \to 0$ can be written for $S = \frac{1}{2}$

$$C = \frac{\pi^2}{6} \frac{c\, Nk^2 T}{\mu} P(0)$$

$$= \frac{\pi^2}{3\lambda\lambda^1} cNk^2 T \cdot \frac{1}{f(Ro)}$$

For low concentrations, f(Ro) can be written

$$f(Ro) = \frac{9\pi J^2}{2Eo} \cdot \frac{1}{(2k_F Ro)^3} = \frac{9\pi J^2}{2Eo} \frac{c}{(2ak_F)^3}$$

where 'a' is the nearest neighbour distance in the metal. For a f.c.c. monovalent metal $(2ak_F)^3 = 24\sqrt{2}\ \pi^2$

$$\text{and } C = \frac{16\sqrt{2}\pi^3}{9\lambda\lambda^1} Nk \frac{kT}{E_F/J^2} \text{ as } T \to 0 \quad \ldots\ldots\ldots\ldots\ldots\ldots 4.19$$

Thus C is proportional to T and independent of concentration c, as $T \to 0$. The origine of the concentration independance is, of course, the dependence of the interaction on $1/R^3$ at large distances.

The result is readily generalised for any spin S, (see appendix 1) to give

$$C = \frac{32\sqrt{2}\pi^3}{9\lambda\lambda^1} \frac{Nk}{2S+1} \frac{kT}{E_F/J^2} \text{ as } T \to 0 \quad \ldots\ldots\ldots 4.20$$

For Cu Mn, C/T tends to the value 2.3 mj/mole $^oK^2$ as $T \to 0$, and S found from entropy measurements, is 5/2. Taking $E_F = 7$ e.v., and $\lambda = \lambda^1 = 1$, eq. 4.20 gives J = 7.6 e.v. This rather excessive value for J can be reduced somewhat if the effective spin coordination number λ is taken to be seven, the number of spins at the distance Ro needed to account for the magnitude of T_n (Blandin and Friedel[89], section 4.5) J is then 2.9 e.v., which is still rather large. It is apparent, therefore, that very large values of the exchange integral are required if the R.K.Y. interaction is to explain the high ordering temperatures observed in dilute magnetic alloys. The mechanism proposed by Blandin and Friedel[89], section 4.5, is therefore to be preferred as it provides an interaction an order of magnitude larger than the R.K.Y.

interaction for the same value of the exchange integral.

Some of the more important assumptions made by Marshall should be considered further. The essential features of the theory are that P(0) should be finite and inversely proportional to c. There is a close analogy between the present problem, and that of computing the N.M.R. line shape in non conducting crystals, where the nuclei are coupled only by magnetic dipole interactions. Anderson[111], and others, have shown that in this case the line shape is a cut off Lorentzian of the form $P(H) = \frac{1}{\pi} \frac{\Delta}{H^2+\Delta^2}$ for $|H| < \alpha$

$= 0$ for $|H| > \alpha$

Δ is shown to be proportional to c, and α is independent of c for low concentrations. Marshall considers that at high temperatures, when spin correlations are negligable, this line shape will obtain for the present problem. At lower temperatures, spin correlations will have the effect of increasing the probability of higher fields, in order to lower the total energy, and P(0) will therefore decrease to give the P(H) curve the shape shown in fig. 3. The required properties of P(0), that is shall be finite and proportional to 1/c, will be retained however.

A more drastic assumption has been the use of the Ising approximation, through the assumption of a unique direction for the magnetic field. The effects on the predictions of the model of relaxing this condition, are catastrophic. The probability function $P(\underline{H})\, d\underline{H}$ now describes the probability of an impurity being in a vector field lying between $\underline{H}$ and $\underline{H} + d\underline{H}$. The probability that the impurity should lie in a scalar field $H \rightarrow H + dH$ is then $4\pi H^2\, P(\underline{H})\, dH$ if the field distribution is isotropic. C/T will then be proportional to T^2 as $T \rightarrow 0$ (see Appendix 1) and the model will no longer

predict the observed results.

As Mossbauer experiments suggest that the anti-ferromagnetic ordering is approximately isotropic, this otherwise attractive theory would appear to be doomed, unless $P(\underline{H})$ varies as $1/H^2$ as $H \to 0$, which seems extremely unlikely, or unless it can be shown that the distribution of very low fields is extremely anisotropic.

4.19 Klein[112]

Klein has adopted the ideas of Marshall[110], developed in the last section, and has attempted to account for the concentration and temperature dependence of the specific heat anomalies of different systems over an extended temperature range on the basis of computed P(H) curves. The energy of the system is treated in the Ising approximation, and is therefore subject to the criticisms considered in the last section.

Starting from an R.K.Y. interaction, written in the form

$$E = \sum_{i<j} JS^2 \, (2k_F)^3 \, \frac{x \cos x - \sin x}{x^4} \, \mu_i \, \mu_j$$

$x = 2k_F r_{ij}$, and JS^2 is approximately the interaction energy at unit separation.

Klein constructs the partition function for the system of impurities, and determines from it the two particle correlation function $\langle \mu_o \mu_j \rangle$, where μ_o is the central spin index. It is found that only spins close to the origine are strongly correlated with μ_o, and that outside some correlation radius R_c, the correlation is zero, being effectively screened by the oscillating interactions of the intermediate spins. At $T = 0$ $Rc(0) \sim 0.51\, c^{-1/3}$ where

Rc is in units of the lattice constant. The correlated volume decreases with the concentration in such a way that it always contains an average of 3.3 spins, one at the origine, and 2.3 others. The P(H) curve can then be constructed by considering the fields at the origine from the two independent regions - inside, and outside, the correlated volume. . In his earlier paper (Klein and Brout), Klein consideredthat the inside, correlated, spins were responsible for the high fields, and the outside spins dominated the shape of the P(H) curve at H = 0. In his latest paper, the correlated spins give the major contribution to the whole P(H) curve, whilst the main effect of the outside spins is to make the discrete spectrum due to the inside spins continuous at low fields.

The final form of the P(H) function may be written

$$P(H) = \frac{1}{3(2\pi)^{\frac{1}{2}}} \sum_{i=1,2,3} \frac{a_i}{\sigma} e^{-\frac{1}{2}\left(\frac{H}{\sigma} - b_i\right)^2} \quad \ldots\ldots\ldots 4.21$$

Where a_i and b_i are functions of H, but are independent of concentration, temperature, and the strength of the interaction. The width σ is given by

$$\sigma\ (T = 0) \sim 7.80\ JS^2\ c \quad \ldots\ldots\ldots\ldots\ldots\ldots\ 4.22$$

and is therefore proportional to the interaction energy and the conentration. In general, P(0) is finite, and is given by

$$P(0) \sim \frac{0.1}{\sigma} = \frac{1}{78JS^2\,c} \quad \ldots\ldots\ldots\ldots\ldots\ 4.23$$

The behaviour of the P(H) curve with concentration can be seen from Fig 23

Fig 23

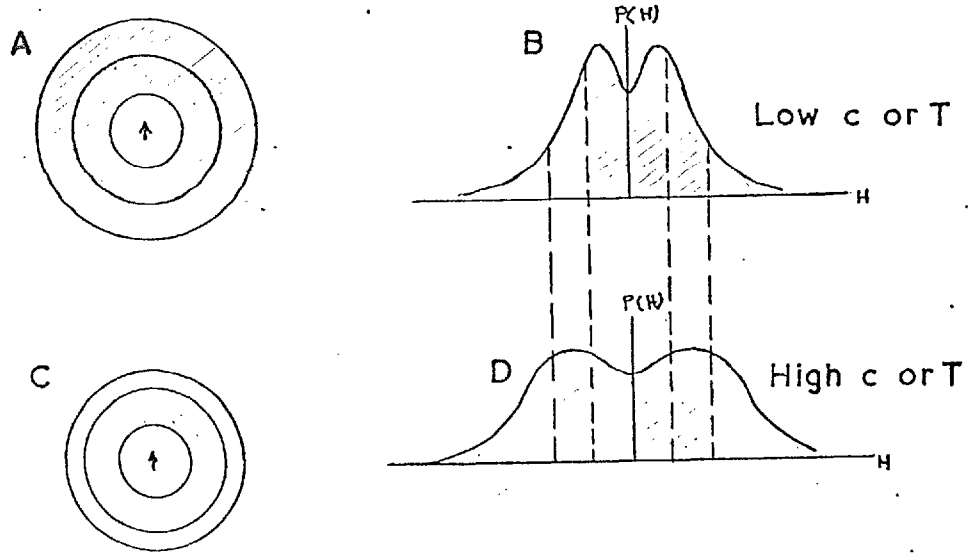

In fig. 23A, the correlated volume is divided into three regions. The region closest to the central spin gives the highest fields, and therefore provides the wings of the P(H) curve (fig 23 B). The region near the edge of the correlated volume provide the central portion of the P(H) curve. Increasing the concentration reduces the correlated radius Rc(fig 23 C) and therefore reduces the probability of low fields. The P(H) curve is normalised, therefore the probability of high fields increases, and the P(H) curve spreads out, fig 23 D. The P(H) curve generally exhibits a maximum at a field H_1, different from zero, and which is approximately given by $H_1 = \frac{JS^2}{R_c^3}$, and comes mainly from the rather large probability of finding a spin near the edge of the correlated volume. Thus $H_1 \sim 8c\, JS^2 \sim \frac{10}{p(0)}$

The effect of increasing the temperature is to randomise the weakly coupled spins at the edge of the correlated volume, and thus to reduce the correlation radius Rc,

$$Rc(T) = Rc(0)\left[\left(\frac{Tc}{T} \right)^2 - 2\,\frac{Tc}{T}\,\log\frac{Tc}{T} \right]^{\frac{1}{3}} \quad \text{for } T > Tc \ldots\ldots 4.24$$

This has a similar effect on the P(H) curve to that of increasing the concentration , and the probability of high fields increases.

The specific heat curve will generally be concentration independent at low temperatures; proportional to concentration at intermediate temperatures, when the spins in the middle region of the P(H) curve are disordering; and to c^2 in the high temperature region corresponding to the wings of the distribution curve, P(H) being proportional to c in this region. It should be noted, however, that at temperatures high compared with $\frac{\mu H_{max}}{k}$, the specific heat per impurity is proportional to $\overline{H^2}$, (see appendix 1) and therefore (probably) to c^2, and thus the total specific heat varies as c^3 in this region.

The differing behaviour of the specific heat curves observed for different systems is accounted for simply by assuming that different parts of the anomaly are falling within the temperature range of the measurement. Thus the Cu Mn measurements between 1.5 and 5°K of Zimmerman and Hoare[73] fall in the concentration independent region; the Cu Fe results of Franck Manchester and Martin[74] between 0.4 and 1°K correspond to the intermediate region proportional to c; and the Cu Co results of Crane and Zimmerman[75] between 2°K and 5°K fall in the c^2 region.

The value of JS^2 found from the intercept of $\gamma_0 = C/T$ as $T \to 0$, (P(0) is proportional to $1/JS^2$), can be used to check this theory. γ_0 found for Cu Fe[74] is 1.6 times smaller than that found for Cu Mn by Zimmerman and Hoare[73]. This would indicate that the anomaly for Cu Fe should extend to higher temperaturesthan that of Cu Mn, which is not consistant with the concentration dependence observed. It would also suggest that the value of

J for Cu Fe is 40 times larger than that for Cu Mn (assuming a spin of 1/2 and 5/2 for the Fe and Mn atom) - a most unlikely result. The source of this ambiguity is that Klein calculates the specific heat assuming a spin of $\frac{1}{2}$, whilst assuming any value of S in the energy JS^2, and the entropy associated with the anomaly is always cN log 2. If the specific heat is calculated assuming a general spin, as in Appendix 1, γ_o is proportional to $\frac{1}{J(2S + 1)}$, and the width σ is proportional to JS.

Thus $\frac{J_{Fe}}{J_{Mn}} \sim 5$ and $\frac{\sigma_{Fe}}{\sigma_{Mn}} \sim 1$ which is rather more reasonable.

The general features of the specific heat anomalies predicted by Klein's theory are not in any significant way different from those predicted by Marshall, as the concentration dependence of different parts of the P(H) curve can be arrived at by very general arguments, provided the Ising approximation and a potential varying as $1/r^3$ are assumed. The original contribution of Klein's work lies in his particular statistical calculation of the P(H) curve. Comparison of his results with experiment is difficult, but the shapes of the specific heat curves in alloys containing Fe, and those in alloys containing Mn, suggest that the internal field distributions are rather different in the two systems, whereas Klein's calculations predict an almost universal P(H) curve. The particular feature that can be compared is the maximum in the P(H) curve, which should be reflected in the C/T curve. This is indeed observed in all of the alloys containing Mn, and in those containing rather high concentrations of Cr or Fe. The magnitude of the hump in the Mn alloys is certainly too large to be accounted for by the P(H) curves described by Klein, though these may be sufficient to explain

those in the other alloys.

It does not appear that the P(H) curves calculated by Klein are any closer to the true curves than those constructed in an arbitrary way by Marshall. The most disheartening features of the theory, is, of course, the use of the Ising approximation. Klein suggests that this may be justified because of the very small number of spins in the correlated volume. It is certainly not justified in calculating the field from the uncorrelated region, but this only contributes in an unimportant way to the P(H) curve.

CHAPTER 5

DESIGN OF APPARATUS AND EXPERIMENTAL TECHNIQUE

5.1 Introduction

The adiabatic calorimeter was originally used by Nernst and Eucken[113] in 1910 for the measurement of low temperature specific heats, and has since been developed to yield results of considerable accuracy over a wide range of temperatures. The principle of the measurement is simple. The specimen is suspended in a container from which it is thermally isolated. Electrical power is dissipated for a limited time, in a heater attached to the specimen, and a thermometer, also attached to the specimen, measures the change in temperature. From a knowledge of the power W, the time t, and the temperature change ΔT, the heat capacity Q of the specimen and heater-thermometer assembly can be calculated from $Q = \frac{Wt}{\Delta T}$.

As it is not possible to obtain completely adiabatic conditions, it is necessary to apply a correction for the amount of heat transferred to the specimen from the surroundings during the heating period. In order that this correction should be as small as possible, the temperature of the enclosure must be maintained close to that of the specimen, the difference being not more than one or two degrees.

Heat can be transferred to the specimen by gas conduction, conduction down the suspension and electrical leads, and by radiation. These are reduced to a minimum by suspending the specimen with nylon threads in a high vacuum, using electrical leads of low thermal conductivity, and having highly polished surfaces fort he specimen and container to reduce radiation, which predominates at high temperatures. Heat can be generated in the region of the specimen by joule heating in the electrical leads, joule heating in the

thermometer (which effectively limits its maximum sensitivity), and by vibration heating. Vibration of the specimen due to pump or building vibrations are damped by frictional processes in the suspension and electrical leads, and a proportion of this heat, of the order of 0.1 to 1 erg/sec, will reach the specimen. The specific heat of metals in the liquid helium range is extremely small, (the specific heat of copper at 1°K is 30,000 times smaller than the value at room temperature) and a typical heating rate in a measurement at 1°K, on one mole of Copper, is 20 ergs/sec. It is therefore essential to keep extraneous heat inputs to the specimen below 1 erg/sec in this temperature region.

For measurements within the range 1.8° to 4.2°K the container can be immersed in a dewer containing liquid Helium under reduced pressure. To reach lower temperatures an arrangement similar to that shown in Fig. 24 can be used.

Fig. 24

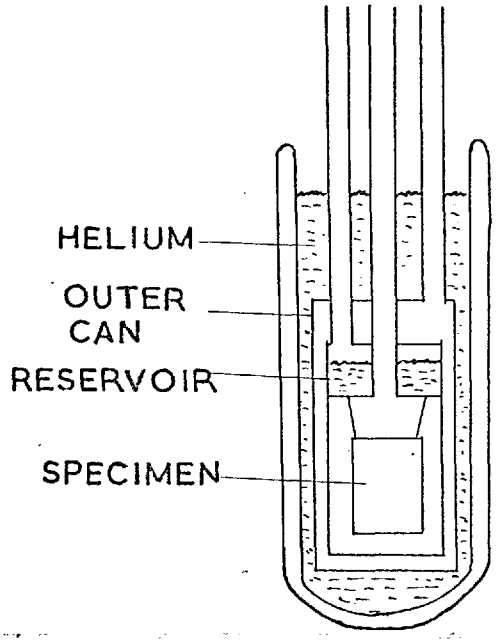

The specimen is suspended in a can attached to a reservoir which

contains a small quantity of liquid Helium. This is thermally isolated from the outer can, which is immersed in liquid Helium boiling at atmospheric pressure (i.e. at 4.2°K). Pumping on the helium in the reservoir will reduce its temperature to around 1.2°K, the lowest temperature being limited by the heat leak to the reservoir and the efficiency of the pumping system. Adiabatic conditions can be achieved above 4.2°K by heating the reservoir to a temperature close to that of the specimen. This type of apparatus can be used successfully between 1°K and 77°K. Examples of this type of calorimeter are described by Rayne[114] and Martin[115].

Above 77°K, radiation between the reservoir and the outer can increases rapidly, and leads to temperature variations over the reservoir shield giving considerable temperature drifts to the specimen. For accurate specific heat measurements above 77°K, therefore, a further shield surrounding the specimens, isolated from the reservoir, becomes necessary. This is called the adiabatic shield. Such an apparatus capable of measuring specific heats to within 0.2% has been described by Dauphinee, Macdonald and Preston Thomas[116].

A fundemental problem in the use of the adiabatic calorimeter, is to cool the specimen initially to the lowest temperatures reached by the reservoir. This was originally achieved by introducing helium exchange gas into the space around the specimen, and when cooling was completed, pumping the gas away until adiabatic conditions were regained. This was unsatisfactory for several reasons. It usually took several hours to pump the gas to a sufficiently low pressure, by which time the specimen would have already started to warm up by vibration heating. More seriously, a film of Helium a few hundred atoms thick is adsorbed on to the surface of the specimen at low temperatures,

which is not removed by pumping away the exchange gas. On warming the specimen, this helium is boiled off, and heat is required to provide the heat of desorption, leading to the anomalously high specific heat values found in many of the early measurements using this technique.

To avoid this problem, Ramanathan and Srivensan[117] originated the mechanical heat switch. The specimen is mechanically connected to the surrounding shield during the cooling period, after which the connection is broken, so that the specimen is again thermally isolated from its surroundings, and measurements may begin immediately.

An essential part of the apparatus is the specimen thermometer, and several possibilities are available, depending on the temperature range in which sensitivity is required. At temperatures above 15°K, platinum or copper resistance thermometers can be used, yielding values of the temperature with an accuracy of around 0.03°K above 25°K. These tend to be rather bulky, and dissipate an appreciable amount of heat if high sensitivity is required, but have the advantage of a high degree of reproducibility and only have to be calibrated at two or three known temperatures.

A thermocouple of, for instance, Au 2.1%Co against Ag 0.2%Au may be used to measure the temperature of the specimen relative to the helium bath. This type of thermometer has the advantage of a very low heat capacity and therefore a very rapid response. It has a sensitivity increasing from 1μv/°K at 1°K to 10μv/°K at 15°K to 40μv/°K at high temperatures, but because of the insolubility of this quantity of Co in Au below 600°C, it is not very reproducible, and has to be calibrated against a standard thermometer during each series of measurements. Undetermined thermal voltages in the leads

limit the accuracy of the temperature measurement with a thermocouple to around 0.05°K. A Au 0.03% Fe against Chromel thermocouple has a sensitivity of around 15μv/°K over the range 1° to 30°K, and is very much more reproducible than the Au 2.1% Co thermocouple, but because of the large thermal conductivity of the Au 0.03% Fe alloy, it can constitute a grave heat leak to the specimen.

Finally there is the carbon resistance thermometer, which is the most popular thermometer in the temperature range 0.3° to 20°K. Several commercial resistors have a large temperature coefficient of resistivity in this temperature range, and have the advantages of a low thermal capacity, and high sensitivity with low heat dissipation. Their main disadvantage is poor reproducibility, making it essential to recalibrate the thermometer against Helium vapour pressure below 4°K, and against a helium gas thermometer above 4°K, after every series of measurements. It seems likely that the commercial carbon thermometer will be superseded in calorimetric work by the germanium thermometer, which combines all of the advantages of the carbon thermometer with excellent reproducibility and the possibility of choosing a thermometer with large sensitivity in any desired temperature range. This thermometer is, unfortunately, very expensive.

5.2 Design of Cryostat

It was decided to build a cryostat capable of measuring specific heats in the temperature range 1°K to 300°K. The cryostat has, therefore, to include an outer can, a reservoir and a reservoir shield, and an adiabatic shield. As a carbon thermometer is to be used in the low temperature range,

a gas thermometer is required for calibration purposes. A diagram of the cryostat with its associated Helium and Nitrogen dewar, is shown in Fig. 25.

The cryostat is suspended by its pumping tubes from a top brass plate, which is bolted to a rigid framework fixed to the wall. The double walled helium dewar, which is 3 7/8" inside diameter and 29" inside length, has a short single walled section at the top, which is turned over in the form of a lip. This is clamped to a flanged brass cylinder, and a gas tight seal is obtained by compressing an annular ring of neopreme between the two. The brass cylinder is bolted to the underside of the brass plate, and is sealed with an "O" ring. The dewar is demounted by unbolting at this point, and dropping down past the cryostat. The helium dewar is surrounded by a double walled Nitrogen dewar, of conventional design, the inside walls of the interspace being silvered, and the space diffusion pumped and sealed permenantly. The inside walls of the interspace between the double walls of the helium dewar are silvered, to reduce the radiation from the N_2 bath. This interspace cannot be pumped and sealed permenantly as Helium gas will diffuse slowly through the glass walls at room temperature and spoil the vacuum. A port is therefore provided to allow this space to be pumped with a rotary pump before each run, after having been flushed with air. The space is then shut off with a tap. The remaining gas in the interspace allows the cryostat to cool to 77°K when the outer dewar is filled with liquid Nitrogen (this takes about 8 hours) and the gas freezes out to provide a high vacuum when liquid helium is transferred to the inner dewar.

The pumping tubes used to evacuate the vacuum interspaces between the cans are made from 3/8" dia 0.006" wall thickness stainless steel tube, stain-

fig 25

Specific Heat

Cryostat

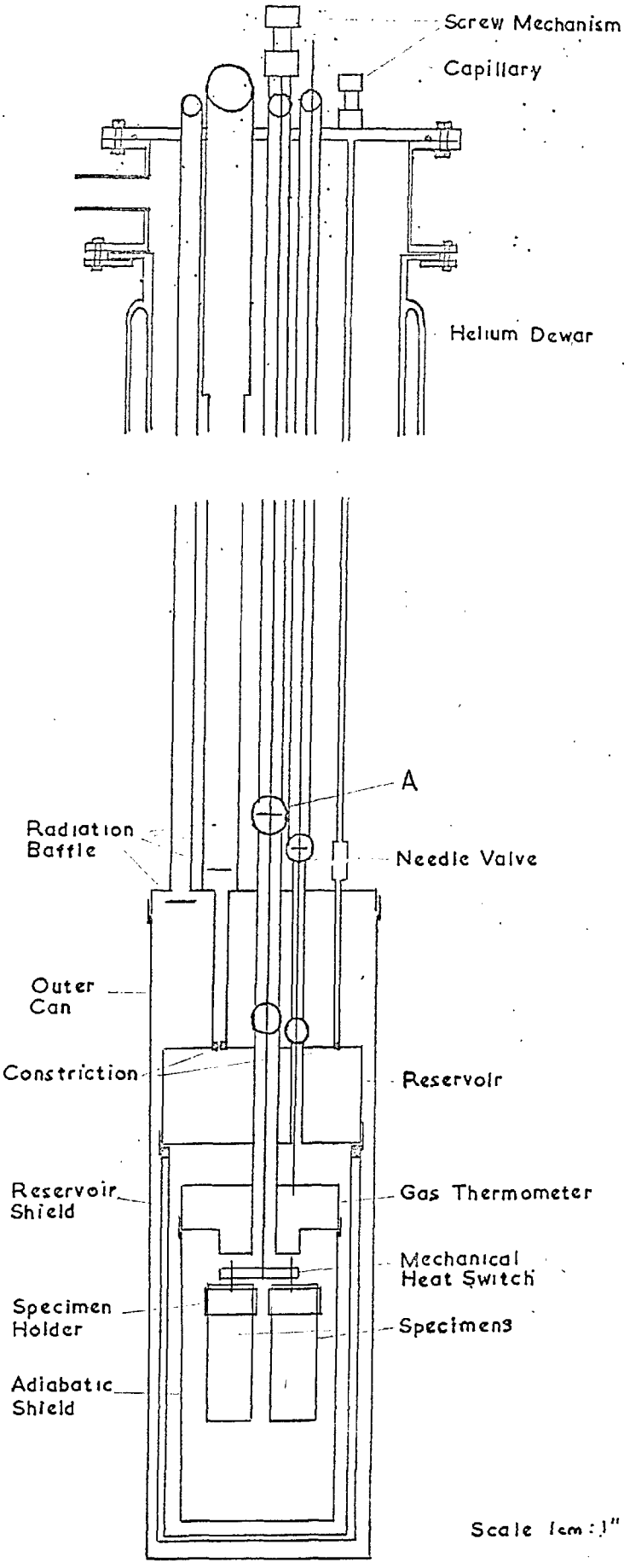

less steel being chosen for its very low thermal conductivity and large physical strength, and the diameter being chosen to provide an adequate pumping speed. All joints in the cryostat are brazed unless otherwise stated.

Liquid helium may be introduced into the helium dewar from a helium storage vessel, by means of a double walled transfer syphon, which can be lowered through a hole in the top brass plate. Below the top plate the transfer syphon slides into a $\frac{1}{2}$" dia. stainless steel tube which projects about 6" into the dewar. The diameter of this tube then decreases to $\frac{1}{4}$" dia., and continues down to the bottom of the dewar. This is to ensure that the liquid helium is taken to the lowest point of the cryostat when the transfer starts, so that the cold vapour produced when it boils, efficiently cools the outer can and the glass dewar walls before leaving the dewar. A gas tight seal between the transfer tube and the dewar is made by tightening an "O" ring coupling above the top plate. This point is capped off when the transfer tube is removed.

To reduce the heat conducted down the stainless steel tubes and dewar walls a 10" long cylinder of polystyrene foam is packed between the tubes, from a level just above the highest level of the liquid helium to a few inches below the top brass plate. A gap of about $\frac{1}{4}$ inch is left around each tube, and between the foam and the glass dewar walls, so that all of the cold gas boiling off from the liquid helium is forced to flow close to the tubes or to the glass wall, and provides efficient cooling. The boil off rate of liquid helium was found to have been reduced from 200 cc/hour without the foam to 100 cc/hour with the foam.

To prevent any radiation that may be funneled down the pumping tubes,

from reaching the reservoir, gas thermometer or specimen, it must all be absorbed at points thermally connected to the liquid helium in the dewar. In the present apparatus it is not convenient to use the usual method of absorbing the radiation by putting right angled bends into the pumping tubes, as several of the tubes have tubes of small diameter passing through them. The method employed was to place discs, of larger diameter than the diameter of the tube, in regions where the diameter of the tube has been temporarily increased, such that there is no 'straight through' path between room temperature and the parts of the cryostat which are cooled to below 4°K. The detailed construction of such a region is shown in Fig. 26. A copper cylinder, with its axis horizontal, is set into the stainless steel tube at a point just above the top brass cap of the outer can. The radiation baffle, a half inch diameter copper disc, is brazed to the smaller diameter tube passing down the middle of the 3/8" dia. pumping tube, there being sufficient clearance between the disc and the cylinder that the pumping speed of the tube is not significantly reduced. The disc is also thermally connected by copper wire to the walls of the cylinder, so that the heat conducted down the small diameter tube, as well as the absorbed radiation, is conducted away to the helium bath. One end cap of the cylinder is demountable, and its shape is shown in Fig. 26. The large number of small diameter copper wires that pass down the inside of the stainless steel tube may be wound several times round the part of the cap that projects into the cylinder, and are connected to it with GE 7031 varnish, a strip of .001" thick condenser paper having been previously cemented to the cap to prevent possible shorting of the wires.

Fig. 26

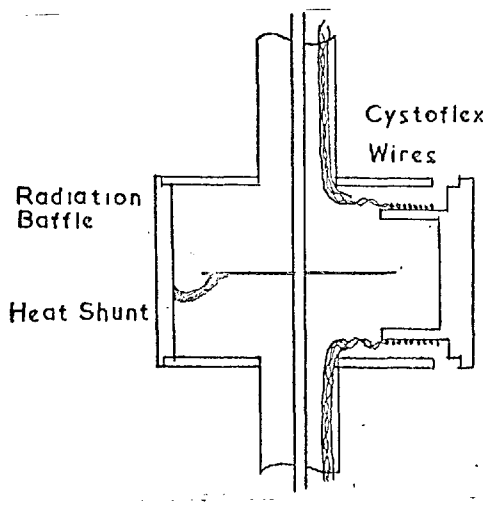

The end cap may then be soldered with low melting point solder, into the copper cylinder. The wires are effectively thermally anchored to the helium bath, and none of the heat conducted down the wires from the room temperature region can reach those parts of the cryostat that are cooled below $4^{o}K$.

5.3 Outer Can

The outer can of the cryostat is 3.4" dia. brass tube with a wall thickness of 0.020" and a length of 10.5", closed at the bottom with a 1/16" thick brass disc. This can is soldered with low melting point solder to the rim of a 0.080" thick top brass cap through which pass the pumping tubes to the inner vacuum spaces and the reservoir. The can and the top cap form an enclosure, at the temperature of the helium bath, which can be evacuated through one of the pumping tubes. Radiation from this pumping tube is absorbed by a 1" dia. copper disc placed directly under the opening of the pumping tube, and soldered to the underside of the top cap.

As the outer can, reservoir shield and adiabatic shield have to be removed and replaced whenever a specimen is changed, they are soldered to the top brass cap, reservoir, and gas thermometer, respectively, with a low melting point solder of composition 70% In, 15%Sn, 9.6%Pb, 5.4% Cd (Indium Corporation of America) which has a melting point of 125°C. The soldering is performed with a gas-air torch, after which a hot soldering iron is run round the top of each joint to ensure that there are no leaks. Each joint is then tested with a helium leak detector, (C.E.C. 112A), though no leaks were ever found in these demountable joints.

5.4 Reservoir and Reservoir Shield

The reservoir is a cylindrical copper vessel, 3" dia. with a wall thickness of .020" and whose base and top are 1/16" thick. The volume of the reservoir is 150 c.c.

Soldered to the underside of the reservoir is the reservoir shield, of high conductivity copper, and double walled (each wall being .020" thick) to reduce thermal gradiants on the inner wall. Small holes drilled through the inner wall allow the interspace to be pumped when the shield is evacuated. The inside diameter of the shield is 2 3/4", and the length is 4 ½".

Liquid helium is let into the reservoir by opening a needle valve in the helium bath, detail of which is shown in Fig. 27

The needle valve consists of a stainless steel needle, with a 10° taper, moving into a 0.020" dia. brass seat. It is actuated by a screw mechanism above the top plate, to which it is connected by a 0.090" dia. stainless steel tube sliding in a 1/8" dia. stainless steel sleeve. It is

Fig. 27

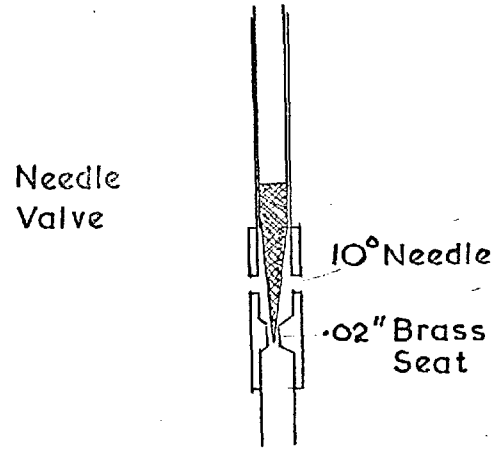

connected to the reservoir by a 1/8 " dia. stainless steel tube, at the bottom end of which is a 0.020" dia constriction to reduce superfluid film flow. Below the λ point (2.14°K) liquid helium becomes a superfluid, and has the property of covering any surface in contact with the liquid or vapour with a superfluid layer 10^{-6} to 10^{-5} cm thick, at a constant temperature equal to that of the bulk liquid. The film will flow to any warmer point in the apparatus, where it may boil. If this is in a pumping tube, the resulting volume of vapour to be removed may be considerably in excess of that leaving the main liquid surface, and if it is not being removed by pumping, it may recondense in the bulk liquid, giving a substantial heat influx.

The film will reach a point in the tube where the heat influx is just sufficient to evaperate the helium creeping up in the film. This is usually a few millimeters below the 4°K point (Ambler and Kurti[118]). The film flow is limited by the minimum perimeter traversed by the film, and at 1°K, the flow rate is approximately 7×10^{-5} p cc/sec., where p cm is the minimum perimeter. It is therefore desirable to introduce constrictions in each of the tubes from the reservoir which go to higher temperatures, though any roughness of

the orifice due to, for instance, condensed air, may increase the effective perimeter considerably.

To obtain very low temperatures, a pumping line with a high pumping speed is essential, and this may be limited by the presence of the constriction. A suitable balance must therefore be achieved between the conflicting conditions of minimum film flow, and maximum pumping speed. In the present apparatus, an orifice of $\frac{1}{2}$ mm dia. and 1mm long was used (although these may not be the optimum dimensions). In the design of the pumping line, the pumping speed of the line, calculated by the formula due to Garfunkle and Wexler[119], was maximised subject to the condition of a tolerable heat leak down the pumping tube between room temperature and the helium bath, and between the bath and the reservoir. In the final design, the tube is 5/16" dia., between the reservoir and the outer can, 5/8" dia. through the helium bath, increasing to 1" dia. five inches below the top plate and continuing as 1" B.S.P. pipe outside. For accurate measurements of the vapour pressure of the liquid in the reservoir, the pressure should be measured at the surface of the liquid, rather than at some point along the pumping line. This is accomplished with a separate sensing tube, 2mm bore, connected between the reservoir and the manometers.

5.5 Gas Thermometer and Adiabatic Shield

The gas thermometer bulb is a cylindrical copper vessel which has a volume of 45.0 cc at 23°C. The adiabatic shield, is a 0.030" wall thickness, 2 3/8" dia. copper cylinder, closed at one end with a 1/16" copper disc, and may be soldered, with low melting point solder, to the underside of the gas-thermometer, forming an isothermal enclosure for the specimen. This space may

be evacuated via a 3/8" dia. stainless steel pumping tube which passes through the centre of the gas thermometer. As the temperature range of the measurements to be described in Chapter 6 is 1.3° to 25°K, the adiabatic shield is not used. The gas thermometer is thermally connected to the reservoir by a cylinder of high conductivity copper, 5/8" long and 5/8" dia., soldered between the top of the gas thermometer and the underside of the reservoir. The isothermal enclosure is then formed by the reservoir and the reservoir shield.

In order that the dead space correction to the gas thermometer pressure should be small (that is, the correction due to the finite mass of gas in tubes at temperatures different from that of the gas thermometer bulb), the pressure sensing tube from the gas thermometer should have as small a diameter as possible, the minimum size being limited by (a) the time required to initially pump the bulb, (b) the response time to pressure changes in the bulb (c) thermomolecular pressure corrections.

With the 1mm bore german silver tube selected, the bulb can be pumped at room temperature from atmospheric pressure to 1mm Hg in about five minutes, and the time increases to about 30 mins when the bulb is at 4°K because of the increased mass of gas in the bulb. By repeatedly flushing with Helium, and repumping, it is assumed that gases other than helium have been reduced to insignificant proportions. Small quantities of other gases (apart from Hydrogen) will not make a significant contribution to the gas thermometer pressure below 30°K as they will have solidified with a negligable vapour pressure.

For the filling pressures used, 4 to 8 cm Hg at 4.2°K, and for temperatures above 3°K, thermomolecular pressure corrections are negligable, being $\sim 10^{-4}$°K at 3°K, and decreasing at higher temperatures. The response time of the gas thermometer was not more than a few seconds at the lowest pressures,

and less than this at higher pressures.

The dead space correction increases to about 1% at 20°K, and as the temperature distribution along the sensing tube as it passes through the cryostat is not known with any confidence, this correction can only be estimated to about ± 30% of its magnitude. In view of the above considerations, a sensing tube of 0.5 mm bore would have been quite acceptable, with a considerable reduction in the dead space correction.

5.6 Specimen Holder

As described in the introduction, a heater and a thermometer have to be attached to the specimen. These may be cemented directly on to the specimen and their heat capacity may be estimated and allowed for, or ignored completely. Considerable improvement in the accuracy of measurement of the specific heat of the specimen, and reduction in the time required to change the specimen, may be effected by mounting the heater and thermometer permenantly on to a specimen holder into which the specimen may be clamped. The heat capacity of the holder, thermometer and heater, known collectively as the addenda, can be measured in a separate experiment and subtracted from the total heat capacity of sample plus addenda in subsequent experiments. The addenda should have a low heat capacity, and should make very good thermal contact with the specimen, Failure to achieve this leads to the addenda being at a higher temperature than the specimen during the heating period, which may in severe cases make difficult the estimation of the temperature change during this period.

The addenda which was finally adopted, and found to give satisfactory

results, is shown in Fig 28.

Fig. 28

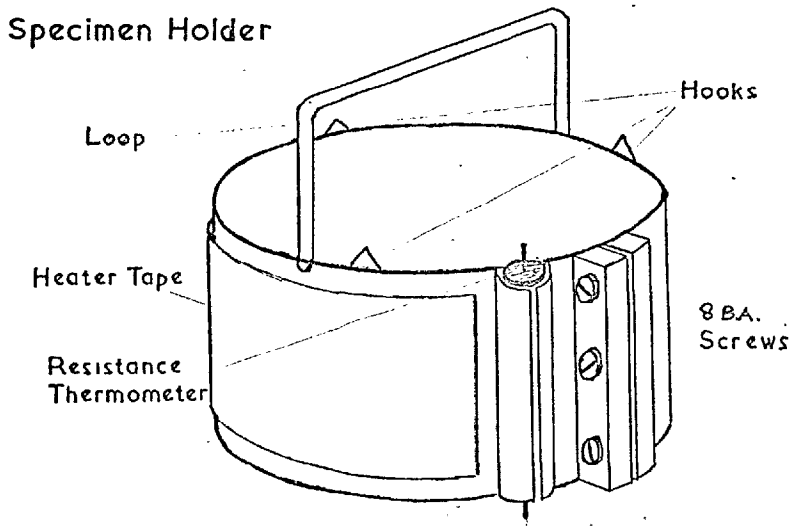

To keep the heat capacity of the clamp as low as possible, it was made in the form of a band cut from 0.0036" thick copper sheet, the band being 3/8" wide and slightly less than $\frac{3}{4}$" dia. The ends of the band can be clamped together with three 8 B.A. screws, between two pieces of square section copper brazed to the band. The specimen is turned in the form of a cylinder $\frac{3}{4}$" dia. and approximately 1" long, and is slipped into the holder, which is then clamped down hard on to the specimen by tightening the three 8 B.A. screws.

To ensure good thermal contact with the specimen, great care was taken during the construction of the holder to maintain a smooth surface inside the band, this surface finally being highly polished. As a final precaution, a small quantity (lessthan 0.01 gms) of silicone grease was smeared on to the inside of the clamp. This quantity of grease was included on the addenda before measuring its heat capacity. No trouble due to bad thermal contact

was ever experienced with this clamp with correctly prepared specimens.

The holder is suspended from the underside of the gas thermometer by three 0.005" thick nylon threads attached to hooks soldered to the top of the clamp. A loop of 20 s.w.g. copper wire is soldered to opposite sides of the top of the holder, for use with the mechanical heat switch in initially cooling the specimen.

The carbon resistance thermometer, which is a nominally 47 ohm Allen Bradley resistor, was prepared by grinding off its outer casing and coating it with a protective coating of G.E. varnish. It is then cemented in with G.E. varnish to ensure good thermal contact with the copper sleeve. The sleeve was split so that there should be no stresses introduced into the resistor on cooling due to the differences in the thermal contraction of the copper and resistor.

The heater consists of two meters of 0.001" dia. nichrome wire, having a total resistance of approximately 4000 ohms. It is advisable, especially with a clamp as thin as the one described above, to distribute the heat dissipated in the heater as evenly as possible over the surface of the clamp. It is not possible to wind a heater round the whole clamp as it does not form a complete ring, and therefore the following procedure had to be adopted. A piece of condenser paper is wrapped round a $1\frac{1}{4}$" dia. bar, and the wire wound on to this in a single layer approximately 1/8" wide. After cementing the wire to the paper with varnish, the paper is slipped off of the bar, and folded flat in the form of a tape roughly 2" in length, and 1/8" wide. This is then cemented onto the clamp, covering most of its surface.

A heater of high resistance was chosen to reduce the current required to give the desired power dissipation. This is so that the current leads to the

specimen can be of a small diameter, with consequent reduction in the heat conducted to the specimen, without excessive dissipation in the leads themselves half of which will reach the specimen, and half the adiabatic shield. Nichrome was chosen because of its high resistivity, and small temperature coefficient - the resistance changes by only 3% in the temperature range 1° to $300^{\circ}K$, and is approximately a linear function of temperature in that range.

As the resistances of the heater and carbon thermometer are measured potentiometrically, two potential and two current leads are required in both cases. The thermal (and therefore electrical) resistance of these leads should be high to reduce the heat conducted to the specimen, but not so high, in the case of the potential leads, that the sensitivity of the voltage measuring system is reduced, or that an excessive amount of heat is dissipated in the current leads. The wires finally chosen were 47 s.w.g. constantin for the resistance thermometer potential and current leads, and the heater potential leads, each having a resistance of around 13 ohms, and 42 s.w.g. constantin for the heater current leads, having a resistance of around 3 ohms each. All the wires were approximately 10 cm in length, and were estimated to have a total heat conductivity of approximately $1 \times T\,\Delta T$ ergs/sec, where ΔT is the difference in temperature between the specimen and the gas thermometer. This may be compared with the measured value of $1.6\,\Delta T$ ergs/sec below $3^{\circ}K$, which must also include a contribution from gas conduction. This is estimated to be of the order of $3\,p\,\Delta T$ ergs/sec, where p is the pressure around the specimen in units of 10^{-6} mm Hg. Radiation makes a quite negligable contribution to the heat reaching the specimen below $20^{\circ}K$.

To keep the total resistance of the leads low, and to reduce the magnitude of the thermal voltages induced in the regions of large temperature gradient, 44 s.w.g. copper leads were chosen to connect the external measuring apparatus with the constantin leads between the gas thermometer and the specimen. The copper wires, having passed down the central pumping tube, and having been thermally anchored at 4°K in the manner described above, were wound several times around the bottom of the gas thermometer, and varnished to it, to be sure that they were at the temperature of the gas thermometer, so that no heat conducted down the wires from the high temperature regions could reach the specimen. After being soldered to the appropriate constantin wire, the first three centimeters of constantin wire were varnished to the gas thermometer. Solder joints on pairs of voltage leads were placed close to one another to reduce temperature differences between the copper constantin connections and the generation of thermal e.m.f's. For similar reasons, the last three centimeters of the leads before soldering to the heater or thermometer were varnished to the specimen holder.

One further lead was soldered to the specimen holder itself. The measurement of the electrical resistance between this wire and the cryostat made it possible to decide when contact of the specimen with the mechanical switch had been broken.

5.7 Mechanical Heat Switch

To thermally connect the specimen to the gas thermometer, a mechanical heat switch was constructed which is based on a design due to Montgomery (unpublished). By suitably positioning the fixing points of the nylon threads, the copper loop soldered to the specimen holder is made to pass

between the bottom of the gas thermometer and a horizontal piece of $\frac{1}{4}$" thick brass strip, without touching either. (See fig. 25). In this position, the specimen is freely suspended by its nylon threads and is thermally isolated from its surroundings. By raising the brass strip, the specimen holder will be lifted up by the copper loop, which is squeezed against the bottom of the gas thermometer, giving the required thermal contact to cool the specimen. The brass strip is rigidly fixed to the bottom of a 0.09" dia. x 0.01" wall thickness stainless steel tube which passes up through the 3/8" dia. central pumping tube. It is raised and lowered by a screw mechanism on the top plate (fig. 25) fixed to the top of the thin stainless steel tube.

The heat transfer across pressed contacts is found to be proportional only to the force applied, and not to the area of contact (Berman[120]). Heat transfer may be improved by making one of the surfaces a very ductile metal, and for this reason the upper surface of the brass strip, and part of the under surface of the gas thermometer, are coated with indium.

It is possible to cool a 1 mole specimen from 77°K to 4°K in approximately fifty minutes, and from 4° to 1.3°K in a further fifteen minutes. One difficulty in the use of a mechanical heat switch is the heat generated by vibration and friction when the switch is broken, which because of the extremely small heat capacities being measured, can lead to a significant temperature rise. With the switch described above, the heat generated is of the order of 200 ergs, leading to a temperature rise of the order of 20 mdeg in 1 mole of Cu at 1.3°K.

As it is essential that the brass plate of the switch is at the same temperature as the gas thermometer, a heat shunt must be connected between the two. This has to be flexible to allow for the movements of the mechanical

switch (approximately $\frac{1}{4}$" in a vertical direction). A similar flexible heat shunt must be provided between the radiation baffle, fixed to the mechanical switch, and the copper cylinder set into the 3/8" pumping line (A in fig. 25). Several methods were tried. Thin copper strip or copper braiding were found to be unsatisfactory as they quickly work hardened and broke on repeated application of the switch. A satisfactory shunt was prepared as follows. Approximately 10 metres of 48 s.w.g. copper wire (insulated with solderable enamel) was doubled up on itself nine times, giving a bundle of 512 strands, approximately 2 cm in length. By applying a hot soldering iron and solder to the ends of the bundle, the enamel melts, and solder flows into the ends. The bundle can then be soldered between the switch and the gas thermometer or copper cylinder. No problems of work hardening were experienced, although the heat shunt has a large area to length ratio.

5.8 Temperature Control of the Reservoir

During the specific heat measurements, it is necessary to keep the temperature of the reservoir stable, and within one or two degrees of the temperature of the specimen, so that temperature drifts are small compared with the temperature change of the specimen during the heating period.

By dissipating electrical power in a heater wound on to the reservoir, its temperature can be raised to a new equilibrium value. Finding the correct heat input to give the required constant temperature becomes rapidly more difficult with increasing temperature, as the time taken to reach thermal equilibrium within the shield and with the surroundings is proportional to the heat capacity Q of the shield, which is increasing rapidly with increasing

temperature.

If it is desired to raise the temperature of the shield by a small amount ΔT, the heat dissipated must be increased by an amount $k_o \Delta T$, where k_o is the effective conductivity between the shield and its surroundings, in order to balance to extra heat conducted away. The temperature will approach the new equilibrium value with a time constant of $\frac{Q}{k_o}$. This time will always be long compared with the time to reach equilibrium in the shield itself because of the much higher effective conductivity of the shield. As k_o is deliberately made as small as possible to reduce helium boil off, Q/k_o may be of the order of several minutes above $10^{\circ}K$.

To reduce the time required to stabilise the temperature, a feedback system is used, in which an electrical signal proportional to the difference in temperature ΔT of a temperature sensing element on the shield and the desired temperature, is amplified, and fed back as electrical power dissipated in the heater wound on the reservoir. If the gain of the system is such that $k_1 \Delta T$ watts are fed back, the time constant is reduced by a factor of $\frac{k_1}{k_o}$ to a value of $\frac{Q}{k_1}$. If the heat input from the surroundings changes by an amount W, the temperature of the reservoir will change by an amount $\frac{W}{k_o}$ without the feedback system, and by W/k_1 with it. The temperature control system therefore reduces random temperature drifts due to changes in heat input, by a factor of $\frac{k_1}{k_o}$.

The temperature sensing element used was a nominally 39 ohm Allen Bradley carbon resistor, which forms one arm of a Wheatstone Bridge. The two equal arms are 1000 ohm high stability resistors, and the variable arm is a five decade resistance box giving a resistance from 0.1 ohm to 9999 ohms in steps of 0.1 ohm. To increase the temperature, the resistance of the variable arm is reduced

below its previous equilibrium value, and the outbalance signal from the bridge is amplified by a D.C. amplifier, with a voltage gain of approximately 1500. The output, in series with a variable resistor to control the gain, is fed back to a 400 ohm constantin heater wound round the reservoir. The circuit diagram of the bridge and amplifier is given in fig. 30C.

With this system, temperature stability of better than one millidegree and a time constant less than one second is obtained below $10^{\circ}K$. At higher temperatures, when the sensitivity of the carbon thermometer is decreasing rapidly, a stability of several millidegrees and a time constant increasing to tens of seconds at $20^{\circ}K$ is found. With the heater and thermometer both on the reservoir, the feedback system was found to be free from oscillation at all temperatures.

The four 44 s.w.g. copper wires connecting the temperature controller with the heater and carbon thermometer are brought up through the pumping tube of the interspace between the reservoir shield and the outer can, and brought out through a hole in a rubber bung at the top of this pumping tube, a vacuum seal being made with black wax. They are thermally anchored at $4^{\circ}K$, and are spiralled between the outer can and the reservoir, to reduce the heat leak to the reservoir.

5.9 Vacuum System

The following pumping facilities are required in the running of the cryostat.

1) The gas pressure must be reduced to less than 10^{-7} mm Hg in the space around the specimen and the space between the reservoir and the outer can, to maintain effective thermal isolation between them.

2) Efficient pumping of the liquid helium in the reservoir is required to reach as low a temperature as possible.

3) Provision must be made for initially pumping the gas thermometer with a diffusion pump, before filling with helium gas.

4) The helium dewar must be evacuated and filled with helium exchange gas before cooling the cryostat, to prevent water vapour or air from solidifying on the needle valve, or in any of the constrictions in the tubes leading to the reservoir.

5) The interspace between the double walls of the helium dewar must be evacuated with a rotary pump before each run.

6) The pressure in the vacuum side of the manometers must be less than 0.01 mm Hg.

The first four facilities are provided by a 1SC 150 Edwards rotary pump, and a 2F4 Edwards Diffusion pump, and the last two by a 1SC 50 Edwards rotary pump. A schematic diagram of the arrangement of the pumps, taps and pumping tubes is shown in Fig. 29.

The pumping lines from each of the vacuum interspaces in the cryostat pass through the top plate and into $\frac{1}{2}$" Edwards taps. The three lines then connect into a common manifold, and go via a 1" flexible coupling to 1" B.S.P. copper pipe. By opening or closing the relevant taps, this point can be connected either to the diffusion pump or the backing pump. The gas thermometer can be evacuated via a tap which also connects into the manifold. The tap has a very small volume to reduce the dead space correction for the gas thermometer, and provides a connecting point for the 1 mm bore german silver tube coming from the gas thermometer, and 2 mm bore stainless steel tube connecting it to the constant volume manometer.

The reservoir pumping line passes through the top plate, into a 1" valve, via a 1" flexible coupling, to either the diffusion pump or the backing pump.

fig29

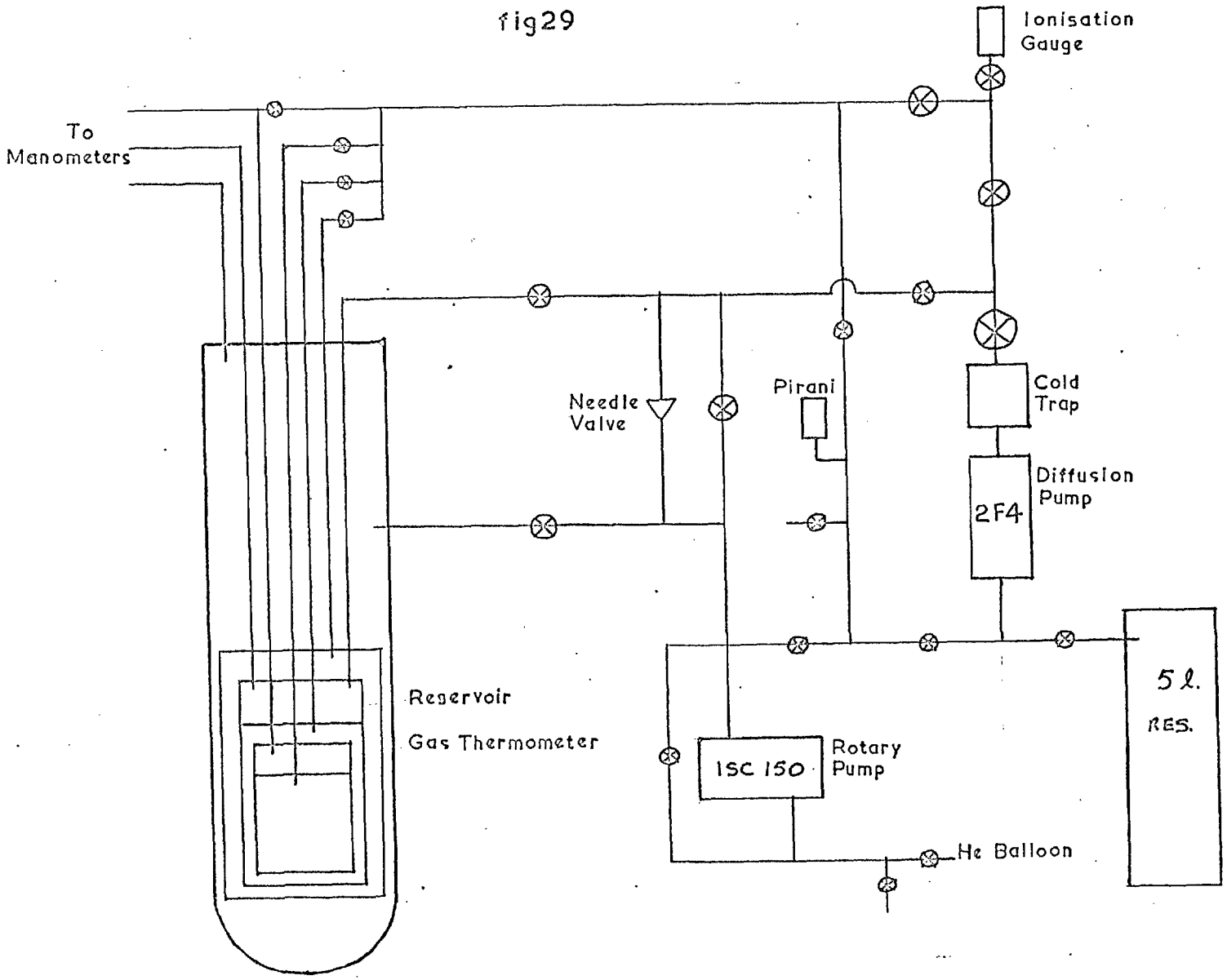
Ionisation Gauge
To Manometers
Needle Valve
Pirani
Cold Trap
Diffusion Pump
2F4
5 l. RES.
Reservoir
Gas Thermometer
ISC 150
Rotary Pump
He Balloon

However, as it was never possible to reduce the pressure of the liquid helium in the reservoir below 0.3 mm Hg, the facility for pumping the liquid with the diffusion pump was not used. To provide a fine control on the pumping speed, when pumping the reservoir, a $\frac{1}{4}$" bore needle valve is connected across the main 1" tap connecting the reservoir pumping line to the backing pump.

A further connection, through a 1" tap and a 1" flexible coupling, is made to the helium dewar. This connection is made into the side of the brass cylinder connecting the glass dewar and the top brass plate.

It is often necessary to pump on the vacuum interspaces with the diffusion pump, and at the same time pump on the reservoir with the backing pump. As this would normally lead to too high a backing pressure for the diffusion pump, the backing side of the diffusion pump can be isolated from the backing pump, and be connected into a five litre reservoir. It is found to be possible, under normal conditions, to leave the diffusion pump connected to this reservoir for at least an hour before the pressure rises above 0.1 mm, which is the maximum allowed backing pressure for the 2F4 diffusion pump.

The backing pressure is measured with a Pirani M6A gauge head, and control unit, type 2A. , and the high vacuum is measured with an Edwards Ionisation gauge head type IG2, and a Lion Electronics type 1075D control unit. The gauge head is situated in the 1" pumping line between the diffusion pump and the manifold, and for several reasons, can be relied on to give only a rough indication of the pressure in the interspaces. The main contribution to the ionisation gauge reading comes from the volatile vapour given off by the walls of the pumping tube. These condense with a negligable vapour pressure in the low temperature region of the cryostat, and do not contribute to the heat leak from the specimen

to the reservoir shield or between the reservoir shield and outer can, this being determined only by the pressure of helium present. The helium pressure increases between the diffusion pump and the manifold, but in the situation when the mean free path of the molecules is large compared with the diameter of the pumping tube, the pressure is lower in the low temperature interspace than at the top of the pumping tube by a factor of $\sqrt{\frac{Tr}{T}}$, where Tr is the room temperature, and T is the temperature of the interspace. These considerations make it very difficult to estimate the pressure in the interspaces, but fortunately such a knowledge is not essential for accurate specific heat measurements. From the measured drift rates of the specimen temperature it may be presumed that the pressure round the specimen is less than 10^{-7} mm Hg when the temperature is below $4^{\circ}K$.

5.10 Manometers

The vapour pressure of the liquid in the reservoir is measured with two manometers, a mercury manometer for the pressure range 7 cm Hg to 100 cm Hg, and an oil manometer containing butyl pthalate for the range 0 - 7 cm Hg (equals 0 to 90 cm butyl pthalate).

The mercury manometer is in the form of a U-tube, 100 cm long and prepared from 0.8 cm bore glass tubing. The oil manometer is the same length, and is made from 0.5 cm bore glass tubing. One arm of each manometer is connecte through a $\frac{1}{4}$" tap (connected to the glass manometer by $\frac{1}{4}$" bore polythene tubing) to the auxilliary vacuum system, and is pumped to approximately 10^{-2} mm Hg. The other arm is connected to the system whose pressure is to be measured, also through a $\frac{1}{4}$" tap. The pressure in the two arms of the manometer can be equalised by means of a further $\frac{1}{4}$" tap. A similar pair of manometers were

provided to measure the pressure of the helium in the helium dewar.

The constant volume manometer, used with the gas thermometer, is shown in fig. 30A. It consists of a long arm (100 cm in length, 1 cm bore) which is connected to the auxilliary vacuum system, and a short arm, also 1 cm dia., and about 4 cm in length which is connected via a vertical length of glass tubing 105 cm long, 0.6 mm bore, along 73 cm of 2 mm bore stainless steel tubing, into 90 cm of 1 mm bore german silver tubing, and into the gas thermometer. The short arm is set into the top of a bulb whose volume is about 80 cc, and the long arm is set into the side of the bulb, at the bottom. For any given pressure in the thermometer bulb, mercury can be brought to a fixed level in the short tube, (thus defining the constant volume of the system) by displacing it from a mercury reservoir with a piston operated by a screw. The pressure in the gas thermometer is then given by the difference in levels of the mercury in the two arms. The mercury reservoir is a stainless steel cylinder with a stainless steel piston sealed with two rubber "O" rings and is connected to the glass system with $\frac{1}{4}$" dia. polythene tubing. The maximum volume of the reservoir is 170 cc, such that it can hold all of the mercury required to fill the glass bulb and the long arm of the manometer.

A metal pointer sealed in the short arm defines the fixed level, the mercury level being raised until it just makes electrical contact with the metal pointer, the resistance between the pointer and the mercury being detected with a Model 8 Avo on the high resistance range. With vacuum in both arms of the manometer, the level of the mercury in the long arm is measured when the mercury in the short arm just touches the pointer. As this level has been found to be reproducable to $\pm$ 0.05 mm Hg in many pressure measurements, the value is subtracted from the height of mercury in the long arm when some

other pressure is being measured, and the level of mercury in the short arm does not have to be measured.

The glass bulb removes the possibility of the level of mercury on the side of the short arm being depressed below the bottom of the long arm, with the risk of losing gas from the gas thermometer. The glass bulb therefore has to contain enough mercury to fill the long arm to a level of at least 76 cm. The length of 0.6 mm bore glass tubing set into the top of the short arm is to prevent mercury from being forced into the capillary tubing and from there into the gas thermometer bulb if the pressure on the vacuum side of the manometer should inadvertantly rise to atmospheric pressure when the gas thermometer pressure is very low.

The five manometers are all mounted on the same wooden panel, and with them their associated $\frac{1}{4}$" taps. The liquid levels in the manometers were all measured with one single steel rule, mounted vertically in the centre of the panel, using a horizontal slide, the slide being set to the level of the meniscus, and the height being read off on the rule to the nearest 0.1 mm using a vernier attached to the slide. The arrangement is shown in Fig 30B. The perspex slide is rigidly attached to two roller bearings, one above the other, and spaced 8" apart. These slide on a 3/8" dia. ground steel rod, (rod A), which is mounted vertically between V-blocks rigidly fixed to the top and bottom of one side face of a seasoned wooden block 40" in length and 2" square cross section, which is itself mounted vertically on the panel. The wooden block has its two side faces milled flat and parallel and the steel rule is mounted vertically on the front face. On the opposite side of the wooden block to the first steel rod, and parallel to it, is fixed a second

Temperature Controller fig30C

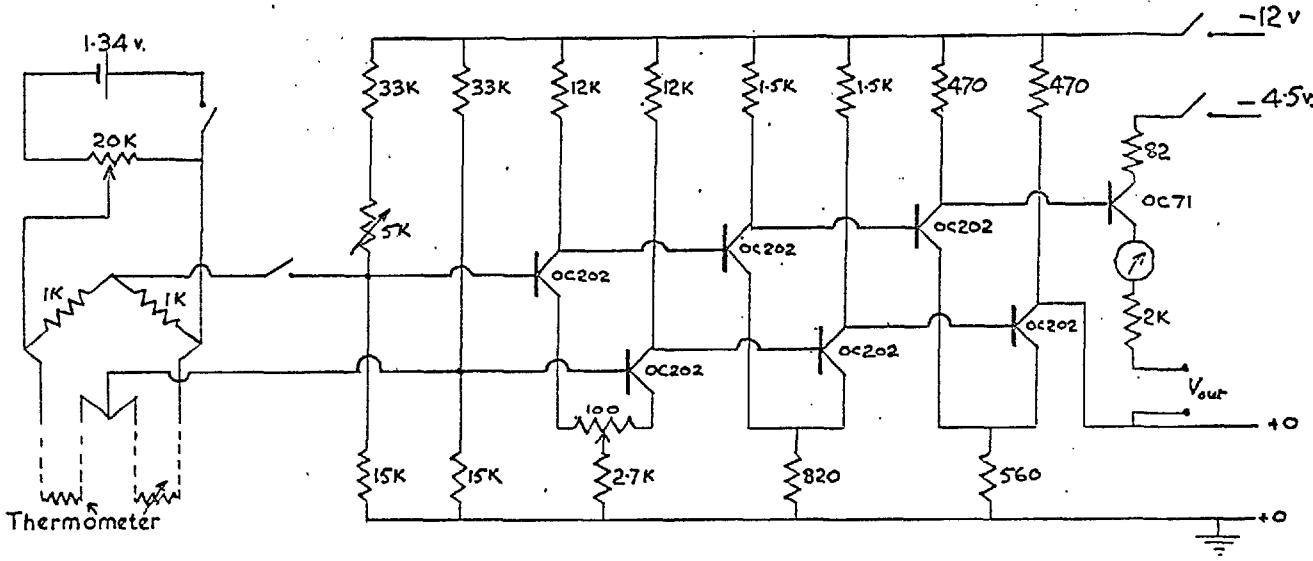

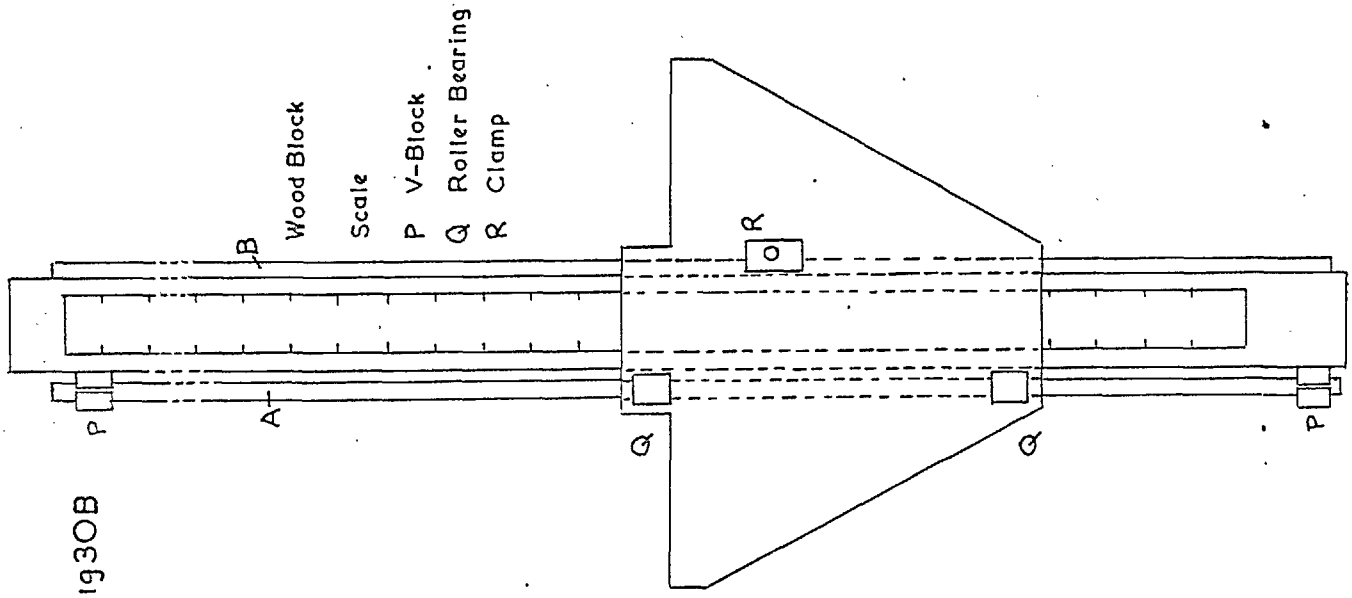

fig30B

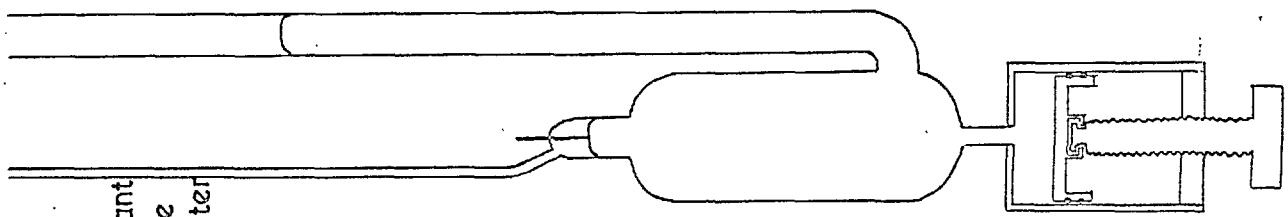

fig30A Constant Volume Manometer

3/8 " dia ground steel rod (rod B), rigidly screwed to the side of the wooden block. A brass block, 3" in length with a vertical 3/8" dia hole drilled through it, and cut away so that only about two thirds of the hole remains, can slide on rod B. The block is also split in a vertical plane so that the two halves can be clamped on to the steel rod by tightening a knurl ended brass screw. The brass block is bolted on to the perspex slide, and together with the roller bearings on rod A forms a rigid three point fixing for the slide. Rod A, carrying the roller bearings, can bend, but is prevented from doing so by the presence of the brass clamp on rod B. The clamp itself has only a short bearing length on rod A, but this is increased considerably by the presence of the two roller bearings on rod B, and angular rocking movements in a vertical plane are not detectable. Thus the accuracy of the measuring system is determined by the straightness and rigidity of rod B. The straightness of the rod was tested after being fixed to the wood by laying it on the table of a milling machine, and measuring the gap with feeler gauges. At no point was it more than 0.010 inches, and this was not found to have increased on recheck.ing some months later.

The slide consists of two shaped perspex sheets, one passing behind, and one in front of the manometers, and bolted together at several points along their length. The top edge of the front one is ground to a knife edge, and is then polished smooth and flat, (the flatness was tested with feeler gauges and found to be better than 0.002" over the entire length). To enable the liquid level to be seen most clearly, a black background was found to be most satisfactory for both the oil and mercury manometers, with illumination from above. This is achieved in the following way. A piece of specially

prepared plastic sheet, which consists of a black plastic covering over a white plaster of paris base, is cut to a rectangle $1\frac{1}{2}$" high by 2" long. A sharp horizontal white line, 1 mm wide, is obtained by milling through the plastic cover 6" below the top edge. The strip is then connected on to the back perspex strip, with the horizontal whiteline at the same level as the top edge of the front perspex sheet. The top of the white line, and the top of the front perspex sheet form the two fiducial lines necessary to determine the level of the liquid l[illegible] without errors due to parallax. One such black strip is fixed behind each manometer, and the illumination is provided by a piece of white card fixed to the back of the slide, projecting three inches above the top of the black strips.

The front edge is adjusted to be horizontal with a spirit level, and the fixing screws are tightened. The black strips are then cemented in place, the top edge of the white line being lined up by eye with the top edge of the front perspex sheet. The accuracy of alignment can be checked by measuring the liquid levels in both arms of each monometer, when the tap which equalises the pressure in the two sides is opened, and checking that they are the same. Repeated measurements on these levels showed that they are the same, within 0.1 mm.

The great advantage of the measuring system described above is the speed with which measurements can be made, because of the clarity with which the liquid level can be seen, and the ease with which the rule and vernier can be read - this is a considerable advantage when a large number of calibration points have to be taken.

The main disadvantage is the inherent inaccuracies of such a mechanical system due to slack in the bearing surfaces, and lack of straightness in the guide rod B. Errors due to the slide not being horizontal or the back and front fiducial lines being not quite parallel, are unimportant, as they will not alter with the position of the slide, and can therefore be measured when the pressures in the two arms are equal, and allowed for in other pressure difference As mentioned above, these errors have been measured, and were not greater than 0.1 mm.

The amount of play in the roller bearings on the $\frac{3}{8}$" ground steel rod, as claimed by the manufacturers, is 0.0003", and no vertical rocking movement of the ends of the slide could be detected, and were certainly less than 0.1mm. Non straightness of the guide rod is a more serious source of error as it is difficult to detect. If the slide makes an angle θ_1 with the horizontal when measuring the liquid level in one arm, and θ_2 when measuring the level in the other arm, the error in the measurement will be $(\theta_1 - \theta_2)\ell$ where ℓ is the mean distance of the manometer from the scale. As the measured maximum bend in the rod was 0.01", and the bearing length is 8", θ can never be greater than $\frac{0.01}{8}$, and as ℓ is 5" for the reservoir mercury manometer, $2\frac{1}{2}$" for the reservoir oil manometer, and 2" for the constant volume manometer, the error could not exceed 0.1 mm. As θ will only vary slowly with height, the error introduced when measuring small differences in pressure, when the effect would be most severe, is quite negligable.

The sensitivity of the mercury manometer is 0.8 mm/mdeg when the vapour pressure is .80 cm Hg, and about 0.16 mm/mdeg when the pressure is 7 cm Hg. At this point, the oil manometer can be used, and its density (12.94 times smaller than that of mercury) can be checked by making

simultaneous measurements of the oil manometer and mercury manometer readings for several pressures. The sensitivity of the oil manometer at a pressure of 7 cm Hg is thus 2 mm/mdeg, and it has fallen to 0.1 mm/mdeg when the pressure is 1.2 mm Hg, and the temperature is $1.3^{\circ}K$. Thus using the two manometers, the temperature may be estimated to within 1 mdeg., over the entire temperature range 1.3° to $4.2^{\circ}K$, if the level difference can be reliably estimated to 0.1 mm. Repeated measurements of the same pressure lead to values which have a scatter of less than $\pm$ 0.1 mm, and systematic errors should not exceed this value, especially when the level difference is small.

The mercury level in the long arm of the constant volume manometer can be read to $\pm$ 0.1 mm, and the fixed level is assumed to remain constant, its value being known to $\pm$ 0.05 mm. If a filling pressure of 8 cm Hg at $4^{\circ}K$ is used, the sensitivity of the thermometer is approximately constant at 2cm Hg/$^{\circ}K$. The temperature can therefore be estimated to $\pm$ 5mdeg. When calibrating the gas thermometer against the vapour pressure of the liquid in the reservoir between $3^{\circ}K$ and $4^{\circ}K$, the difference in the calculated temperaturesare found to be consistant with the estimated gas thermometer corrections, and have a scatter of between 5 to 10 mdeg.

5.11 Measurement of the Resistance of the Specimen Resistance Thermometer

The change in temperature of the specimen as a function of time is calculated from the observed changes in potential across the carbon resistance thermometer when a known current is passing through it. The change in temperature during the heating period is

about 3% of the mean temperature, corresponding to a change in voltage of about 10% at 1°K and 1% at 20°K. As it is desired to measure the change in temperature with an accuracy of 0.1%, the measuring circuit must be capable of measuring changes of the order of 10^{-5} times the total voltage.

The current through the carbon resistor is limited by the joule heat generated in the resistor, which, because of the poor thermal conductivity of the carbon granules, leads to a rise in temperature of the resistor core, and a consequent lowering of its resistance. As the resistance increases very rapidly, and the thermal conductivity decreases, as the temperature is reduced, the effect is more acute at the lowest temperatures, but using an empirical formula due to Berman[121], which relates the temperature rise to the power dissipated, it can be shown that the rise in temperature is always less than 0.3 mdeg if the voltage across the resistor is less than 10 mv. The voltage across the resistor does not exceed 10 mv in practise. The voltage discrimination of the detecting circuit therefore has to be of the order of 1 μv at 1°K, and 0.1 μv at 20°K.

The resistance is measured potentiometrically, requiring two current and two potential leads to the carbon resistor. The potential is backed off with a Tinsley 4025 potentiometer on its most sensitive range (0-10 mv in 1 μv steps), and the small difference voltage is amplified by a Keithley type 149 D.C. amplifier, and the output is displayed on a Honeywell Brown 10 mv potentiometric chart recorder. Fullscale deflection of 10" on the chart recorder may be chosen to be 10 μv, 30 μv, 100 μv, 300 μv or 1 mv by an appropriate setting of a sensitivity switch on the Keithley amplifier. The most sensitive range could not always be used for two reasons. At the

lowest temperatures, where the sensitivity of the thermometer is greatest, typical drift rates of 0.1 mdeg./sec make it impracticable to use a more sensitive range than the 100 μv range (full scale deflection on this range at 1.3°K is about 4 mdeg).

The second factor limiting the maximum usable sensitivity is the electrical noise superimposed upon the output signal. The Keithly amplifier incorporates a mechanical chopper operated at 100 c/s, and has a 10 c/s bandwidth. The second harmonic of all mains frequency pick up does not average to zero as do all other frequencies above 10 c/s, but appears as noise at the output. Pick up at this frequency may be considerable, and strenuous efforts have to be made to reduce it as far as possible by using screened leads, and earthing the screening, potentiometer case, and the chassis of the unit supplying the current to the thermometer, to a common point on the top plate of the cryostat. None of the leads to the resistance thermometer is earthed as to do so is found to increase the pick up considerably. Screening is provided in the cryostat by the stainless steel pumping tube through which the wires pass. These measures provide good electrostatic screening, but afford little protection against varying magnetic fields. The effects of these fields are minimised by twisting the wires together where possible to reduce the loop area. Other sources of noise, such as Johnson noise and noise generated in the amplifier are much smaller than the electrostatic and magnetic pick up.

It was found that the noise level was roughly proportional to the resistance of the carbon resistor, and could not be reduced below 0.5 R μv, where R is in k ohms, that is, about 5 μv at 1.3°K and 0.1 μv at 15°K.

As the resistance of the thermometer decreases very rapidly with increasing temperature, the thermometer current has to be increased to maintain sensitivity. Thus, whenever the voltage across the resistor falls below about 3 mv, the current is increased to bring the voltage up to 10 mv. The thermometer currents used are approximately 0.3 μA between 1.1° and 1.3°K, 0.9 μA between 1.3° and 1.9°K, 3 μA between 1.9° and 2.9°K, 8 μA between 2.9° and 4.9°K, 22 μA between 4.9°K and 9.2°K, and 45 μA above 9.2°K.

These currents are provided by switching appropriate resistors in series with a 1.34 volt Mallory mercury cell, and the resistance thermometer. The circuit is shown in Fig. 31A. This cell was chosen because of its large capacity, around 1 amp hour, and its long term voltage stability. The current through the resistor is found by measuring the voltage across a 14,510 ohm wire wound resistor which is also in series with the thermometer. The voltage is taken to the second pair of input terminals on the potentiometer, and can be measured to five significant figures with the aid of the Keithley amplifier.

Thermal voltages in the voltage leads are eliminated by switching off the thermometer current and backing off any residual voltage with a backing off control incorporated into the D.C. amplifier. Uncorrected but constant thermal voltages of up to 1 μv are unimportant, as they would lead to an error in the absolute temperature of less than 1 mdeg. If the thermal voltage should vary by more than 0.1 μv during the heating period of the specific heat measurement (typically of the order of 25 secs) it would introduce a significant error into the measurement of ΔT, but under normal conditions it was seldom found to vary by more than one tenth of this amount.

fig 31A

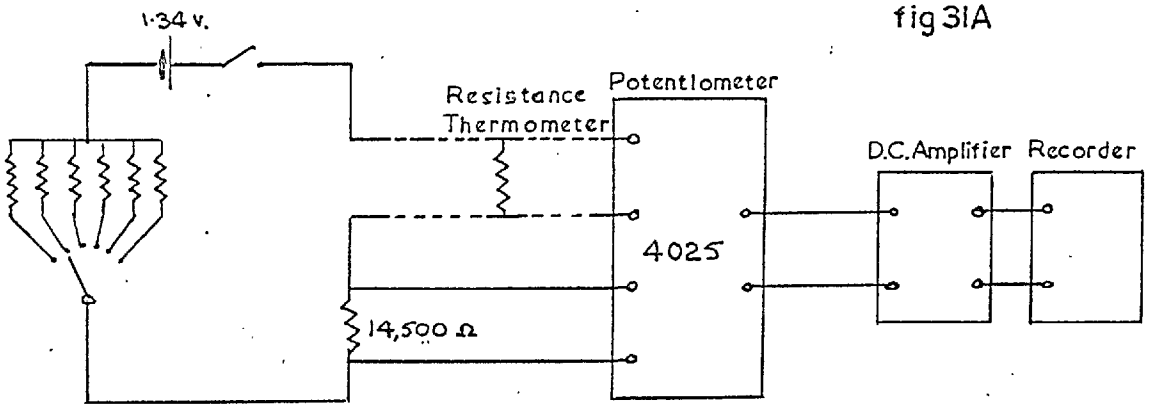

Specimen Thermometer Circuit

fig 31B

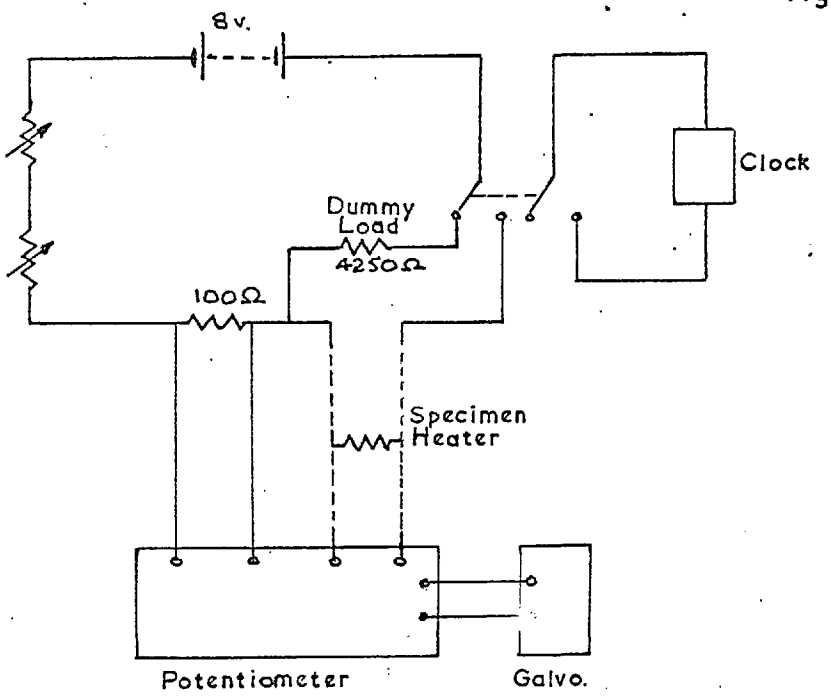

Specimen Heater Circuit

The gain and linearity of the amplifier-recorder system for different amplifier sensitivity ranges has to be measured at regular intervals, usually before and after the series of specific heat measurements, by changing the potentiometer setting by known amounts, and measuring the change in reading of the pen recorder. The pen recorder automatically readjusts its gain every ten minutes, and this varies by up to 1%. The gain of the system is also non-linear by up to 1%, but using the method of measurement to be described below, the errors introduced into ΔT by errors in the amplifier-recorder system never exceed 0.1%, and are generally far less than this value.

5.12 Specimen Heater Current Supply

With a specimen heater resistance of 4250 ohms, heater currents of between 20 μA and 2 mAs are required to provide a heating rate of between 1 mdg/sec and 10 mdeg/sec in a specimen of one mole, in the temperature range 1° to 20°K. The current must also be constant to within 1 in 10^4 during the heating period of between 20 and 30 secs. The circuit providing this current is shown in fig. 31B. Six Mallory cells, connected in series, provide a voltage of approximately 8 volts. The current is controlled by two variable resistors in series with the cells, giving course and fine controls. The current can be switched from a dummy lead to the heater resistor with one pair of contacts of a two pole two way toggle switch. The second pair of contacts are used to switch the Leybold electric clock which measures the time for which the current is flowing.

The electric clock is driven by a mains operated synchronous motor,

and is started and stopped by a clutch operated by a relay energised by current flowing in the switching circuit. The clock is graduated in 10 msec. intervals, and when calibrated against a crystal controlled electronic timer, was found to be in error by up to 20 msecs. for time intervals less than 10 secs, increasing to 50 msecs for time intervals of about 100 msecs. These variations are made up of switching delays and variations in mains frequency. As these would not introduce errors of more than about ± 0.1% in a typical heating time (20 - 30 secs), the clock was considered to be adequate. Differences between the times when the two pairs of contacts of the toggle switch close was also checked with the crystal controlled timer, and were found to be of the order of 5 to 10 msecs.

The potential across the heater resistor is measured with a second Tinsley 4025 potentiometer, the outbalance being detected with a Tinsley type 4500 galvonometer (5Ω 34mm/μA). The voltage across a standard 100 ohm resistor (accuracy 0.1%) in series with the heater current is measured with the same potentiometer, and determines the magnitude of the heater current.

As the potentials across the heater resistor and 100 ohm standard are never less than 100 mv and 2.5 mv respectively, it was considered unnecessary to include a reversing switch in the current and potential leads to illiminate thermal voltages, as these are unlikely to exceed 1μv. The heater current and voltage are therefore measured to four significant figures, with an error of ± 1 in the last figure.

5.13 Measuring Proceedure

The following is a brief account of the proceedure adopted during the

measurement of the specific heat of a specimen in the temperature range 1.3° to 20°K.

The specimen, which has been turned to size, polished, and carefully weighed, is inserted into the specimen holder, and the clamping screws are tightened, and then retightened after a few hours. The reservoir shield is soldered to the reservoir, and the outer can to its top cap using low melting point solder, and the system is checked for leaks with a helium leak detector. The helium and nitrogen dewars are mounted, and the vacuum interspace of the helium dewar is evacuated with the auxilliary pump, and is then shut off. The helium dewar is pumped out and filled with helium exchange gas at atmospheric pressure. The space between the reservoir and outer can, (the outer space), is pumped, a small pressure (about 1mm Hg) of helium exchange gas is let in and the space is shut off. The space around the specimen (the inner space) is then pumped with the diffusion pump backed by the helium leak detector, and the mechanical heat switch is closed. Liquid Nitrogen is poured into the Nitrogen dewar, and the cryostat is allowed to cool over night - the outer can and reservoir being cooled by conduction through the exchange gas, and the specimen by conduction through the mechanical switch. Any leak appearing in the inner space at low temperatures will let in helium, which will be detected by the leak detector.

When the entire system is at liquid nitrogen temperatures, the helium exchange gas in the outer vacuum space can be pumped away, (having first shut off the inner space pumping line) and the two vacuum spaces are then pumped to a high vacuum with the diffusion pump. At no time before the specific heat measurements are completed is any helium gas allowed into the space

round the specimen because of the difficulty in removing it at low temperatures. The sensitivity of the amplifier-recorder system is measured at this stage.

The helium transfer syphon, one arm of which is dipped into the liquid helium storage vessel, is lowered into the helium dewar and the "O" ring seal is tightened to provide a gas tight seal on to the transfer tube. The reservoir is pumped with a backing pump, and the needle valve is opened. The helium dewar is closed off, and as the pressure in the dewar falls, (the gas is being pumped away through the needle valve) liquid helium is drawn through the transfer syphon. On leaving the transfer tube at the bottom of the dewar, the liquid evaporates and the cold gas cools the outer can and the dewar walls as it rises. The cold gas is then pumped through the reservoir, which is also cooled, and leaves by the reservoir pumping line. This method of transfer removes the need for helium exchange gas in the outer vacuum space, with a consequent reduction in the time required to reach the lowest temperatures and commence measurements. As the reservoir cools, the gas thermometer is cooled through the thermal short to the reservoir, and the specimen is cooled through the mechanical heat switch.

After transferring for about fifty minutes, liquid helium is observed in the bottom of the dewar, and if the speed of transfer has been carefully controlled the reservoir and specimen quickly reach $4.2^{\circ}K$. The needle valve is closed, and the dewar is opened to the helium gas balloon. More liquid helium is now transferred by closing off the boil off line of the storage vessel and pumping with the rubber bladder sealed into its neck. This is continued until the outer can of the cryostat is covered with liquid to a

depth of about 15 cm, when it contains about 1.5 litres of liquid helium. The transfer syphon can now be removed, and the top of the transfer tube sealed off. Approximately 3 to 3.5 litres of helium are used in the transfer, so that approximately 1.8 litres of liquid are required to cool the cryostat from 77°K to 4°K.

The needle valve is again opened, and helium is allowed into the reservoir to a depth of about 3 cm, the amount being estimated from the fall in level in the dewar. The needle valve is shut, and the reservoir pumped with the maximum pumping speed available. The temperature of the reservoir falls to about 1.2°K, and after about 15 mins., the specimen is at its lowest temperature, and the mechanical switch is opened. This must be done very carefully, as excessive vibration may raise the temperature of the specimen very considerably. The temperature rise is usually found to be between 10 and 20 mdegs. The specimen is now at its lowest temperature, and thermally isolated, and specific heat measurements may be commenced immediately.

The thermometer current is set at 0.3 μA, and the voltage across the thermometer is backed off with the potentiometer until the difference voltage is less than the full scale deflection of the pen recorder using the maximum convenient amplifier sensitivity (usually the 100 μV range at this temperature). The slow variation of the recorder trace with time corresponds to the temperature drift of the specimen. Under these initial conditions, the temperature is rising at a rate of about 10^{-2} mdeg/sec, even though the shield surrounding it is colder than the specimen, because of vibration heating of about 0.5 erg/sec. It is this temperature drift, and the noise level on the signal that limit the

maximum usable sensitivity of the amplifier.

The recorder trace of a typical specific heat measurement is shown in Fig. 32 A, and the corresponding variation of temperature is shown in Fig 32 B (the temperature drifts before and after the heat having been greatly exaggerated for clarity).

Fig. 32

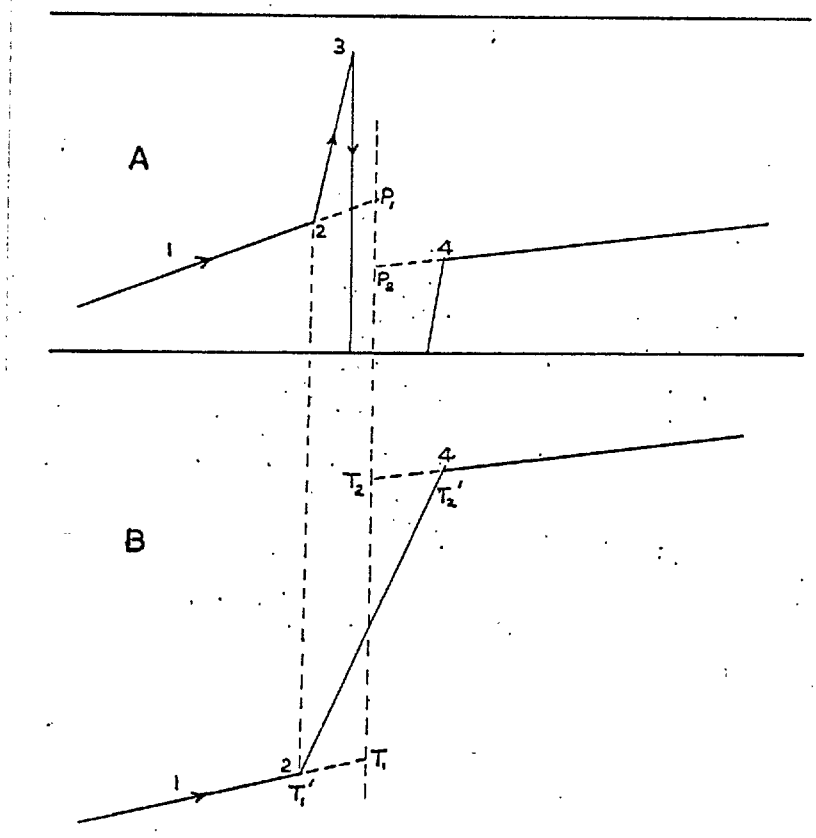

The temperature drift is recorded for two to three minutes (1) and then the heater current is turned on (2). The voltage on the potentiometer is reduced by a predetermined amount (3), (an amount corresponding to a change in temperature ΔT of 3% of the mean temperature). This voltage change will

be between 10 and 100 times full scale deflection on the pen recorder and the direction of the unbalanced voltage will be equivalent to a chart reading well below the bottom of the chart. As the specimen temperature rises, the unbalanced voltage rapidly decreases, and when this is again within the range of the pen recorder, the heater current is switched off (4), and the temperature of the specimen again drifts slowly for a further three minutes, ready for the next heat.

The magnitude of the heater current is chosen to give the desired temperature change in 20 to 30 secs., this being the minimum time in which the heater current or voltage can be conveniently measured, and which also allows the extrapolation of the temperature drifts before and after the heat, which are necessary to estimate ΔT, to be made with confidence. The heater current (or voltage), the time of duration of the heat, and the thermometer potential reading before and after the heat, are recorded.

This procedure is repeated until the thermometer potential falls below 3 mv, when the current is increased to bring the potential back to 10 mv. As the temperature rises, and the resistance falls, the noise level also falls. Also as the temperature increments traversed during the approximately constant heating period are increasing, the drift rate becomes a smaller fraction of the heating rate. These two factors enable the more sensitive ranges of the amplifier to be used, and compensate for the decreasing sensitivity of the thermometer. As full scale deflection on the recorder corresponds to between 5% and 10% of the voltage change during the heat, any errors in the calculated resistance change, due to inaccuracies in the sensitivity of the amplifier-recorder system are reduced by the same factor.

As the specific heat is increasing with temperature, and the temperature increment is also increasing, the heater current has to be increased every five or six heats to keep the heating time within 20 to 30 secs. Only the heater current or the heater voltage are measured in any one heat, first one and then the other being measured for several consecutive heats, so that the heater resistance, which only varies very slowly with temperature, can be checked.

When the temperature reaches about 2.2°K, the heat conducted along the leads and through the residual gas to the reservoir shield just balances the vibration heating, and the temperature drift rate falls to zero. At about 3°K, the drift rate has increased sufficiently to necessitate increasing the temperature of the reservoir to about 3.5°K. Readjustment of the reservoir temperature is necessary every degree or so around 4°K, and every two or three degrees between 10 and 20°K.

After between 90 and 100 heats, the temperature of the specimen has reached 20°K. The sensitivity of the amplifier-recorder system is again checked. The first part of the experiment has now been completed, and it remains to calibrate the thermometer against the vapour pressure of the liquid helium in the reservoir in the temperature range 1.3 to 4.2°K, and against the gas thermometer between 4°K and 25°K.

5.14 Thermometer Calibration (i) Below 4.2°K

The temperature of the liquid in the reservoir can be found from a measurement of its vapour pressure. Providing that the reservoir liquid and the resistance thermometer are at the same temperature, the temperature

corresponding to the particular value of the resistance of the thermometer can be determined.

The reservoir is refilled with helium to a depth of about 2cm. Pure helium gas that has boiled off from the liquid in the dewar is let into the gas thermometer to a pressure of about 8cm Hg at $4^{\circ}K$. The mechanical heat switch is closed, and helium exchange gas at approximately 0.05 mm Hg pressure is let into the inner space round the specimen. This is to ensure that the temperatures of the specimen and reservoir are the same. That this is the case is suggested by the very rapid response of the specimen thermometer to changes in the reservoir temperature, though it would be hard to detect small, constant, differences in temperature between the two.

The reservoir is warmed to about $4.0^{\circ}K$, and is very gently pumped. This prevents the formation of a hot surface layer, and provides favourable conditions for the mixing of the liquid by convection currents. By carefully adjusting the pumping speed of the needle valve, and watching the changes in temperature of the specimen thermometer on the recorder, the temperature can be brought to an almost constant value. When the temperature has remained constant to within 0.5 mdeg for several minutes, the vapour pressure is measured on the manometer, and the specimen thermometer voltage and current are noted. The gas thermometer pressure is also determined for all measurements down to about $2.5^{\circ}K$, to calibrate the gas thermometer. The reservoir is then pumped down to a slightly lower temperature, and the pumping speed is readjusted to stabilise the temperature, approximately fifteen minutes being required to obtain sufficiently stable conditions

and to take the necessary readings. Two complete sets of readings are taken at each temperature. This is repeated about fifteen times in the temperature range 4.2° to $1.3^{\circ}K$. The temperature stabiliser is not used below $4^{\circ}K$ when calibrating the thermometer because of the danger of setting up unknown temperature gradients in the liquid and the reservoir walls.

When the pressure is down to about 7 cm Hg, the oil manometer may be used, the level difference being about 90 cm at this pressure. For three or four calibration points between 7 cm Hg and 4 cm Hg, both the oil and the mercury manometers are measured to check the density of the oil with the value found previously using a density bottly. It becomes extremely difficult to obtain accurate calibration points below about $1.4^{\circ}K$ using the vapour pressure of Helium 4, as the pressure change with temperature is falling rapidly, and thermomolecular pressure corrections rapidly increase with further decrease in temperature.

(ii) Between $4^{\circ}K$ and $25^{\circ}K$

Having obtained the calibration points below $4^{\circ}K$, the liquid helium in the reservoir is pumped away, and the temperature controller is set to stabilise the temperature of the reservoir at about $4.5^{\circ}K$. The reservoir temperature stabilises very rapidly, but the specimen may take up to several minutes to come into equilibrium with the reservoir. When the thermometer voltage is stable, the voltage and current are recorded and the gas thermometer pressure is measured. This is repeated twice at each temperature. About fifteen such calibration points are taken in the temperature range $4^{\circ}K$ to $25^{\circ}K$.

5.15 Errors in the Calibration Points (i) Below 4.2°K

For calibration points below 4.2°K, the helium vapour pressure measured in the manometer is compared with the "1958 Helium Vapour Pressure Scale" to obtain the temperature T. To obtain more accurate values of the temperature, certain corrections must be applied. The 1958 temperature scale assumes a mercury column at 0°C, and must therefore be corrected for the lower density of mercury at the ambient temperature of the column. If this temperature is 24°C, the correction decreases from a value of 4 mdeg at 4°K and is negligable below 1°K, the correction being subtracted from T. This correction is shown in fig. 33A.

The second correction is that for the thermomolecular pressure difference between the high and low temperature ends of the pressure sensing tube, and is important when the mean free path of the molecules becomes comparable with the diameter of the tube. In the extreme case when the mean free path is long compared with the diameter, the ratio of the pressures at each end is given by $\frac{P_{hot}}{P_{cold}} = \sqrt{\frac{T_{hot}}{T_{cold}}}$. For intermediate cases, Roberts and Sydoriak[143] have given numerical values of $\frac{P_{hot}}{P_{cold}}$ in terms of the parameter $\frac{P_{hot}}{R}$, where R is the radius of the tube. A graph of the correction to be applied to the temperature calculated from P_{hot} is shown in fig 33A for a sensing tube of 2 mm bore.

A further source of error in the temperature comes from the increase in temperature with depth below the liquid surface due to the increase in hydrostatic pressure. The estimation of this correction is difficult, as its maximum value is reduced by the instability of such a temperature gradient,

and turbulence in the liquid, and also by the presence of the copper walls of the reservoir. It is most severe just above the λ point (2.2°K), when it can have a maximum value of about 2 mdeg/cm of liquid helium. Because of the large surface area and small depth (around 1 cm) of the liquid in the reservoir, and as the liquid is being continually pumped, it is considered that the conditions are most favourable for good mixing of the liquid, and therefore this correction is ignored. Below the λ point the liquid becomes superfluid, and cannot support a temperature gradient, and therefore the correction is zero. There is also a further source of error to be considered below the λ point. Superfluid helium flows up the sensing tube, boils, and refluxes back into the reservoir, setting up a pressure gradient in the sensing tube. Roberts and Sydoriak have concluded that this correction is negligable above 1°K.

Random errors of approximately ± 0.1 mm in the measurement of the liquid levels in the manometers lead to errors of approximately ± 0.1 mdeg at 4.5°K, to ± 0.6 mdeg at 2.4°K using the mercury manometer, and from 0.05 mdeg at 2.4°K to 1 mdeg at 1.3°K to 7 mdeg at 1.0°K with the oil manometer. Incomplete mixing of the liquid, especially serious near 4.2°K, where the pumping rate to maintain a constant temperature is very low, may lead to temperature variations of one or two millidegrees. A final source of error is the 1958 temperature scale itself. The resistance of the thermometer is measured to better than 1 part in 10^4, which gives an equivalent error in temperature of less than 0.2 mdeg throughout the range.

One may therefore hope to measure the temperature in a calibration

measurement between 1.4 and 4.2°K to within a millidgree of two. That the random errors do not exceed this value is supported by the scatter of the calibration points from the calibration curve.

Fig 33

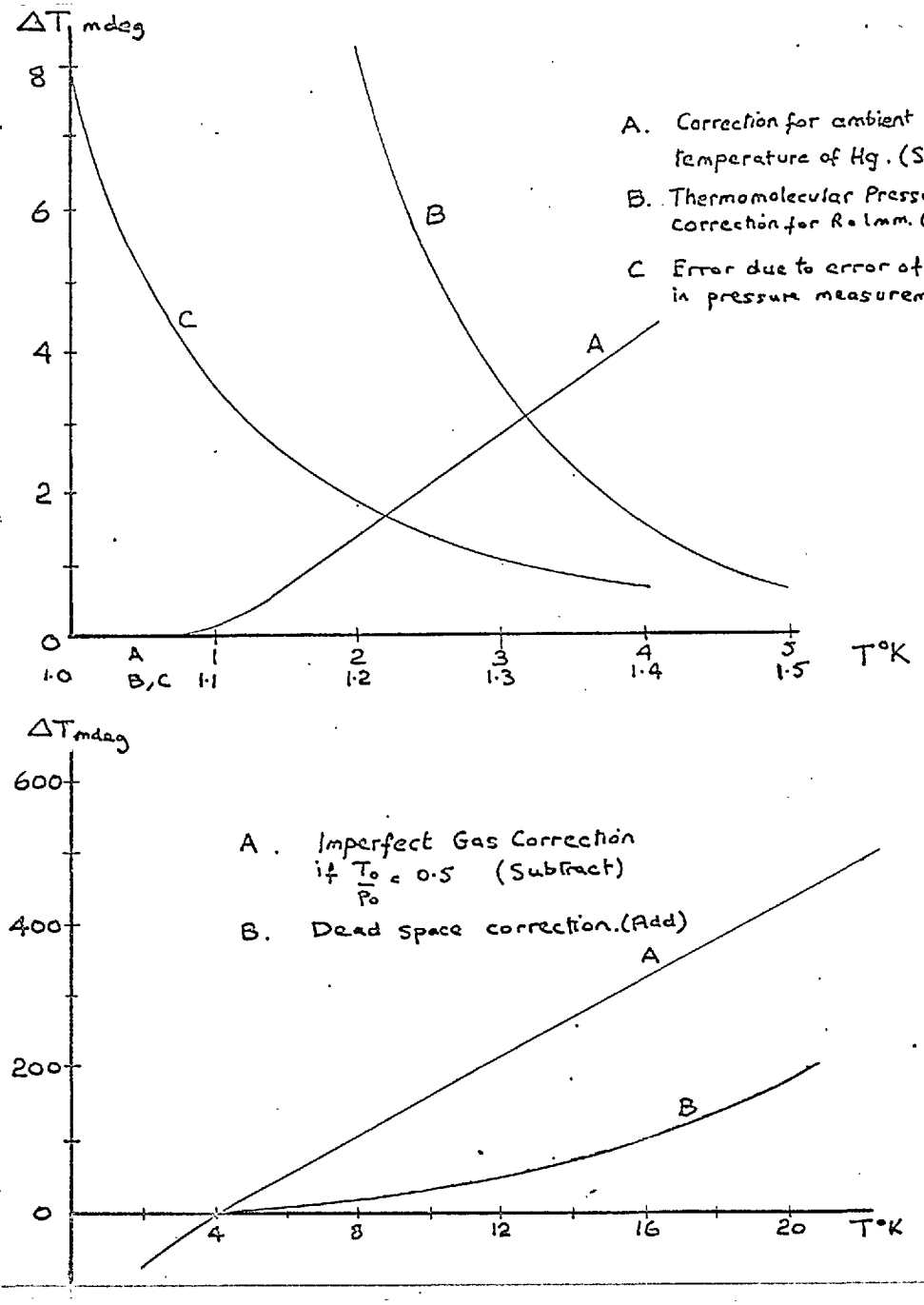

(ii) Above $4.2^{\circ}K$

In this region the temperature is calculated from the gas thermometer pressure. To a first approximation the pressure p of the gas in a constant volume gas thermometer, is proportional to its temperature, and the pressure at one known temperature is sufficient to establish the pressure-temperature scale. In practise two corrections have to be applied to take account of the non-linearity of the system - the imperfect gas correction and the dead space correction.

Helium is not a perfect gas, and exhibits increasing departures from Charles' Law ($p \propto T$) at low temperatures and high pressures. The gas thermometer pressure p_o is measured at a known temperature To (the temperature is measured from the vapour pressure of the liquid in the reservoir at say, $4^{\circ}K$) and other temperatures T at higher pressures p are calculated assuming a linear relation $T = p\frac{To}{po}$. The method of evaluating the correction ΔT to be applied to T because of the non-ideality of the helium is given in Appendix 3, and it is found to be proportional to the filling pressure for low pressures. For the filling pressure used (p_o = 8 cm Hg at $T_o = 4^{\circ}K$, i.e. $\frac{To}{po} = 0.5$) the correction increases from zero at $T = To \simeq 4^{\circ}K$ to $0.45^{\circ}K$ at $20^{\circ}K$, and is to be subtracted from the calculated temperature. This correction is known with a confidence of about 10%, and is shown for $\frac{To}{po} = 0.5$ in Fig. 33B.

The dead space correction arises from the finite mass of gas in the pressure sensing tube and manometer, which is at a temperature different from that of the bulb. This correction is calculated in Appendix 3, and is shown in Fig. 33B. The calculation assumes a knowledge of the temperature

distribution along the sensing tube, and as this is not known with any real assurance within the cryostat, it is estimated that this correction may be in eror by ± 15% of its magnitude. The magnitude of the correction varies from zero at T=To ~ 4°K, to about 0.17°K at 20°K, and has to be added to the calculated temperature. Unlike the first correction, it is independent of the filling pressure of the thermometer. A further correction is that for the thermomolecular pressure difference along the pressure sensing tube. If $\frac{To}{po} = 0.5$, and for a 1 mm bore sensing tube this correction is approximately 0.1 mdeg at 3°K, and falls at higher temperatures, and is therefore ignored.

The random measuring error of ±0.1 mm Hg is equivalent to a random temperature error of ± 5 mdeg if $\frac{To}{po} = 0.5$. However since the pressure p_o is used to calculate the sensitivity, any error in p_o will result in a systematic error increased by a factor $\frac{T}{To}$ at a higher temperature T. Thus there is an uncertainty of ± 25 mdeg at 20°K from this source. This error is reduced by taking five or six gas thermometer-vapour pressure thermometer calibration points between 4.2°K and 2.5°K, calculating $\frac{T}{p}$ for each, plotting against T for each point. From this plot the value of $\frac{T}{p}$ at 4°K is taken to be the value $\frac{To}{po}$ in calculating the higher temperature points. The variation of T/p with T affords an opportunity to check the estimated correction curves in this range. Satisfactory agreement is found within the experimental error.

The resistance of the thermometer is measured with an accuracy corresponding to 0.2 mdeg at 4°K, and less than 5 mdeg at 20°K.

The rather large correction to be applied to the calculated temperature could be reduced by a factor of approximately five, ($\frac{20°K}{4°K}$), if the gas

thermometer could be calibrated against the vapour pressure of liquid Hydrogen at 20°K. Unfortunately such a facility is not available in this cryostat though it is hoped to add a hydrogen vapour pressure bulb at a later stage. The non ideal gas correction has been checked by calibrating the carbon resistor against the gas thermometer using a filling pressure of $\frac{To}{po} = 0.5$, and repeating the calibration with a filling pressure of $\frac{To}{po} = 1$ (in the same low temperature run). From the differences in calculated temperature corresponding to the same resistance, (and therefore, presumably, the same true temperature) the temperature correction due the non-ideality of the gas can be estimated. It was found to be in satisfactory agreement with the calculated curve. The dead space correction can only be checked by calibrating against a known high temperature.

Thus the magnitude of the corrections to be applied assuming a filling pressure of $\frac{To}{po} = 0.5$ at 4°K, vary between + 0.04° ± 0.01°K at 3°K, zero at 4°K, to 0.29° ± 0.07°K at 20°K, with a random error of 0.005°K.

5.16 The Calibration Curve

It has been demonstrated on many occasions that the temperature dependence of an Allen Bradley resistor can be well described by a function of the form

$$\sqrt{\frac{\log R}{T}} = a_o + a_1 \log R$$

Such a function has been found to fit the calibration points of the present resistor to better than 1% in the temperature range 1.3° to 4.2°K, and also in the range 2.5 to 25°K, and to better than 2% over the entire range

1.3 to 25°K.

The systematic deviation from the above curve can be removed almost entirely by including two more terms in the formula, giving

$$\sqrt{\frac{\log R}{T}} = a_0 + a_1 \log R + a_2 (\log R)^2 + a_3 (\log r)^3 \quad \ldots \quad 5.1$$

The problem remains to find the most satisfactory criteria for choosing the coefficients a_i. As the error in any particular calibration point arises almost entirely from the measurement of T, R will be assumed to be known exactly.

Choosing the coefficients to minimise the R.M.S. deviation of T from the value predicted by eq.5.1, would not be very satisfactory in fitting a curve over the entire range 1.3 to 25°K, for the following reasons. The temperature measurements in the range 4° to 25°K have a far greater random scatter than those below 4°K, and this criterion would lead to a calibration curve which deviated from the low temperature points by an amount far larger than their actual errors. The criterion would lead to a fractional error in T, which increased as the temperature is reduced. It is therefore preferable to minimise the R.M.S. fractional deviations $\frac{\delta T}{T}$, where δT is the deviation of a calibration point from the calibration curve. Although this would probably be the most satisfactory criterion, considerable simplification in the computation of the coefficients can be effected if mean square deviations in the quantity $\sqrt{\frac{\log R}{T}}$ are minimised. These deviations are of the form $\sqrt{\frac{\log R}{T}} \frac{\delta T}{T}$ and are therefore the fractional deviations weighted by a slowly decreasing function of T which still further decreases the influence of errors in the high temperature points.

Thus writing $\sqrt{\frac{\log R}{T}}$ as y and $\log R$ as x, the polynomial $y = a_0 + a_1 x + a_2 x^2 + a_3 x^3$ is determined which is the best fit to the points y_i, x_i subject to the condition that $\sum_i (y_i - y)^2$ is a minimum. This computation is performed on an Elliott 803 computer using the Elliott Library Programme 803 Y2. In the discussion of the results of particular runs, the R.M.S. deviation of the quantity $\sqrt{\frac{\log R}{T}}$ is quoted. This may be converted to a fractional deviation in T by multiplying this quantity by a factor increasing from 1 at 1.3°K to 4 at 20°K. The fractional deviation in the temperature is of the order of 0.1%

The calculation of ΔT in each specific heat measurement involves, effectively, the multiplication of ΔR, the change in resistance during a heat, by the gradient of the calibration curve $\frac{dR}{dT}$. Under certain circumstances the gradient of a curve which fits all of the calibration points with considerable accuracy may deviate quite considerably from the gradient of the true calibration curve. This would be the case if the number of terms in the polynomial were comparable to the number of calibration points, and this situation is therefore to be avoided. It may also be the case at the ends of the temperature range, and errors of up to 1% in the estimation of ΔT, and therefore of the specific heat, are to be expected within about 10% of the temperature of the extremal calibration points.

5.17 Calculation of the Specific Heat

The heat capacity Q(T) of the specimen + addenda is calculated from either of the two equations,

$$Q(T) = \frac{i^2 R_H(T)\, t}{\Delta T} = \frac{V^2 t}{R_H(T)\, \Delta T} \qquad \ldots\ldots\ldots\ldots 5.2$$

where $R_H(T)$ is the resistance of the specimen heater, t is the heating time, i is the heater current and V is the heater voltage.

If $Q_A(T)$ is the heat capacity of the addenda at temperature T, the specific heat C per mole of a specimen of N moles, is given by

$$C = \frac{Q(T) - Q_A(T)}{N}$$

The quantities T and ΔT are computed from the resistanceof the thermometer before and after the heat, using the calibration polynomial described above. Because of the rapidly varying sensitivity of the thermometer, ΔT cannot be found by simply multiplying the change in resistance by the gradient of the R-T curve. The temperatures before and after the heat have to be calculated separately, and subtracted to find ΔT. To find ΔT to three significant figures, the resistances must be measured, and the temperatures computed, to five significant figures. To reduce the considerable labour involved in these and subsequent calculations, a programme has been developed for use with an Elliott 803 computer which allows the specific heat to be computed given the necessary information obtained in the run. An outline of the stages of this calculation will now be given, and the detailed programme is given in Appendix 4.

Fig. 32 B shows the variation of temperature with time during a heat.

Before and after the heat, the drift rate depends only on the heat leak to the specimen from the surroundings. During the heating period, the heat reaching the specimen is equal to the power dissipated in the heater plus the heat leak from the surroundings, which will vary over the duration of the heat because of the increasing temperature of the specimen. It may be shown that if the temperature drifts before and after the heat are small, and vary as a linear function of the temperature of the specimen, and if the specific heat of the specimen does not vary significantly over the temperature range T to T+ΔT, then the effects of the heat leaking from the surroundings may be eliminated by taking $\Delta T = T_2 - T_1$, the temperatures found by extrapolating the temperature drifts before and after to a time half way through the heat, rather than taking $\Delta T = T_2^1 - T_1^1$, the actual temperature increase during the heat.

The resistance R_1 at the point P_1 (corresponding to T_1) is found from the relation

$$R_1 = \frac{V_1 - s\,d_1}{V_i} \times R_i$$

where V_1 is the potentiometer reading (μv) before the heat, s is the sensitivity in μV/inch of the amplifier-recorder system for the particular range in use, and d_1 is the recorder deflection in inches of the point P_1. Vi is the voltage in millivolts across the standard resistor R_i (kΩ) in the thermometer current circuit, (thus $\frac{Vi}{R_i}$ is the thermometer current in μA). V_i is a slowly varying function of V_1 for any given range, varying by about 0.5% as V_1 changes from 10 to 3mv. As V_i is only measured at the beginning and end of the series of measurements using the particular thermometer current range, its value at any particular value of V_1 is found from

$$V_i = V_{io} \left(1 - \frac{V_1}{V_o} \right)$$

where V_o is the voltage of the cell providing the current (1.34v) and V_{io} is the value of V_i when $V_1 = 0$ (found by extrapolating the measured values of V_i to $V_1 = 0$). Thus for a given heat, only the value V_{io} need be known, and is common to all heats in the given current range.

R_2 is calculated in a similar manner from

$$R_2 = \frac{V_2 - sd_2}{V_i} R_i$$

where V_2 is the potentiometer reading after the heat. Using the calibration formula, T_1 and T_2, and thus the quantities $T = \frac{T_1 + T_2}{2}$ and $\Delta T = T_2 - T_1$ may be calculated.

The resistance of the heater $R_H(T)$ increases approximately linearly with temperature, and can be represented approximately by the function

$$R_H(T) = R_1 + R_2 T$$

over the entire range 1° to $300^\circ K$, R_1 taking values between 4122 and 4128 ohms for different runs, and R_2 being approximately 0.3 ohms/$^\circ K$. Thus over the range 1° to $20^\circ K$, the resistance changes by less than 0.2%. With the calculated value of T, $R_H(T)$ can be determined and with the values of i (or V), t and ΔT, the heat capacity can be computed.

The heat capacity of the addenda is presented as a six constant polynomial in T, of the form

$$Q_A = A_1 T + A_2 T^2 + ... + A_6 T^6,$$

and its value is calculated at the temperature of the heat, and is subtracted from the total heat capacity to give the heat capicity of the specimen, Dividing by N gives the specific heat per mole, C of the specimen. Since in this study it is the excess specific heat ΔC due to the magnetic impurities whi is of interest, the specific heat C_o of the pure metal (also presented in the form of a polynomial in T) is calculated at the Temperature T, and is subtracted from C to give ΔC.

Thus in the calculation of the specific heat, the following information must be provided which is common to each heat.

1) Number of moles of specimen N,

2) Thermometer calibration curve,

3) R_1 and R_2

4) Addenda polynomial

5) Pure metal polynomial.

For each heat the following information is required.

S, V_i, V_1, d_1, V_2, d_2, V or i, t.

From these quantities, the following information is printed out for each heat

$$T \quad T_2 - T_1 \quad C \quad C/T \quad C-Co \quad \frac{C-Co}{T}$$

5.18 Summary of Errors

Uncertainty in the temperature arises almost entirely from errors in the calibration curve, as an error in the measurement of the resistance of

the thermometer will not introduce an error greater than 0.01%. As seen above, errors in the calibration curve may arise from three sources, - random errors in the manometer pressure measurements (less than ± 1 mdeg between 1.4° and 4.2°K, ± 5 mdeg above 4.2°K), uncertainties in the corrections (less than ± 1 mdeg between 1.4° and 4.2°K, increasing to ± 10 mdeg at 5°K and ± 70 mdeg at 20°K). Thirdly there is the inability of a polynomial of the form discussed above to represent the true calibration curve. The deviation varies between 1 mdeg at 1.4°K and 50 mdeg at 20°K, though allowance can be made for this where necessary. Thus the accumulated errors in T increase from ± 2 mdeg at 1.5°K, ± 20 mdeg at 5°K, to ± 100 mdeg at 20°K.

Random errors in ΔT may arise from the uncertainties in the resistance before and after the heat. The values of the quantities d_1, d_2 can be read to 0.01 inches, with an associated error of less than 0,01%, but these may differ from the true values of d by a significant amount. At the lowest temperatures the large noise level on the signal makes extrapolation of the drift difficult. This noise voltage may be as much of 0.5% of the voltage change during the heat, and ΔT may therefore be in error by up to 0.3%. For the higher temperature points the noise level is about 0.1% of the voltage change, and ΔT can be estimated to slightly better than this amount. The sensitivity of the amplifier-recorder system varies by up to 1% over several hours, and this may introduce a maximum error of 0.1% if d_1 and d_2 differ by a whole chart width, but as d_1 and d_2 are usually rather close together the error will be smaller than this value. As the potentiometer is only changed in units of 100μv, and these units are calibrated with an accuracy of 0.01%, the errors introduced by the potentiometer in ΔT can not be greater

than 0.03%. Thus random errors of 0.3% at 1.5°K, decreasing to 0.1% at 20°K are expected in ΔT.

As discussed above, a rather large systematic error can be introduced because of the differences between the gradient of the polynomial and the true calibration curve. This error may be as great as 1%, near the ends of the range. It can be allowed for in the following way. The deviations between the calibration points and the calculated calibration curve are plotted against temperature. A smooth curve is drawn through any systematic deviation of these points. Such a curve will generally have as many zeros as the order of the polynomial. ΔT is then multiplied by a factor equal to one plus the gradient of this curve, to give the corrected value of ΔT.

Errors in the quantities i and V, and therefore also $R_H(T)$, are less than 0.01%, and the random error in T is of the order of 0.1%.

There is a further systematic error in the heat capacity calculated from eq.5.2, as Q(T) is in fact an average value over the temperature range ΔT. This differs from the true heat capacity at the temperature $T = \frac{T_1 + T_2}{2}$ by an amount

$$\Delta Q \simeq \frac{1}{24} \frac{d^2 Q}{dT^2} (\Delta T)^2$$

For a metal whose specific heat varies as

$$Q = AT + BT^3$$

$$\frac{\Delta Q}{Q} = \frac{6BT (\Delta T)^2}{24(A + BT^3)} < 4 \frac{(\Delta T)^2}{T^2}$$

$\frac{\Delta T}{T}$ is approximately 1/30 for every heat, and the systematic error introduced

is therefore less than 0.03%, and is therefore ignored.

Thus combining the various sources of error, and eliminating the systematic error introduced by the calibration curve where necessary, random errors of approximately 0.4% at 1.4°K decreasing to 0.2% at 20°K are expected in the heat capacity. The temperature may in the error by 0.1% below 4°K, increasing to 0.5% at 20°K.

CHAPTER 6

EXPERIMENTAL RESULTS

6.1 Introduction

The specific heats of several dilute magnetic alloys have been measured in the temperature range 1.3° to 20°K. These fall into three groups.

A. Cu, Cu 0.6% Fe, Cu_3 Au 0.6% Fe, Cu Au 0.6% Fe, Cu Au_3 0.6% Fe, Au 0.6% Fe, Cu 0.6% Fe 0.1% Mn

B. Rh, Rh 0.5% Fe

C. Pd 0.19% Fe

The specific heat of the addenda was also measured.

A. It has been suggested by Martin[122] that the anomalous specific heat of systems exhibiting a resistance minimum only, such as Cu Fe, show a different concentration and temperature dependence to those systems, such as Cu Mn and Au Fe, which exhibit both a low temperature minimum and maximum. In particular it was suggested that the temperature of the maximum in the specific heat is independent of concentration in the first group, and proportional to concentration in the second group, whilst at very low temperatures $\Delta C/T$ is concentration dependent in the first group, and concentration independent in the second group. This conclusion was based on the specific heat measurements of Franck Manchester and Martin[74] on the Cu Fe system, and those of Zimmerman and Hoare[73] and of du Chatenier[76] on Cu Mn alloys. It was suspected that the magnetic ordering in the two systems differed in a

significant way, and that this lead to the differing resistive behaviour. To test this hypothesis, it was decided that measurements should be made of the specific heat and resistivity of a series of copper-gold alloys containing a fixed amount of iron, to determine whether the appearance of a resistance maximum with increasing gold concentration was accompanied by a change in character of the specific heat anomaly. To this end specific heat measurements were made on the following alloys. Cu 0.6% Fe, Cu_3Au 0.6% Fe, Cu Au 0.6% Fe, Cu Au_3 0.6% Fe and Au 0.6% Fe. The specific heat of pure Cu was also measured to increase the significance of the Cu 0.6% Fe results and as a check on the accuracy of the measuring technique. The specific heat of a Cu 0.6% Fe 0.1% Mn specimen was measured to investigate the effect of a small amount of Mn (which itself gives rise to a resistance maximum in Cu) on the ordering of the Fe atoms.

B. Coles has observed remarkable behaviour in the resistivity of dilute Rh Fe alloys at low temperatures (section 1.9). His results, shown in Fig. 2(C), show that the excess resistance decreases monatonically below about 50°K, tending to a value at 0°K of about one third of its high temperature value. The relative excess resistance (that is $\frac{\Delta R(T)}{\Delta R(0)}$) is independent of concentration at all temperatures. The low temperature magnetoresistance is positive, and this, together with the concentration independence of the relative excess resistance, are unusual in systems of localised magnetic moments ordering in internal fields. The specific heat of Rh 0.5% Fe was therefore measured to throw light on this unusual system. As no reliable measurements over an extended temperature range are available for pure Rh,

tho specific heat of Rh was also measured.

C. The magnetic properties of Pd containing small amounts of 1st row transition metals have been investigated by Gerstenberg[123], Crangle[124], Clogston[45], and Bozorth[25]. They observe long range ferromagnetic ordering in Pd containing (apparently) any finite amount of Fe, even though Pd itself is paramagetic, and observe a saturation moment per Fe atom of around 12 μ_B. Such large moments have been accounted for by assuming that the neighbouring Pd atoms are polarised by the Fe impurity, and that their moments add to that of the Fe atom. It was considered that the excess entropy of a dilute Pd Fe alloy at the Curie temperature might yield a value for the spin of the Fe-Pd complex, and might give evidence for the possible dissociation of the Pd and Fe atoms at the Curie temperature. Measurements were therefore made of the specific heat of a Pd 0.1% Fe alloy. During the course of these measurements Veal and Rayne[126] published the results of measurements of the specific heat of a series of dilute Pd Fe alloys.

6.2 Preparation of Specimens

The Cu 0.6% Fe, Cu_3Au 0.6% Fe, Cu Au 0.6% Fe, Cu Au_3 0.6% Fe, Au 0.6% Fe and Cu 0.6% Fe 0.1% Mn specimens were prepared by Johnson Matthey and Co. They were all cast, swaged, annealed at 850°C, and quenched in water to prevent precipitation of the iron, and to ensure complete disorder in the ternary alloys.

No metallographic examinations of the specimens were made to determine the state of solution of the Fe, and as the concentration of Fe in the

Cu 0.6% Fe alloys is considerably in excess of the room temperature solubility limit, the actual amount of Fe in solid solution is in some doubt. No great difficulty is found in producing wire specimens with this quantity of Fe in solution, but the rate of cooling during quenching is very much longer for large specific heat specimens (3/4" dia x 1" long) than is possible for thin wires, giving a greatly increased danger of precipitation. The large entropy found for the Cu 0.6% Fe sample, (slightly larger than that found for the Au 0.6% Fe sample) suggests that most, if not all, of the Fe is in solution in the CuFe alloy. The Au 0.6% Fe alloy is well within the room temperature solubility limit, so that precipitation of Fe in this alloy is unlikely. The solubility of Fe in binary Cu-Au alloys has not been measured, but again the specific heat anomaly for these alloys suggests that most of the iron is in solid solution.

The results of chemical analysis of the Fe content is given with the description of individual runs, but this does not differentiate between Fe in and out of solution. As samples for analysis are taken from one part of the specimen only, variation in Fe concentration over the volume of the alloy is not known. The exact proportions of Cu and Au in the ternary copper-gold-iron alloys were not determined by chemical analysis. As a comparison of specific heat and resistance measurements are made on the same specimen, this is not of importanceproviding the alloys are completely disordered.

The pure Rh specimen, and the Rh 0.5% Fe specimen were kindly loaned by the International Nickel Co (Mond) Ltd. The Rh 0.5% Fe specimen was melted in a high frequency induction furnace, forged, and annealed at 1100°K.

Quenching was not considered necessary because of the high solubility of Fe in Rh.

The Pd 0.19% Fe specimen was prepared by melting existing Pd Fe arc melted buttons with extra Pd in an induction furnace. The Fe concentration was estimated from the known concentrations of Fe in the buttons, and from the amount of Pd added. This specimen was not quenched or annealed, but precipitation or inhomogeneity are not expected because of the high solubility of Fe in Pd, and because of the use of an induction furnace to melt the specimen (this technique provides good mixing of the components). I am indepted to Mr. J. Tibble, Metallurgy Department, Imperial College, for his assistance in preparing this specimen.

All specimens were turned, (or ground in the case of the Rh and Rh 0.5% Fe alloys) into cylinders 0.75" dia., and approximately 1" in length. They were then polished and cleaned.

6.3 Errors

Sources of random and systematic error have been discussed in detail in section 5.18 Random errors in C arise mainly from errors in ΔT, and decrease from about 0.4% at 1.5°K to 0.2% at 20°K. The random error in T is negligable. Systematic errors in T increase from 0.1% for T = 4°K, to 0.5% at 20°K. Systematic errors in C, due almost entirely to systematic errorsin ΔT of up to 1% arising from errors in the slope of the calibration curve, have been partially corrected. Other sources of error are negligable.

6.4 Addenda

A plot of Q/T against T^2, where Q is the heat capacity of the addenda, is shown in Fig. 34A. This was one of the earliest runs, and some difficulty was experienced with the calibration of the carbon thermometer. As the calibration in later experiments was found to vary by only a few tenths of one per cent from run to run, the calibration obtained in the Cu_3Au 0.6% Fe run was used to calculate the addenda specific heat. This calibration was used as it corresponded most closely to those addenda calibration points in which confidence could be placed. The error introduced in this way is not expected to be more than one or two per cent, and as the heat capacity of the addenda is never more than 8% of the total for addenda plus specimen, and is generally much less, this will not introduce an error into the specific heat of the specimen of more than 0.2%.

The polynomial

$$\frac{Q}{T} = 2.400 \times 10^{-2} + 5.617 \times 10^{-3}\, T^2 - 8.656 \times 10^{-5}\, T^3 - 1.356 \times 10^{-6}\, T^4 + 4.154 \times 10^{-8}\, T^5 \qquad mj/^{\circ}K^2$$

was found to fit the addenda specific heat results to within 2%. For the reasons given above, this will introduce a maximum error of about 0.2% into a specific heat measurement, though the error will usually be smaller than this.

6.5 Pure Cu

The specific heat of 0.785 moles of copper was measured between 1.4°K and 20°K. The copper contained as its main impurity 0.002% Fe.

In the following graphs, C is expressed in mj/mole °K

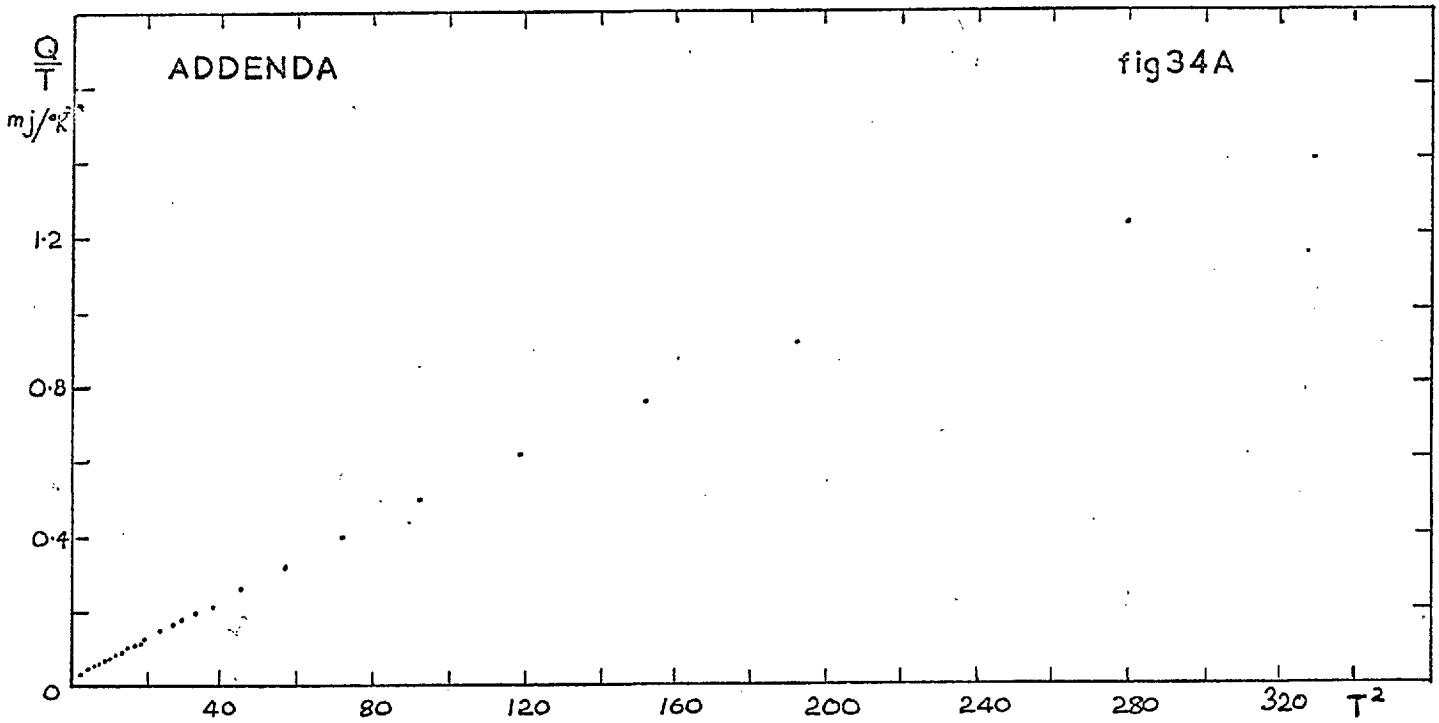

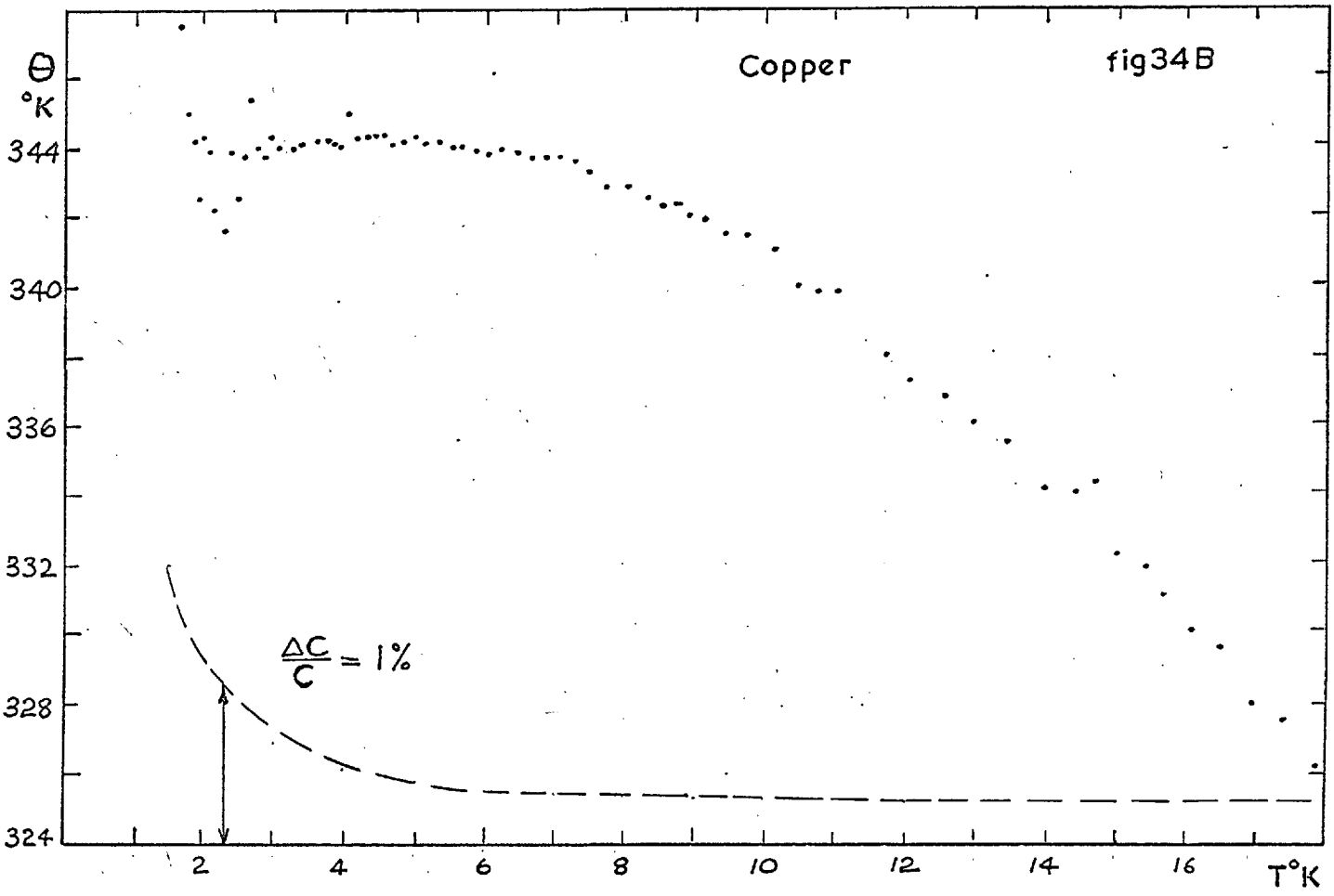

Sixteen calibration points were taken between 1.3°K and 4.2°K, and a further sixteen between 4.2°K and 23°K. A least squares fit of the points to the polynomial $\sqrt{\frac{\log R}{T}} = \sum_{a=0}^{3} a_i (\log_e R)^i$ gave the following calibration curve.

$$\sqrt{\frac{\log R}{T}} = -2.164 + 0.6561 \log R - 0.02880 (\log R)^2 + 0.001491 (\log R)^3$$

The R.M.S. deviation of measured values of $\sqrt{\frac{\log R}{T}}$ from this calibration curve was 0.5×10^{-3}, corresponding to a fractional deviation $\frac{\delta T}{T}$ of 0.7×10^{-3} at 1.5°K and 2.2×10^{-3} at 23°K.

The experimental values for C/T against T^2 in the temperature range 1.4° to 4.5°K are shown in Fig. 35A. A least squares fit of these points to a straight line give

$$\gamma = 0.706 \pm .006 \text{ mj/mole } {}^\circ K^2 \qquad \theta = 344.3 \pm 1.1 \ {}^\circ K$$

The errors represent 95% confidence limits from the least squares analysis, and include an estimated systematic error. These values may be compared with other recent measurements of the specific heat of Cu.

	γ mj/mole $^\circ K^2$	θ(0°K)	Temperature Range °K
This work	0.706 ± .006	344.3 ± 1.1	1.4 - 20
Corak[134](1955)	0.688 ± .002	343.8 ± 0.5	1.2 --5.4
Rayne[135](1957)	0.687 ± .012	344.5 ± 3	1.2 - 4.2
Veal[136](1962)	0.692 ± .009	342.7	1.2 - 4.2
Franck[74](1961)	0.697 ± .005	344 ± 2	1.5 - 30
Griffel[137](1957)	0.691 ± .006	347 ± 2	1.8 - 4.2
Zimmerman[73](1960)	0.690	344	1.3 - 15
du Chatenier[72](1964)	0.721 ± .010	338.9 ± 0.8	1.4 - 30

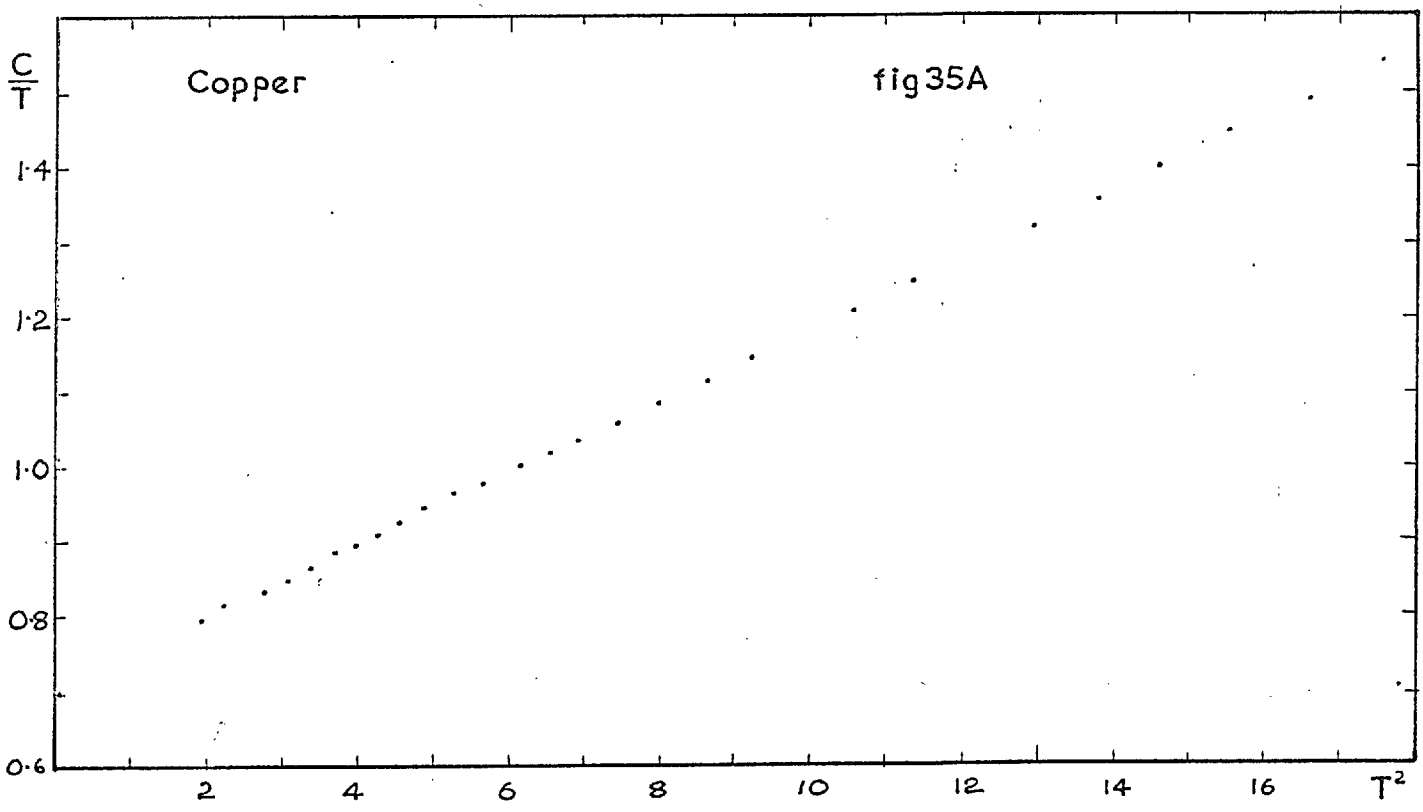
Copper
fig 35A
C/T
1·4
1·2
1·0
0·8
0·6
2
4
6
8
10
12
14
16
T²

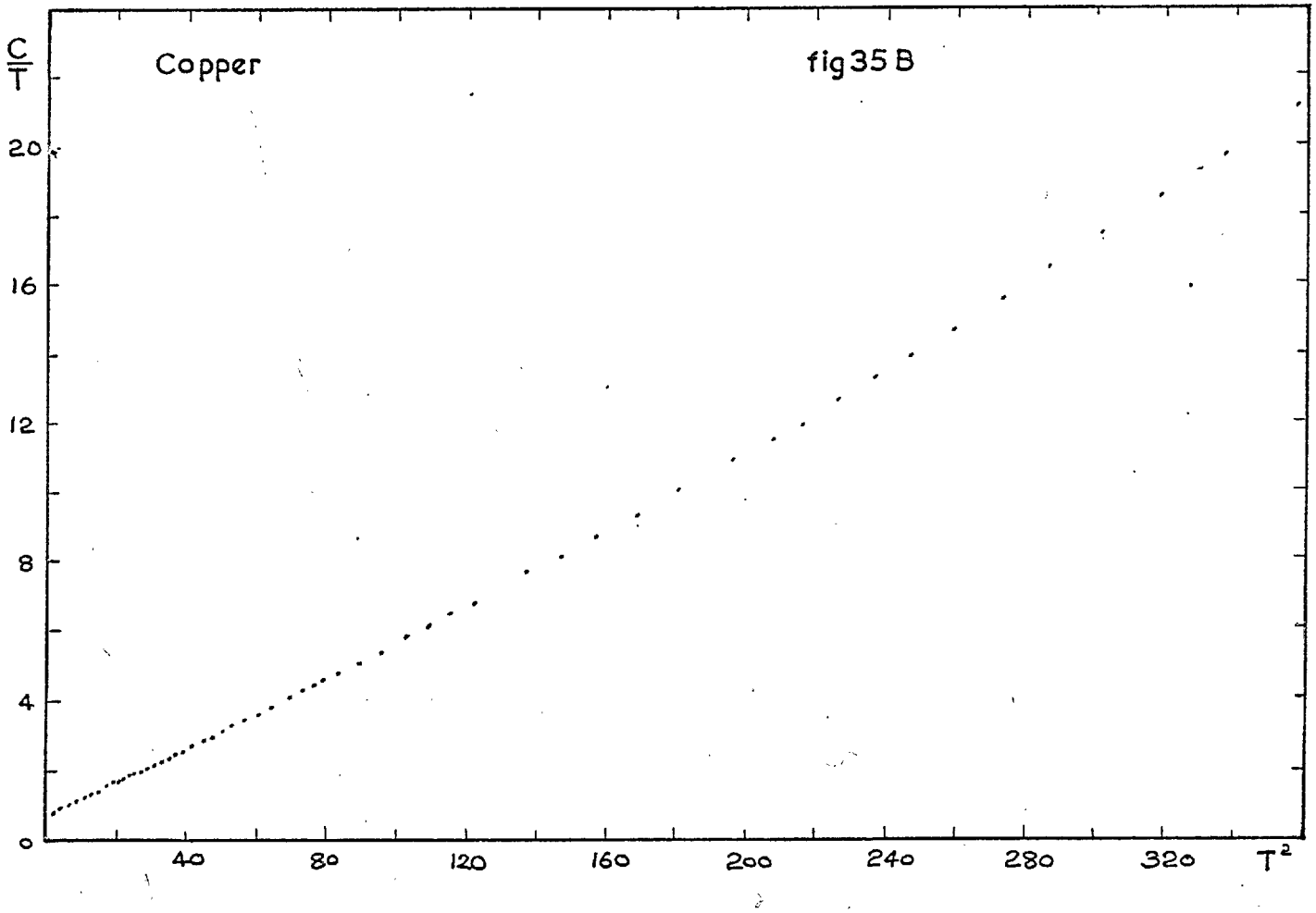
Copper
fig 35 B
C/T
20
16
12
8
4
0
40
80
120
160
200
240
280
320
T²

The value of $\theta(0)$ is in good agreement with that found by other workers. The slightly higher value found for γ may be due to the small smount of Fe present in the sample.

Assuming a value of $\gamma = 0.706$ mj/mole$^{\circ}K^2$ a value of θ can be computed for each specific heat measurement. The variation of θ with temperature in the range 1.5 - 20°K is shown in Fig. 34B. The results are in close agreement with those of Franck Manchester and Martin[74] below 11°K, but differ by about 1½% from their value at 20°K.

In order to compute the excess specific heat in the Cu 0.6% Fe and Cu 0.6%Fe 0.1% Mn specimens, the specific heat results for pure Cu were fitted to a polynomial in T.

$$\frac{C}{T} = 7.294 \times 10^{-1} - 2.350 \times 10^{-2}\, T + 5.451 \times 10^{-2}\, T^2 - 1.030 \times 10^{-3}\, T^3$$

$$+ 8.101 \times 10^{-5}\, T^4 - 6.147 \times 10^{-7}\, T^5 \qquad \text{mj/mole } {}^{\circ}K^2$$

The deviation of the points from this polynomial is never greater than 0.5%, and is less than 0.2% above 4°K (where the excess specific heat in the dilute alloy is only a small fraction of the total specific heat). The deviations may be almost entirely attributed to random scatter of the points, except at the lowest temperatures, and very little error is introduced by the use of an analytic expression for the specific heat of pure copper.

6.6 Cu 0.6% Fe

The specific heat of 0.997 moles of Cu 0.6% Fe was measured between 1.3° and 20°K. Chemical analysis showed that a one gram sample taken from the specimen contained 0.56% Fe.

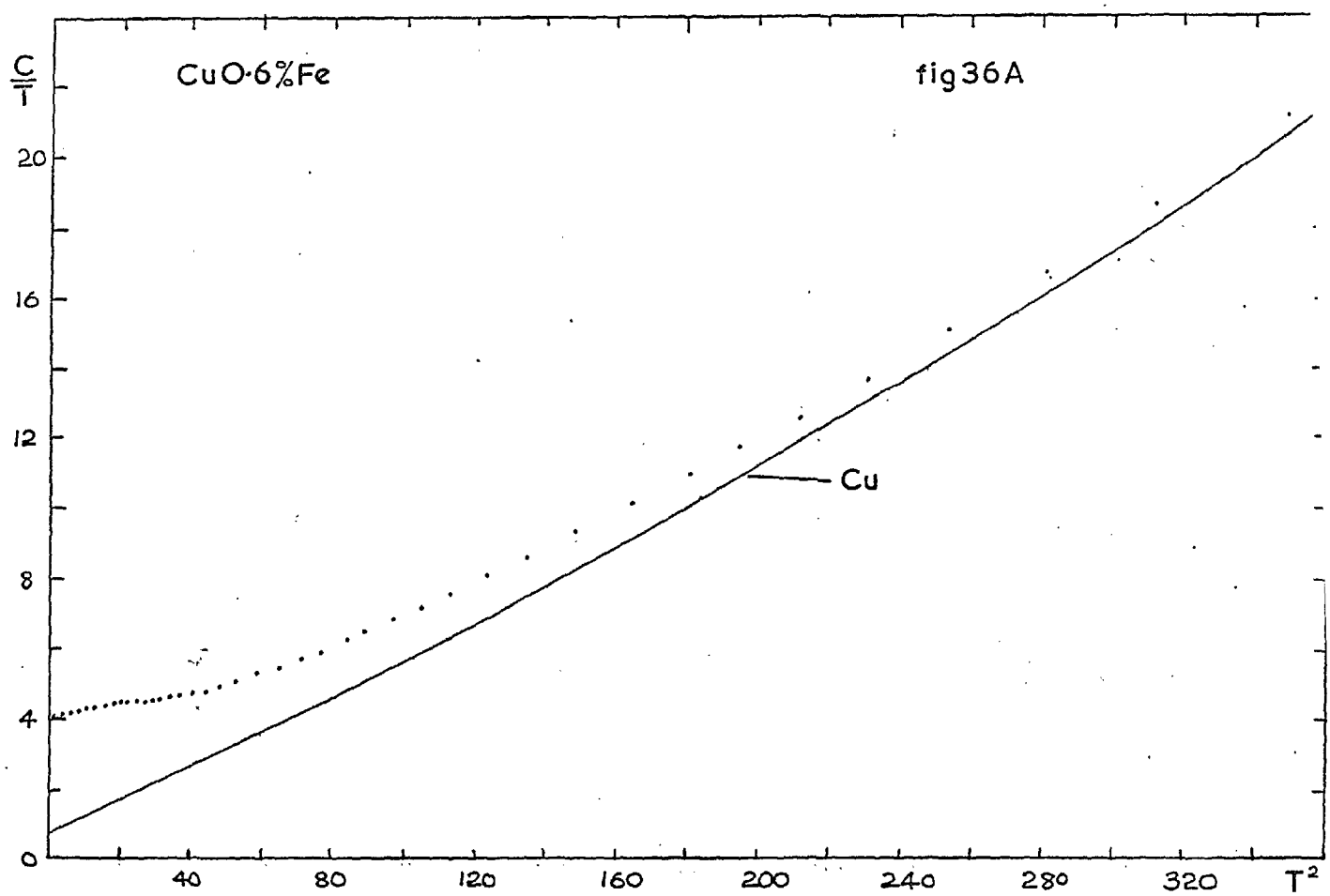
C/T
CuO·6%Fe
fig 36A
20
16
12
8
4
0
Cu
40
80
120
160
200
240
280
320
T²

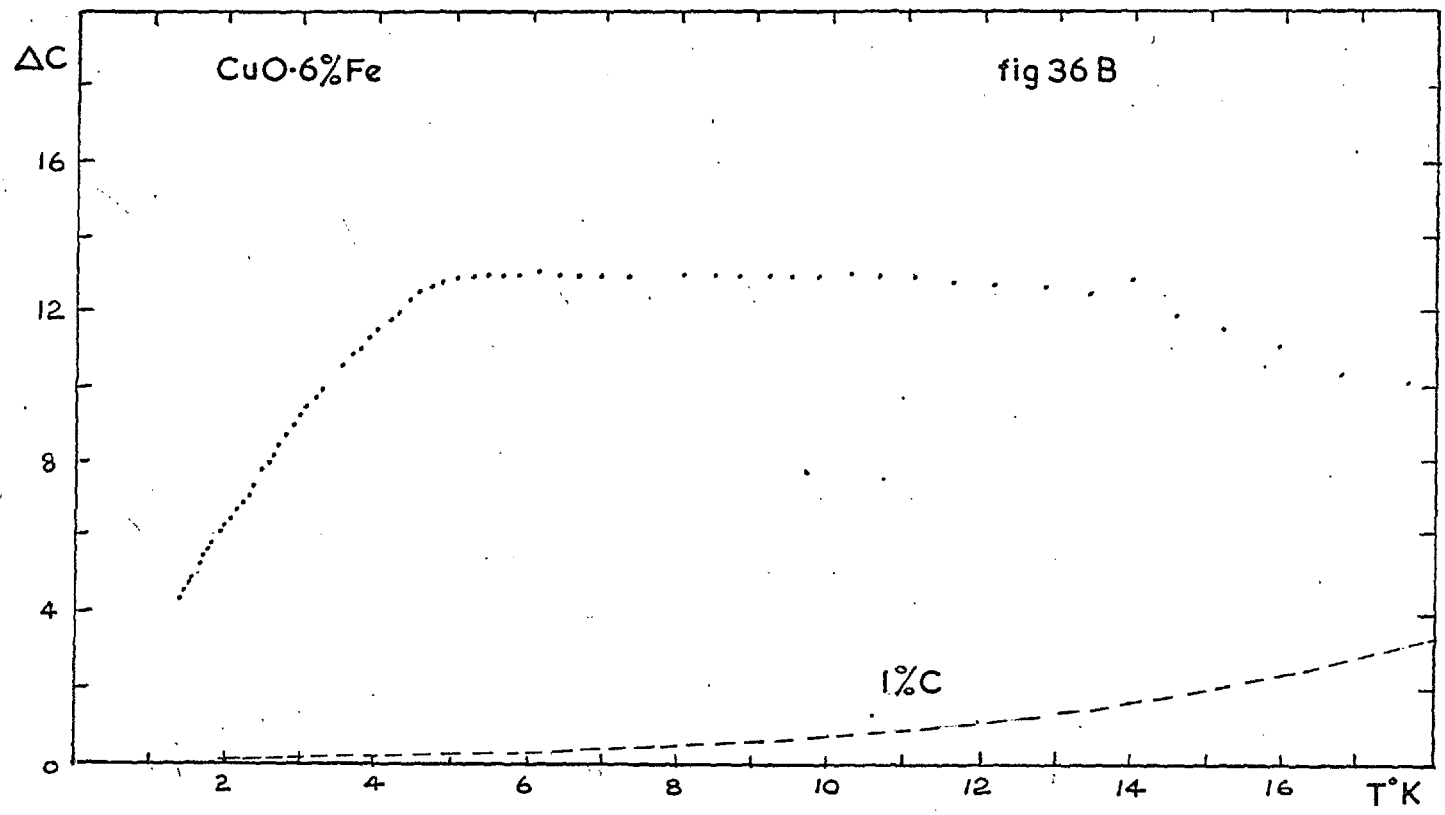
ΔC
CuO·6%Fe
fig 36 B
16
12
8
4
0
1%C
2
4
6
8
10
12
14
16
T°K

Calibration points below 3.6°K were considered to be unreliable as satisfactory equilibrium conditions could not be obtained. This behaviour was traced to the presence of the adiabatic shield, which prevented the specimen and reservoir reaching the same temperature, in spite of the presence of helium exchange gas between the specimen and adiabatic shield, and adiabatic shield and reservoir shield. The adiabatic shield was removed after this run and the thermal short (see section 5.5) connected between the gas thermometer and reservoir. Equilibrium between the specimen and reservoir liquid was rapidly established in subsequent runs.

Above 3.6°K, the calibration points were reliable, and twelve calibration points were obtained between 3.6°K and 26°K. The R.M.S. deviation of $\frac{\log R}{T}$ from the calculated calibration curve is 0.4×10^{-3}. Values of C/T against T^2, calculated using this calibration curve, are shown in fig. 36A, together with a curve for pure Cu.

A plot of ΔC against T is shown in fig. 36B, and $\frac{\Delta C}{T}$ against T in fig 37. The values have been obtained by subtracting from the total specific heat of the Cu 0.6% Fe alloy the specific heat of Cu calculated at the particular temperature from the polynomial discussed in section 6.5. The results at temperatures between 3.6°K and 20°K have been calculated using the Cu 0.6% Fe calibration curve. Below 5°K the results are calculated using the Cu_3Au 0.6% Fe calibration curve. This curve lies within 2 mdeg of the reliable Cu 0.6% Fe calibration points between 3.6°K and 5°K, and within 4 mdeg of all other calibration curves in this temperature region. This spread between calibration curves does not increase down to 1.3°K, and the specific heat curve is therefore expected to be in

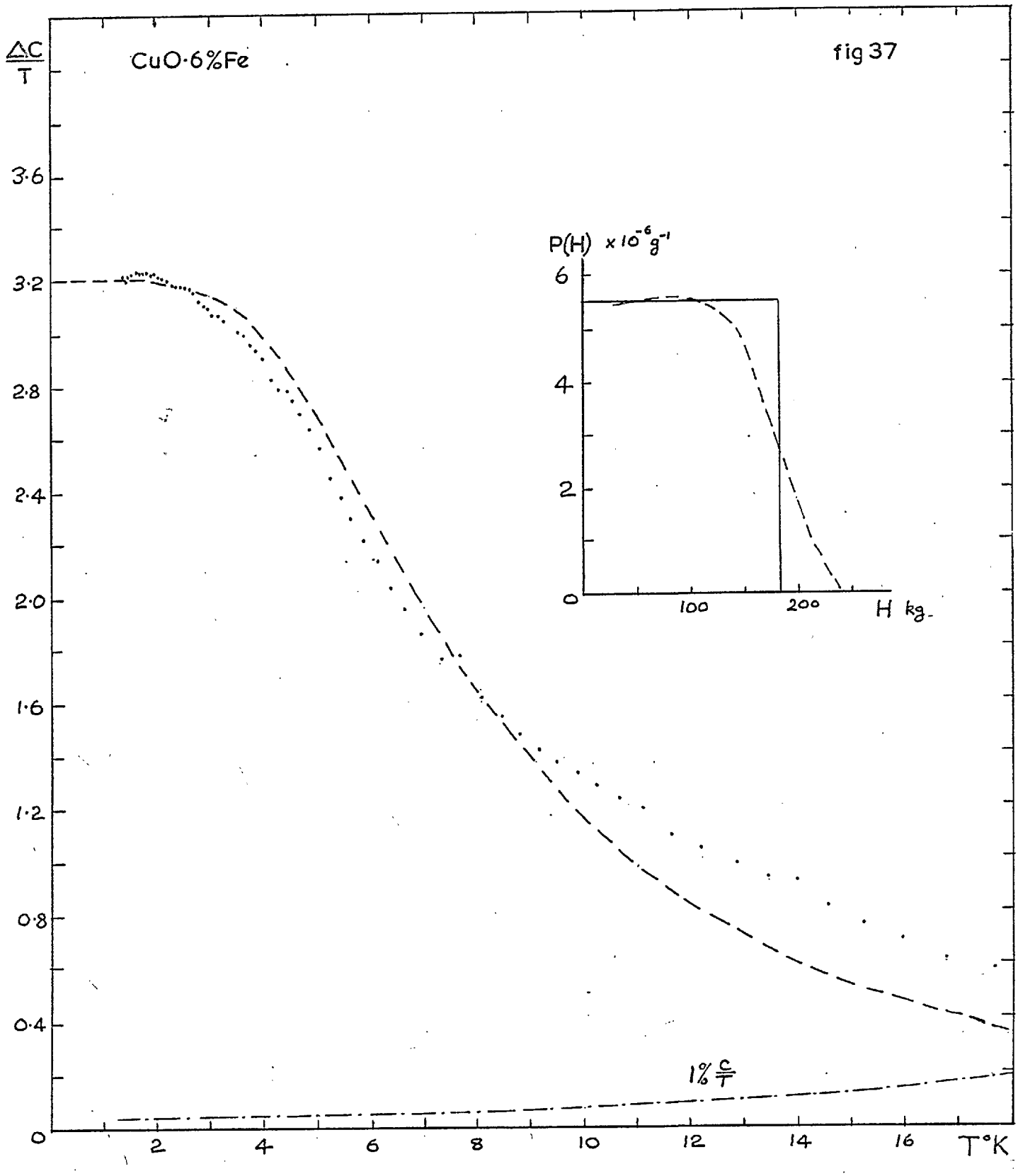
ΔC/T
CuO·6%Fe
fig 37
3·6
3·2
2·8
2·4
2·0
1·6
1·2
0·8
0·4
0
2
4
6
8
10
12
14
16
T°K
P(H) x 10⁻⁶ g⁻¹
6
4
2
0
100
200
H kg.
1% C/T

error by not more than one or two per cent due to the use of this calibration curve. In the temperature region 3.6°K to 5°K, where calculations using the two calibration curves overlap, the calculated values differ by less than 1%. The use of the Cu calibration curve lowers the points shown in figs. 36B and 37 by approximately 1% below 2°K, and by less than 0.5% between 3° and 4°K. It therefore seems unlikely that an error of more than 2% has been introduced into ΔC or $\frac{\Delta C}{T}$ by the use of the Cu_3Au 0.6 % Fe calibration curve below 3.6°K.

The dotted curve at the bottom of figs 36B and 37 represent 1% of the total C or C/T for the Cu 0.6% Fe sample This is a guide to the possible errors in ΔC resulting from accumulated errors in the specific heats of Cu 0.6% Fe and Cu.

6.7 Cu_3 Au 0.6% Fe

The specific heat of 0.879 moles of Cu_3Au 0.6% Fe was measured between 1.3°K and 20°K. Chemical analysis showed that a one gram sample taken from the specimen contained 0.61% Fe.

Fifteen calibration points were taken between 1.3°K and 4.2°K, and a further sixteen between 4.2°K and 23°K. The R.M.S. deviation of the meausred values of $\sqrt{\frac{\log R}{T}}$ from the calibration curve was 0.6×10^{-3}.

Fig. 38A shows a plot of $\frac{C}{T}$ against T^2 for this alloy. To determine the excess specific heat due to the iron, a knowledge of the specific heat of the solvent is required over the entire temperature range 1° - 20°K. Unfortunately this information is not available for any of the binary

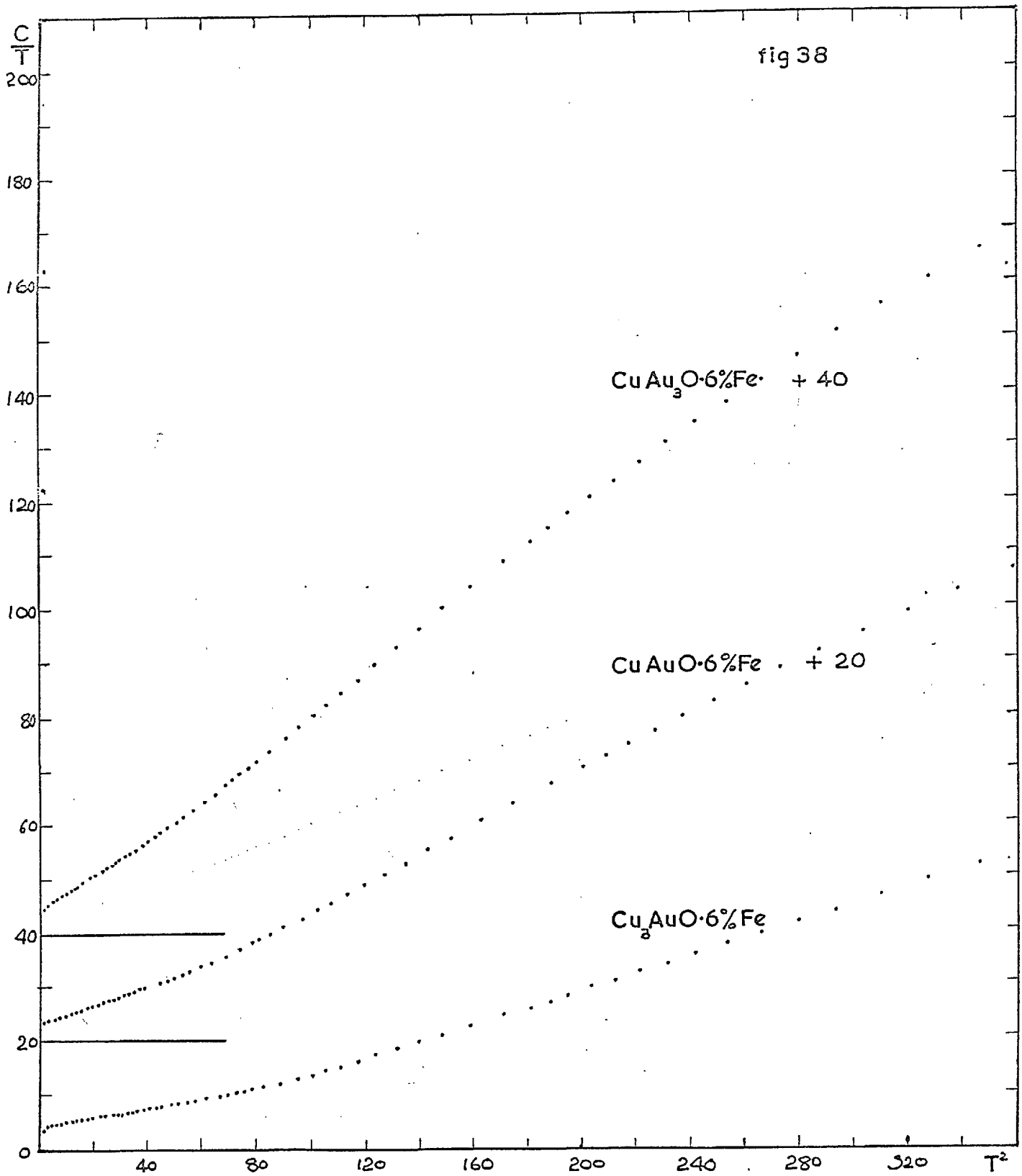
fig 38
C/T
200
180
160
140
120
100
80
60
40
20
0
40
80
120
160
200
240
280
320
T²
CuAu₃O·6%Fe· + 40
CuAuO·6%Fe · + 20
Cu₃AuO·6%Fe ·

copper-gold alloys, but as the purpose of this series of measurements is to compare the shapes of the specific heat anomalies in these alloys, some attempts must be made to estimate the specific heat of the solvents.

The specific heat of Cu_3Au has been measured in the temperature range 1° to $4^\circ K$ by Rayne[127] and by Montgomery (unpublished), who were examining the effect of atomic ordering on the values of γ and θ. Rayne found a value of $\gamma = 0.66$ mj/mole $^\circ K^2$ and $\theta = 278^\circ K$, whilst Montgomery found $\gamma = 0.67$ mj/mole $^\circ K^2$ and $\theta = 268.6^\circ K$ for the disordered alloy. The small difference in γ will only have the effect of raising or lowering $\frac{\Delta C}{T}$ by a small amount, and will not alter its shape. A value of 0.67 mj/mole $^\circ K^2$ has therefore been assumed.

The value chosen for θ has a much more profound effect on the shape of $\frac{\Delta C}{T}$, especially at higher temperatures when the lattice specific heat is a large fraction of the total specific heat, and it is therefore unfortunate that Rayne and Montgomery found different values for θ between 1° and $4^\circ K$. Calculations of $\frac{\Delta C}{T}$ have been made based on both values, and the results are shown as curves X and X' in fig 39A.

The temperature dependence of θ at higher temperatures has been estimated in the following way, making the plausible assumption that the general shape of the anomaly at high temperatures is similar to that in other dilute alloys.

If the excess specific heat is assumed to be zero at all temperatures above $12^\circ K$, a value of θ can be obtained from each of the measured specific heat values above $12^\circ K$. These values are shown in fig. 40B as curve x_1. If, on the other hand, the excess specific heat above $12^\circ K$ is assumed to be

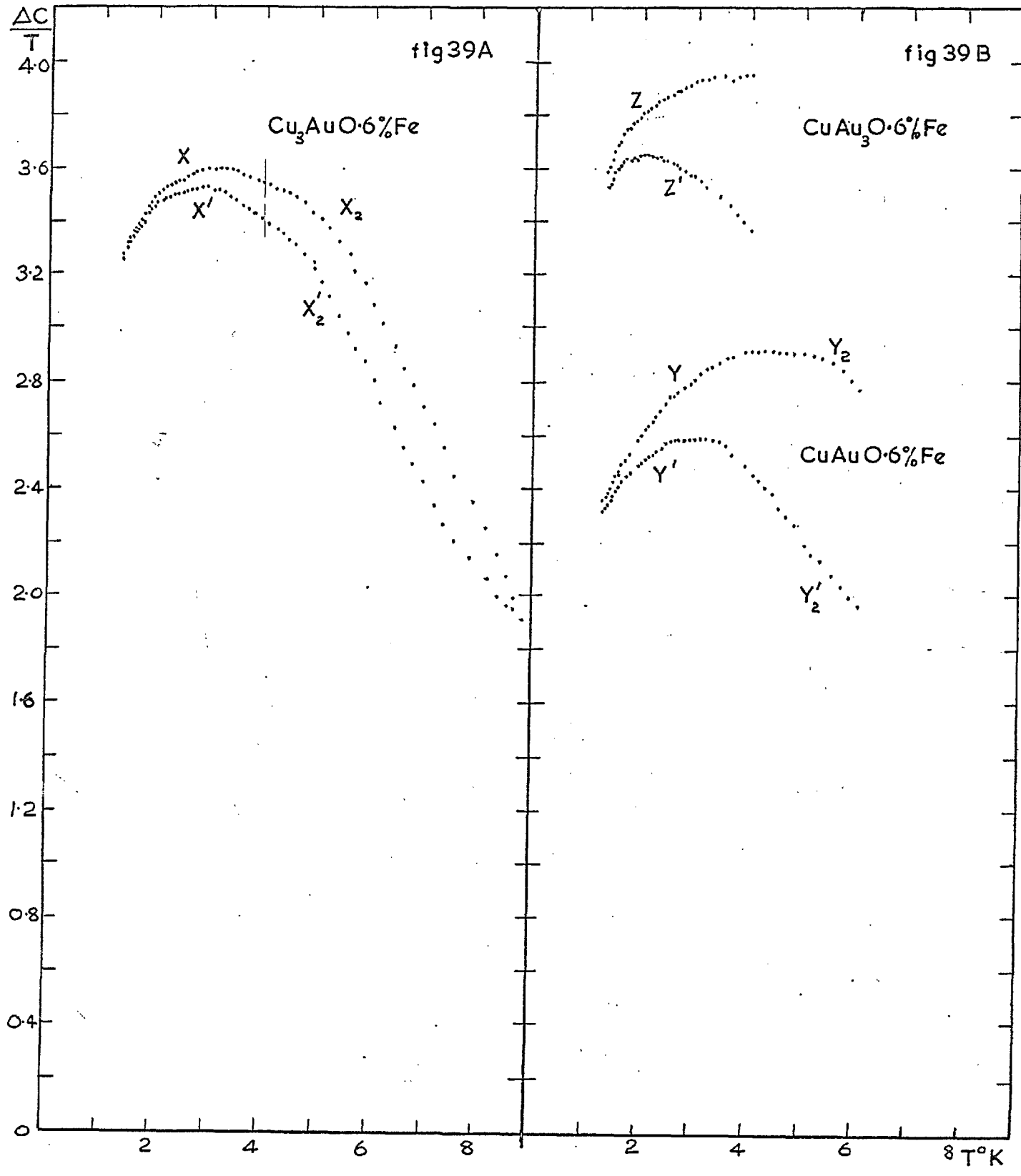
ΔC/T
fig 39A
Cu3Au O·6%Fe
X
X'
X2
X'2
fig 39 B
Z
Z'
CuAu3 O·6%Fe
Y2
Y
CuAu O·6%Fe
Y'
Y'2
4·0
3·6
3·2
2·8
2·4
2·0
1·6
1·2
0·8
0·4
0
2
4
6
8
T°K

the same as that in the Cu 0.6% Fe alloy, this excess may be subtracted from the total specific heat, and new values of θ calculated for all points above 12°K. These values of θ are shown as curve x_1' in fig. 40 B, which is seen to lie slightly above x_1, corresponding to a slightly lower value of the lattice specific heat. Curves x_1 and x_1' therefore represent probable limits on the values of θ above 12°K. These curves lie significantly below the values found for θ below 4°K, though the high temperature θ is increasing with decreasing temperature in such a way that the regions can be joined by smooth curves such as x_2 and x_2'.

The general form of these θ-T curves is typical of many crystal lattices, and is due to a low frequency peak in the phonon frequency spectrum. Calculation of the frequency spectrum is difficult for a diatomic lattice, especially when the alloy is disordered, and has not been attempted for the disordered binary copper-gold systems. A minimum occurs in the θ-T curve for Cu at around 30°K, and the depth of the minimum is about 10% of $\theta(0)$. The minimum in the curve $x - x_2 - x_1$ is approximately 15% of $\theta(0)$, and that for the curve $x' - x_2' - x_1'$ is approximately 12% of $\theta(0)$.

Values of $\frac{\Delta C}{T}$ against T, calculated from these possible θ-T curves, are shown in fig. 39A. From the two curves $X-X_2$, and $X' - X_2'$, which are derived from the θ-T curves $x - x_2$, and $x' - x_2'$, the effects on $\frac{\Delta C}{T}$ of uncertainties in θ can be seen. The effect of quite a large error in θ at low temperatures (below 3°K) is rather small, (the effect is of course zero at T=0), and the shape of the anomaly in this temperature region is therefore quite reliable. Errors in θ have an effect which increases rapidly

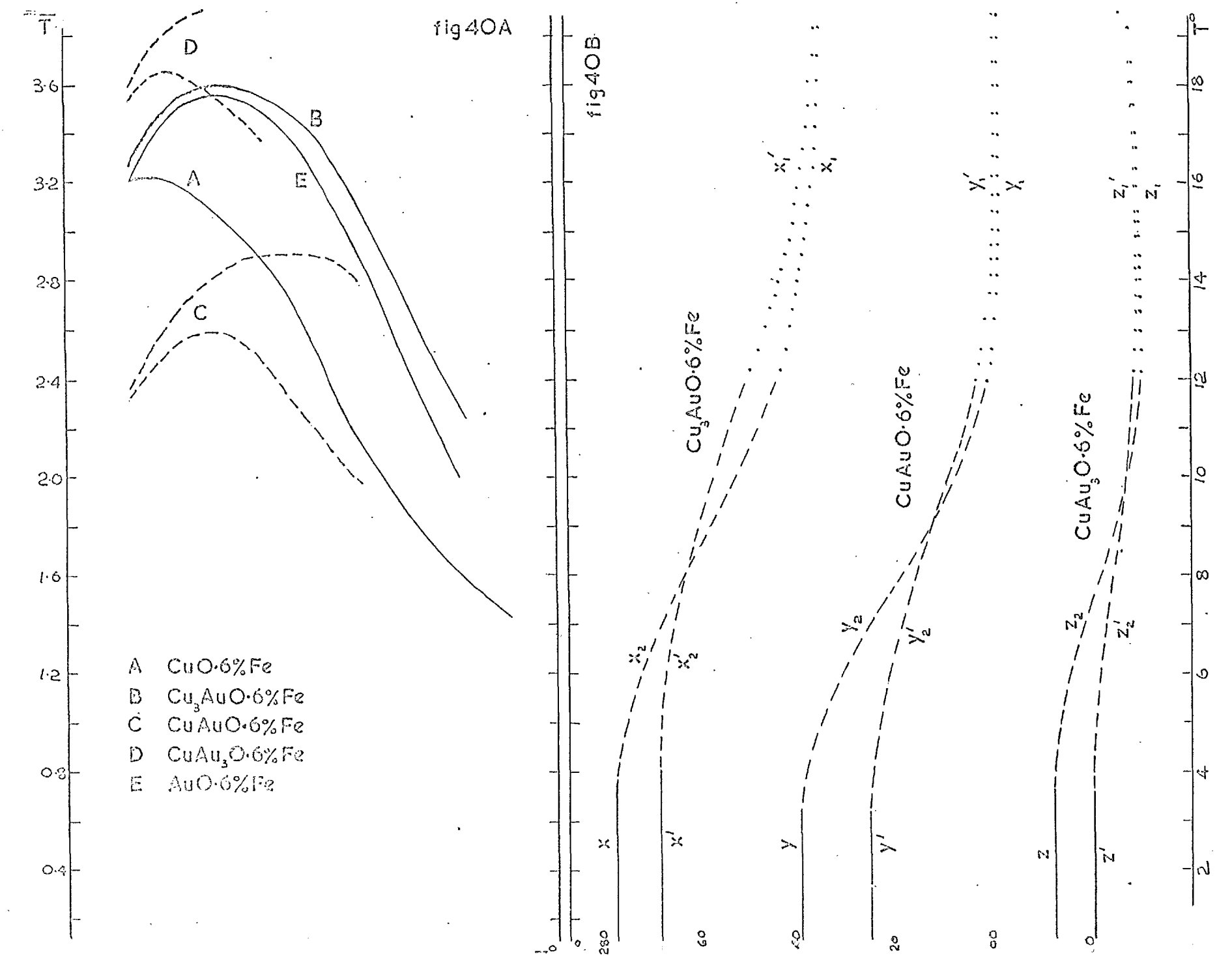
fig 40A
fig 40B
T
T°
A CuO·6%Fe
B Cu3AuO·6%Fe
C CuAuO·6%Fe
D CuAu3O·6%Fe
E AuO·6%Fe
Cu3AuO·6%Fe
CuAuO·6%Fe
CuAu3O·6%Fe

with increasing temperature, and at high temperatures the shape of the anomaly is in considerable doubt. Some confidence can beplaced in the maximum value of 3.5 to 3.6 mj/mole $^{o}K^{2}$ in $\frac{\Delta C}{T}$ at a temperature close to $3^{o}K$, and in the shape of the anomaly below this temperature.

6.8 CuAu 0.6% Fe

The specific heat of 0.843 moles of Cu Au 0.6% Fe was measured between $1.3^{o}K$ and $20^{o}K$. Chemical analysis showed that a one gram sample taken from the specimen contained 0.63% Fe.

Thirteen calibration points were taken between 1.3^{o} and $4.2^{o}K$, and a further fourteen between 4.2^{o} and $23^{o}K$. The R.M.S. deviation of the measured values of $\sqrt{\frac{\log R}{T}}$ from the calibration curve was 0.76×10^{-3}.

A plot of C/T against T^{2} for this alloy is shown in fig 38 B. The temperature variation of θ above $12^{o}K$ for the solvent has been calculated in the manner described in section 6.7, yielding curves y_1 and y_1' in fig. 40B. γ has been taken arbitrarily as 0.71 mj/mole $^{o}K^{2}$, the mean of the values for Cu and Au. This assumption has a negligable effect on the shape of the $\frac{\Delta C}{T}$ curve. An increase in θ with decreasing temperature is evident from these curves, and it is assumed that this is a result of a minimum in the θ-T curve of similar magnitude to that for pure copper. As no experimental values for θ below $4^{o}K$ are available, two values of $\theta(0)$ have been chosen, $226^{o}K$ and $248^{o}K$, such that the depth of the minimum is 11% and 17% for the two curves $y' - y'_1$ and $y - y_1$.

The values of $\frac{\Delta C}{T}$ against T calculated from these θ-T curves, are shown in fig. 39 B. The specific heat curve $Y - Y_2$ derives from the θ-T curve $y - y_2$, and the specific heat curve $Y' - Y_2'$ has been calculated from the $y' - y'_2$ θ - T curve. The shape of the $\frac{\Delta C}{T}$ curve at low temperatures is seen to be little effected by the choice of θ, but the results become rapidly more uncertain with increasing temperature. The existance of a maximum in the $\frac{\Delta C}{T}$ curve is again established, of a magnitude between 2.5 and 3.0 mj/mole$^\circ K^2$, and at a temperature between 2.5 and 5°K.

6.9 $Cu Au_3$ 0.6% Fe

The specific heat of 0.760 moles of $CuAu_3$ 0.6% Fe has been measured between 1.3° and 20°K. Chemical analysis showed that a one gram sample taken from the specimen contained 0.61% Fe.

Fourteencalibration points were measured between 1.3° and 4.2°K, and a further eleven points between 4.2°K and 23°K. The R.M.S. deviation of the measured values of $\sqrt{\frac{\log R}{T}}$ from the calibration curve was 0.63×10^{-3}.

A plot of C/T against T^2 for this alloy is shown in Fig. 38C. Assuming a value of $\gamma = 0.73$ mj/mole$^\circ K^2$, values of θ for the solvent have been calculated for temperatures above 12°K in the manner described in section 6.7. This yields the curves z_1, z_1' in fig. 40 B. θ is not increasing with decreasing temperature above 12°K, but a close study of the C/T against T^2 curve shows that it must in fact do so at lower temperatures if the excess specific heat is to remain positive. Arbitrary values of $\theta(0)$ of 180°K and 188°K have been assumed, giving a depth of the maximum of 5% and 10%, and smooth curves $z-z_2-z_1$ and $z'-z_2'-z_1'$ have been

drawn to represent the variation of θ with temperature.

Values of $\frac{\Delta C}{T}$ against T based on these θ-T curves are shown in fig. 39B, curve $Z - Z_2$ being derived from curve $z - z_2$, and curve $Z' - Z_2'$ from $z' - z_2'$. The general behaviour below $2^{\circ}K$ is probably significant provided θ does not vary in an unusual way below this temperature, but the sensitivity of the results to the value assumed for θ make the values at higher temperatures of little significance. Once more a maximum in $\frac{\Delta C}{T}$ is evident, the value at the maximum being approximately 3.8 mj/mole$^{\circ}K^2$. It is not possible to decide the temperature of the maximum.

6.10 Au 0.6%Fe

The specific heat of 0.708 moles of Au 0.6% Fe has been measured between $1.3^{\circ}K$ and $19^{\circ}K$. Chemical analysis showed that a one gram sample taken from the specimen contained 0.71% Fe.

Twelve calibration points were taken between $1.3^{\circ}K$ and $4.2^{\circ}K$, and a further ten between $4.2^{\circ}K$ and $22^{\circ}K$. The R.M.S. deviation of the measured values of $\sqrt{\frac{\log R}{T}}$ from the computed calibration curve was 0.55×10^{-3}.

A plot of C/T against T^2 for this alloy is shown in fig. 41 A. The specific heat of the pure metal was not measured, and therefore to find the excess specific heat, values of the specific heat of pure gold found by other workers, must be used. Recent values are given below.

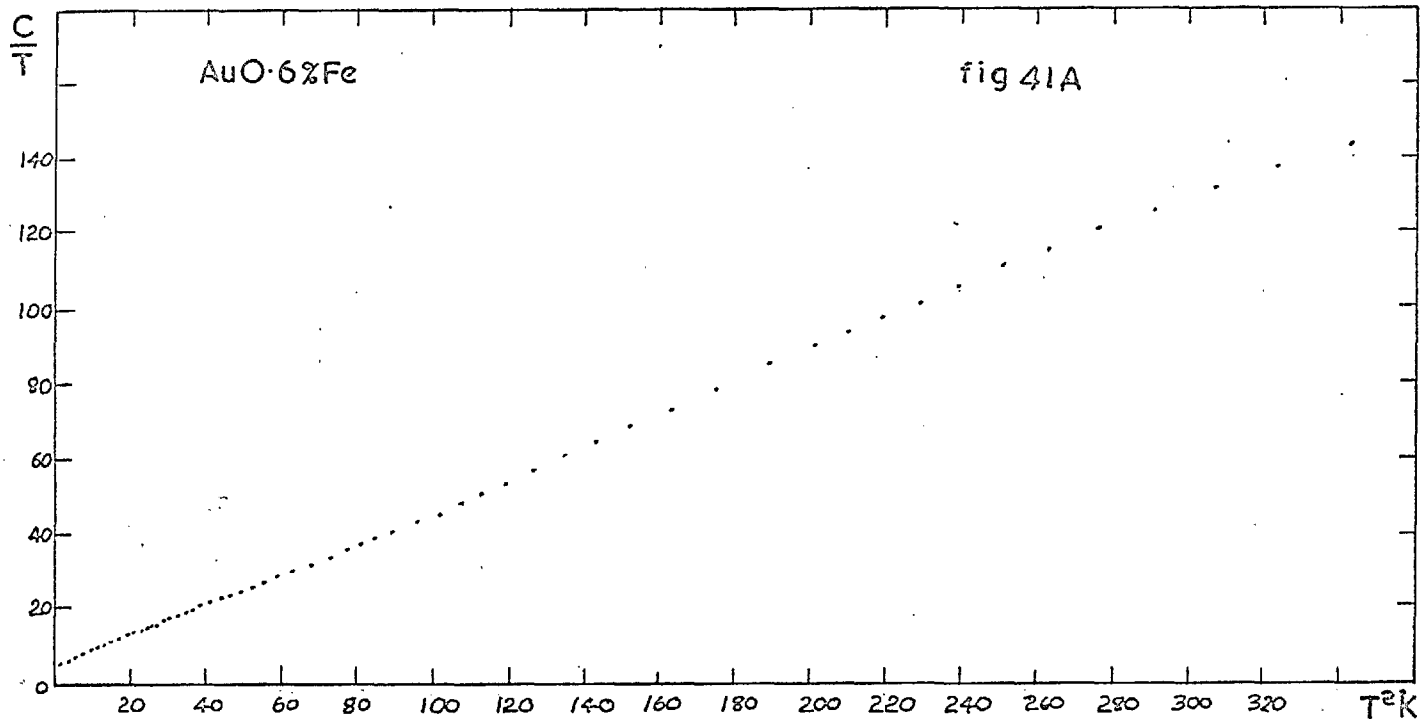
C/T
AuO·6%Fe
fig 41A
140
120
100
80
60
40
20
0
20
40
60
80
100
120
140
160
180
200
220
240
260
280
300
320
T°K

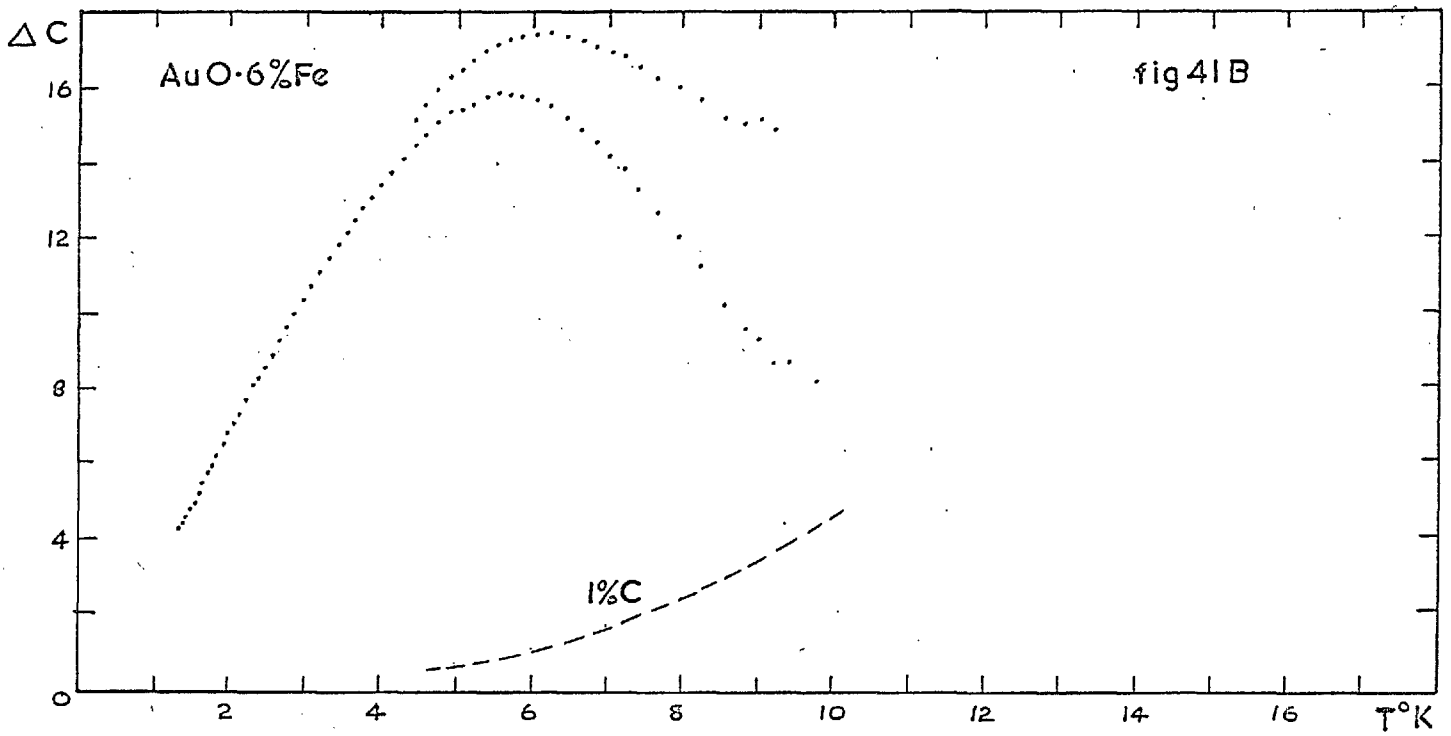
ΔC
AuO·6%Fe
fig 41B
16
12
8
4
0
1%C
2
4
6
8
10
12
14
16
T°K

Author	Temperature Range °K	γ mj/mole°K^2	$\theta(0)$	$\theta(10)$	$\theta(20)$	$\theta(30)$
Corak[128](1955)	1 - 5	0.70	164			
Zimmerman[138](1962)	1 - 5	0.74	164.6			
du Chatenier[96](1962)	1 - 30	0.74	165.2	165.2	167.0	169.8
N.B.S.	1 - 5	0.74	165			
Dreyfus[77](1964)	1 - 4	0.74	165			

ΔC against T is shown in fig. 41 B and $\frac{\Delta C}{T}$ against T in fig. 42. In calculating these results a value of $\gamma = 0.74$ mj/mole°K^2 was assumed. Curve A was found taking $\theta = 164^\circ K$, and curve B taking $\theta = 165^\circ K$. The effect of this small change in θ is seen to be marked at high temperatures, but does not effect the results significantly below 4°K.

A plot of $\frac{\Delta C}{T}$ against T for each of the alloys Cu 0.6% Fe, Cu_3Au 0.6% Fe, CuAu 0.6% Fe, $CuAu_3$ 0.6% Fe and Au 0.6% Fe is shown in fig. 40 A so that the anomalies in these systems can be compared.

6.11 Cu 0.6% Fe 0.1% Mn

The specific heat of 0.960 moles of Cu 0.6% Fe 0.1% Mn was measured between 1.3°K and 20°K. Chemical analysis showed that a one gram sample taken from the specimen contained 0.59% Fe and 0.10% Mn.

Fifteen calibration points were taken between 1.3° and 4.2°K, and a further fifteen between 4.2°K and 23°K. The R.M.S. deviation of the measured values of $\sqrt{\frac{\log R}{T}}$ from the calibration curve was 0.60×10^{-3}.

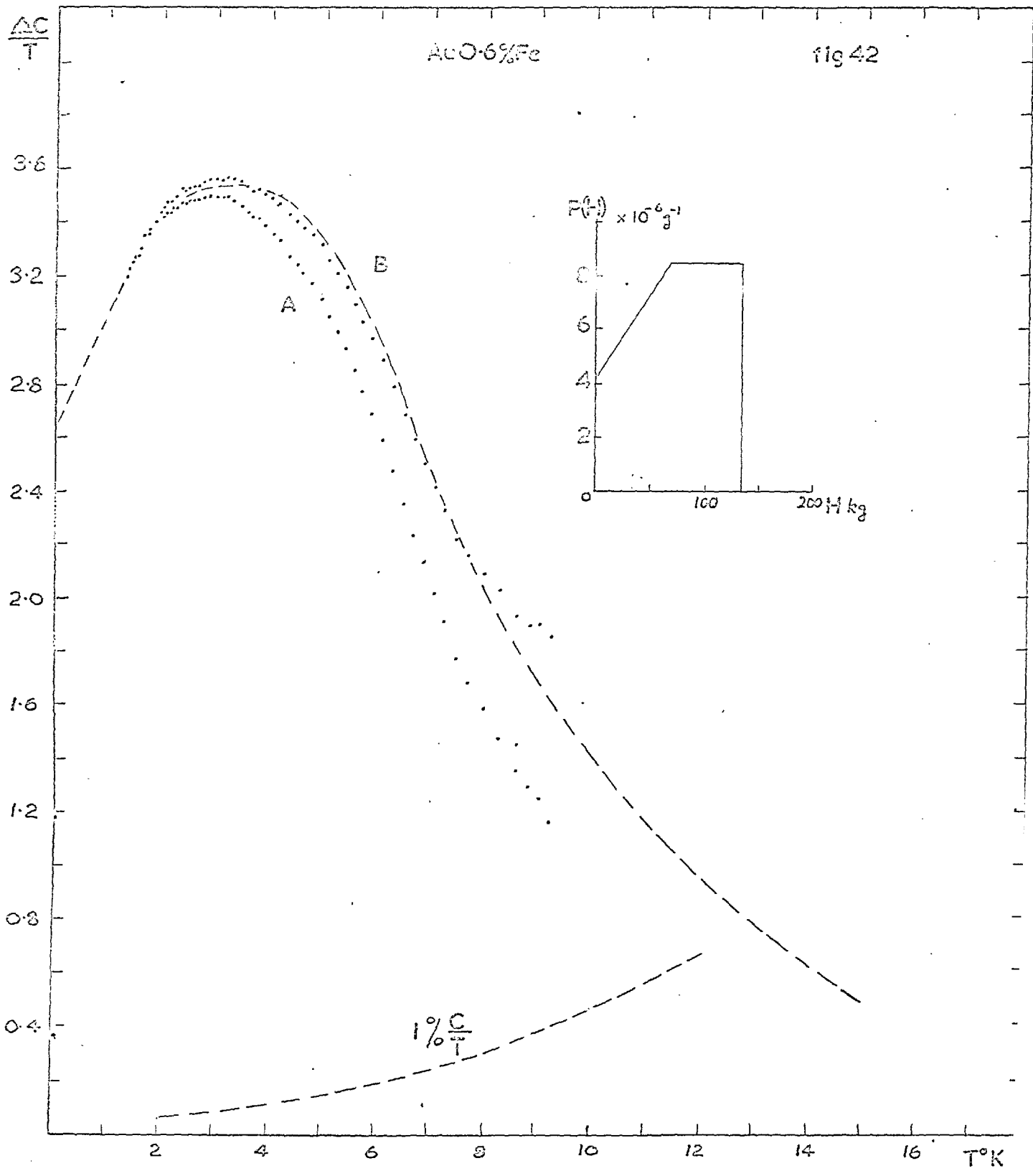
ΔC/T
Au 0·6% Fe
fig 42
3·6
3·2
2·8
2·4
2·0
1·6
1·2
0·8
0·4
A
B
P(H) × 10⁻⁶ g⁻¹
6
4
2
0
100
200 H kg
1% C/T
2
4
6
8
10
12
14
16
T°K

A plot of C/T against T^2 for this alloy is shown in fig 43A. The curve for pure Cu is also shown. A plot of ΔC against T is shown in fig 43 B, using the analytic expression for the specific heat of pure copper described in section 6.5. Values of $\frac{\Delta C}{T}$ against T are shown in fig 44, and the Cu 0.56% Fe results are included for comparison.

6.12 Rh

The specific heat of 0.653 moles of Rh was measured between 1.4° and 20°K. The specimen was expected to contain not more than 0.002% Fe impurity. Eighteen calibration points were measured between 1.3°K and 4.2°K, and a further sixteen between 4.2° and 23°K. The R.M.S. deviation of the measured values of $\sqrt{\frac{\log R}{T}}$ from the computed calibration curve was 0.77×10^{-3}.

A plot of C/T against T^2 is shown in Fig 45A for temperatures below 6°K, and in Fig 45B for temperatures below 20°K. It is evident that this plot is linear only between about 4.5° and 8°K, and in this region a value of $\gamma = 4.66$ mj/mole°K^2 and $\theta = 472$°K is obtained. The curvature observed above 8°K may be interpreted in terms of a rapid decrease in θ with increasing temperature. A plot of θ against T is shown in Fig 46A, θ values being calculated from each of the specific heat values above 4.7°K assuming a value of $\gamma = 4.66$ mj/mole°K^2. The curve at the bottom of Fig 46A marked $\frac{\Delta C}{C} = 1\%$ shows the error in θ due to an error of 1% in the specific heat.

The increasing departure of the results from a straight line as the temperature is reduced below 4.5°K is surprising and very difficult to account for. The magnitude of the deviations, almost 5% at 1.4°K, are too large to be accounted for by systematic errors in the calibration curve or

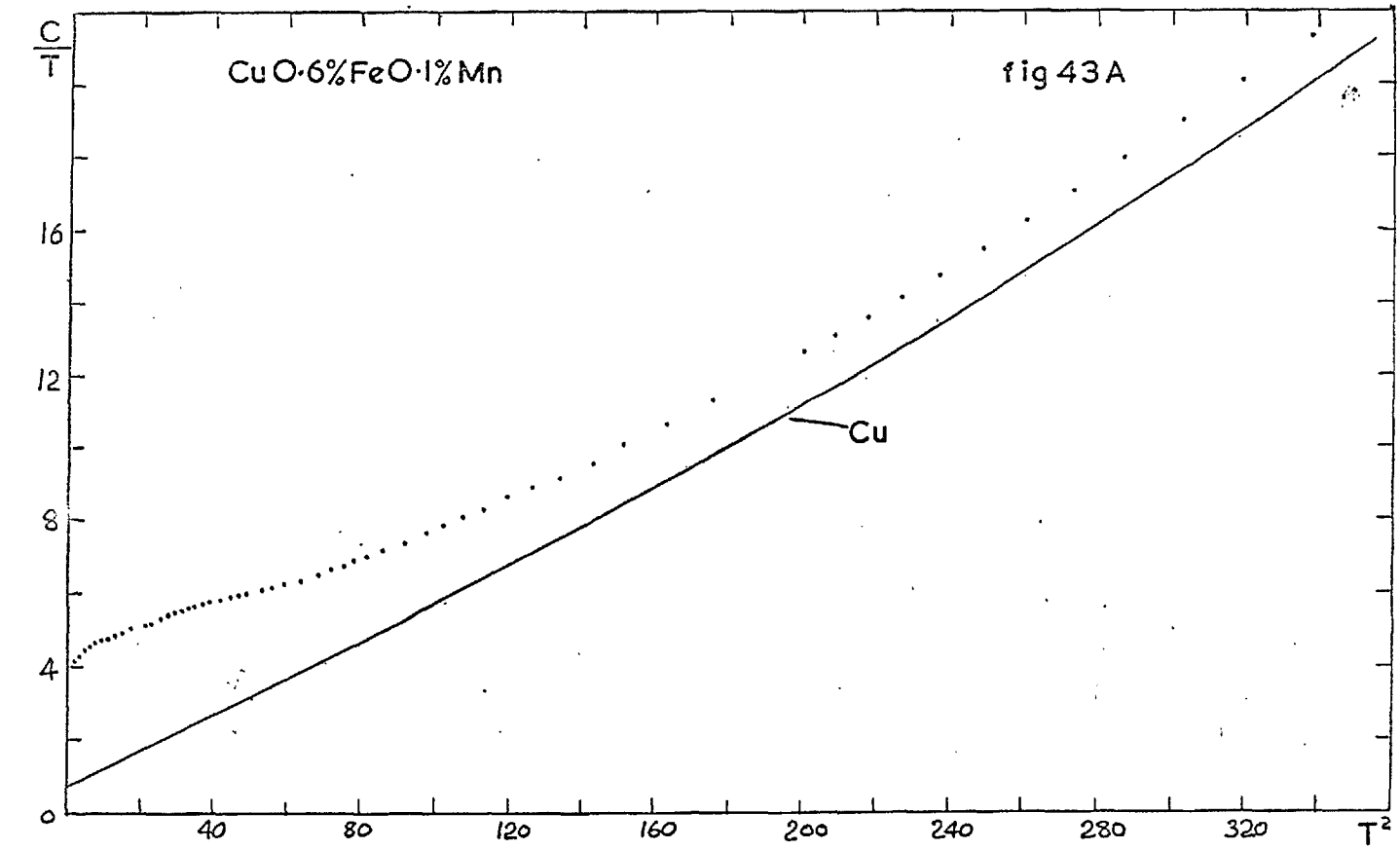
C/T
CuO·6%FeO·1%Mn
fig 43A
16
12
8
4
0
Cu
40
80
120
160
200
240
280
320
T²

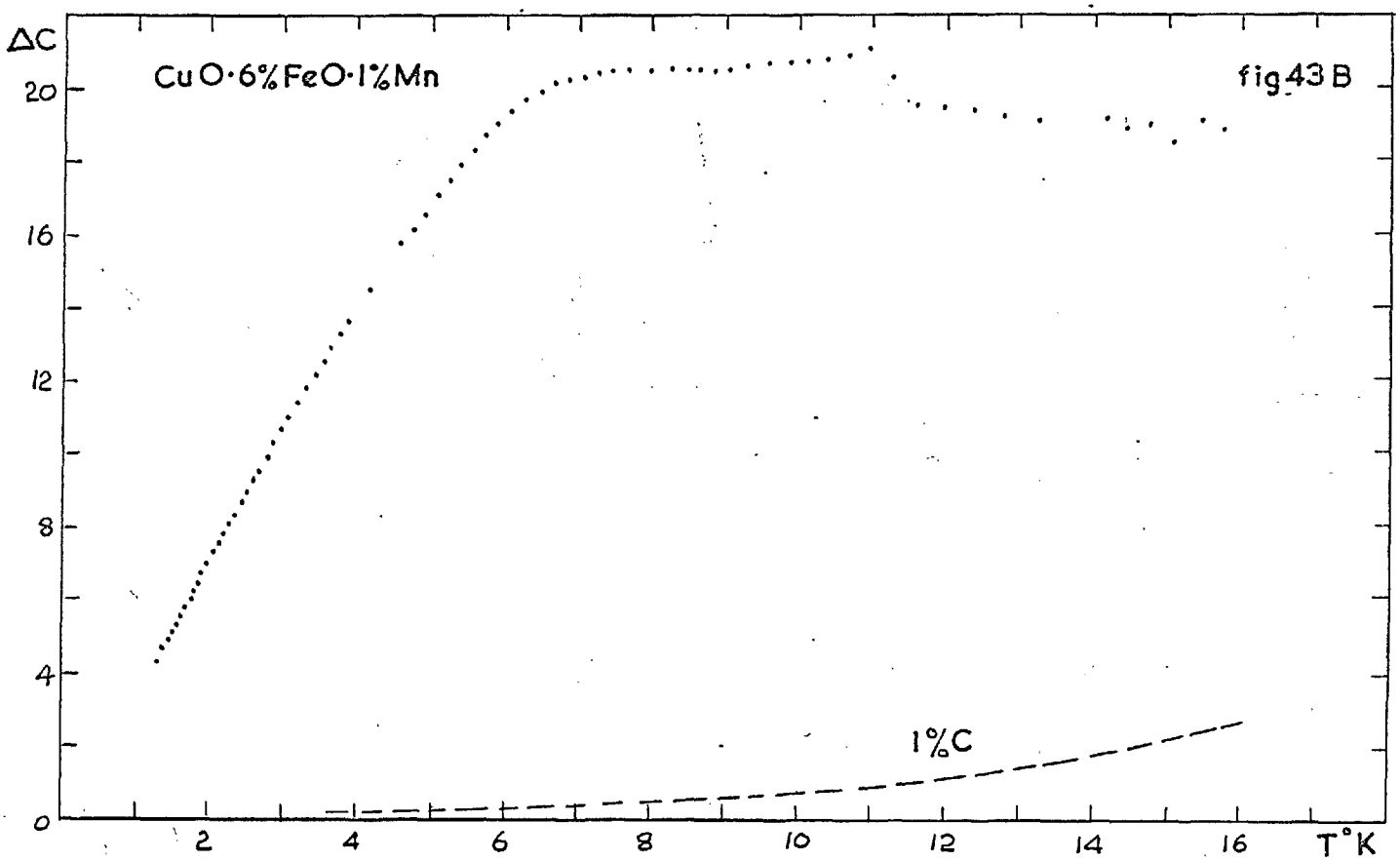
ΔC
CuO·6%FeO·1%Mn
fig 43B
20
16
12
8
4
0
1%C
2
4
6
8
10
12
14
16
T°K

in other measured quantities. The most obvious explanation is that the extra specific heat is due to magneticimpurities. A comparison with the C/T against T^2 curve for the Rh 0.5% Fe, fig. 46B, shows that if the magnitude of the excess specific heat at $2^{\circ}K$ isproportional to the Fe concentration, the extra specific heat in the Rh specimen could be accounted for by the presenceof 0.03% Fe. This more than an order of magnitude larger than the expected concentration of Fe.

It is possible that there is an unknown source of error in the method of measurement that manifests itself below $4^{\circ}K$, but this seems unlikely as the measurements on Rh were followed within two days by the measurements on Cu, described above, which showed no such unusual behaviour, no changes having been made in the apparatus or measuring technique between the runs.

Alternatively the calibration may be in error below $4.5^{\circ}K$. This also seems unlikely, as the calibration points fit the calibration curve for Cu within 2 mdeg below $4.2^{\circ}K$, and the systematic deviations of the calibration points from their respective calibration curves are almost identical for the Rh and Cu runs.

The values of γ and θ for Rh found by other workers are shown below

Author	γ mj/mole$^{\circ}K^2$	$\theta(0)$	$\theta(10)$	$\theta(20)$	Temperature Range $^{\circ}K$
Wolcott[129] (1955)	4.9	478	478	425	1.2 - 20
Clusius[130] (1955)	4.2	512±17	439		10 - 273
Budworth[131] (1960)	4.65 ±.018	512±17			2.5 - 4.2
This work	4.66	472	469	420	4.5 - 20

It should be noted that if the low temperature increase in C/T is due to magnetic impurities, the excess specific heat will not be zero above

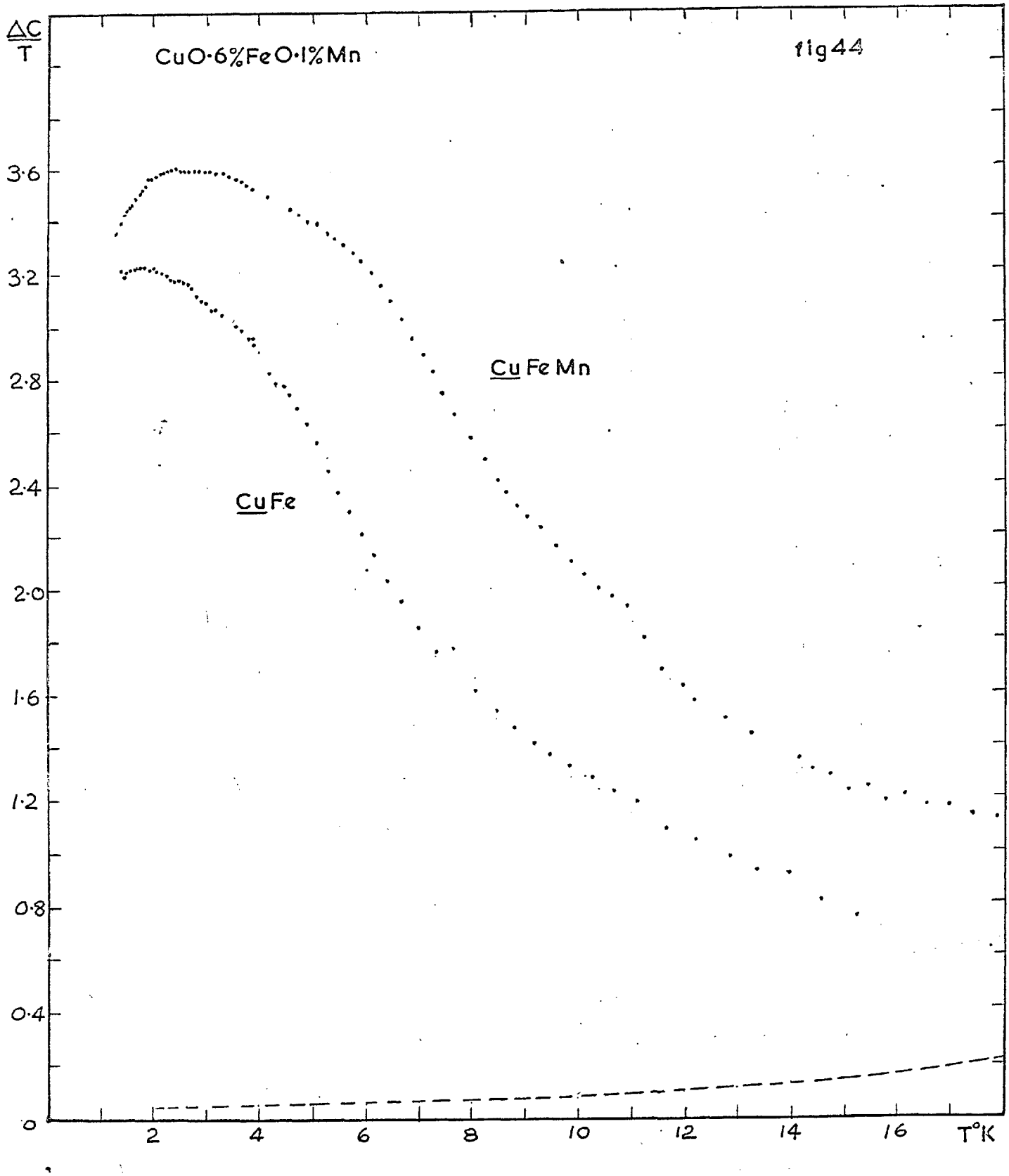
ΔC/T
CuO·6%FeO·1%Mn
fig 44
3·6
3·2
2·8
2·4
2·0
1·6
1·2
0·8
0·4
0
CuFeMn
CuFe
2
4
6
8
10
12
14
16
T°K

$4.5^{\circ}K$, and the values of θ and γ given above will be slightly too large.

The following polynomial was found to fit 42 randomly selected specific heat values for pure Rh.

$$\frac{C}{T} = 5.041 - 1.643 \times 10^{-1} T + 4.520 \times 10^{-2} T^2 - 2.496 \times 10^{-3} T^3 + 1.249 \times 10^{-4} T^4 - 1.400 \times 10^{-6} T^5 \quad mj/mole^{\circ}K^2$$

The R.M.S. deviation of the points from the polynomial is 0.018 $mj/mole^{\circ}K^2$, corresponding to a fractional error of 0.35% below $5^{\circ}K$, decreasing to 0.12% at $20^{\circ}K$.

6.13 Rh 0.5% Fe

The specific heatof 0.629 moles of Rh 0.5% Fe was measured between 1.3° and $20^{\circ}K$. Ten calibration points were taken between 1.3° and $4.2^{\circ}K$, and a furthereleven between $4.2^{\circ}K$ and $26^{\circ}K$. The R.M.S. deviation of the measured values of $\sqrt{\frac{\log R}{T}}$ from the computed calibration curve was 0.8×10^{-3}.

A plot of C/T against T^2 for this alloy is shown in fig. 46B, together with a smooth curve representing the values for pure Rh.

The quantities ΔC against T and $\frac{\Delta C}{T}$ against T are shown in figs 47A and 47B, and have been obtained with the aid of the polynomial for the Rh specific heat described in section 6.12. Curve A has been calculated assuming that $\gamma = 4.66$ $mj/mole^{\circ}K^2$, and θ isconstant at $472^{\circ}K$ below $4.5^{\circ}K$, whilst curve B has been calculated from the measured specific heat values for pure Rh below $4.5^{\circ}K$.

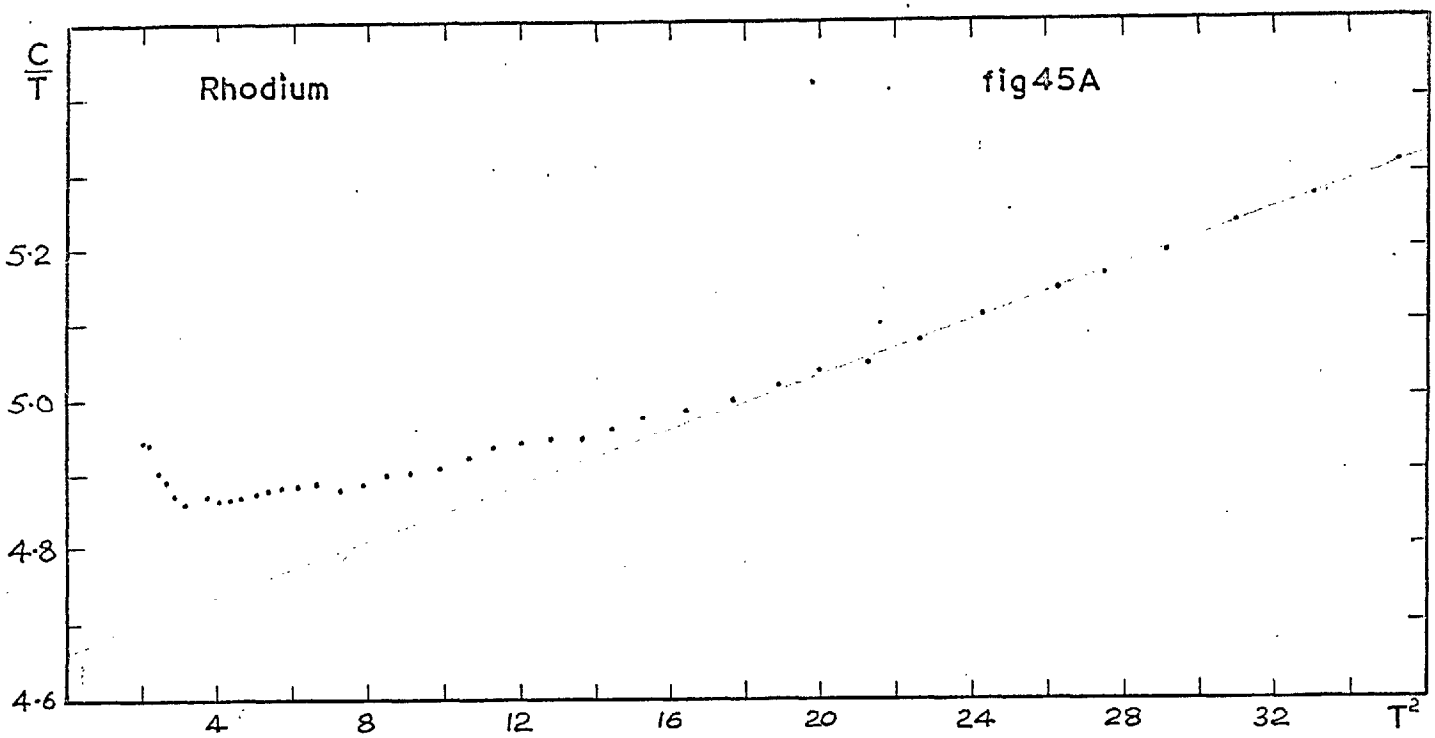
C/T
Rhodium
fig45A
5·2
5·0
4·8
4·6
4
8
12
16
20
24
28
32
T²

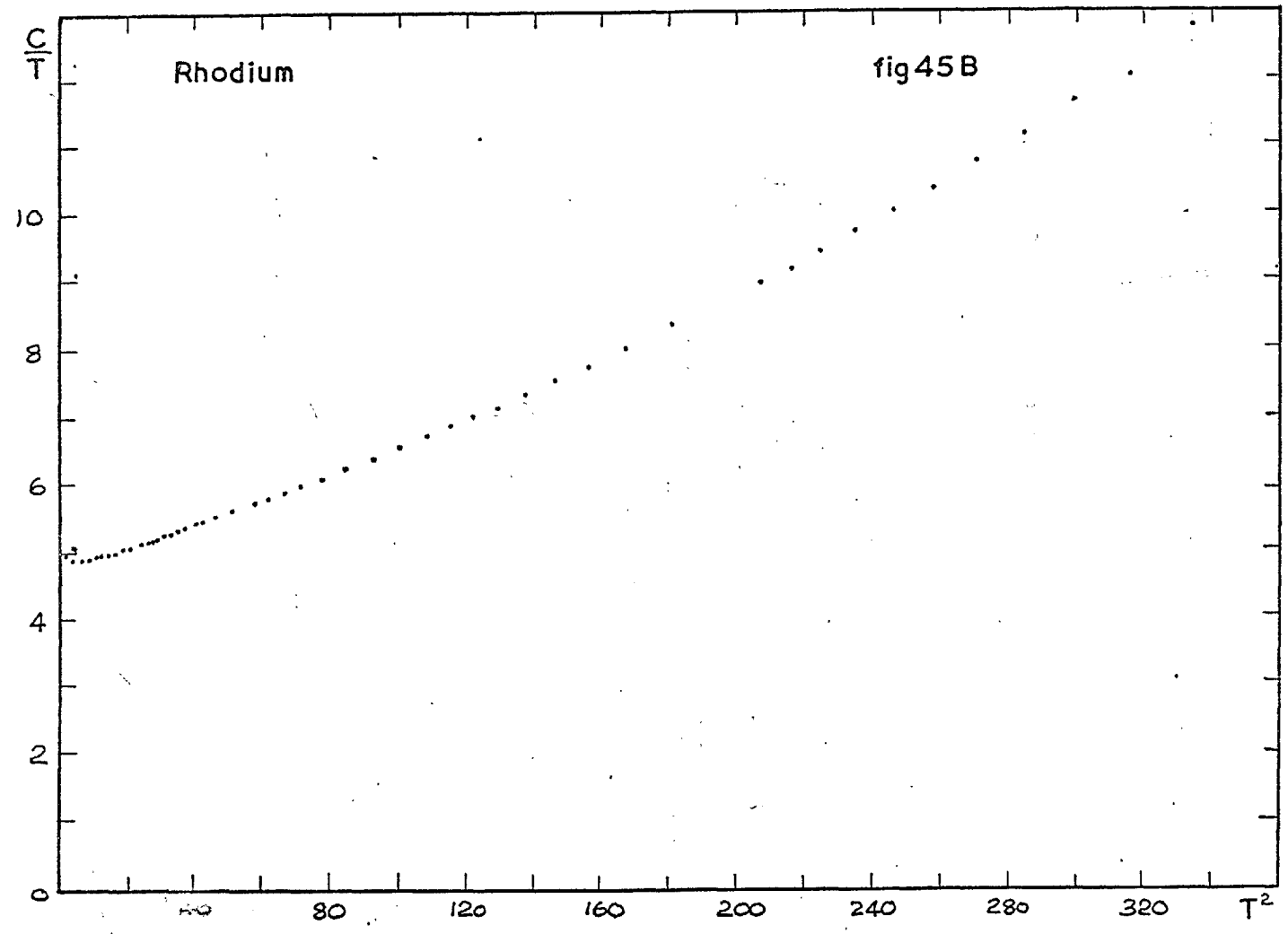
C/T
Rhodium
fig45B
10
8
6
4
2
0
80
120
160
200
240
280
320
T²

6.14 Pd 0.19% Fe

The specific heat of 0.328 moles of Pd 0.19% Fe were measured between 1.3° and 17° K. Satisfactory equilibrium conditions were not obtained during the thermometer calibration below 3°K, and the calibration points are unreliable below this temperature. The calibration curve was computed from eleven calibration points between 3.3°K and 20°K, with an R.M.S. deviation of the measured values of $\sqrt{\frac{\log R}{T}}$ from the calibration curve of 0.15×10^{-3}. This calibration curve has been used to compute the specific heat values above 3.5°K. Below this temperature the Cu_3Au 0.6% Fe calibration curve was used to compute the results as it most closely fitted these Pd Fe calibration points below 4°K in which confidence could be placed. For the reasons outlined in section 6.6, this is not expected to introduce an error of more than one or two per cent in the total specific heat.

A plot of $\frac{C}{T}$ against T^2 for this alloy is shown in fig. 48A. The specific heat of pure Pd was not measured, and therefore to obtain the excess specific heat due to the Fe, values of the specific heat of Pd found by other workers must be considered.

Author	γ mj/mole°K^2	$\theta(0)$	Temperature Range
Hoare and Yates[132] (1957)	9.31 ± .05	274 ± 3	1.4 - 4.2
Veal and Rayne[133] (1964)	9.42 ± .02	273.6 ± 1.4	1.4 - 4.2
Montgomery and Pells	9.53 ± .07	278.1 ± 4.0	1.3 - 4.2

Rayne quotes values of the specific heat of Pd between 4°K and 100°K, and these values are plotted as circles in fig. 48A. He also shows a plot of θ against T in this temperature range. θ is shown to be

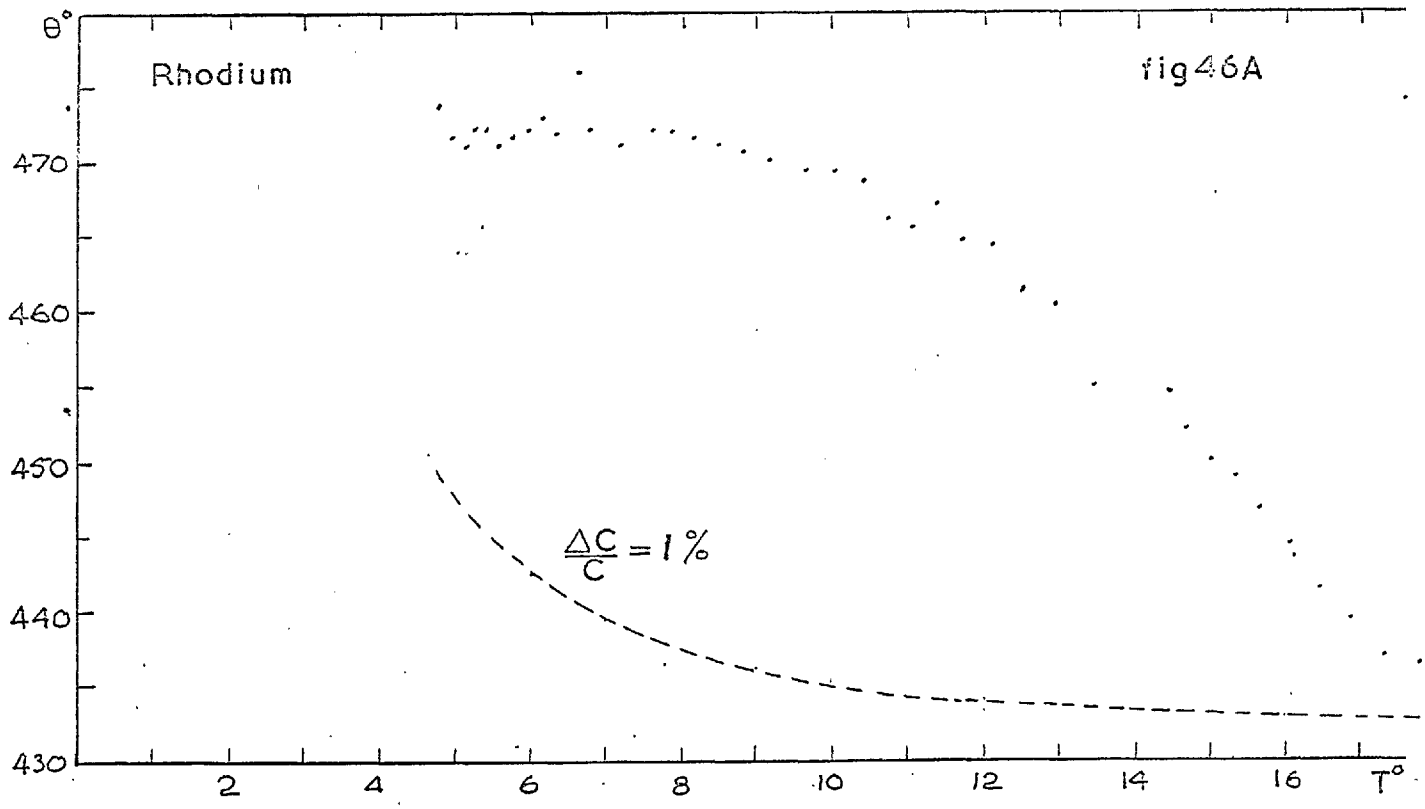
θ°
Rhodium
fig 46A
470
460
450
440
430
$\frac{\Delta C}{C} = 1\%$
2
4
6
8
10
12
14
16
T°

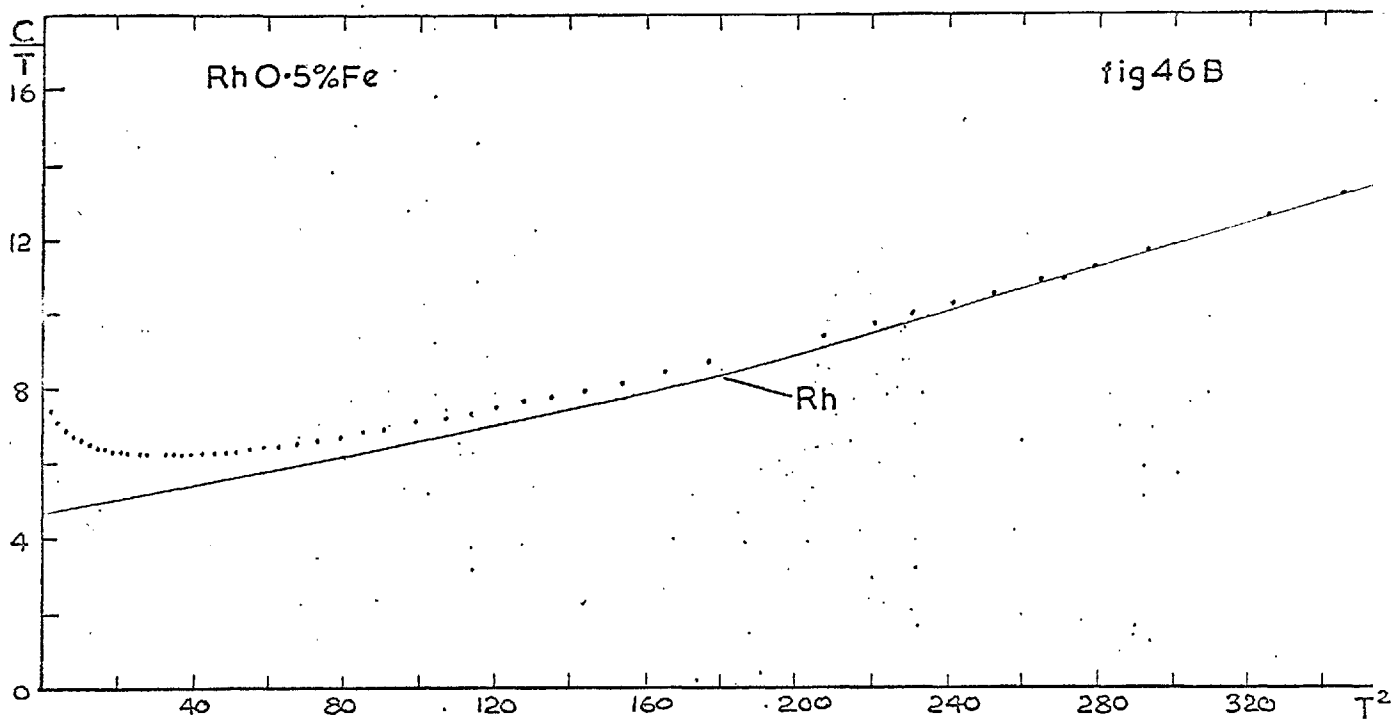
C/T
RhO·5%Fe
fig 46B
16
12
8
4
0
Rh
40
80
120
160
200
240
280
320
T²

approximately constant at about 277°K up to 25°K, and then to increase slightly. Unfortunately these values of θ are not consistant with the numerical values of the specific heat quoted, which suggest that θ has fallen to a value of about 266°K at 13°K and is then approximately constant. Because of this uncertainty in the values of the specific heat of Pd above 4°K, the following procedure has been adopted. The excess specific heat is assumed to be zero above 17°K, and a value of θ has been computed at that temperature assuming that γ = 9.42 mj/mole°K^2, and is found to be 265.4°K. The straight line in fig. 48A corresponds to the specific heat of Pd assuming that θ is constant at that value.

Assuming these values for γ and θ, $\frac{\Delta C}{T}$ is plotted against T in fig 48 B, and ΔC is plotted against T in fig. 49. The discontinuity in these curves at 3.5°K, by an amount of the order of 0.8% of the total specific heat, arises from the overlap of the two calibration curves. As a value of θ = 273.6°K would seem to be more appropriate for temperatures below 4°K, the effect on $\frac{\Delta C}{T}$ and ΔC of increasing θ from 265.4° to 273.6° is shown in curve A. The effect is seen to be small below 2°K, but increases rapidly at higher temperatures.

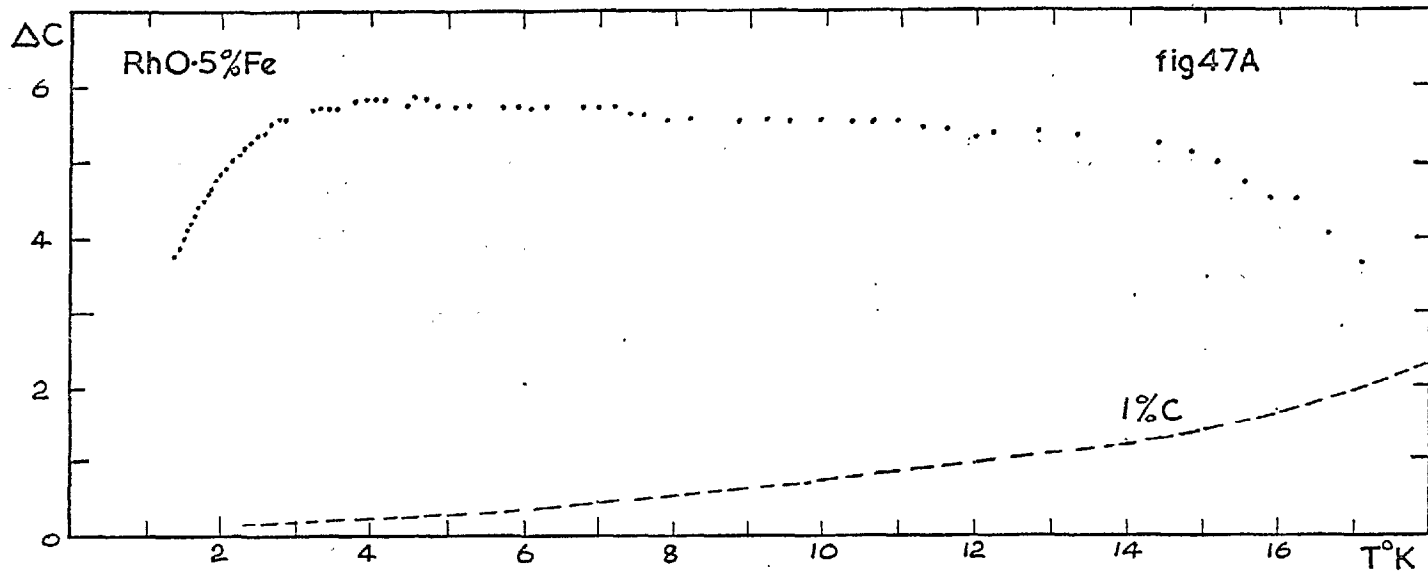
ΔC
RhO·5%Fe
fig47A
6
4
2
0
1%C
2
4
6
8
10
12
14
16
T°K

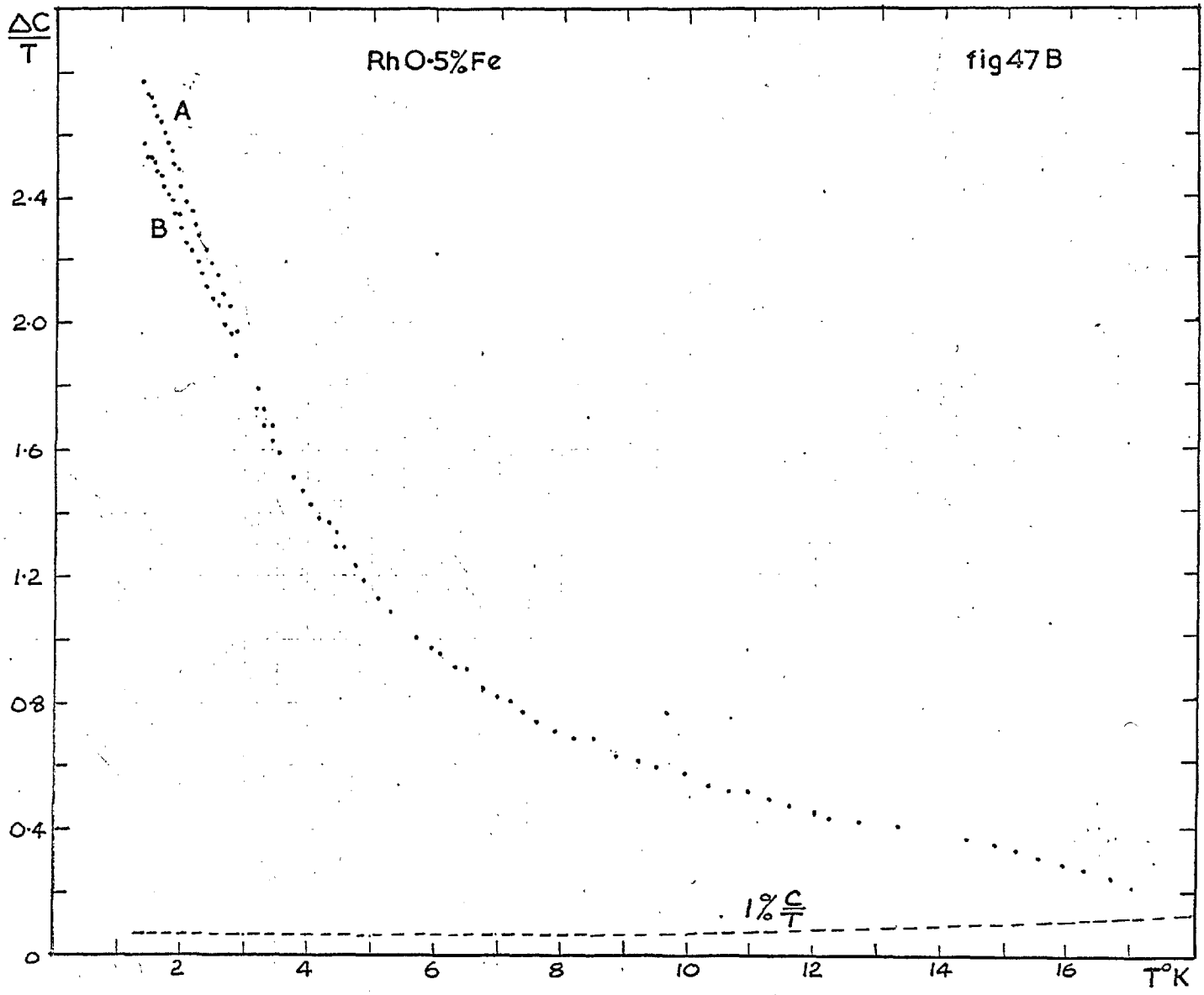
ΔC/T
RhO·5%Fe
fig47B
A
B
2·4
2·0
1·6
1·2
0·8
0·4
0
1% C/T
2
4
6
8
10
12
14
16
T°K

CHAPTER 7

INTERPRETATION OF RESULTS

7.1 Introduction

The theories of Friedel, Anderson, Wolff and Clogston show that the excess charge of an impurity may be screened by conduction electrons from a relatively narrow energy range (or the order of 1 e.v. in width), and these screening electrons may therefore enhance the density of states atthe Fermi surface, giving an enhanced electronic specific heat. As discussed in section 4.16, the extra specific heat, which is linear in temperature, will be small compared with the specific heat of the pure metal, and cannot account for the large anomalies observed with magnetic impurites.

Recent theories of Kondo[108], Doniach[139] and Nagaoka[140] have shown that the resistance minimum may result from spin dependent scattering from isolated magnetic impurities, in which the scattering probability of a conduction electron increases rapidly as its momentum approaches the Fermi momentum. Associated withthis increased scattering therewill be a rather narrow peak in the density of states of the conduction electrons which may be centred about the Fermi energy, and which will give a contribution to the specific heat which is linear in temperature as $T \to 0$. The magnitude of this contribution is uncertain, but Nagaoka[140] estimates that for a 1% alloy it may be only 10% of the electronic specific heat of the pure metal. As, on this model, the anomaly is due to non interacting magnetic impurities, its magnitude will be proportional to concentration at all temperatures. Thus although it may account for the finite value of $\frac{\Delta C}{T}$ as $T \to 0$, it cannot account for the approximate concentration independence of $\frac{\Delta C}{T}$

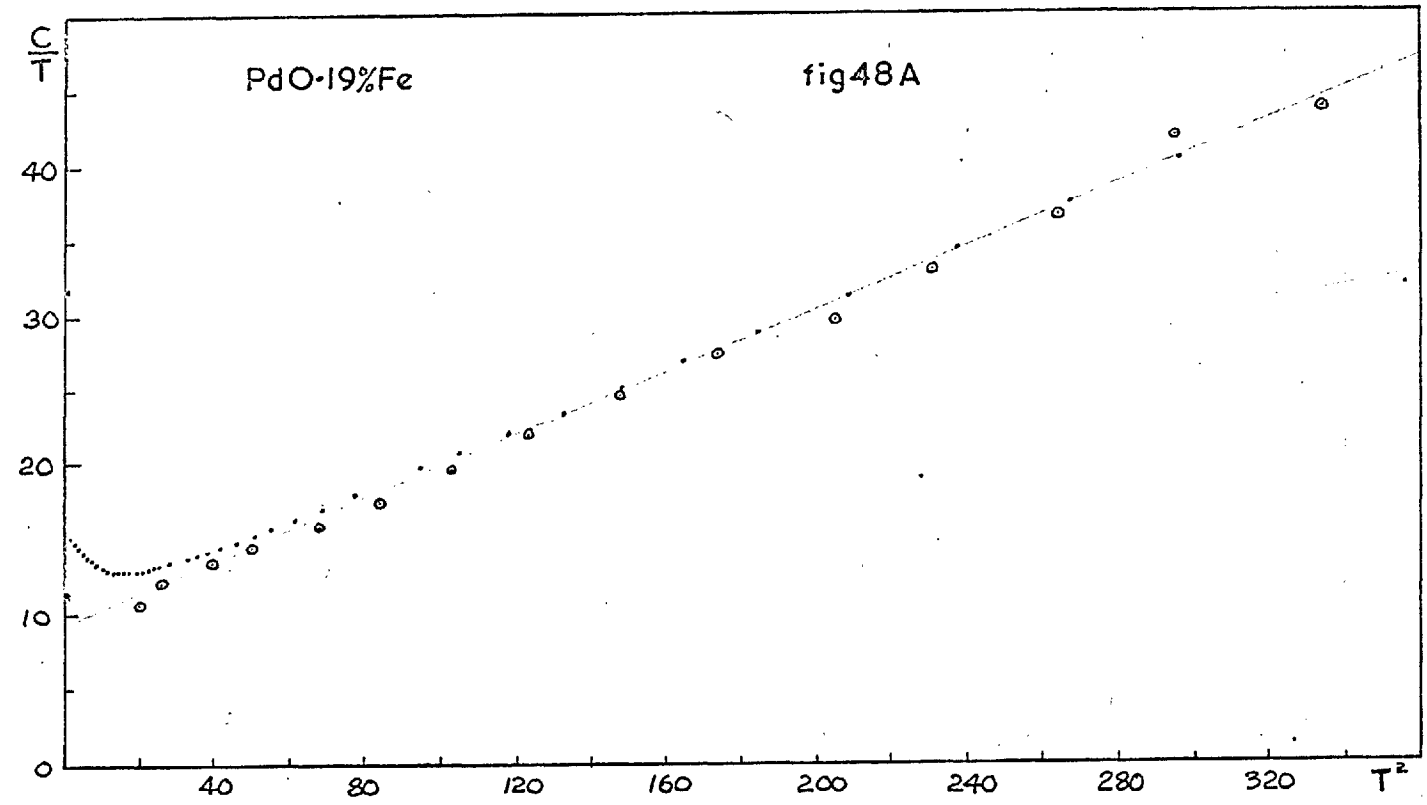
C/T
PdO·19%Fe
fig48A
40
30
20
10
0
40
80
120
160
200
240
280
320
T²

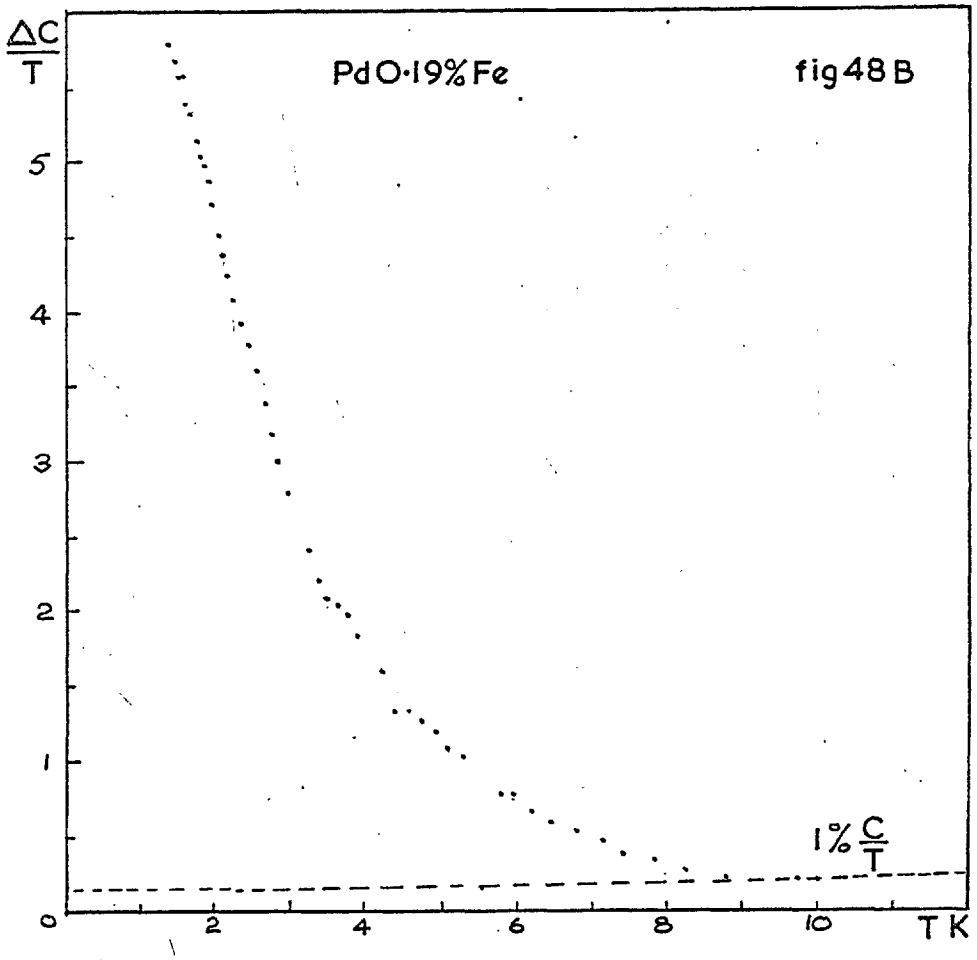
ΔC/T
PdO·19%Fe
fig48B
5
4
3
2
1
0
1% C/T
2
4
6
8
10
T K

at low temperatures, or the increasing temperature of the maximum in the specific heat with increasing concentration.

It therefore seems that the specific heat anomalies can only be accounted for in terms of the interaction between the impurities, and their subsequent ordering at sufficiently low temperatures. As the entropy of the anomaly is proportional to the concentration, within experimental error, the degeneracy of each impurity state may be calculated, and a spin value obtained by assuming that the degeneracy is equal to 2S + 1. As current theories (Anderson, Friedel) suggest that the magnetised impurity state is a many electron state whose total spin may have any value between 0 and 5/2, and not only half integral values, it is not certain how far this procedure is justified. In the absence of a theory capable of handling non half-integral spins, it is essential to assume that the degeneracy of each impurity state is well defined. The shape of the specific heat anomaly can then be calculated using simple quantum statistics, for any given distribution of local fields, and the resulting specific heat curve compared with the experimental results. Thus although such an analysis may not be justified, the specific heat anomalies will be considered in terms of localised impurities with well defined degeneracies, ordering in a distribution of internal fields represented by a P(H) curve.

Series A

7.2 Cu 0.6% Fe

$\frac{\Delta C}{T}$ against T for this specimen is shown in fig. 37 and ΔC against T in fig. 36B, and these curves are compared with those of Franck Manchester

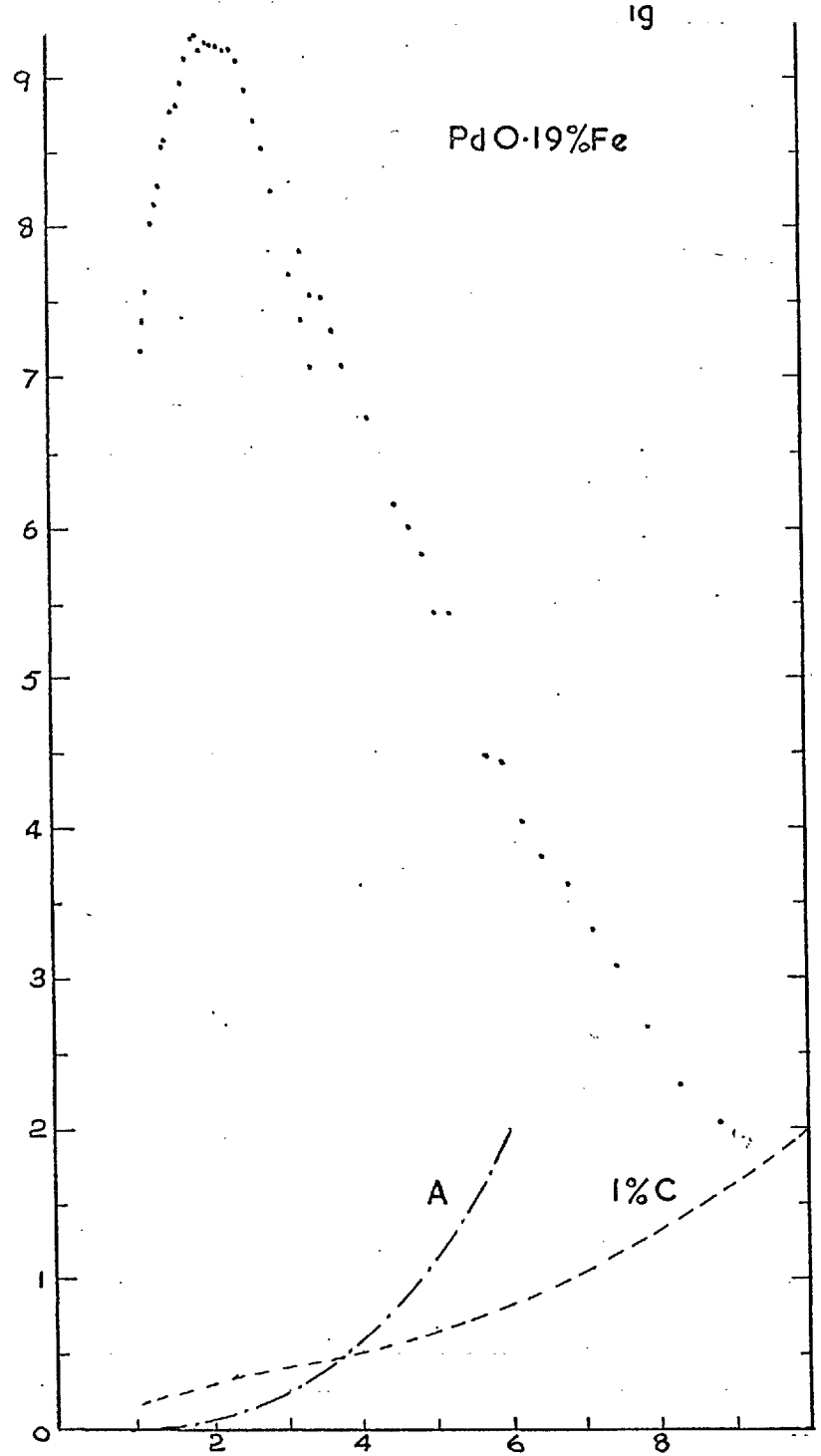
Pd 0·19%Fe
A
1%C
0
1
2
3
4
5
6
7
8
9
2
4
6
8

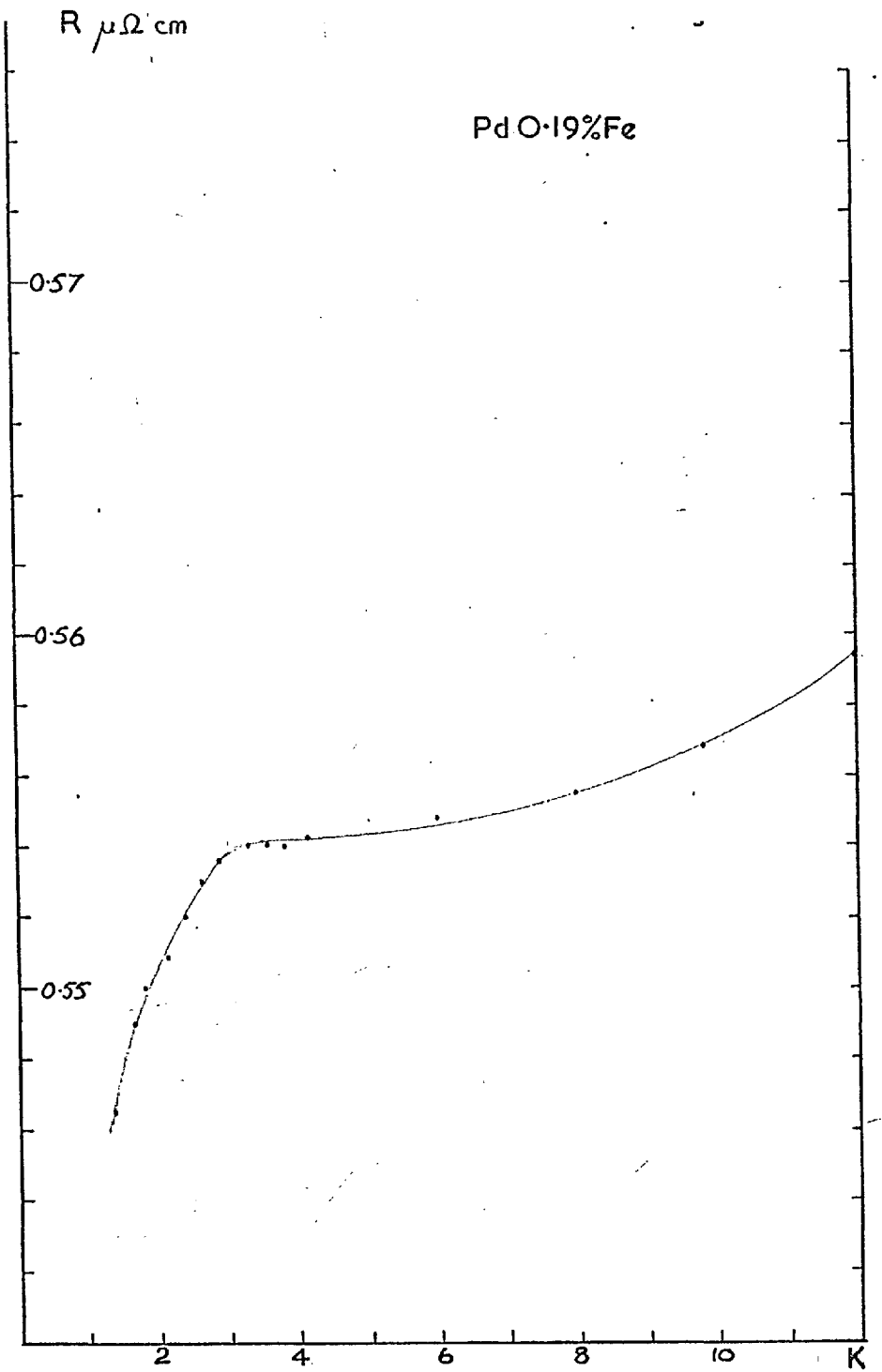
R μΩ cm
Pd 0·19%Fe
0·57
0·56
0·55
2
4
6
8
10
K

and Martin[74] for more dilute Cu Fe alloys in figs. 9 and 10. The excess specific heat initially increases approximately linearly with temperature, and reaches a maximum at about 5.5°K. It then decreases very slowly with increasing temperature, though the rate of decrease above 10°K is uncertain due to the increasing lattice specific heat. The anomaly is therefore similar to those found by Franck et al[74] for lower concentration alloys, with the beginning of the broad maximum occuring at a temperature which increases with concentration.

Fig. 37 shows that $\frac{\Delta C}{T}$ may pass through a maximum at about 1.8 °K, falling to a value at 1.3°K which is less than 1% lower than the value at the maximum. The existance of the maximum is by no means certain however, as the specific heat may be in error by up to 2% below 3.6°K due to uncertainties in the thermometer calibration.

It is not possible to say from these measurements whether a concentration independent region exists at very low temperatures (below 0.4°K), but if so it will occur over a very much smaller portion of the anomaly than the concentration independent region in the Mn alloys.

The increase in entropy between 1.3°K and 20°K is 28 ± 2 mj/mole °K. If $\frac{\Delta C}{T}$ is assumed to be constant below 1.3°K the entropy at 1.3°K is 4.2 mj/mole°K, and a plausible extrapolation of the anomaly above 20°K suggests that the entropy increase above 20°K is 2 ± 1 mj/mole°K. The total entropy associated with the anomaly is therefore 34 ± 3 mj/mole°K (if the estimated entropy below 1.3°K is not in error by more than 30%). Assuming that the Fe concentration is 0.56% as found by chemical analysis the spin per Fe atom is 0.54 ± 0.07, and is therefore consistant with the spin of $\frac{1}{2}$ found by Franck et al for their Cu 0.05, 0.1 and 0.2% Fe specimens.

A $\frac{\Delta C}{T}$ against T curve has been calculated (dashed curve in fig 37) assuming an Fe spin of $\frac{1}{2}$ and a rectangular, temperature independent P(H) curve (fig. 37 inset) in which there is a constant probability of local fields up to 182 Kg, and zero probability of fields greater than this. (A rectangular P(H) curve which is symmetrical about H=0, and with a value of P(0) half that shown in fig. 37, will give an identical curve). Deviation of the experimental points from this curve suggest that the high field cut off is not as sharp as this, and the dotted P(H) curve (inset) is a more likely distribution of fields. The shape of the specific heat curve above 1.3°K is insensitive to details of the P(H) curve at very low H.

7.3 Au 0.6% Fe

A plot of $\frac{\Delta C}{T}$ against T is shown in fig. 42 for this alloy, and ΔC against T in fig. 41B, and these are compared with the measurements of Dreyfus[77] et al and those of du Chatenier[72] on other Au Fe alloys in fig. 8. The excess specific heat increases approximately linearly at low temperatures, and passes through a maximum value at about 6°K, and decreases at higher temperatures. Uncertainties in the specific heat of pure gold, which increase rapidly above 6°K, make the rate of decrease above this temperature uncertain, but it is apparently rather more rapid than for the Cu 0.6% Fe alloy.

$\frac{\Delta C}{T}$ passes through a pronounced maximum at 3.0 ± 0.2°K, and at 1.3°K has a value approximately 10% lower than the value at the maximum. The measurements of Dreyfus[77] et al for Au 0.2, 0.5 and 1.0% Fe alloys, and the present measurements on the Au 0.6% Fe alloy show that the specific heat is almost concentration independent at 1.3°K for these alloys, and may possibly approach

the curve of du Chatenier for a Au 0.092% Fe alloy at very low temperatures.

Assuming a linear extrapolation of $\frac{\Delta C}{T}$ below 1.3°K to a value of 2.65 mj/mole°K^2 at T=0, and a reasonable extrapolation of the curves above 12°K, the entropy associated with the anomaly (curve B, θ = 165°K for pure Au) is 35 ± 4 mj/mole°K, of which about 10% comes from the region below 1.3°K, and a further 10% from the region above 12°K. If the Fe concentration is assumed to be 0.71%, as found by the chemical analysis of a one gram sample taken from the specific heat specimen, then the value of the spin per Fe atom is 0.41 ± 0.09. If the concentration is taken to be 0.6% Fe, as the initial proportions of Fe and Au used in the preparation of the sample would suggest, the spin value per Fe atom is 0.50 ± 0.08. The residual electrical resistance of a sample taken from the specimen indicated an Fe concentration of 0.5%, and therefore it is possible that there may be some inhomogeneity or precepitation in this alloy. The entropy calculated assuming curve A (θ = 164° for pure Au) yields a spin value of 0.32 if the concentration is 0.71%, and 0.40 if the concentration is 0.6%. The results are therefore probably consistant with a spin of $\frac{1}{2}$ for the Fe atom.

The dashed curve in fig. 42 has been calculated assuming a concentration of 0.6%, a spin of $\frac{1}{2}$, and the P(H) curve shown in fig. 42 (inset). A pronounced dip in the P(H) curve at low H is necessary to reproduce the maximum in $\frac{\Delta C}{T}$, though it is not possible to decide from measurements above 1.3°K whether P(0) is zero or finite.

7.4 Cu_3Au 0.6% Fe, CuAu 0.6% Fe and $CuAu_3$ 0.6% Fe

$\frac{\Delta C}{T}$ against T for these alloys is shown in fig. 39. A and B. As discussed

in section 6.7, the specific heat of the solvents were not measured, and errors in the assumed lattice specific heats make the shapes of these anomalies very uncertain at high temperatures.

Data is available for the specific heat of Cu_3Au below $4^\circ K$, and plausible assumption for the heat capacity of Cu_3Au above this temperature allow the shape of the anomaly to be obtained with some confidence below $10^\circ K$. $\frac{\Delta C}{T}$ exhibits a maximum at about $3^\circ K$, and is 10% lower at $1.3^\circ K$ than at $3^\circ K$. Uncertainty in the shape of the anomaly at higher temperatures make a calculation of a spin value impossible, but the results are consistant with a spin of $\frac{1}{2}$.

There is no data available on the specific heat of CuAu or $CuAu_3$, and the situation is aggravated by the rapidly increasing lattice specific heat with increasing gold concentration. The curves for $\frac{\Delta C}{T}$ against T for CuAu 0.6% Fe and $CuAu_3$ 0.6% Fe therefore have little significance above $3^\circ K$. However the existance of a maximum in $\frac{\Delta C}{T}$ at a temperature between 2° and $5^\circ K$ seems to be established for both of these systems, as the lattice specific heat is a very small fraction of the total specific heat below $2^\circ K$, where $\frac{\Delta C}{T}$ is increasing rapidly.

The $\frac{\Delta C}{T}$ against T curves for the copper-gold-iron series are compared in fig. 40A. The shape of the anomalies in Au 0.6% Fe and Cu_3Au 0.6%Fe are very similar, with a maximum in $\frac{\Delta C}{T}$ occuring at about $3^\circ K$ in each system, and it is possible this is also true in the CuAu 0.6% Fe and $CuAu_3$ 0.6% Fe anomalies. The magnitude of $\frac{\Delta C}{T}$ at the maximum expressed in $mj/mole\,^\circ K^2$, is 3.56 for Au 0.6% Fe, 3.5 for Cu_3Au 0.6% Fe, 2.7 for Cu Au 0.6% Fe and 3.8

for $CuAu_3$ 0.6% Fe. The rather low value for CuAu 0.6% Fe compared with those for the other systems may suggest that there is less Fe in solution than the value of 0.63% suggested by chemical analysis, or alternatively that the distribution of internal fields is similar to that of the other alloys, but spreads to higher fields, with a decreased probability of lower fields.

It is not possible to decide from the measurements whether the shape of the anomaly in Cu 0.6% Fe is similar to that in Au 0.6%Fe, but with a maximum occuring at a lower temperature (1.8°K compared with 3°K), or whether the shape of the curves differ significantly at low temperatures, with $\frac{\Delta C}{T}$ approximately constant below 1.3°K for Cu 0.6% Fe, and falling rapidly for Au 0.6% Fe. Evidence in favour of the latter conclusion comes from the very much stronger concentration dependence of $\frac{\Delta C}{T}$ at 1.3°K in the Cu Fe system than in the Au Fe system (see figs. 9 and 8), thus requiring an extremely rapid fall off of $\frac{\Delta C}{T}$ at low temperatures for Cu Fe if a concentration independent region is to be reached. Measurements are required to very much lower temperatures in both systems before any definite conclusions can be reached.

7.5 Cu 0.6% Fe 0.1% Mn

A plot of $\frac{\Delta C}{T}$ against T for this alloy is shown in fig. 44, the Cu 0.6%Fe results being included for comparison. A maximum in $\frac{\Delta C}{T}$ occurs at about 3°K, with a magnitude of 3.6 mj/mole°K^2, which is about 7% higher than the value at 1.3°K. The curve is thus very similar to that for Au 0.6% Fe below about 4°K. The difference in entropy between the Cu 0.6% Fe 0.1% Mn and Cu 0.6% Fe anomalies is consistant with a spin of 5/2 per Mn atom.

ΔC against T for the Cu 0.6% Fe 0.1% Mn alloy is shown in fig. 43B. The shape of this curve is similar to that for Cu 0.6% Fe, with a maximum at about $8^{\circ}K$, and a gradual decrease at higher temperatures. An interesting feature of this curve is the sharp peak at $11^{\circ}K$ which resembles a λ anomaly. The peak is much too sharp to be the result of inaccuracies in the calibration curve. A possible explanation is that some of the Fe has precipitated in the γ phase, and undergoes an antiferromegnetic transition at $11^{\circ}K$.

7.6 Some Conclusions from the Specific Heat Results

The specific heat anomalies of dilute magnetic alloys do not resemble the λ anomalies typical of the disordering of spacially ordered ferro or antiferromagnetic systems, in which the very rapid decrease in specific heat above the maximum is the result of a very rapidly decreasing sublattice magnetisation and molecular field with increasing temperature. Short range order above the transition temperature, in which large fields persist in small regions of the system, tends to broaden the peak, although the rate of decrease of the specific heat above the maximum is still very rapid.

In dilute alloys, the random distribution of the impurities and the alternating strength of the interaction with separation, lead to a wide range of internal fields which may differ greatly in magnitude and direction on neighbouring sites. It seems unlikely therefore, that there exists a transition temperature, or even a transition region, of the type normally associated with a cooperatively ordering system, but rather that the magnitude and distribution of the internal fields is essentially the same in the high temperature magnetically disordered state, and the magnetically ordered state

at low temperatures, in which the spins are lined up along their randomly oriented local fields. Thus when a spin lines up in its local field, the energy of the system is reduced mainly by the fall in energy of the given spin, and not by a lowering of the energy of neighbouring impurities through an increase in the average internal field, as is the case for spacially ordered magnetic systems with well defined sublattices. The fact that the experimental $\frac{\Delta C}{T}$ curves for Cu 0.6% Fe and Au 0.6% Fe (and those investigated by other workers) decrease less rapidly with increasing temperature than curves calculated from a temperature independent P(H) curve with a sharp cut off, is consistant with this picture.

The finite value of $\frac{\Delta C}{T}$ at $T=0$, and therefore of $P(0)$, may be consistant with an interaction of the R.K.Y. type for impurities of spin $\frac{1}{2}$. The spin polarisation of the conduction electrons produced by spin dependent scattering from a given impurity will always be parallel or antiparallel to the direction of the impurity spin. A second impurity of spin $\frac{1}{2}$ can only line up parallel or antiparallel to this spin polarisation, and therefore will remain parallel or antiparallel to the original spin. The Ising approximation will then be appropriate for such a system. This will not be the case for spins greater than $\frac{1}{2}$ at finite temperatures, and this may account for the very strong dip in $\frac{\Delta C}{T}$ as $T \to 0$, and thus in $P(H)$ as $H \to 0$, observed in the alloys of Mn in Cu, Ag and Au.

The concentration independence on the Marshall, Klein theories, as a result of the assumption of a $1/r^3$ dependence of the strength of the interaction with distance. This is only true in the R.K.Y. interaction at large distances,

and depends on certain arbitrary assumptions concerning the nature of the exchange integral (section 3.9). The weak concentration dependences of $\frac{\Delta C}{T}$ as T -> 0 for AuFe and Cu Fe may result from the breakdown of the validity of these assumptions, especially at high concentrations.

It is of interest to compute the values of the exchange integral J required if the R.K.Y. interaction is to account for the magnitude of the maximum fields in the P(H) distribution. Eq. 4.15 may be used to relate the internal field to the exchange integral, by summing the interaction from all neighbouring impurities. As a simple approximation, it may be assumed that the largest field on an impurity results from the addition of the interaction of an effective number 'm' of impurities at the nearest neighbour distance R_m to the central impurity. Assuming that E_F for Cu is 7 e.v., $F(2k_FR_m) = 2.2 \times 10^{-3}$, and that the spin is $\frac{1}{2}$, a simple calculation gives $J = \frac{1.4}{\sqrt{m}}$ e.v. for a maximum field of 182 Kg. Since the probability of any value of the field which can result only from the presence of more than one or two impurities which are nearest neighbours to the central impurity is rather small for a 0.6% alloy, J would have to take a value of the order of 1 e.v. It is possible that the contributions from impurities at more distant sites may reduce the value of J required to 0.7 e.v., though this figure requires that all impurities give contributions which add constructively at the central impurity. This value for J is rather large compared with the spectroscopic value of 0.1 to 0.3 e.v. but not unreasonably so. As remarked in section 3.10, the interaction via oscillations in the tail of the virtual bound state proposed by Blandin and Friedel can account for the magnitude of H with a considerably lower value of J.

COMPARISON WITH OTHER PROPERTIES

7.7 Mossbauer Effect

Mossbauer measurements on Au Fe alloys suggest the existance of a rather well defined transition temperature at $7^{\circ}K/\%$ Fe, with a temperature spread of not more than about 10%. The thermal average of the nuclear spin increases rapidly just below this temperature, and is zero at higher temperatures. For the Au 0.6% Fe sample investigated here, this transition would occur at about $4^{\circ}K$, close to the temperature of the maximum in $\frac{\Delta C}{T}$, and it is difficult to reconcile the absence of a Mossbauer splitting above $4^{\circ}K$ with the persistance of high internal fields to very much higher temperatures suggested by specific heat measurements.

A possible explanation is as follows. In the model suggested in the last section, the field at a given site is the resultant of fields from neighbouring spins which will be randomly separated, and whose spins will be randomly oriented with respect to the given spin at all temperatures. At high temperatures this resultant field, which may have any magnitude, will be changing direction (and magnitude) rapidly. At intermediate temperatures, the local field may be large enough to align the spin, but as the field is produced by spins which are themselves flipping, its direction, and thus the direction of the spin and the hyperfine field at the nucleus, will change rapidly, and the average value of the hyperfine field over a period of 10^{-7} seconds will be zero. Thus although the spin is partially aligned to its local field, and contributes to the specific heat, it will give a zero Mossbauer splitting. As the temperature is further reduced, the number of spins in

very low fields falls, and the direction of the field on a given site may remain constant for a time long compared with 10^{-7} seconds, and a Mossbauer splitting will be observed. Such a freezing of the orientation of the local fields may be quite rapid (in terms of a temperature change) if there is a strong minimum in the P(H) curve at low fields, as the specific heat curve suggests for Au Fe. In this case the freezing out may be expected to occur at a temperature close to the maximum in $\frac{\Delta C}{T}$, as is observed.

Other features of the Mossbauer spectra are then consistant with the specific heat results. The sharpness of the lines for Au Fe at temperatures rather below the transition temperature suggest that the distribution of internal fields is confined to a rather narrow range around some mean field. The specific heat results, however, suggest a rather broad distribution of fields. On the present model, the spins are already mostly aligned at the Mossbauer transition temperature, T_c, and only a few spins have $\mu H < kT_c$.

It is possible also that the absence of an observed paramagnetic line at temperatures well below T_c is consistant with a finite P(0). It may be shown, using the analysis in Appendix 1, and assuming the internal field distribution shown in fig. 42 for Au 0.6% Fe, that at $1^{\circ}K$, only 1/20% of the impurities have a relative magnetisation of less than 1%, and which would give rise to a spectrum whose width is 1% of the maximum width of the Mossbauer spectrum, and which could therefore be said to contribute to the paramagnetic line. Such a small amount may easily remain unobserved.

The Mossbauer spectrum of Cu Fe does not show a well defined transition temperature, but appears gradually at a temperature of the order of $6^{\circ}K/\%$ Fe,

and is unresolved into well defined lines even at the lowest temperatures of measurement. The results could be interpreted simply in terms of a broad distribution of internal fields, but these fields would be far too low to account for the observed specific heat anomaly. On the model discussed above, it may be supposed that even though the spins are more or less aligned with their local fields. in the liquid helium temperature range, the direction of the fields is still changing significantly over a period of 10^{-7} secs., giving a blurred Mossbauer spectrum. The more gradual freezing out of the field orientations may result from the absence of a strong dip in the P(H) curve at low fields. It would be of considerable interest to observe the Mossbauer spectrum of Cu_3Au 0.6% Fe, which shows a maximum in $\frac{\Delta C}{T}$, and therefore presumably has a dip in the P(H) curve at low H, to see whether its spectrum is similar to that of Au Fe or Cu Fe.

7.8 Electrical Resistance

The temperature variation of the electrical resistivity between 1.5° and 30°K for the series of copper - gold iron alloys is shown in Fig 50A.‡ The resistance of each specimen has been measured with an accuracy of a few parts in 10^5, but because of the complicated shape of the specimens, (they are turnings taken from the specific heat samples) the absolute resistivity is not known with confidence. This has therefore been estimated from the room temperature and 77°K values of the resistance, assuming that the excess

‡ I am indepted to Dr. B. R. Coles for measuring the resistivity of the Cu_3Au 0.6% Fe, CuAu 0.6% Fe, $CuAu_3$ 0.6% Fe, Au 0.6% Fe, Rh 0.5% Fe and Pd 0.19% Fe alloys, and for making the results available for presentation in this thesis. I am also indepted to S. Mozumder for measuring the resistivities of the Cu 0.6% Fe and Cu 0.6% Fe 0.1% Mn alloys.

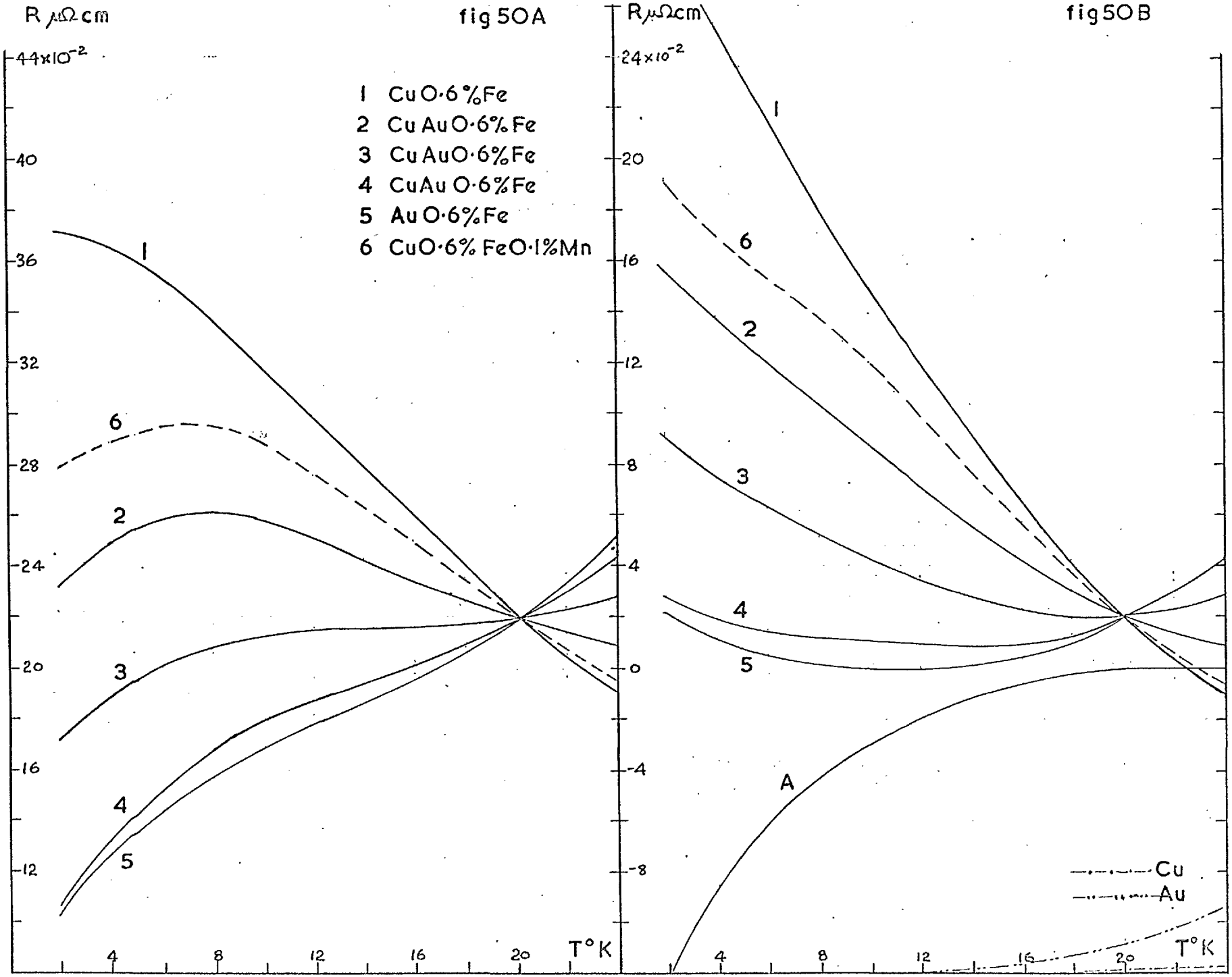
R μΩ cm
fig 5OA
44×10⁻²
40
36
32
28
24
20
16
12
1 CuO·6%Fe
2 CuAuO·6%Fe
3 CuAuO·6%Fe
4 CuAuO·6%Fe
5 AuO·6%Fe
6 CuO·6% FeO·1%Mn
1
6
2
3
4
5
4
8
12
16
20
T°K
R μΩcm
fig 5OB
24×10⁻²
20
16
12
8
4
0
-4
-8
1
6
2
3
4
5
A
Cu
Au
4
8
12
16
20
T°K

resistance is independent of temperature between these two temperatures.

The actual magnitude of the termperature dependent parts of the resistance curves are of more physical significance than their magnitudes relative to, for instance, the resistance at the minimum, providing the scattering processes leading to the temperature dependent and temperature independent resistivities are independent of one another. To enable the magnitudes of the temperature variations (which are never more than a few per cent of the total resistance) to be clearly compared, they have been arranged to pass through the same point on the graph at 20°K, by subtracting different amounts from each specimen's resistivity. Approximately 5, 17, 19, 15 and 4 μΩ cm have been subtracted from the Cu 0.6% Fe, Cu_3Au 0.6% Fe, CuAu 0.6%Fe, $CuAu_3$ 0.6% Fe, and Au 0.6% Fe resistances respectively. The values for the Cu 0.6% Fe and Au 0.6% Fe residual resistivities suggest Fe concentrations of 0.6% and 0.5% in the two systems respectively. This value is comparable with the value of 0.56% obtained by chemical analysis for the Cu 0.6% Fe specimen, but is significantly lower than the value of 0.7% found by chemical analysis for the Au 0.6% Fe specimen. The large values for the residual resistivities of the other three alloys result mainly from the large scattering from the disordered matrix.

The resistance curve for Cu 0.6% Fe passes through a minimum at about 45°K, the depth of the minimum being about 0.29 μΩ cm, or about 5.6% of $R_{min.}$. There is no low temperature maximum, but there is some flatening of the curve at low temperatures. There is a smooth resistance maximum at about 8°K for Cu_3Au 0.6% Fe and a minimum at 30°K, 0.057 μΩcm below the value at the maximum.

The resistance curve for CuAu 0.6% Fe shows neither a maximum or minimum, but passes through a horizontal point of inflexion at 14°K, and falls off rapidly below this temperature to a value at 2°K which is about 0.044μΩ lower than the value at 14°K. The $CuAu_3$ 0.6% Fe and the Au 0.6% Fe curves also show points of inflexion at approximately 14°K, with the rate of decrease below this temperature increasing with increasing Au concentration. The lattice resistance is also increasing rapidly with increasing Au concentration, and curves for the lattice resistivity of Cu and Au are shown in Fig. 50. The increasing lattice resistivity is much too small in the temperature range of interest to account for the disappearance of the minimum.

It is rather surprising that if the scattering processes operating in those systems which exhibit a resistance minimum only, differ in some fundemental way from those in systems exhibiting both a maximum and minimum, that the relatively minor changes in the electronic structure of the matrix that occur when the matrix changes from Cu to Cu_3Au should result in the appearance of a maximum in the resistivity. It will be assumed, therefore, that there is no such fundemental change. The curves suggest that there are two competing scattering processes. one which increases with decreasing temperature (the increasing component) and one which decreases with decreasing temperature (the decreasing component), and that the magnitude of the decreasing component is increasing with increasing gold concentration. All recent theories of the decreasing component (Yosida[105], Schmitt[104]) suggest that it is due to the freezing out of inelastic scattering when the thermal energy of the impurity falls below its energy splitting in the internal field. The total increase in resistance due to inelastic scattering from the value of zero at T=0 to its

value at very high temperatures is independent of the distribution of internal fields in the sample, and depends only on the magnitude of the s-d exchange integral and the spin of the impurity. There is no obvious reason why these quantities should be very different for Fe in Cu, Cu_3Au or Au (entropy measurements suggesting a spin of $\frac{1}{2}$ in all cases), and therefore the total magnitude of this component should be the same through the whole series of copper-gold-iron alloys.

The rate of increase with increasing temperature will, however, depend on the field distribution, and this rate should only be large when the specific heat anomaly (or rather, $\frac{\Delta C}{T}$) is large, that is, up to a temperature which increases with the concentration. A maximum in the restivity will only result if the slope of the decreasing component is greater than the slope of the increasing component at low temperatures. Thus if the internal fields in Cu Fe extended to very much higher values than those in Au Fe, the more gradual increase in inelastic scattering in Cu Fe could result in the absence of a maximum, whilst the more rapid increase in Au Fe could be sufficient to produce a maximum.

The differences in the P(H) curves for Cu 0.6% Fe and Au 0.6% Fe found from specific heat measurements, do not seem to be sufficient to account for the differences in their resistance curves.

The only striking difference is the maximum in $\frac{\Delta C}{T}$ in Au Fe and its absence in Cu Fe. The decrease in $\frac{\Delta C}{T}$ at low T, and thus in P(H) at low H, would lead to a rapid decrease in the inelastic scattering at temperatures rather below the maximum in $\frac{\Delta C}{T}$. This is therefore consistant with the appearance

of a resistance maximum in such systems, and with its absence in Cu 0.6% Fe, which shows no maximum in $\frac{\Delta C}{T}$. This feature cannot explain the results however. Firstly, the temperature of the maximum in $\frac{\Delta C}{T}$ ($3^{\circ}K$) is considerably below the temperature of the resistance maximum ($8^{\circ}K$) in Cu_3Au 0.6% Fe, and secondly, it cannot account for the apparently different magnitudes of the decreasing components, which should be independent of the distribution of the fields.

So far it has been assumed that the behaviour of the resistance curves is the result of a decreasing component which increases in magnitude with increasing gold concentration, and although this is consistant with the resistance curves, it is difficult to understand in terms of the theory of the decreasing component. An alternative possibility should therefore be considered, in which the curves result from the addition of a decreasing component having approximately the same magnitude and shape for each of the systems, to an increasing component which varies in magnitude from alloy to alloy. Fig. 50 B shows the results of separating each resistance curve into two such components. (The increasing component includes the resistivity due to phonon scattering). Such a separation is obviously not unique, and the decreasing component (curve A) which is common to each system, has been chosen simply to give increasing components which increase smoothly without points of inflexion. As the Fe concentration is not quite the same for each alloy, the shape and magnitude of the decreasing component is not expected to be quite the same for each. For this reason, and also because the resistivities themselves are not known very accurately, small wiggles in the increasing curves are to be expected from the simple analysis attempted here. The smoothness of all of the increasing curves must

therefore be considered as evidence for the physical significance of this analysis. Curve A has been assumed arbitrarily (and probably incorrectly) to be constant above 20°K, and has decreased by 0.12μΩ cm by 2°K. If this analysis is justified, the following conclusions may be drawn.

(1) The temperature of the maximum has no special significance as a transition temperature, but only occurs as the balance of two competing curves.

(2) The absence of a resistance maximum in the Cu Fe system is due to the large magnitude of the increasing component, and not to the small magnitude of the decreasing component.

(3) The appearance of a maximum in Cu_3Au 0.6% Fe, a flat region in Cu Au 0.6% Fe, and a point of inflexion for $CuAu_3$ 0.6% Fe and Au 0.6% Fe is due to the rapid decrease of the magnitude of the decreasing component with increasing gold concentration.

It is evident that (on this analysis) the temperature of the maximum (when it appears) will increase with increasing gold concentration, even though the Fe concentration remains constant. The possibility should therefore be considered that the increase in temperature of the resistivity maximum with increasing impurity concentration is entirely due to a decrease in the relative magnitude of the increasing component (that is, the magnitude relative to R_{min}), with increasing concentration, combined with a decreasing component whose relative magnitude is independent of concentration. (Such a decreasing component could evidently not be due to the inelastic scattering described above, as that spreads to higher temperatures with increasing concentration). The very rapid decrease in the relative depth of the minimum

with increasing concentration found in all systems which exhibit a resistance maximum lends support to this suggestion. (The decrease in depth is not due to the decreasing component itself, as this is much too small. In Au 0.006% Fe (Macdonald[13]) the relative depth of the minimum is around 20%, and it has disappeared altogether for Au 0.2% Fe, whereas the magnitude of the decreasing component is not more than about 3% R_{min}). It would also account for the non linearity of the temperature of the maximum with increasing concentration, and the persistance of a rather rapid change in slope in the resistance curve at a temperature which increases very little when the concentration increases considerably above the value for which the resistance minimum and maximum disappear.

Although it is difficult to say with certainty because of the lack of published resistance values over a wide range of temperatures for both high and low concentration alloys, the Au Fe resistance curves of Macdonald[13] and the Cu Fe curves of Kjekshus and Pearson[16], and of Knook[15], seem to be consistant with the above suggestion. The Cu Mn results of Schmitt and Jacobs[25], however, would seem to require a decreasing component which spreads to higher temperatures with increasing concentration.

It would evidently be of the greatest interest if it could be shown unambiguously that the relative magnitude of the decreasing component in Au Fe or Cu Fe is independent of temperature, as it could not then be attributed to inelastic scattering from interacting impurities. If this is the case, the Rh Fe resistivity differs from the resistivity of Au Fe or Cu Fe only by having a negligably small increasing component.

The resistance curve of Cu 0.6% Fe 0.1% Mn is also shown in Fig 50A. It exhibits a maximum at 8°K, and a minimum at about 50°K, approximately 0.18 μΩ cm or 3.3% below the value at 8°K. The existance of a resistance maximum at this temperature is difficult to understand if there is a fundemental difference between the scattering mechanisms operating in Cu Fe and Cu Fe Mn. If this were the case, the anomalous resistivities would be approximately additive and a maximum in the Cu 0.6% Fe 0.1% Mn would be expected at about 3°K, the temperature at which it appears in Cu 0.1% Mn.

It is very much more simple to understand the results in terms of two competing scattering processes. The effect of adding Mn to Cu Fe is to reduce the magnitude of the increasing component and to increase the magnitude of the decreasing component. This can be seen from the irregular shape of the increasing component in fig. 50 B(6) obtained by subtracting curve A from the resistance curve. A decreasing component at least 0.03 μΩ cm (25%) deeper than curve A at 2°K is necessary to give a smooth increasing curve. This is to be expected from the much larger spin (5/2) of the Mn ions, and is consistant with the considerably larger decreasing component found in dilute alloys containing Mn compared with those containing Fe.

Summarising the conclusions drawn from the copper-gold-iron resistance curves, it appears that the important property which determines whether or not a system will exhibit a resistance maximum is the rate of decrease of the increasing component with increasing concentration. Kjekshus[16] et al have shown that the depth of the minimum decreases rather slowly in Cu Fe and Cu Cr, which do not exhibit resistance maxima, and decreases very rapidly in Cu Mn which does. As mentioned above, it also decreases rapidly in all other systems

which exhibit resistance maxima. Current theories of the increasing component suggest that its magnitude should decrease with increasing interaction between impurities, though explicit calculations of this effect have not been made. It is not clear why this should be more rapid for Fe in Au than for Fe in Cu. It is not possible to decide from existing experimental data whether the increase in temperature of the resistance maximum with increasing impurity concentration is due entirely to a decreasing component that spreads to higher temperatures with increasing concentration, or an increasing component which decreases with increasing concentration, or to a combination of the two.

7.9 Magnetic Susceptibility

Unfortunately the magnetic susceptibility of Cu Fe has not been measured below 14°K, so that is is not possible to compare its behaviour with that of Au Fe. Above 14°K, both systems have been shown to exhibit Curie Weiss behaviour with a moment which increases with concentration below 300°K, (section 1.3) and which for Cu Fe is effectively concentration independent at 4.7 μ_B (S = 1.9) above 1000°K. Between 14° and 300°K the moment of Fe in Cu increases from 2.6μ_B (S = 0.6) for C = 0.006% to 4.7μ_B (S = 1.9) for c = 0.56%. For Fe in Au, the moment is 3.4μ_B (S = 1.3) for concentrations between 0.5 and 1% and increases to 4.9μ_B (S = 2.0) at 6.6%. These values of the spin are inconsistant with the value of $\frac{1}{2}$ found from the specific heat of the Cu Fe and Au Fe alloys of concentration up to 0.6% Fe. As $1/\chi$ is not linear in T below 77°K for several of the alloys, it is possible that the true Curie Weiss region had not been reached even at 300°K, and variations in effective moments

found by fitting the curves to straight lines may be expected to give concentration dependent moments. This curvature in the $1/\chi - T$ plot at high temperatures is consistant with the conclusion from specific heat measurements that large internal fields persist to high temperatures, and that magnetic ordering takes place over a very extended temperature range. It seems rather unlikely however, that this effect is sufficient to account for the very large variations of moment observed.

The observation that the spin value from magnetic measurements at very high temperatures, where a more realistic value for the moment might be expected, is very much larger than that obtained from low temperature entropy measurements, may suggest that the entropy continues to increase considerably above 20°K. The fact that the large moment at high temperatures is associated with very large paramagnetic Curie temperatures even for very low concentration alloys suggests, however, that the whole interpretation of the susceptibility measurements may be in error. Thus the behaviour of Fe in the noble metals may be intermediate between the behaviour of Mn and Co. Mn has a well behaved moment and paramagnetic Curie temperature at high temperatures. Co, on the other hand, has an almost temperature independent susceptibility at high temperatures, and when this is interpreted in terms of a Curie Weiss law, yields very large and concentration dependent values of the effective moment and paramagnetic Curie temperature.

It is noteworthy that the temperature of the susceptibility maximum in all systems in which it has been observed correlates well with the temperature of the maximum in $\frac{\Delta C}{T}$ (see figs. 5, 7 and 8), the temperature of the maximum in each property varying from about 4°K/%Mn for Au Mn to 12°K/%Cr for Au Cr.

This lends support to t he assumption that the susceptibility maximum and the specific heat anomaly can both be attributed to the same mechanism - presumably magnetic ordering.

Magnetic remenance on the application and removal of a magnetic field is only observed below the temperature T_c of the maximum in $\frac{\Delta C}{T}$ and χ. This is consistant with the suggestion that the internal fields are flipping rapidly above T_c, so that at such temperatures any remenance would decay in less than 10^{-7} secs. At lower temperatures, when the directions of the internal fields progressively freeze out, the decay rate drops rapidly, until at temperatures well below T_c it may persist for several hours. If this interpretation is correct, a very much smaller remenance would be expected for Cu Fe, as Moss bauer measurements suggest very short relaxation times to very low temperatures in this system.

7.10 Thermopower.

The large thermopowers at low temperatures observed in dilute magnetic alloys have not been satisfactorily explained. Molecular field theories (de Vrooman[109] et al Geunault[141] et al) attribute the large thermopower to the rapid energy dependence for inelastic scattering which results from the splitting of the impurity energy levels in the internal field. This mechanism can only give large thermopowers at temperatures for which the specific heat is large. Although there is a rather tempting association of the concentration independences of the thermopower and specific heat at low temperatures, this mechanism cannot account for the fact that the thermopower in very dilute alloys is large to very much higher temperatures than is the specific heat.

For example, at 20°K the thermopower of Au 0.004% Fe (Macdonald[13]) has only fallen to about half of its maximum value, whereas the specific heat, assuming a linear extrapolation from the Au 0.6% Fe values, will have fallen to less than 0.1% of its maximum value, The contrast may be even greater than this for, as mentioned in section 1.8, the fall off in the thermopower at high temperatures can be almost, if not entirely, attributed to the rapidly increasing thermal scattering.

Recent theories of the resistance minimum, based on spin dependent scattering from independent ions, predict large thermopowers extending over a wide range, though explicit calculations by Doniach[139] give values very much smaller than those observed experimentally. The concentration independence (the observed magnitude of the thermopower depends on the ratio of anomalous to normal scattering), and the correlation of the onset of the decrease in relative depth of the resistance minimum with the decrease in magnitude of the thermopower in the low temperature linear region, suggest strongly that these phenomena are related.

7.11 B. Rh0.5% Fe

$\frac{\Delta C}{T}$ against T is shown in Fig 47B for this alloy, and ΔC against T in fig. 47A. The excess specific heat rises to a maximum value of about 5.8 mj/mole°K, and decreases slowly at higher temperatures. The rate of decrease above 10°K is uncertain because of the increasing lattice specific heat. The rather rapid fall off above 15°K may not be significant as it could result from a combined error in the specific heats of the Rh and Rh 0.5% Fe alloys of less than 1%.

$\frac{\Delta C}{T}$ increases continually with decreasing temperature, down to 1.3°K. The uncertainty in the specific heat of pure Rh below 4°K makes the rate of increase of $\frac{\Delta C}{T}$ uncertain, but neither possible curve shows any sign of leveling off to a constant value. Comparison with figs. 9 and 10 shows that the anomaly is similar to that which might be expected for a Cu 0.3% Fe alloy.

The $\frac{\Delta C}{T}$ curve A yields a value for the entropy between 1.3°K and 18°K of 13 mj/mole°K. A linear extrapolation of $\frac{\Delta C}{T}$ below 1.3°K to a value of 3.4 mj/mole°K² at T=0 yields a further 4 mj/mole°K, and extropolation above 18°K a further 1 mj/mole°K, giving a total entropy of 18 mj/mole °K. This corresponds to a spin of 0.28 assuming a concentration of 0.5% Fe. If a spin of $\frac{1}{2}$ is assumed, an extra entropy of 10 mj/mole°K is unaccounted for. If this were all to appear below 1.3°K, $\frac{\Delta C}{T}$ would have to reach a value of the order of 20-30 mj/mole°K² at 0°K. It is possible that there is less than 0.5% Fe in solution (a chemical analysis or a resistance measurement of samples taken from this specimen were not performed). An entropy of 18 mj/mole °K, and a spin of $\frac{1}{2}$, would result from a concentration of 0.31% Fe in solution.

7.12 Discussion

The specific heat anomaly in the Rh Fe system is therefore similar to that observed in noble metal-transition metal alloys (though measurements on alloys of different concentration are required to compare the concentration dependences of the anomalies in the two systems). Magnetic susceptibility measurements by Waszink[49] (section1.9) on a Rh 0.85% Fe sample yield an effective moment at high temperatures of 3.4 μ_B (S=1.3) and a large negative paramagentic Curie temperature (-41°K). At lower temperatures $1/\chi$ decreases

more rapidly than linearly with decreasing temperature. The behaviour is therefore similar to that observed by Bitter[30] et al in rather more dilute Cu Fe alloys. As in the Cu Fe and Au Fe system, the spin deduced from high temperature susceptibility measurements is significantly higher than that obtained entropy measurements.

The specific heat anomaly throws no light on the origins of the striking resistive behaviour, in which the excess resistance increases by a factor of almost three as the temperature increases from 1°K to 50°K. If the resistive anomaly were due to interactions between ions, the specific heat anomaly might have been expected to extend to higher temperatures than is observed.

The concentration independence of the relative excess resistance suggests that it is due to scattering from independent ions. Kondo[108] (section 4.13) has suggested that a positive value of the exchange integral J in his theory would give a resistance which decreased with decreasing temperature. Doniach[139] has shown that spin dependent scattering from single impurities yields a resistive component which increases with decreasing temperature for either sign of J, if the conduction band is half filled (as for a noble metal matrix) but that a component which decreases with decreasing temperature may result if the conduction band is almost filled (as for Rh).

As mentioned in section 1.9, although the magnitude of the change in resistance relative to its magnitude at 0°K is very much larger than is observed in other dilute alloys, this results entirely from the very small temperature independent component in Rh Fe. This may also account for the positive magnetoresistance observed in this system. A small resistance implies a long mean free path, and therefore a large normal positive magnetoresistance.

Waszink's susceptibility measurements usggest that the magnetisation of this system remains low even at 1.5°K (because of the large negative θ). Assuming that the negative component of the magnetoresistance is proportional to the square of the magnetisation, it may be shown that the negative component is unlikely to exceed 20% of the normal positive component, and Kohler's rule will be approximately obeyed, as observed. However, the scattering mechanism proposed by Doniach[139] or Kondo[108] should also decrease in magnitude in an external field, and should therefore also yield a positive magnetoresistance in Rh Fe in addition to the negative magnetoresistance component usually attributed to the decrease in the spin dependent elastic scattering with increasing magnetic alignment. In order that this positive component be distinguished from the large positive mean free path effect, the mean free path should be reduced by the addition of a third, non magnetic, component. The continued existance of a positive magnetoresistance in such an alloy would give valuable support to Doniach's theory.

7.13 C. Pd 0.19% Fe

ΔC against T for this alloy is shown in fig49, and ΔC against T in fig 48 B. The excess specific heat increases to a maximum value of 9.2 mj/mole°K, and falls rapidly at higher temperatures. Because of the uncertainties in the specific heat of Pd above 4°K, the rate of decrease at higher temperatures is uncertain. At temperatures between 2.5°K and 4°K the lattice specific heat is small, and the rapid decrease is fairly well established. This is very much more rapid than is observed in any of the other dilute alloys containing Fe, and is rather more rapid than those containing Mn. It is possible, though

difficult to establish with certainty, that the rate of decrease is too rapid to be accounted for by a temperature independent distribution of internal fields, and must be considered in terms of internal fields whose magnitudes increase with decreasing temperature.

$\frac{\Delta C}{T}$ increases continuously on cooling, and reaches a value of 6.0 mj/mole$^{\circ}K^2$ at 1.2°K. The entropy associated with the anomaly between 1.2°K and 10°K is 14 mj/mole$^{\circ}$K. An arbitrary extrapolation of the curve to a value of 6.5 mj/mole$^{\circ}K^2$ at T=0 yields an entropy at 1.2°K of 7 mj/mole$^{\circ}$K, and a plausible extrapolation above 10°K yields a further 1 mj/mole$^{\circ}$K. The total entropy is therefore 22 mj/mole$^{\circ}$K. If the concentration is 0.19%, this corresponds to a spin value of 1.5, and therefore to a moment of 3.9μ_B. This value of the spin, the temperature of the maximum, and the shape of the specific heat anomaly are in good agreement with the results obtained by Veal and Rayne[126] also on a Pd 0.19% Fe alloy.

7.14 Discussion

Crangle has shown from saturation magnetisation measurements that a Pd 0.15% Fe has a ferromagnetic transition at 4.3°K, and a magneton number in the ferromagnetic region of 9.5 μ_B. Similar large values for the moment, (between 9 and 12μ_B), have been observed by Gerstenberg[123], Crangle[124], Clogston[45] and Bozorth[125] for higher Fe concentrations. These values are very much larger than the maximum values of 5.9μ_B (S = 5/2) allowed by the Pauli Exclusion principle. These large moments have been interpreted (Clogston[45]) by assuming a polarisation of the Pd atoms in the neighbourhood of each Fe atom, and recent neutron diffraction measurements by Low[48] have shown that

this polarisation may extend to a distance of at least 10Å, and effect up to 120 nearest Pd atoms.

The moment per Fe atom in the paramagnetic region well above the transition temperature has been measured by Clogston[45] for a Pd 1% Fe alloy, who finds a value of 9.7 μ_B. It is evident therefore that the polarised Pd atoms remain bound to the Fe atom above the magnetic ordering temperature. Mossbauer measurements of Craig[142] et al at 4°K on very dilute Pd Fe alloys, which are in the paramagnetic region down to 1.5°K show that the hyperfine splitting with applied field is a function of $\frac{H}{T}$, and can be fitted to a Brillouin curve corresponding to a magnetic moment of 12.6μ_B, and thus to a spin of 6.

As the entropy associated with the specific heat anomaly suggests a value of the spin of 1.5, two conclusions may be drawn.

(1) The polarised Pd atoms are rigidly bound to the Fe atom below the transition temperature, and do not have degrees of freedom independent of those of the Fe-Pd complex.

(2) In the ferromagnetic region, the degeneracy of the magnetised state depends only on the spin of the Fe atom, (assuming that this is 1.5) and not on the spin of the complete Fe-Pd complex (assuming this to be 6 as found by magnetic measurement). The Mossbauer measurements of Craig[142] suggest that this is not the case in the paramagnetic region, as the shape of the Brillouin curve is determined primarily by the degeneracy of the impurity state, and not directly by its magnetic moment.

The resistivity of a sample taken from the Pd 0.19% Fe sample is shown in fig. 49 (inset). The curve exhibits a sharp change of slope at 3.3 ± 0.3°K,

falling off rapidly at lower temperatures. Above the transition, the excess resistance is independent of temperature, showing no sign of a resistance minimum. The sharpness of the transition, which occurs at a temperature slightly higher than the maximum in the specific heat curve ($2.3^{\circ}K$), is consistant with the rather rapid onset of magnetic ordering indicated by the specific heat.

If the decrease in resistance below the transition is due to the freezing out of inelastic scattering with decreasing temperature, it might be expected that this would be sensitive to short range order, varying with temperature wherever the magnetic energy of an impurity is comparable to its thermal energy, and would give a rather more broad transition than is actually observed, extending over a region in which the specific heat anomaly is large. Alternatively the decrease may be due to the decrease in spin diffuse scattering, resulting from increasing interference of conduction electrons scattered from the magnetic impurities with increasing magnetic alignment. Such interference might be expect to be important in a ferromagnetically ordering system such as Pd Fe, but would probably be unimportant in the random antiferromagnetically ordered arrangement of spins which is presumed to obtain in other dilute magnetic alloys. This mechanism, which depends rather strongly on the bulk magnetisation, may therefore be less sensitive to short range order than is inelastic scattering and is therefore more likely to provide a sharp resistive transition.

SUMMARY

Series A

The specific heat anomalies in the copper-gold-iron alloys differ only in the details of the P(H) curve, especially at low fields. A maximum in $\frac{\Delta C}{T}$ at about $3^{\circ}K$ (and therefore a deep minimum in P(H) at low H) is observed for all of the alloys containing Au. It appears that $\frac{\Delta C}{T}$ may be rather more concentration dependent at low temperatures for Cu Fe alloys than for Au Fe alloys. The entropy of the specific heat anomalies is consistant with a spin of $\frac{1}{2}$ for the Fe atoms in each system.

It is considered that the specific heat anomalies and the Mossbauer effect for Cu Fe and Au Fe alloys may be mutually consistant if it is assumed that the distribution of internal fields varies little with temperature, but that the orientations of the local fields freeze out at a rather well defined low temperature in Au Fe, and rather more gradually in Cu Fe. It is considered that the magnetic ordering and scattering mechanisms in Cu Fe alloys are not fundementally different from those in Au Fe alloys, but that the absence of a resistance maximum in Cu 0.6% Fe, the resistance maximum in Cu_3Au 0.6% Fe, and the points of inflection is the resistance curves of CuAu 0.6% Fe, $CuAu_2$ 0.6%Fe, and Au 0.6% Fe are due to the rapid decrease, with increasing gold concentration, in the magnitude of a component of resistivity which increases with decreasing temperature.

B. It is concluded that the specific heat anomaly in the Rh 0.5% Fe alloy is similar to that observed in other dilute alloys containing Fe, and is probably not intimately related to the unusual resistive behaviour (though measurements

of the concentration dependence of the specific heat anomaly are needed to confirm this). It is also considered that only the resistive behaviour is unusual, and that the magnetoresistance and susceptibility are basically similar to these properties observed in other dilute magnetic alloys containing Fe.

C. The shape of the specific heat anomaly in the Pd 0.19% Fe alloy suggests that magnetic ordering in this system occurs over a much narrower temperature range than is found in other systems, which is consistant with the behaviour of the restivity and magnetisation in this system. The spin value of 1.5 found from the entropy associated with the specific heat anomaly is much lower than the value of 5 to 6 suggested by magnetisation and Mossbauer measurements.

APPENDIX 1

CALCULATION OF SPECIFIC HEAT FROM THE P(H) CURVE

It may be shown (Cusack p.282) by the application of Maxwell Boltzman statistics to a set of n magnetic carriers of spin S, and magnetic moment $\mu = g\mu_B \sqrt{S(S+1)}$, in a magnetic field H, and at a temperature T, that the magnetisation is given by

$$m = \frac{ng\mu_B}{2} \left[(2S+1) \operatorname{Coth} (2S+1) \frac{g\mu_B H}{2kT} - \operatorname{Coth} \frac{g\mu_B H}{2kT} \right] \quad \ldots\ldots\ldots \text{A.1}$$

g is the spectroscopic splitting factor, and μ_B is the Bohr magneton. The total energy is $E = -mH$.

If there is a probability P(H) dH that a carrier is in a field between H and H + dH, and the total number of atoms is N of which a fraction c are magnetic carriers

$$E = -\frac{Nc\, g\mu_B}{2} \int_{-\infty}^{\infty} H\, P(H)\, dH\, (\alpha \operatorname{Coth} \alpha x - \operatorname{Coth} x) \quad \ldots\ldots\ldots\ldots \text{A.2}$$

where $\alpha = 2S + 1$ and $x = \frac{g\mu_B H}{2kT}$

P(H) will in general be a function of temperature, but in the calculation of the specific heat, P(H) will be assumed to be independent of temperature. Thus from A.2

$$C = cNk \int_{-\infty}^{\infty} P(H)\, dH\, (-\alpha^2 x^2 \operatorname{Cos\,eah}^2 \alpha x + x^2 \operatorname{cos\,ech}^2 x)$$

$$= \frac{2cNk^2 T}{g\mu_B} \int_{-\infty}^{\infty} P(H)\, dx\, f(x)$$

where $f(x) = x^2 \operatorname{cosech}^2 x - \alpha^2 x^2 \operatorname{cosech}^2 \alpha x$

From a knowledge of P(H), subject to the condition

$$\int_{-\infty}^{\infty} P(H)\, dH = 1$$

the specific heat may be calculated. This will be done exactly for the two extreme cases $T \to 0$ and $T \to \infty$.

<u>$T \to 0$</u>

If P(H) is finite at H=0, and is assumed to be constant and equal to P(0) for $H \lesssim \frac{2kT}{g\mu_B}$, i.e. for those values of x for which $f(x)$ is large,

$$C = 2c \frac{Nk^2 T}{g\mu_B} P(0) \int_{-\infty}^{\infty} f(x)\, dx$$

If $I = \int_{-\infty}^{\infty} x^2 \operatorname{cosech}^2 x\, dx = \frac{\pi^2}{3}$

$$= \int_{-\infty}^{\infty} \alpha^2 x^2 \operatorname{cosech}^2 \alpha x\, d(\alpha x)$$

then $\int_{-\infty}^{\infty} f(x)\,dx = I(1 - 1/a) = \frac{2S}{2S+1} I$

$\therefore C = \frac{2\pi^2}{3} c Nk \frac{kT}{g\mu_B} P(0) \frac{2S}{2S+1}$

Thus in the limit as T -> 0, C/T is constant and proportional to P(0).

The temperature dependence of C/T close to T=0 can be found if P(H) is any polynomial in H for very low H.

e.g. if $P(H) = \sum_n |a_n H^n| = \sum_n a_n \left(\frac{2kT}{g\mu_B}\right)^n x^n$

as T -> 0 $C = \frac{2c\,Nk^2 T}{g\mu_B} \sum_n \int_{-\infty}^{\infty} a_n \left(\frac{2kT}{g\mu_B}\right)^n x^n f(x)\,dx$

$\frac{C}{T} = c Nk \sum_n \left(\frac{2k}{g\mu_B}\right)^{n+1} a_n I_n T^n$ where $I_n = \int_{-\infty}^{\infty} x^n f(x)\,dx$

Thus the shape of the C/T against T curve as T -> 0 reflects the shape of the P(H) against H curve as H -> 0.

<u>T -> ∞</u>

At very high temperatures, such that $kT >> \frac{g\mu_B H}{2}$ for all H, f(x) takes the form,

$f(x) = x^2 \operatorname{cosech}^2 x - \alpha^2 x^2 \operatorname{cosech}^2 \alpha x \to \frac{x^2}{3} (\alpha^2 - 1) = \frac{4x^2}{3} S(S+1)$

$= \frac{g^2 \mu_B^2 H^2}{3k^2 T^2} \qquad S(S+1) = \frac{1}{3}\left(\frac{\mu H}{kT}\right)^2$

$$\therefore C = \frac{c\,Nk\,\mu^2}{3k^2\,T^2} \int_{-\infty}^{\infty} H^2\, P(H)\, dH$$

writing $\int_{-\infty}^{\infty} H^2\, P(H)\, dH = \overline{H^2}$

$$C \to c\,Nk\,\frac{\mu^2\,\overline{H^2}}{3k^2T^2} \quad \text{for T large.}$$

Thus in the high temperature limit, the specific heat decreases as $1/T^2$ for any distribution of fields, provided the distribution does not change with temperature. This will be a good approximation for $T \gtrsim 3\,\frac{\mu\,H_{max}}{k}$.

APPENDIX 2

SPECIFIC HEAT RESULTS

In the following columns, C is expressed in mj/mole°K and T in °K.

Copper

T	C/T	T	C/T	T	C/T	T	C/T
1.388	.7914	3.598	1.320	6.665	2.830	12.52	8.685
1.493	.8173	3.712	1.357	6.883	2.971	12.97	9.344
1.666	.8334	3.821	1.398	7.074	3.106	13.46	10.03
1.753	.8492	3.942	1.444	7.281	3.248	13.99	10.90
1.835	.8640	4.074	1.489	7.506	3.406	14.41	11.48
1.926	.8828	4.194	1.540	7.750	3.594	14.71	11.92
1.994	.8928	4.304	1.583	8.020	3.800	15.03	12.62
2.064	.9080	4.404	1.624	8.317	4.050	15.37	13.24
2.133	.9249	4.538	1.683	8.554	4.251	12.72	13.93
2.300	.9620	4.683	1.745	8.728	4.396	16.11	14.70
2.386	.9762	4.843	1.821	8.909	4.557	16.51	15.55
2.477	1.004	5.005	1.894	9.137	4.763	16.93	16.45
2.557	1.021	5.156	1.969	9.440	5.060	17.37	17.41
2.635	1.035	5.319	2.051	9.772	5.391	17.84	18.54
2.725	1.058	5.500	2.146	10.14	5.766	18.35	19.78
2.827	1.088	5.673	2.239	10.46	6.120	18.89	21.59
2.932	1.113	5.836	2.333	10.74	6.431	19.46	22.84
3.034	1.145	6.015	2.438	11.05	6.789	20.07	24.28
3.250	1.209	6.212	2.546	11.73	7.625		
3.366	1.244	6.427	2.681	12.11	8.120		

Cu 0.6% Fe 0.997 Moles

T	C/T	ΔC/T	T	C/T	ΔC/T	T	C/T	ΔC/T
1.387	4.003	3.217	3.168	4.251	3.065	7.673	5.327	1.770
1.428	3.984	3.192	3.272	4.262	3.044	8.075	5.468	1.610
1.476	4.007	3.209	3.514	4.303	3.005	8.451	5.709	1.540
1.530	4.027	3.220	3.638	4.331	2.990	8.793	5.947	1.477
1.639	4.056	3.233	3.756	4.341	2.958	9.176	6.230	1.417
1.691	4.061	3.229	3.871	4.358	2.933	9.470	6.465	1.370
1.746	4.072	3.230	3.999	4.375	2.902	9.862	6.803	1.330
1.801	4.080	3.229	4.159	4.358	2.822	10.25	7.177	1.280
1.926	4.094	3.220	4.293	4.384	2.794	10.66	7.545	1.232
1.993	4.109	3.222	4.413	4.421	2.780	11.11	8.041	1.191
2.061	4.113	3.212	4.543	4.441	2.744	11.62	8.571	1.095
2.131	4.120	3.204	4.687	4.454	2.694	12.19	9.276	1.041
2.213	4.133	3.199	4.847	4.468	2.635	12.84	10.13	0.980
2.300	4.133	3.180	5.043	4.486	2.560	13.44	10.96	0.931
2.375	4.145	3.175	5.256	4.483	2.453	13.97	11.73	0.920
2.454	4.168	3.179	5.453	4.502	2.372	14.56	12.56	0.812
2.531	4.180	3.173	5.647	4.560	2.293	15.21	13.70	0.752
2.606	4.190	3.163	5.864	4.601	2.205	15.94	15.10	0.693
2.691	4.196	3.147	6.108	4.644	2.132	16.75	16.71	0.617
2.789	4.186	3.11	6.385	4.710	2.032	17.65	18.65	0.568
2.883	4.196	3.097	6.658	4.797	1.946	18.68	21.02	0.467
2.968	4.214	3.088	6.974	4.914	1.855	19.52	23.09	0.362
3.067	4.217	3.062	7.325	5.068	1.760	"o.15	24.60	0.193

Cu_3Au 0.6% Fe 0.879 Moles

T	C/T	T	C/T	T	C/T	T	C/T
1.315	3.852	2.904	5.075	5.998	7.142	11.46	18.16
1.365	4.150	3.016	5.124	6.193	7.310	11.82	19.40
1.417	4.204	3.120	5.192	6.406	7.503	12.21	20.79
1.469	4.244	3.228	5.250	6.598	7.693	12.63	22.37
1.520	4.279	3.339	5.310	6.767	7.869	13.08	24.21
1.572	4.310	3.452	5.373	6.951	8.077	13.45	25.78
1.624	4.339	3.565	5.436	7.147	8.312	13.71	26.86
1.681	4.376	3.693	5.513	7.360	8.582	13.98	28.04
1.740	4.416	3.819	5.592	7.593	8.897	14.26	29.38
1.804	4.469	3.941	5.667	7.847	9.279	14.56	30.82
1.868	4.508	4.077	5.761	8.125	9.735	14.87	32.34
1.940	4.545	4.202	5.839	8.350	10.12	15.20	33.93
2.009	4.588	4.313	5.923	8.512	10.42	15.55	35.68
2.081	4.621	4.434	6.006	8.683	10.77	15.92	37.49
2.152	4.659	4.569	6.109	8.862	11.12	16.30	39.55
2.224	4.693	4.717	6.222	9.087	11.61	16.71	41.69
2.299	4.735	4.881	6.329	9.385	12.28	17.15	43.97
2.375	4.778	5.032	6.430	9.713	13.06	17.61	46.41
2.452	4.813	5.184	6.543	10.01	13.82	18.10	49.14
2.529	4.862	5.351	6.658	10.26	14.50	18.62	52.03
2.605	4.902	5.509	6.774	10.53	15.25	19.18	55.28
2.69s	4.954	5.657	6.879	10.82	16.13	19.77	58.53
2.791	5.009	5.820	7.009	11.13	17.10	20.41	62.17

Cu Au 0.6% Fe 0.843 Moles

1.296	3.295	2.792	4.571	5.710	8.600	10.95	28.84
1.336	3.320	2.885	4.661	5.877	8.935	11.26	30.71
1.381	3.357	2.985	4.760	6.059	9.317	11.61	32.89
1.431	3.392	3.093	4.872	6.258	9.766	11.96	35.17
1.484	3.442	3.198	4.978	6.678	10.78	12.35	37.67
1.538	3.486	3.306	5.087	6.850	11.22	12.77	40.56
1.594	3.528	3.429	5.221	7.038	11.75	13.25	43.86
1.659	3.584	3.554	5.364	7.242	12.34	13.75	47.49
1.729	3.638	3.681	5.500	7.464	13.02	14.16	50.45
1.796	3.692	3.925	5.794	7.705	13.81	14.45	52.63
1.931	3.808	4.060	5.957	7.967	14.72	14.75	54.86
2.003	3.869	4.183	6.114	8.258	15.79	15.07	57.23
2.073	3.928	4.292	6.259	8.578	17.05	15.41	59.80
2.144	3.983	4.412	6.417	8.835	18.12	15.76	62.52
2.212	4.042	4.543	6.601	9.024	18.95	16.14	65.42
2.284	4.107	4.688	6.820	9.222	19.86	16.54	68.47
2.368	4.183	4.850	7.072	9.479	21.04	16.96	71.76
2.455	4.268	5.032	7.370	9.811	22.66	17.41	75.10
2.532	4.332	5.184	7.628	10.11	24.21	17.88	78.72
2.608	4.402	5.350	7.918	10.37	25.60	18.39	82.67
2.693	4.481	5.534	8.264	10.65	27.14	18.93	86.66

$CuAu_3$ 0.6% Fe 0.760 Moles

T	C/T	T	C/T	T	C/T	T	C/T
1.315	4.826	2.844	7.005	5.967	15.39	11.13	49.02
1.364	4.882	2.937	7.178	6.158	16.12	11.46	52.93
1.411	4.949	3.039	7.363	6.370	16.97	11.82	55.35
1.461	5.021	3.146	7.560	6.563	17.78	12.20	59.30
1.511	5.083	3.257	7.779	6.727	18.52	12.62	63.08
1.562	5.144	3.372	8.396	6.904	18.32	13.07	67.64
1.618	5.222	3.490	8.234	7.097	20.27	13.44	71.29
1.679	5.299	3.608	8.485	7.308	21.34	13.70	73.97
1.738	5.366	3.742	8.772	7.536	22.53	13.97	76.78
1.794	5.443	3.873	9.076	7.784	23.93	14.26	79.74
1.848	5.506	4.002	9.376	8.054	25.54	14.56	82.74
1.912	5.595	4.145	9.725	8.275	26.89	14.87	86.01
1.982	5.687	4.278	10.05	8.433	27.91	15.20	89.58
2.053	5.780	4.396	10.37	8.596	28.99	15.55	93.07
2.126	5.881	4.526	10.71	8.771	30.18	15.92	96.96
2.206	5.993	4.670	11.12	8.958	31.47	16.31	101.0
2.284	6.112	4.828	11.59	9.195	33.21	16.71	105.2
2.358	6.219	4.980	12.05	9.504	35.53	17.15	109.8
2.434	6.334	5.127	12.51	9.781	37.69	17.61	114.3
2.509	6.448	5.287	13.02	10.02	39.60	18.10	119.2
2.582	6.566	5.465	13.60	10.27	41.59	18.61	124.4
2.664	6.694	5.635	14.18	10.53	43.85	19.17	129.9
2.757	6.859	5.794	14.74	10.82	46.29		

Au 0.6% Fe 0.708 Moles

T	C/T	ΔC/T	T	C/T	ΔC/T	T	C/T	ΔC/T	T	C/T
1.336	4.700	3.199	2.859	7.829	3.560	5.695	17.67	3.030	10.63	50.80
1.376	4.769	3.221	2.979	8.131	3.560	5.861	18.40	2.963	10.93	53.70
1.422	4.853	3.249	3.087	8.426	3.572	6.043	19.24	2.881	11.25	56.84
1.475	4.436	3.265	3.190	8.704	3.569	6.243	20.19	2.789	11.58	60.34
1.531	5.014	3.271	3.297	8.994	3.560	6.462	21.26	2.684	11.95	64.24
1.587	5.120	3.301	3.418	9.335	3.549	6.659	22.26	2.588	12.35	68.58
1.643	5.252	3.355	3.541	9.687	3.529	6.834	23.17	2.501	12.79	73.39
1.703	5.341	3.357	3.649	10.01	3.514	7.022	24.19	2.414	13.26	78.82
1.769	5.453	3.371	3.752	10.34	3.521	7.225	25.33	2.329	13.77	84.91
1.838	5.589	3.398	3.867	10.70	3.501	7.446	26.59	2.219	14.19	89.95
1.914	5.750	3.435	3.994	11.12	3.488	7.687	28.03	2.154	14.49	93.68
1.988	5.891	3.452	4.137	11.60	3.465	7.951	29.67	2.088	14.80	97.53
2.061	6.039	3.473	4.298	12.15	3.421	8.242	31.59	2.029	15.13	101.6
2.129	6.164	3.473	4.449	12.69	3.400	8.560	33.77	1.932	15.48	105.9
2.219	6.353	3.492	4.585	13.19	3.379	8.820	35.63	1.896	15.84	110.5
2.314	6.569	3.522	4.735	13.76	3.355	9.008	37.04		16.23	115.3
2.392	6.718	3.514	4.902	14.40	3.313	9.205	38.54		16.63	120.5
2.473	6.898	3.523	5.057	15.00	3.247	9.459	40.60		17.06	125.8
2.566	7.111	3.532	5.212	15.21	3.205	9.792	43.34		17.51	131.5
2.659	7.325	3.534	5.382	16.34	3.156	10.10	49.57	18.00	137.3	
2.752	7½560	3.550	5.544	17.01	3.097	10.35	48.26		18.51	143.5

Cu 0.6% Fe 0.1% Mn 0.960 Moles

T	C/T	ΔC/T	T	C/T	ΔC/T	T	C/T	ΔC/T	T	C/T	ΔC/T
1.291	4.137	3.355	2.852	4.685	3.595	6.467	5.800	3.089	11.93	9.587	1.632
1.361	4.190	3.399	2.961	4.712	3.592	6.665	5.862	3.024	12.33	10.06	1.574
1.423	4.222	3.423	3.066	4.742	3.592	6.841	5.912	2.956	12.75	10.61	1.505
1.479	4.249	3.442	3.178	4.768	3.584	7.029	5.978	2.894	13.23	11.25	1.443
1.532	4.267	3.453	3.295	4.800	3.581	7.232	6.051	2.824	14.14	12.65	1.357
1.590	4.284	3.460	3.460	3.403	4.828	7.452	6.136	2.748	14.42	13.08	1.308
1.650	4.319	3.487	3.512	4.848	3.559	7.691	6.232	2.664	14.73	13.60	1.290
1.708	4.349	3.507	3.633	4.879	3.549	7.957	6.352	2.579	15.05	14.14	1.229
1.766	4.372	3.521	3.752	4.909	3.536	8.246	6.504	2.491	15.39	14.78	1.241
1.824	4.398	3.536	3.865	4.936	3.522	8.476	6.626	2.418	15.75	15.44	1.195
1.892	4.437	3.564	4.134	5.014	3.498	8.643	6.722	2.370	16.13	16.23	1.210
1.962	4.448	3.562	4.568	5.145	3.448	8.819	6.828	2.319	16.53	17.05	1.175
2.035	4.468	3.568	4.715	5.183	3.421	9.006	6.957	2.277	16.95	17.98	1.175
2.105	4.495	3.581	4.880	5.236	3.397	9.256	7.144	2.229	17.40	18.98	1.140
2.175	4.516	3.588	5.061	5.305	3.381	9.570	7.38s	2.159	17.87	20.11	1.121
2.249	4.539	3.596	5.216	5.358	3.357	9.851	7.607	2.100	18.38	21.38	1.108
2.326	4.560	3.600	5.386	5.418	3.329	10.09	7.809	2.049	18.92	22.76	1.058
2.406	4.583	3.605	5.547	5.477	3.304	1035	8.045	2.007	19.49	24.32	1.012
2.490	4.596	3.598	5.699	5.533	3.276	10.62	8.310	1.964	20.10	26.09	0.960
2.573	4.615	3.597	5.867	5.595	3.245	10.92	8.620	1.930	20.76	27.96	0.764
2.653	4.631	3.593	6.049	5.661	3.205	11.23	8.866	1.808	21.47	30.22	0.669
2.746	4.660	3.598	6247	5.725	3.150	11.57	9.175	1.694			

Rh 0.653 Moles

T	C/T	T	C/T	T	C/T	T	C/T
1.417	4.940	3.147	4.905	5.947	5.311	12.51	7.742
1.481	4.938	3.260	4.920	6.138	5.352	12.95	7.998
1.555	4.900	3.363	4.931	6.347	5.402	13.44	8.389
1.625	4.884	3.467	4.939	6.580	5.439	14.39	8.967
1.695	4.867	3.582	4.943	6.787	5.509	14.69	9.189
1.766	4.856	3.694	4.940	7.166	5.614	15.00	9.443
1.843	4.837	3.803	4.957	7.614	5.723	15.33	9.708
1.939	4.866	3.922	4.970	7.870	5.794	15.69	10.02
2.014	4.861	4.056	4.981	8.150	5.885	16.06	10.37
2.087	4.862	4.206	4.997	8.456	5.980	16.46	10.78
2.160	4.866	4.346	5.018	8.799	6.096	16.88	11.19
2.238	4.870	4.471	5.036	9.186	6.234	17.31	11.65
2.316	4.875	4.607	5.045	9.612	6.392	17.78	12.05
2.394	4.879	4.759	5.075	10.02	6.544	18.28	12.79
2.485	4.880	4.928	5.110	1041	6.713	19.39	14.41
2.582	4.884	5.125	5.147	10.75	6.871	19.99	15.12
2.694	4.876	5.245	5.166	11.06	7.005		
2.810	4.884	5.401	5.196	11.38	7.122		
2.922	4.896	5.565	5.233	11.72	7.325		
3.031	4.898	5.746	5.270	12.10	7.517		

Rh 0.5% Fe 0.629 Moles

T	C/T	ΔC/T	T	C/T	ΔC/T	T	C/T	ΔC/T	T	C/T	ΔC/T
1.357	7.467	2.772	2.638	6.878	2.092	5.903	6.248	0.974	11.28	7.609	0.486
1.418	7.425	2.728	2.728	6.847	2.052	6.088	6.253	0.930	11.62	7.770	0.470
1.478	7.419	2.720	2.831	6.784	1.973	6.291	6.271	0.915	11.99	7.946	0.444
1.526	7.397	2.695	3.178	6.638	1.795	6.515	6.319	0.911	12.39	8.168	0.436
1.578	7.365	2.660	3.294	6.592	1.732	6.763	6.315	0.848	12.82	8.418	0.422
1.631	7.351	2.642	3.401	6.555	1.678	6.990	6.342	0.819	13.30	8.710	0.405
1.687	7.320	2.609	3.508	6.519	1.630	7.190	6.377	0.802	14.39	9.391	0.365
1.747	7.291	2.576	3.760	6.464	1.548	7.407	6.400	0.766	14.84	9.708	0.344
1.801	7.272	2.554	3.895	6.437	1.501	7.643	6.440	0.739	15.17	9.951	0.330
1.856	7.226	2.501	4.025	6.406	1.448	7.903	6.482	0.704	15.52	10.21	0.305
1.921	7.217	2.486	4.171	6.377	1.397	8.212	6.554	0.681	15.88	10.48	0.285
1.987	7.175	2.440	4.306	6.387	1.374	8.527	6.657	0.681	16.27	10.83	0.277
2.055	7.133	2.391	4.427	6.325	1.296	8.877	6.722	0.625	16.68	11.20	0.241
2.128	7.107	2.361	4.560	6.335	1.289	9.209	6.824	0.607	17.11	11.62	0.211
2.207	7.069	2.319	4.707	6.306	1.239	9.518	6.922	0.586	18.05	12.60	0.126
2.287	7.032	2.277	4.870	6.274	1.183	9.939	7.067	0561	18.56	13.17	0.079
2.371	6.992	2.231	5.096	6.254	1.127	10.32	7.205	0.536	19.11	13.86	0.062
2.457	6.956	2.188	5.277	6.249	1.092	10.66	7.343	0.519	19.70	14.64	0.027
2.547	6.934	2.157	5.704	6.242	1.007	10.96	7.471	0.507	20.33	15.54	0.084

Pd 0.19% Fe 0.328 Moles

1.290	15.45	5.855	2.631	13.53	3.384	6.189	14.08	0.653
1.385	15.40	5.780	2.735	13.38	3.182	6.484	14.39	0.587
1.438	15.30	5.666	2.839	13.26	2.997	6.811	14.78	0.532
1.486	15.21	5.559	2.961	13.12	2.784	7.143	15.20	0.465
1.536	15.23	5.560	3.206	12.89	2.398	7.472	15.63	0.389
1.592	15.07	5.387	3.359	12.79	2.199	7.850	16.18	0.341
1.652	15.01	5.308	3.493	12.85	2.161	8.289	16.85	0.276
1.714	14.86	5.136	3.624	12.86	2.075	8.805	17.73	0.232
1.778	14.79	5.039	3.758	12.84	1.946	9.741	1954	0.237
1.838	14.74	4.965	3.890	12.82	1.819	10.25	"o.62	0.254
1.903	14.66	4.866	4.215	12.87	1.594	11.52	23.41	0.160
1.972	14.54	4.712	4.386	12.75	1.321	10.86	21.88	0.177
2.037	14.36	4.507	4.577	12.95	1.346	12.18	25.05	0.158
2.102	14.27	4.390	4.750	13.04	1.266	12.84	26.73	0.142
2.171	14.15	4.243	4.907	13.12	1.189	13.57	28.78	0.160
2.252	14.03	4.084	5.087	13.19	1.069	14.43	31.27	0.168
2.338	13.91	3.9ss	5.296	13.37	1.026	15.42	34.30	0.117
2.430	13.81	3.777	5.772	13.67	0.776	16.35	37.32	0.041
2.527	13.69	3.604	5.966	13.87	0.745	17.21	40.22	-0.076

Addenda Heat capacity Q in mj/°K

T	Q/T	T	Q/T	T	Q/T	T	Q/T
1.452	.0375	2.296	.0545	3.899	.1044	7.524	.3162
1.458	.0383	2.347	.0557	4.056	.1105	8.488	.3996
1.546	.0388	2.475	.0576	4.253	.1175	9.599	.4938
1.548	.0384	2.607	.0590	4.452	.1273	10.91	.6174
1.567	.0394	2.682	.0591	4.908	.1499	12.37	.7590
1.646	.0403	2.807	.0631	5.220	.1668	13.88	.9110
1.761	.0430	3.022	.0697	5.445	.1798	16.73	1.232
1.876	.0459	3.217	.0750	5.747	.1952	18.14	1.400
2.033	.0481	3.442	.0827	6.162	.2209	19.64	1.592
2.174	.0524	3.680	.0913	6.766	.2616	20.90	1.761

APPENDIX 3

GAS THERMOMETER CORRECTIONS

1. Correction for Non Ideality of Gas

The equation of state of a gas may be written

$$pv = A_o \alpha T \left(1 + \frac{B}{v} + \frac{C}{v^2} + \ldots\right)$$

expressing the variables in Amagat units, that is p in atmospheres, and v in units of the volume that would be occupied by the gas at N.T.P.

$\alpha = \frac{1}{273.15}$ and $A_o = 0.999488$. For the filling pressures employed in the present work, only the correction involving the second virial coefficient B need to considered, higher order corrections being negligable.

If the thermometer is filled to a pressure p_o at temperature T_o,

$$p_o v = A_o \alpha T_o \left(1 + \frac{B_o}{v}\right)$$

and at temperature T, p is given by

$$pv = A_o \alpha T \left(1 + \frac{B}{v}\right)$$

Therefore $T = p \frac{T_o}{p_o} \cdot \frac{1 + \frac{B_o}{v}}{1 + \frac{B}{v}} = T_m \frac{1 + \frac{B_o}{v}}{1 + \frac{B}{v}}$

where $T_m = \frac{pT_o}{p_o}$ is the temperature calculated assuming the validity of Charles' Law. The correction ΔT to T_m is therefore

$$\Delta T = T - T_m = \frac{T_m}{v} \left(\frac{B_o - B}{1 + \frac{B}{v}} \right)$$

If p_o is expressed in cm Hg,

$$v = \frac{T_o}{p_o} \times \frac{76}{273} = 0.28 \frac{T_o}{p_o}$$

The corrections shown in fig. 33B have been calculated assuming the temperature variation of B quoted by Keesom in "Helium", 1942.

2. Dead Space Correction

This correction eliminates the effects of the gas in those parts of the pressure sensing tube that are at temperatures different from that of the bulb. In estimating this correction, non ideality of the gas in the sensing tube can be ignored. Thus the equation of state of the gas in the system can be written

$$\sum_i \frac{pv_i}{T_i} = \text{constant}$$

for a fixed mass of gas in the system. The summation is taken over all parts of the system.

If the thermometer is filled to a pressure p_o at temperature T_o

$$\frac{p_o V_o}{T_o} + p_o I_o = \frac{pV}{T} + pI$$

where V_θ is the volume of the thermometer bulb at temperature T_o, and V is the volume of the thermometer bulb at temperature T, and $V = V_o + \delta V$

$I_o = \int_v \frac{dv}{T}$, the integration being taken over the whole volume of the sensing tube when the temperature of the bulb is T_o, and I is the same integral, taken when the temperature of the bulb is T.

Therefore $T = T_m \quad \frac{1 + \Delta + \delta V}{1 + \Delta_o}$

where $\Delta = \frac{T}{V_o} I$ and $\Delta_o = \frac{T_o}{V_o} I_o$

and $T_m = P \frac{T_o}{p_o}$ is the temperature calculated assuming the validity of Charles' Law.

$$\Delta T = T - T_m \quad \left\{ \frac{\Delta - \Delta_o + \delta V}{1 + \Delta_o} \right\}$$

APPENDIX 4

SPECIFIC HEAT PROGRAMME

Programme for Use with the Elliott 703 Computer

```
SETS 1(5)J(6)K(6)LM(2)
SETV A(50)NP(6)Q(6)R(3)S(6)T(2)U(2)V(9)W(2)
SETF LOG
SETR 9
1)READ N . . . . . N = No. of moles
WAIT
VARY 1=0:1:5
READ PI . . . . . sqrt(logR/T) = Po/LOGR + P1 + P2 LOGR + P3 (LOGR)^2
PRINT PI,6                                    + P4 (LOGR)^3
REPEAT I
LINE
WAIT
READ R1
READ R2 . . . . . R_H = R1 + R2 * T
PRINT R1,4
PRINT R2,3
LINE
WAIT                                          6
VARY J=1:1:6                                  ∑   Q(J) T^J
READ QJ . . . . . Qaddenda =                  J=1
PRINT QJ,4/
REPEAT J
LINE
WAIT                                          6
VARY K=1:1:6                                  ∑   S(K) T^K
READ SK . . . . . C pure metal                K=1
PRINT SK,4/
REPEAT K
LINES 3
TITLE
     T       T²      T2-T1       C       C/T       C-CO       C-CO/T
LINES 2
WAIT
2)READ L . . . . . L = Number of Heat
READ V1 . . . . . V1 = S μv/inch
JUMP IF V1= 0to3
A1=V1
3)READ V2 . . . . . V2 = V_i mv
JUMP IF V2=C to4
A2=V2
4)VARY M=1:1:2
READ UM . . . . . UM = V1 or V2
READ WM . . . . . WM = d1 or d2
A3=A2/1340000
A4=A3*UM
A5=A2-A4
A6=A5/14.51
A7=WM*A1
```

```
A8=UM-A7
A9=A8/A6
A10=LOG A9
A11=0
VARY 1=4:-1:5
A11=A11+P1
A11=A11*A10
REPEAT 1
TM=A10/A11
TM=TM*A10
TM=TM*TM
TM=TM*A10
REPEAT M
A12=T1+T2
A13=A12/2
A14=T2-T1
A15=A13*A13
A16=R2*A13
A17=R1+A16
READ V3 . . . . . V3 = V mv
READ V4 . . . . . V4 = i μA
JUMP IF V3=0 to5
A18=V3*V3
A19=A18/A17
A20=A19/1000
5)JUMP IF V4=0 to6
A21=V4*V4
A22=A21*A17
A20=A22/1000000000
6)READ V5 . . . . . V5 = t secs
A23=A20*V5
A24=A23/A14
A25=0
VARY J=6:-1:6
A25=A25+QJ
A25=A25*A13
REPEAT J
A26=A24-A25
A27=A26/N
A28=A27/A13
A29=0
VARY K=6:-1:6
A29=A29+SK
A29=A29*A13
REPEAT K
A30=A27-A29
A31=A30/A13
PRINT L,3
PRINT A13,4
PRINT A15,4
PRINT A14,4
PRINT A27,4
PRINT A28,4
```

```
PRINT A30,4
PRINT A31,4
LINE
JUMP to2
STOP
START 1
```

REFERENCES

1. G.J. Van den Berg.Prof. Low Temperature Physics 4, 194,1964.
2. W.J. de Haas, J. de Boer, G.J. Van Berg, Physica 1, 115, 1933
3. A.N. Gerritsen and J.O. Linde, Physica 17 573, 1951
4. J. Owen, M.E.Browne, W.D.Knight, and C.Kittel, Phys Rev. 102, 1501, 1956
5. D.A. Spohr and R.T. Webber, Phys. Rev. 105, 1427, 1957
6. M.S.R. Chari and J. De Nobel, Physica 25, 60, 1959.* See also Cryogenics 3,70,1963.* Report No. 140/64 Clarendon Laboratory, Oxford.
7. R. Berman, J.C.F. Brock, D.J.Huntley *
8. M. Hansen, Constitution of Binary Alloys, McGraw-Hill, 1958.
9. A.N. Gerritsen and J.O.Linde, Physica 18, 877, 1952
10. C.A. Domenicali and E.L. Christenson, J.Appl.Phys., 32, 2450, 1961
11. A.J. Croft, E.A. Faulkner, J.Hatton, E.F. Seymour, Phil.Mag7 44,289,1953
12. J.S. Dugdale and D.K.C.Macdonald, Can.J.Phys., 35, 271, 1957
13. D.K.C. MacDonald, W.B. Pearson, and I.M. Templeton, Proc.Roy.Soc. A266, 161, 1962
14. G.K. White, Can. J. Phys., 33,119,1955.
15. B.Knook, Thesis, Leiden, 1962
16. A.Kjekshus and W.B.Pearson, Can. J. Phys. 40, 98,1962
17. Y.Muto, J.Phys.Soc.Japan15,2119,1960. See also ref. 34.
18. A.N. Gerritsen, Physica 23, 1087,1957
19. F.T.Hedgecock, W.B. Muir, F.T.Wallingford, Can.J.Phys. 38,376,1960, G.Gaudet, F.T.Hedgecock, G.Lamarche, F.T.Wallingford. Can.J.Phys.38, 1134,196.
20. G.J.Los and A.N.Gerritsen, Physica 23, 633, 1957
21 A.N.Gerritsen, Physica 25, 489, 1959
22. I.S. Jacobs and R.W.Schmitt. Physica 24, S.174,1958
23. J.Owen, M.E.Browne, V.Arp, and A.F.Kip, J.Phys.Chem.Solids
24. A. Van Itterbeek, W.Peelaers, F.Steffens App.Sci.Res. B8, 337, 1960
25. R.W. Schmitt, and I.S. Jacobs, J.Phys.Chem.Solids 3, 324 1957
26. O.S.Lutes and J.L.Schmit, Phys.Rev.134, A676,1964

27. G. Gustafson. Ann. der Physik 25, 545, 1936

28. A.R. Kaufmann, S.T.Pan. J.R. Clark, Rev. Mod. Phys. 17, 87, 1945.

29. W.E.Henry. Phys.Rev.Letters 11, 468,1963.

30. F.Bitter, A.R.Kaufmann, C.Starr, and S.T.Pan. Phys.Rev.60, 134,1941.

31. E.Hildebrand, Ann.derPhysik 30, 593, 1936.

32. E.W.Pugh, B.R.Coles, A.Arrott, J.E.Goldman. Phys.Rev.105,814,1957.

33. E.W.Collings and F.T.Hedgecock. Phys.Rev. 126, 1654,1962.

34. E.W.Collings, F.T.Hedgecock, W.B.Muir, Proc. 8th Int.Cont. Low Temp. Phys. Butterworths, 1963.

35. E.W. Collings, F.T.Hedgecock, and T.Sakudo, Can.J.Phys.39, 1233, 1961

36. A.N.Gerritsen, Physica 19, 61, 1953.

37. Y.Muto, K.Noto, F.T.Hedgecock, CanJ.Phys. 42, 15, 1964.

38. W.Marshall, T.E.Cranshaw, C.E.Johnson, M.S.Ridout, Rev.Mod.Phys.36,399,1964

39. M.S.Ridout, T.E.Cranshaw, C.E.Johnson, Int.Conf.Mag. Nottingham 1964.

40. R.J.Borg, R.Booth, C.E.Violet. Phys.Rev.Letters,11, 464,1963.

41. P.P.Craig, and W.A.Steyert, Phys.Rev.Letters 13,802,1964

42. A.V.Gold, D.K.C.MacDonald, W.B.Bearson, I.M.Templeton, Phil.Mag.5, 765,1960

43. G.Borelius, Proc.Roy.Acad.Sci.Amst.35,15,1932

44. B.T.Matthias,M.Peter.H.J.Williams,A.M.Clogston.E.Corenswit,R.C.Sherwood. Phys.Rev.Letters, 5, 542,1960

45. A.M.CLogston,B.T.Matthias,M.Peter,H.J.Williams,E.Corenzwit,R.C.Sherwood, Phys. Rev. 125, 541,1962.

46. D.Gerstenberg Ann.Physik 2, 236,1958.

47. J.Crangle Phil.Mag. 5, 335, 1960

48. C.G.E.Low Proc.Int.Conf.Mag.(Nottingham) 1964

49. J.H.Waszink Thesis. London University 1965.

50. B.R.Coles. Phil.Mag.8, 335,1962.

51. B.R.Coles. Physics Letters 8, 243, 1964.

52. B.R.Coles, J.H.Waszink, J.W.Loram Proc.Int.Conf.Mag.(Nottingham)1964

53. M.P.Sarachik, E.Corenzwit, L.D.Longinotti, Phys.Rev.135, A1041,1964.

54. M.P.Sarachik, J.Appl.Phys.Suppl. 35,1094, 1964.

55. M.P.Sarachik, Phys.Rev. 137, A659, 1965.

56. B.W.Veal and J.A.Rayne, Phys.Rev.135, A442,1964

57. J.A.Cape and R.R.Hake Int.Conf.Mag.

58. M.Blackman, Rep.Prog.Phys. 8, 10, 1941.

59. R.B.Leighton. Rev. Mod.Phys. 20, 165, 1948

60. J.R.Neighbours and G.A.Alers Phys.Rev. 111, 707, 1958.

61. J. de Launey. J.Chem.Phys. 22, 1676,1954.

62. J.Friedel Nuovo Cimento Supp. 7, 287,1958

63. H.Montgomery. unpublished

64. G.L.Guthrie, S.A.Friedberg, J.E.Goldman, Phys.Rev. 113,45,1958.

65. J.A.Rayne, Phys.Rev. 108, 22, 1957

66. L.L.Isaacs and T.B. Massalski, Phys.Rev.138 A134, 1965

67. J.M.Ziman, Advan. Phys. 10, 1, 1961.

68. C.H.Cheng, C.T.Wei, P.A.Beck. Phys.Rev.120, 426,1960

69. M.M.Cohen and V.Heine, Advan.Phys. 7, 395, 1951

70. H.Jones Phys.Rev. 134, 958, 1964.

71. J.Friedel Can. J.Phys.34, 1190, 1956.

72. F.J. du Chatenier Thesis Leiden 1965

73. J.E.Zimmerman And F.E.Hoare J.Phys.Chem.Solids, 17, 52, 1960

74. J.P.Franck, F.D.Manchester, D.L.Martin, Proc.Roy.Soc.A263 494, 1961

75. L.T.Crane and J.E.Zimmerman, Phys.Rev.123, 113,1961 L.T.Crane Phys.Rev. 125, 1902,1962

76. J.de Nobel and F.J. du Chatenier Physica 25, 969,1959

77. B.Dreyfus, J.Souletie, R.Tournier, L.Weil, Compte Rendu 259, 4266,1964

78. J.K.Logan, J.R.Clement,H.R.Jeffers, Phys.Rev.105, 1435,1957

79. D.L.Martin, Can.J.Phys.39, 1385,1961

80 D.L. Martin, Proc.Phys.Soc.78 1489,1961

81. J.Friedel Ann. Phys. 9, 166, 1954. See also ref.62

82. G.G.E.Low and M.F.Collings J.App.Phys. 34 1195, 1963

83. W.Kohn and S.H.Vosko Phys.Rev. 119, 912, 1960

84. J.Friedel, PhilMag. 43, 153,1952. See also ref 62.

85. P. de Casteljau, and J.Friedel J.Phys.Rad.17, 27,1956.

86. G.F.Koster and J.C.Slater Phys.Rev.96 1208,1954

87. N.F.Mott and H.S.W.Massey Atomic Collisions Oxford 1949.

88. L.I.Schiff Quantum Mechanics McGraw-Hill 1955

89. A.Blandin and J.Friedel. . J.Phys.Rad.20, 160,1956.

90. J.Friedel, CanJ.Phys. 34, 1190,1956

91 E.Daniel, J.Phys.Chem. Solids 23, 975,1962

92. P.A.Wolff, Phys.Rev.124,1030,1961

93. A.M.Clogston, Phys.Rev. 125,439,1962. See also ref.45

94. P.W.Anderson Phys.Rev. 124, 41,1961

95. K.Yosida, Phys.Rev.106 893 1957

96. C.Zener Phys.Rev. 81 440, 1951

97. A.A.Abrikosov and L.P.Gorkov, J.E.T.P.16, 1575, 1963.

98. M.A. Ruderman and C.Kittel Phys.Rev. 96, 99, 1954

99. A.W. Overhauser J.Phys.Chem.Solids 13, 71, 1960

100. A.J.Dekker, Physica 24, 697, 1958

101. W.Opechovski, Physica 4, 181, 1937

102. H.Sato, A.Arrott, R.Kikuchi J.Phys.Cehm.Solids 10, 19, 1959

103. J.Korringa, A.N.Gerritsen Physica 19 457,1953

104. R.W.Schmitt PhysRev. 103, 83, 1956

105. K.Yosida. Phys.Rev.107, 396,1957

106. A.D.Brailsford, A.W.Overhauser J.Phys.Chem,Solids15, 140,1960

107. A.J.Dekker, Physica 25, 1244, 1959

108. J.Kondo, Prog.Theoret.Phys.(Kyoto) 32, 37,1964.

109. A.R. de Vroomen, M.L.Potters. Physica 27, 1083, 1961

110. W.Marshall Phys.Rev. 118, 1519, 1960

111. P.W.Anderson, Phys.Rev. 82, 342, 1951, see also C.Kittel and E. Abrahams Phys.Rev. 90, 238, 1953

112. M.W.Klein and R. Brout, Phys. Rev. 132,2412,1963.
M.W.Klein, Phys Rev. Letters 11, 408, 1963
M.W.Klein, Sporry Rand Report No. SRRC-RR-64-40 (1964)

114. J.A.Rayne Aust.J.Phys. 9, 189, 1956

115. D.L.Martin Can.J.Phys.38,17,1960;40,1166,1962
F.D.Manchester Can.J.Phys.37,989 1959

116. T.M.Dauphinee, D.K.C.MacDonald, H.Preston Thomas Proc Roy.Soc.A221, 267,1954

117. K.G.Ramanathan and T.M.Srivenšan Phil.Mag. 46, 338, 1955

118. E.Ambler, N.Kurti Phil. Mag.43, 1307, 1952.

119. See ref. 128

120 R.Berman, J.Appl. Phys.27, 318, 1956

121. R.Berman, Rev.Sci.Inst.2594,1954

122. D.Martin, Proc. 8th Int.Conf. Low Temp Phys. Butterworths, 1963.

123. D.Gerstenberg, Ann Physik, 2, 236, 1958

124. J.Crangle Phil.Mag. 5, 335, 1960

125. R.M.Bozorth, P.A.Wolff, DD.Davis, J H.Wernick,V.B.Compton, Phys.Rev.122, 1157, 1961

126 B.W.Veal and J.A.Rayne Phys.Rev.135, A442,1964

127 J.A.Rayne, Phys.Rev. 108, 649 1957

128. W.S.Corak, M.P.Garfunkle,C.B.Satterthwaite, A.Wexler, Phys.Rev.98,1699, 1955

129. N.M.Wolcott, Conf.Low.Temp.Phys.(Paris)108,1955.

130. A.K.Clusius and C.G.Losa. Conf.Low.Temp.Phys.(Paris)53,1955

131. D.W.Budworth, F.E.Hoare,J.Preston, Proc.Roy.Soc.A257, 250, 1960

132. F.E.Hoare and B.Yates Proc.Roy.Soc.A240, 42, 1957

133. See ref. 126

134. W.S.Corak, Phys.Rev.98, 1699 1955

135. J.A.Rayne, Phys.Rev. 108, 22,1957

136. B.W.Veal and J.A.Rayne Phys.Rev128,551,1962

137. M.Griffel, R.W.Vest and J.F.Smith, J.Chem.Phys.27,1267,1957

138. J.E.Zimmerman, PhysRev. 126, 573, 1962

139. S.Doniach - to be published

140. Y.Nagaoka, Phys.Rev.138, A1112,1965

141. A.M.Guenault and D.K.C.MacDonald, Phil Mag6, 1201, 1961

142. P.P.Craig, D.E.Nagle, W.A.Steyart, R.D.Rayler, PhysRev. Letters 9, 12,1962

143. T.R.Roberts and S.G.Sydoriak, Phys.Rev. 102, 304, 1956.